GROUNDWATER – SURFACE WATER INTERACTION UNDER THE EFFECTS OF CLIMATE AND LAND USE CHANGES

by

Gopal Chandra Saha

B.Sc., Bangladesh University of Engineering & Technology, Bangladesh, 2003
M.Sc., Stuttgart University, Germany, 2006
M.Sc., Auburn University, USA, 2009

DISSERTATION SUBMITTED IN PARTIAL FULFILLMENT OF
THE REQUIREMENTS FOR THE DEGREE OF
DOCTOR OF PHILOSOPHY
IN
NATURAL RESOURCES AND ENVIRONMENTAL STUDIES

UNIVERSITY OF NORTHERN BRITISH COLUMBIA

September 2014

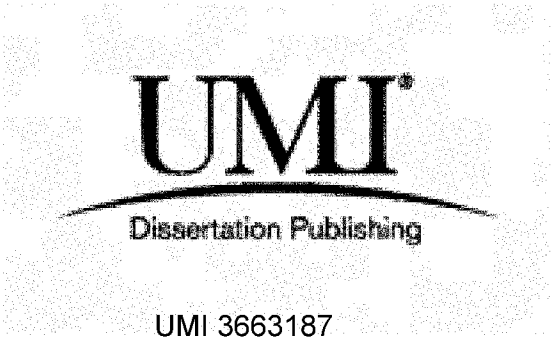

ProQuest LLC
789 East Eisenhower Parkway
P.O. Box 1346
Ann Arbor, MI 48106-1346

ABSTRACT

Historical observed data and future climate projections provide enough evidence that water resources systems (i.e., surface water and groundwater) are extremely vulnerable to climate change. However, the impact of climate change on water resources systems varies from region to region. Therefore, climate change impact studies of water resources systems are of interest at regional to local scales. These studies provide a better understanding of the sensitivity of water resources systems to changes in climatic variables (i.e., precipitation and temperature), and help to manage future water resources. In addition to climate change, human-induced land use changes also significantly affect water resources systems. Therefore, climate and land use changes can provide offsetting and additive impacts on water resources systems depending on the region and watershed characteristics. In this dissertation research, groundwater-surface water (GW-SW) interaction under the effects of climate and land use changes were investigated through the development of a Gridded Surface Subsurface Hydrologic Analysis (GSSHA) modeling system using a case study in Kiskatinaw River watershed (KRW), British Columbia, Canada. Based on the simulation results, it was found that the mean annual groundwater contribution to stream flow in the study area during the short-term period (2012-2016) under the A2 and B1 climate change scenarios of the Intergovernmental Panel on Climate Change (IPCC) is expected to decrease by 3.3% and 1.8%, respectively, with respect to that during the reference period (2007-2011). This was due to increased precipitation (on average 6.1% under the A2 and 3.6% under the B1 scenarios) and temperature (on average 0.64°C under the A2 and 0.36°C under the B1 scenarios). The climate change would result in increased stream flow (on average 6.7% and

3% under the A2 and B1 scenarios, respectively) and groundwater discharge (on average 2.8% and 1.2% under the A2 and B1 scenarios, respectively), but the major increase occurred in surface runoff (on average 22.5% and 11.2% under the A2 and B1 scenarios, respectively). Under the effect of climate change, the mean groundwater contribution to stream flow illustrated monthly, seasonal, and annual variation due to precipitation variability. The mean seasonal groundwater contribution to stream flow under both climate change scenarios is the lowest and highest during summer and winter, respectively. Similar results were found for the long-term period (2020-2040).

When land use/land cover (LULC) changes (i.e., increasing forest clear cut area, and decreasing forest and agricultural areas) were combined with climate change scenarios, similar results of climate change effects were found, but with a decreasing rate except in stream flow and surface runoff. Compared to the reference period (2007-2011), the mean annual groundwater contribution to stream flow from 2012 to 2016 under the combined effect of A2 or B1 climate change scenario and LULC changes is expected to decrease by 6.4% and 4.3%, respectively. Under the combined LULC changes with A2 and B1 scenarios, on average stream flow increased by 10.1% and 5.8%, groundwater discharge increased by 2.1% and 0.7%, and surface runoff increased by 42% and 29%, respectively. The results indicate that the flow patterns were shifted to the regime with more surface runoff and stream flow but less groundwater discharge, which implies that land use change has an important role in GW-SW interaction within a watershed. In addition, uncertainty analysis of GW-SW interaction in the study area was conducted using a Monte Carlo method, and the cumulative frequency distributions of groundwater contributions to stream flow under the A2 and B1

climate change scenarios were obtained. These results also illustrated different monthly, seasonal, and annual variation patterns.

The key contribution of this dissertation research was the inclusion of climate and LULC changes scenarios in the developed numerical model to assess GW-SW interaction. The modeling results will help better understand the dynamics of GW-SW interaction due to climate change or combined climate and LULC changes. The results will also provide useful information for effective short-term and long-term water resources decision making in the study area in terms of seasonal and annual water extractions from the river and water allocation to the stakeholders for future water supply, as well as for evaluating the ecological conditions of the stream. The developed numerical model would serve as a useful tool for dealing with GW-SW management problems in the context of climate and land use changes.

TABLE OF CONTENTS

LIST OF FIGURES

LIST OF TABLES

ACKNOWLEDGEMENT

First of all, I would like to thank my co-supervisors Professors Jianbing Li and Ronald Wallen Thring for their enormous guidance, suggestion and inspiration in completing the dissertation. Their constructive criticism has helped me to organize the work properly. I would also like to thank Professors Youmin Tang, Adam Wei and Liang Chen for serving as my committee members, and for their comments and supports. In addition, I would like to thank Professor Lei Liu for serving as the external examiner, and for his comments to improve the dissertation.

I would like to appreciate Faye Hirshfield, Peter Caputa, Siddhartho Shekhar Paul, Malyssa Maurer, Arlinda Banaj, Reg Whiten, Chelton van Geloven, Vanessa Ford, Deepa Filatow, Richard Kabzems, and Trevor Murdock for their assistance in data collection, conducting field work, and providing data during this study. Special thanks to You Qin Wang, Jutta Koehler, Ju Zhang, Xinyuan Song, Sissy, Kara Taylor, Scot, and Tammera Kostya for their numerous help during my whole study at UNBC.

I would also like to show my deepest gratitude to my parents (Santosh Kumar Saha and Niva Rani Saha), my brother (Sujit Kumar Saha) and sister (Shilpi Rani Saha), and my relatives, especially Late Prahllad Saha and Badal Saha, for encouraging me during my whole degree program at UNBC. In addition, my wife, Pinki Saha, and my little son, Adhrit Saha, motivated and encouraged me lots to do work very efficiently although it was difficult for me sometimes to leave them at home for long time during my long hours working at UNBC. This research was funded by Peace River Regional District, the City of Dawson Creek, Geoscience BC, EnCana, and BP Apache.

CHAPTER 1

INTRODUCTION

1.1 Background

Groundwater-surface water (GW-SW) interaction is a common phenomenon observed in nature. During flooding season, surface water can recharge groundwater, but during drought season groundwater acts as an important source to feed the surface water flow. As a result, groundwater and surface water are closely linked components of the hydrologic system. The development and exploitation of any one component can affect the other component. It is thus crucial to quantify the exchange processes between these two components for sustainable water resources management (Sophocleous, 2002).

It has been recognized that the water resources system is extremely vulnerable to changes in climate (McCarthy et al., 2001; Kundzewicz et al., 2008). The IPCC (Intergovernmental Panel on Climate Change) reported that the global atmospheric concentrations of greenhouse gases (GHG) will continue to increase in the following decades and lead to continuing climate change (Solomon et al., 2007). Climate change impact studies have been conducted by more focusing on surface water bodies than on groundwater because groundwater is less visible and has a more complex relationship with climate (Scibek et al., 2006a; Kundzewicz et al., 2009). Due to the importance of groundwater resources, climate change impact studies on groundwater have received increasing attention from many scientists during the last decade. For example, Scibek et al. (2006a) conducted a case study of an unconfined aquifer

in the Grand Forks valley in south-central British Columbia, and they developed a methodology for linking climate models, hydrologic model (i.e., HELP), and groundwater flow model (i.e., Visual MODFLOW) in order to investigate the impacts of climate change on groundwater resources. Van Roosmalen et al. (2007) used the DK model (The National Water Resource model for Denmark) based on MIKE SHE code to study climate change impacts on groundwater system for two study areas in Denmark. Krause et al. (2007) used the IWAN (Integrated Water Balance and Nutrient Dynamics Model) model to simulate exchange fluxes between the groundwater of the floodplain and the surface water within the direct catchment of Lower and Central Havel River, Germany. Jenkins (2006) used the GSSHA (Gridded Surface Subsurface Hydrologic Analysis) model to investigate GW-SW interaction in the floodplain of Rio Grande River, New Mexico, USA during high and low flows in Rio Grande River. Goderniaux et al. (2009) examined the climate change impacts on the groundwater reserve in Geer Basin catchment in Belgium using a finite element model called HydroGeoSphere. Jackson et al. (2011) used the ZOODRM model and the ZOOMQ3D finite difference code to assess the impacts of climate change on groundwater in the Chalk aquifer system in England. Dams et al. (2012) used a coupled model of WetSpa and MODFLOW to study climate change impacts on the groundwater system in the Kleine Nete basin in Belgium. Vansteenkiste et al. (2012) compared the estimations of climate change impacts on the flow regime in the Grote-Nete catchment in Belgium by using two spatially distributed models, MIKE SHE and WetSpa.

In general, most of the previous studies reported how the mean annual groundwater level and groundwater recharge or discharge (i.e., mean of 20 to 40 years) would change under different climate change scenarios. Only a few studies (Van Roosmalen et al., 2007; Jackson

et al., 2011; Dams et al., 2012; Vansteenkiste et al., 2012) reported how the mean monthly groundwater recharge and discharge, stream flow, as well as groundwater level would change between current and projected future climates. There is little knowledge regarding how the mean monthly groundwater contribution to stream flow will change under different climate change scenarios. These monthly changes could determine the monthly status of groundwater resources and site conditions for groundwater-dependent terrestrial ecosystems (Naumburg et al., 2005). They will also determine the monthly, seasonal and annual variations of stream flow dependency on groundwater, and these will provide useful information for monthly, seasonal and annual water extractions from the river, and allocation to the stakeholders for future water supply. In addition to climate change, land use changes can also significantly affect groundwater recharge and discharge, and surface water flow patterns by altering soils' infiltration rate (Jinno et al., 2009). For example, increasing urban area resulted in decreasing groundwater discharge, and increasing stream flow and surface runoff (Klocking et al., 2002; Chang, 2007; Lin et al., 2007; Dams et al., 2008; Zhou et al., 2013); the conversion of perennial vegetation to seasonal growing crops in the Mississippi River Basin resulted in increased groundwater discharge and stream flow, and decreased surface runoff (Zhang et al., 2006b; Schilling et al., 2010); changing agricultural area into grasslands in a sub catchment of Havel River, Germany, resulted in decreased groundwater discharge (Krause et al., 2004); the conversion of grassland into forest in the western part of Jutland, Denmark, resulted in decreased groundwater discharge (Van Roosmalen et al., 2009); a decrease of grassland area with concurrent increases of shrub land rain-fed agriculture, bare ground irrigated agriculture and urban area led to an increase in the surface runoff and a decrease in the groundwater discharge and stream flow (Ghaffari et al., 2010). A number of studies (Klocking et al., 2002;

Batelaan et al., 2003; Krause et al., 2004; Lin et al., 2007; Dams et al., 2008; Van Roosmalen et al., 2009; Wijesekara et al., 2012; Zhou et al., 2013) have investigated the combined impacts of climate and land use changes on watershed hydrology. Many of the previous studies reported how the mean annual groundwater recharge and discharge, stream flow, as well as groundwater level would change under different land use change scenarios. However, little attention was paid to investigate how the mean monthly, seasonal and annual groundwater contributions to stream flow will change under both changing land use and climatic conditions. Moreover, most of the parameters (e.g., precipitation, soil properties, topography) of hydrologic models used for GW-SW interaction simulation require measurements from resources-intensive field exercises (Benke et al., 2008), and they are always associated with uncertainty. Such parameter uncertainty would also lead to uncertainty in modeling outputs (Muleta et al., 2004). A number of studies have conducted uncertainty analysis of stream flow in watershed due to parameter uncertainty using various uncertainty analysis methods in different hydrologic models (Beven et al., 1992; Kuczera et al., 1998; Vrugt et al., 2003; Benke et al., 2008; Mishra, 2009; Dotto et al., 2012; Shen et al., 2012; Shen et al., 2013). However, few studies have reported regarding the uncertainty analysis of the mean monthly, seasonal and annual groundwater contributions to stream flow in a watershed.

1.2 Objectives

This dissertation research is proposed to fill the gaps identified above using a study area along the river of the Mainstem sub-watershed of Kiskatinaw River Watershed (KRW) in

north-eastern British Columbia as a case study. The mean monthly, seasonal and annual groundwater contributions to stream flow under different GHG emission scenarios (i.e., A2 and B1), as well as combined climate and land use changes were investigated using the GSSHA model. The related objectives include (1) development of a GSSHA model for the study area of the Mainstem sub-watershed, (2) investigating climate change impacts on GW-SW interaction in the study area using the GSSHA model under different GHG emission scenarios (i.e., A2 and B1 scenarios of IPCC), (3) examining the combined impacts of land use/land cover and climate changes on GW-SW interaction, and (4) uncertainty analysis of GW-SW interaction under different GHG emission scenarios.

1.3 Organization of dissertation

This dissertation is organized into eight chapters. Chapter 1 introduces the research importance and objectives. Chapter 2 provides details of literature review of GW-SW interaction. Chapter 3 describes the study area, GW-SW monitoring network development, field data collection, and development of the GSSHA numerical model. Chapter 4 presents the generation of future climate and land use/land cover change scenarios. Chapter 5 discusses the modeling results of climate change impacts on GW-SW interaction under different GHG emission scenarios. Chapter 6 presents the modeling results of climate and land use/land cover changes impacts on GW-SW interaction. Chapter 7 describes the uncertainty analysis results of GW-SW interaction. Chapter 8 presents the summary and conclusions of this study and recommendations for future research.

CHAPTER 2

LITERATURE REVIEW

2.1 Background

Investigation of GW-SW interaction in a watershed has been continued since the last several decades (Lee, 1977; Woessner et al., 1984; Workman et al., 1991; Geist et al. 1998; Krause et al., 2007; Van Roosmalen et al., 2007; Goderniaux, 2010; Dams et al., 2012). This interaction occurs throughout the year because groundwater and surface water are closely linked components of the hydrologic system. In a watershed, groundwater interacts with surface water (i.e., stream or river) in four basic ways depending on the elevations of surface water and groundwater table as described below (Woessner, 1998; Winter et al., 1998):

(1) If groundwater levels at both banks are higher than surface water level in the river/creek, groundwater contributes to river/creek, which is shown in Fig. 2.1a (i.e., gaining stream or groundwater discharging).

(2) If groundwater levels at both banks are lower than surface water level in the river/creek, river/creek contributes to groundwater, which is shown in Fig. 2.1b (i.e., losing stream or groundwater recharging).

(3) If groundwater levels at both banks are equal to surface water level in the river/creek, zero exchange occurs, which is shown in Fig. 2.1c (i.e., parallel flow stream).

(4) If groundwater level at one bank is higher than surface water level in the river/creek but lower at the opposite bank, a flow-through channel occurs, which is shown in Fig.

2.1d (i.e., gaining at one side of the river/creek and losing at other side of the river/creek).

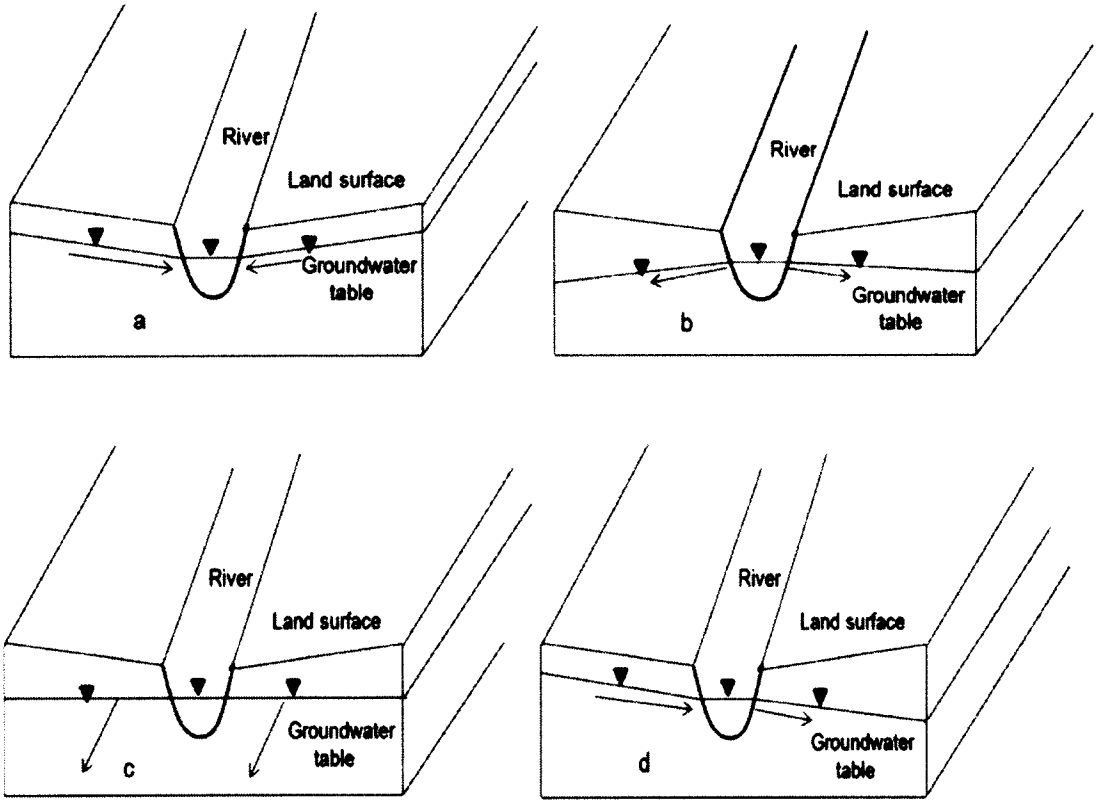

Figure 2.1 Groundwater-surface water interaction in a (a) gaining, (b) losing, (c) parallel flow and (d) flow-through stream (modified from Woessner, 1998). The arrow indicates groundwater flow direction.

During the last several decades, numerous studies have been done for investigating GW-SW interaction using different methods. This chapter will review the methodologies used in

previous research on the investigation of GW-SW interaction, and highlight the critical issues that need to be further explored.

2.2 Methods used for investigating groundwater-surface water interaction

GW-SW interaction and base flow (groundwater discharge) quantification have been investigated by researchers using different methods, including field investigation and measurement, numerical models, analytical methods, and experimental methods. Various field measurement methods (e.g., seepage meters, piezometer methods, tracer methods) have been used to investigate GW-SW interaction and determine base flow, but they are usually site and case specific (Kalbus et al., 2006). Due to limited data availability, the understanding of the temporal and spatial variation of complex GW-SW interaction processes is very limited (Zhang et al., 2004). Sophocleous (2002) pointed out that base flow determination is a major challenge due to heterogeneities and the problem of integrating measurements at various scales. Analytical methods use analytical equations and graphs to determine base flow, but they cannot provide future forecasting. Experimental methods consider homogenous formation of soil, and are used in small-scale application. In contrast, numerical models are cost-effective for investigating and predicting GW-SW interaction and quantifying base flow (Kalbus et al., 2006). In the following sections, different types of methodologies used in GW-SW interaction studies are discussed.

2.2.1 Field measurement methods

2.2.1.1 Using conventional wells and piezometers

Workman et al. (1991) and Jagucki et al. (1995) collected daily groundwater levels and river elevation at the Ohio Management Systems Evaluation Area (OMSEA) from August 1991 to December 1995 to investigate the GW-SW interaction. Eleven wells (152 mm diameter PVC casing, and 6.1 m long) were installed in a 260 ha (2.6 km^2) area surrounding the OMSEA site to monitor groundwater levels, and all the wells were installed on one side of Scioto River. The closest and farthest wells were installed 215 m and 2100 m away from the Scioto River bank, respectively. Groundwater levels were recorded hourly using electronic data loggers. In addition, a stream gauge at Higby, Ohio (approximately 21 km upstream from the OMSEA site) used to monitor river stage (i.e., surface water level) and stream flow provided over 60 years of data. The GW-SW interaction was then determined qualitatively by plotting the temporal variation of groundwater and surface water levels. This plot only indicates the GW-SW interaction by showing the almost similar patterns of temporal variation of groundwater and surface water levels, and the type of GW-SW interaction will be one of the four types as shown in Fig. 2.1 depending on groundwater and surface water levels. However, it cannot quantify groundwater discharge due to lack of other data (e.g., hydraulic conductivity and porosity of soil) to estimate groundwater discharge. Similarly, Durand et al. (2007) developed a riverbed hyporheic zone monitoring network over a 200 m river reach in the River Tame to assess GW-SW interaction. The network consisted of an array of 22 hybrid multilevel sampler (MLS) piezometer drive point devices that have a 1-cm diameter central piezometer tube for recording hydraulic head, and ten

multilevel Teflon sampling tubes (3.2 mm OD, 1.6 mm ID) located at 10-cm depth intervals below the riverbed for groundwater quality sampling. The MLS piezometer drive points were distributed in eight transects with each transect containing two or three devices. A single bank-side extraction well was installed for monitoring groundwater level in the bank, and eight customized devices were also installed for automatic head measurements at 12 locations. The hydraulic conditions were continuously recorded by using one pressure transducer within the extraction well and one other within the river, and were then used to determine GW-SW interaction through plotting surface water and groundwater levels against time period. Gonzales et al. (2009) conducted a field work of GW-SW interaction in a temperate lowland area of 51.7 km^2 in the Netherlands from December 2007 to March 2008. Their field work consisted of the drilling of observation wells, the collection and characterization of soil samples at different locations and depths, setting up a groundwater monitoring network, and water sampling during floods and low flows. Five observation wells were installed surrounding a canal, with four of them on the same site of the canal, and another one in the canal close to the surface water level recorder. In order to monitor GW-SW interaction, the water levels in the observation wells and canal were recorded by automatic data loggers. The water levels of groundwater and surface water were then plotted against time period to indicate the discharge of groundwater to the canal.

Geist et al. (1998) installed piezometers in the Hanford Reach (72 km) of Columbia River to understand GW-SW interaction. Piezometers were installed into streambed using a hand-operated 27-kg air-powered impact hammer attached via hose to an air compressor. In total, 14 piezometers were installed in the Hanford Reach in 1995. Most of the piezometers were installed to a depth of > 1 m. Water surface elevations inside the piezometer (groundwater

table elevation) and river levels were measured manually using an electrical interface measuring tape (Solinst) during 11 days in October and November 1995. Groundwater table elevation, river level and the depth of piezometer perforations below the river bed were used to calculate vertical hydraulic gradient (VHG) at each piezometer location.

$$VHL = \frac{\Delta h}{\Delta L} \qquad (2.1)$$

Where Δh is the difference between the water surface elevation inside the piezometer and the water surface elevation of the river (m), and ΔL is the distance below the river bed to the top of the piezometer perforations (m). Positive value of VHG indicates upwelling (i.e., groundwater discharge zones), while negative value indicates down-welling (i.e., groundwater recharge zones).

Kalbus et al. (2006) pointed out that the piezometer/well provides only point measurement of the hydraulic head. The equipment is quick and easy to install, and the measurement analysis is straightforward although this method is more appropriate for small scale applications and allows for a detailed survey of the heterogeneity of flow conditions in subsurface. However, groundwater levels fluctuate with time. All measurements of the hydraulic head at a study site should be made approximately at the same time, and the resulting contour and flow field maps are representative only of the particular time. Pressure transducers and data loggers can be installed in piezometers/wells in order to facilitate automatic temporal data collection which can then be used in numerical models to simulate groundwater levels and flow paths.

2.2.1.2 Using seepage meters

Lee (1977) used a bag-type seepage meter to measure water flux across GW-SW interface. The meter consisted of a bottomless cylinder vented to a deflated plastic bag. The cylinder was inserted into the sediment, and the water flow from groundwater to surface water was collected in the plastic bag. From the collected volume, the cross section area of the cylinder, and the collection period, the seepage flux was calculated. In case of surface water seeping the sediment, a known volume of water was filled into the plastic bag before the installation, and from the volume loss the infiltration rate was calculated. Kelly et al. (2003) developed a modification of seepage meter fitted with piezometer along the axis of a pan, which is also called piezo-seepmeter. A manometer was used to measure the difference of hydraulic head between the piezometer screen and the inside of the pan, which was temporarily attached to a pump. The pumping flow rate was correlated to the head difference between piezometer and pan, and the fluxes into the seepage meter pan were then estimated. To overcome the inconvenience of manual measurement, various automated seepage meters, which monitor seepage variations with time, have also been developed. For example, Krupa et al. (1998) used a heat pulse meter, which is based on the relationship between the travel time of a heat pulse in the flow tube and the flow velocity. Paulsen et al. (2001) used an ultrasonic meter that relates the travel time of an ultrasonic signal through a flow tube to the flow velocity. Sholkovitz et al. (2003) used dye-dilution meter, which is based on the principle that the rate at which a dye solution is diluted by the inflow or outflow of water is directly proportional to the seepage flow rate. Rosenberry et al. (2004) used an

electromagnetic meter, which measures the voltage induced by water passing through an electromagnetic field, while the voltage is proportional to the flow velocity.

Rosenberry (2008) designed a seepage meter for using in moving water of a side channel of South Platte River, Colorado. In that meter, a conical seepage cylinder, made of plastics drums, was partially inserted into the sediment bed, and the above portion of the cylinder was covered by a plastic or metal lid and was connected through plastic tubing to a seepage bag or flow meter, which was positioned inside a rigid shelter. That shelter, made of plastics boxes, was located nearby the cylinder and close to the bank where current velocity is very slow. Seepage flux was monitored using a flow meter when the seepage bag was full by getting water from the conical seepage cylinder. It was found that no significant relationship exists between seepage flux and current velocity, and this meter is not suitable for high current velocity as the errors are proportional to the current velocity.

Kalbus et al. (2006) pointed out that the inexpensive seepage meters are useful for the detection of groundwater discharge or recharge zones, as they are based on a simple concept. They provide base flow quantification at a certain reach of a stream/river. Therefore, they cannot determine base flow for the whole catchment or watershed. However, for better results, more seepage meters are required to be installed at many locations. In stream, the fluxes measured by seepage meter might not be entirely attributed to groundwater discharge, and they may also include shallow throughflow or hyporheic exchange flow. In addition, seepage meters themselves create obstacles to stream flow that might include interstitial flow into the seepage meter pan. Anibas et al. (2011) also pointed out about the uncertainties in the measured flux due to operational problems in the field. Similar to piezometers, seepage

meters cannot quantify future groundwater discharge because they can only quantify groundwater discharge at observed time period.

2.2.1.3 Using tracer methods

Harvey et al. (1997) used an electrical conductivity mapping method to map groundwater discharge zones in a large lake by measuring the variations in sediment pore water electrical conductivity using YSI model 34 electrical conductance meter. This method was tested within the Hamilton Harbor at the western end of Lake Ontario. Systematic variations of electrical conductivity were found between near shore and offshore sediments, and three anomalous zones of elevated electrical conductivity were identified to represent groundwater discharge. The onshore and offshore piezometers were also used to find out the elevated electrical conductivities and the upward hydraulic gradients, which indicate groundwater discharge. Similarly, Geist et al. (1998) measured the electrical conductivity of water samples collected from the Hanford Reach (72 km) of Columbia River and three in-stream piezometers (L2, L5, and L8) to understand GW-SW interaction. Electrical conductivity measurement was conducted manually during eleven days of October and November 1995 using a conductivity/temperature meter (YSI model 30). For piezometer, a 500-mL water sample was extracted to measure its electrical conductivity. Electrical conductivity measured within the river at all locations averaged 132.9 $\mu S / cm$ (S.D. = 4.4 $\mu S / cm$), whereas electrical conductivity values measured within piezometers L2 and L8 were similar with an average of 131.9 $\mu S / cm$ (S.D. = 3.5 $\mu S / cm$) and 144.1 $\mu S / cm$ (S.D. = 20.4 $\mu S / cm$), respectively. The relative similarity between electrical conductivity values suggests that the

hyporheic zone at these locations was comprised predominantly of river water. Electrical conductivity within piezometer L5 was higher, with an average of 281.4 $\mu S / cm$ (S.D. = 16.4 $\mu S / cm$), indicating a higher proportion of groundwater present in the hyporheic zone at that location than the other observed sites.

Becker et al. (2004) used a heat balance equation to calculate groundwater discharge by measuring stream temperature and stream flow, where the stream temperature was a function of groundwater discharge, stream flow, and additional heat gains and losses through the stream surface. Conant (2004) and Schmidt et al. (2006) estimated water fluxes through the streambed using streambed temperatures by assuming that variations in temperature are attributed to spatial variations in water flux through the streambed. Essaid et al. (2008) also used heat as a tracer to study the temporal and spatial variability of fluxes through streambed by continuously monitoring temperature and head in stream reaches within four agricultural watersheds: Leary Weber Ditch (7.2 km^2), Indiana (IN); Maple Creek (956 km^2), Nebraska (NE); DR2 Drain (5.5 km^2), Washington (WA); and Merced River (822 km^2), California (CA). Two locations in Leary Weber Ditch and DR2 Drain, and one location in Maple Creek and Merced River were monitored. At the NE, WA and CA sites, piezometers installed in the streambed were constructed using 5-cm inner diameter PVC pipe with 15-cm long screen. At IN site, piezometers were constructed from 3-cm inner diameter PVC. At IN and WA sites, piezometers were extended above the highest stream water level, and were open to the atmosphere. At NE site, piezometers were vented to the atmosphere by plastic tubing that ran under the stream and came out on the stream bank (above flood stage). Because of the size of Merced River, such installations were not feasible and the piezometers were extended 15 cm above the river bed and sealed with waterproof caps. Piezometers were installed using the

hydro jetting method, which uses high pressure water to flush sediment. Two piezometer nests were installed at IN site, and one piezometer nest was installed at other sites. The temperature of water in the streams and the piezometers was monitored at a 15-min (IN, NE, and CA sites) and a 60-min (WA site) recording interval at multiple depths below the streambed by suspending StowAway TidbiT Temperature Loggers (Onset Computer Corp., Pocasset, MA; range: −4 to 30°C; accuracy: ±0.2°C at 20°C) within the piezometer clusters. Water levels in the stream and in each piezometer were monitored continuously using Solinst Levelogger (range: 4 m; resolution: 0.1 cm; accuracy: 4 mm) and Solinst Barologger (Model M5) for atmospheric-pressure-change compensation at the same recording interval as for temperature. One-dimensional (vertical) models of water and heat flow with 0.02 m thick grid-blocks were developed to simulate temperature and groundwater head, and to estimate groundwater and surface water fluxes through the streambed. Flux was found to be influenced by the physical heterogeneity of stream channel and temporal variability in stream and groundwater levels. More related research can be found in Clow et al. (2003), Hood et al. (2006), and Hannah et al. (2007).

For better results, tracer sampling at many locations is needed. Tracer methods are applicable to small scale study areas (Kalbus et al., 2006). Similar to piezometers and seepage meters, they cannot quantify future groundwater discharge because they can only quantify groundwater discharge during the observed time period.

2.2.2 Hydrograph separation

A hydrograph is a graphical representation of observed stream flow over time at a specific point in a stream/river. Different types of hydrograph separation methods are used in quantifying base flow (groundwater discharge) from stream flow. These include (1) simple graphical approach, (2) filtering method, (3) stream flow partitioning method, (4) recursive filtering method, (5) unit hydrograph method, (6) rating curve method, and (7) environmental tracer method. The main problem of hydrograph separation methods is that they can only separate base flow from observed stream flow, and cannot predict future base flow.

2.2.2.1 Simple graphical approach

There are various graphical approaches available to separate base flow from stream flow hydrograph. Among them, three methods are very common. These are constant-discharge method, constant-slope method, and concave method. These methods were used in Linsley et al. (1958), Hewlett et al. (1967), Anderson et al. (1980), McNamara et al., (1997), Sujono et al. (2004), Blume et al. (2007), and Gonzales et al. (2009). In the constant-discharge method, base flow is assumed as constant regardless of stream flow (discharge) (Karamouz et al, 2012). Base flow is separated from discharge by a straight line beginning at the point of the lowest discharge prior to the start of the rising limb (due to storm) of the hydrograph and extending at a constant discharge until it intersects the recession limb (due to end of storm) of the hydrograph. In Fig. 2.2, q_s indicates the lowest discharge prior to the start of the rising limb of the hydrograph, and the straight line indicates the base flow separation line. The flow

under this line is called base flow, and the flow above the line is called direct runoff or surface runoff. This method is the simplest and easiest method to separate base flow from discharge, but there are some weaknesses in this method. Generally base flow decreases beyond the start of the rising limb, and continues to decrease until the maximum discharge of the hydrograph, which is not seen in this method. In addition, flow from groundwater aquifer starts prior to the start of the rising limb, which is also not considered in this method.

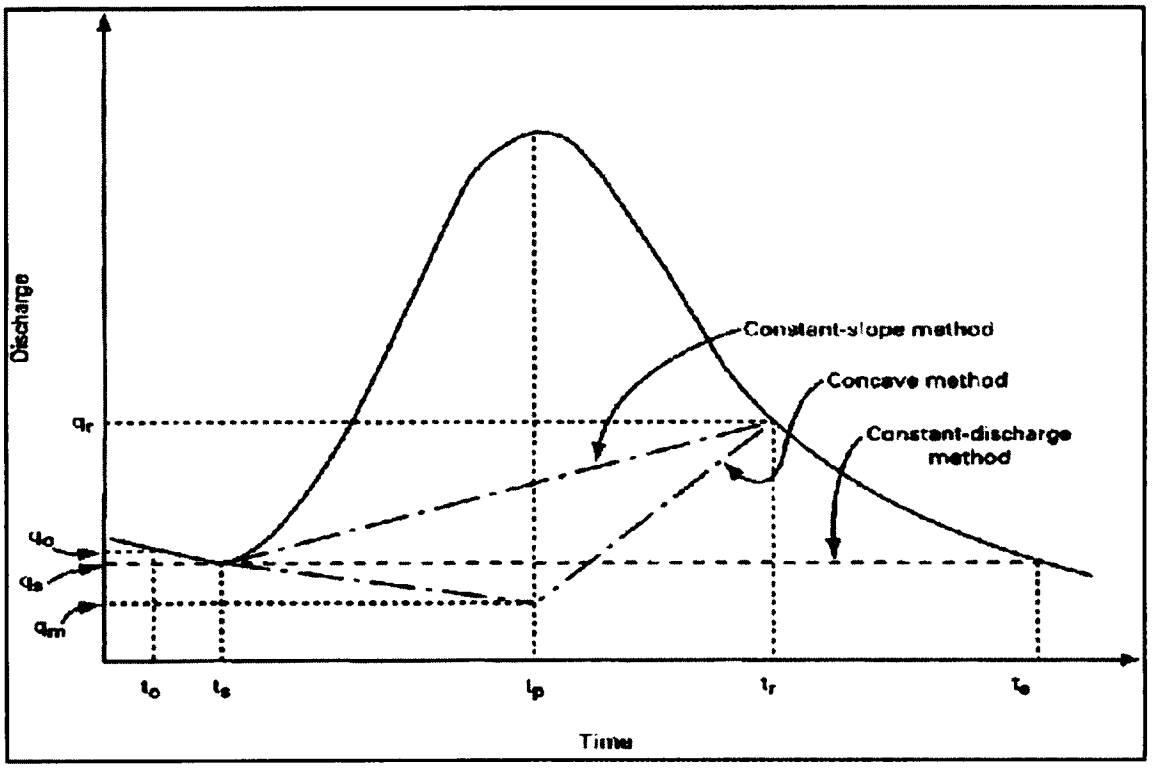

Figure 2.2 Base flow separation methods (taken from McCuen, 2004).

In the constant-slope method, a point (inflection point) is selected on the recession limb of the hydrograph where direct runoff ends because in this method it assumes that flow from groundwater aquifer begins prior to the start of the rising limb (Karamouz et al., 2012).

Different methods are used for identifying this inflection point. The most common method used is by using an empirical equation (Pettyjohn et al., 1979).

$$N = A^{0.2} \tag{2.2}$$

Where N is the number of days from the peak of the hydrograph to the point where the direct runoff ends, and A is the area of the catchment in mi^2. After identification of this inflection point, base flow and direct runoff are separated from stream flow by connecting this point and the point of the lowest discharge prior to the start of the rising limb of hydrograph using a straight line. In Fig. 2.2, t_p and t_r indicate the time when the peak of the hydrograph occurs and direct runoff ends, respectively, q_s indicates the lowest discharge prior to the start of the rising limb of the hydrograph, and q_r indicates the discharge when the direct runoff ends on the recession limb. The straight line connecting q_s and q_r indicates the base flow separation line.

In the concave method, base flow is assumed to decrease while stream flow increases. At first, base flow decreases with a constant slope from the start of the hydrograph until the time of the peak discharge of hydrograph. Then the peak discharge point and the inflection point on the recession limb are connected by a straight line. The inflection point is estimated using the same approach used in the constant-slope method. In Fig. 2.2, q_0 indicates the discharge at the start of the hydrograph, q_r indicates the discharge when the direct runoff ends, and t_p, t_0, and t_r indicate the time when the peak of the hydrograph occurs, the hydrograph starts, and direct runoff ends, respectively. The line starting from t_0 to t_r indicates the base flow separation line, and the flow under this line is called base flow. This is the most realistic method compared to other two methods, but it requires more computational efforts than the other two methods. In cases where drainage from bank storage, lakes or wetlands, soils or

snow packs contributes to stream discharge, the assumption that base flow represents groundwater discharge may not hold (Halford et al., 2000). The limited number of stream gauging stations constrains the resolution of this method, and the results are usually averaged over long stream reaches.

2.2.2.2 Filtering methods

Pettyjohn et al. (1979) developed three base flow separation methods to process long records of groundwater discharge data: (i) fixed-interval (also known as Hysep 1), (ii) sliding-interval (Hysep 2), and (iii) local-minimum (Hysep 3) methods, which are also called filtering separation methods. The advantage of these methods is that they are standardized (objective) and systematic. As a result, they can be easily translated into computer code to reduce computation time and to avoid inconsistencies resulting from manual methods (Sloto et al., 1996). Pettyjohn et al. (1979) and Sloto et al. (1996) used the analysis interval size (i.e., $2N^*$days) in these filtering methods as the odd integer between 3 and 11 nearest to 2N. An empirical equation (Eq. 2.2) is used for estimating this N. In the fixed-interval method, the lowest discharge within each analysis interval ($2N^*$ days) of the hydrograph is assigned as base flow to all days in that interval starting with the first day of stream flow record (Pettyjohn et al., 1979). This method can be visualized by moving a bar of $2N^*$days width upward until the bar first intersects the hydrograph (Fig. 2.3a). The discharge at that point is assigned as base flow to all days in the analysis interval. Then the bar is moved by $2N^*$days horizontally, and the same procedure is repeated for each analysis interval. Pettyjohn et al. (1979) used 5 days as the analysis interval size to separate base flow at French Creek,

Pennsylvania. In Fig. 2.3a, for example, in the analysis interval from April 5 to April 9, the lowest discharge (49 ft^3/s) was assigned as base flow to every day in that interval. Similarly, the other minimum values of discharge were assigned for other intervals, and then connected to define base flow hydrograph. Therefore, in this method, the stream flow hydrograph is partitioned into non-intersecting intervals. On the other hand, in the sliding-interval method, the analysis interval is continuously moved over the hydrograph. In this method, the lowest discharge in one half of the analysis interval minus 1 day [i.e., $0.5(2N^*-1)$ days] of the hydrograph before and after the day is considered and assigned on that day (Pettyjohn et al., 1979). This method can be visualized by moving a bar of $2N^*$ days width upward until the bar first intersects the hydrograph (Fig. 2.3b). The discharge at the point is assigned as base flow to the median day in the analysis interval. Then the bar is moved over to the next day, and the same procedure is repeated. In Fig. 2.3b, for example, in the analysis interval from April 16 to April 20, the lowest discharge (42 ft^3/s) was assigned as base flow to April 18, which is the median day in the interval. In the local-minimum method, the discharge on each day is checked to determine if it is the lowest discharge in one half of the analysis interval minus 1 day [i.e., $0.5(2N^*-1)$ days] of the hydrograph before and after the day being considered (Pettyjohn et al., 1979). If it is, then that discharge in that day is a local minimum, and is connected to the adjacent local minimums by straight lines (Fig. 2.3c). The base flow values for each day between two local minimums are approximated using linear interpolation. This method can be visualized by connecting the lowest points on the hydrograph by straight lines. In Fig. 2.3c, the local minimums were found on April 9, 15, 21 and 24.

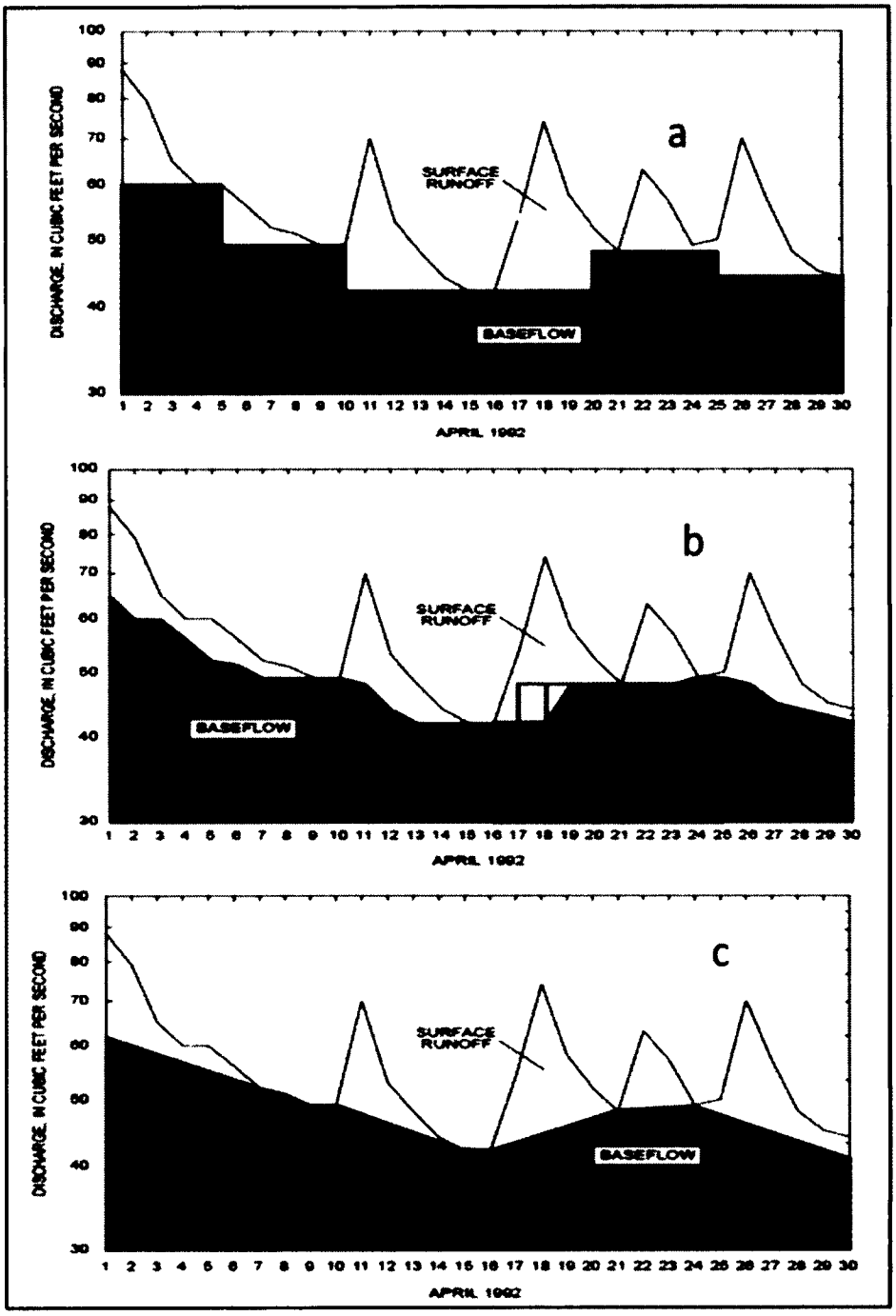

Figure 2.3 Filtering separation using (a) fixed-interval, (b) sliding-interval and (c) local-minimum methods at French Creek, PA (taken from Pettyjohn et al., 1979).

These base flow separation methods were used in Eckhardt (2008) and Gonzales et al. (2009). Zhang et al. (2006b) used HYSEP hydrograph separation method and regression analysis to assess the effects of land use changes on stream flow and base flow in the Mississippi River, USA, from 1940 to 2000. Land use maps between 1940 and 2000 were collected from the government agencies. Base flow was separated from stream flow using HYSEP hydrograph separation method (Sloto et al., 1996). Then the relationship between base flow and soybean fractional area, which is the major land use change between 1940 and 2000, was established using regression analysis. The results indicate a positive correlation between these two parameters. It is also found that the conversion of perennial vegetation to seasonal growing crops, especially soybeans, in the basin since 1940's might have reduced evapotranspiration, increased groundwater recharge, and therefore, increased base flow and stream flow.

2.2.2.3 Stream flow partitioning method

Rutledge (1998) developed a stream flow partitioning method called PART (A computerized method of base-flow-record estimation) program, a USGS base flow separation method, to separate base flow component from daily records of stream flow. This program works by 1) searching the period of stream flow records for days that fit a requirement of antecedent stream flow recession, which is that the decline of daily stream flow is less than 0.1 log cycle, 2) designating base flow to be equal to stream flow on these days, and 3) interpolating linearly the base flow on other days in the stream flow record that do not fit the

requirement of antecedent stream flow recession. This method was used to separate base flow from stream flow in Neff et al. (2005), Eckhardt (2008) and Saha et al. (2013).

2.2.2.4 Recursive filtering method

Eckhardt (2005) developed a low pass filtering technique to separate base flow from stream flow hydrograph. This recursive filter requires the determination of two parameters: (i) the recession constant a, which can be derived from statistical analysis of the recession curve of hydrograph, and (ii) the maximum value of base flow index (BFI_{max}), which cannot be measured, but obtained from the suggested values given in Eckhardt (2005). The base flow is calculated using the following equation:

$$b_k = \frac{(1-BFI_{max})ab_{k-1}+(1-a)BFI_{max}y_k}{1-aBFI_{max}} \qquad (2.3)$$

Where y_k (m^3/s) and b_k (m^3/s) are stream flow and base flow, respectively, at time k (subject to $b_k \leq y_k$), BFI_{max} is the maximum value of base flow index, and a is the recession constant. This method was also used in Eckhardt (2008) and Gonzales et al. (2009).

2.2.2.5 Unit Hydrograph method

This method is based on the principle that an impulse of recharged water into the subsurface system produces a similar response as that to surface runoff by an impulse of effective precipitation. Since the unit hydrograph is a linear hydrologic system model, its solution procedure follows the principles of proportionality and superposition (Su, 1995). Su

(1995) proposed the Nash's cascade reservoir model to represent the base flow unit hydrograph mathematically, where the groundwater watershed is presented by a series of identical linear reservoirs, and each of them having the same storage constant. Base flow is then calculated using the following equation:

$$Q_{(t)} = R\frac{1}{k\Gamma(\varepsilon)}\left[\frac{t}{k}\right]^{\varepsilon-1} e^{-t/k} \qquad (2.4)$$

After simplification, $$Q_{(t)} = At^{\theta}e^{\phi-t} \qquad (2.5)$$

Where $Q_{(t)}$ is base flow (m^3/s), A (m^3/s), Θ (dimensionless), and ϕ (1/s) are model parameters, which can be determined by fitting the model using information from the recession limbs of the hydrograph. This method was used in Gonzales et al. (2009).

2.2.2.6 Rating curve method

This method is based on the assumption that there is a relationship between groundwater levels and discharge in the stream during recession periods. Kliner et al. (1974) attempted to determine this relation by fitting an envelope to all the available data from groundwater levels against discharge measurements. Sellinger (1996) proposed to fit a curve only to the data corresponding to the recession limbs. Theoretically, both approaches should give similar results. The rating curve was developed using the following equation:

$$Q = Ae^{Bh} + Q_0 \qquad (2.6)$$

Where Q is the discharge (m^3/s) at the outlet of the catchment, Q_0 is the constant discharge (m^3/s) coming from the deeper aquifer, h (m) is the groundwater level in an observation well or an average groundwater level over the catchment, and A (m^3/s) and B (1/m) are fitting parameters, which can be determined by the least squares method using observed discharge (Q) and groundwater level data (h). This method was used in Blume et al. (2007), and Gonzales et al. (2009).

2.2.2.7 Using environmental tracers

Hydrograph separation using environmental tracers, such as isotopic and geochemical tracers, provides information on the temporal and spatial origin of stream flow components (Kalbus et al. 2006). Stable isotopic tracers, such as stable oxygen and hydrogen isotopes, are used to distinguish rainfall event flow from pre-event flow because rain water often has a different isotope composition than water already in the catchment (Kendall et al., 1998). Geochemical tracers, such as major chemical parameters (e.g., sodium, nitrate, silica, conductivity) and trace elements (e.g., strontium), are often used to determine the fractions of water flowing along different subsurface flow paths (Cook et al., 2000). In order to separate the stream flow components using environmental tracers, mixing models (Pinder et al., 1969), and diagrams (Christophersen et al., 1992) based on mass conservation are used. The main assumption is that the chemical composition of all investigated components is constant and significantly different, and the mixing is conservative. The stream flow separation is calculated by solving the following linear mixing equation:

$$C_T Q_T = C_P Q_P + C_E Q_E \quad (2.7)$$

After rearranging Eq. (2.7) and using $Q_T = Q_P + Q_E$,

$$\frac{Q_P}{Q_T} = \frac{C_T - C_E}{C_P - C_E} \quad (2.8)$$

Where C_T is the tracer concentration in the stream water, C_P is the tracer concentration in the pre-event water (groundwater), C_E is the tracer concentration in the event water (surface runoff/quickflow), Q_T is the stream flow measured at the outlet of the study area, Q_P is the pre-event water discharge, and Q_E is the event water discharge. Moratatti et al. (1997) used isotropic tracer analysis to separate base flow from stream flow hydrograph. Water samples from the main channel of upper Solimões River and lower Amazon River were collected for analyzing stable oxygen (^{18}O). Stream flow data were collected from neighboring gauges. Then mass balance based equation (Eq.2.8) was used to calculate base flow. Similarly, Gonzales et al. (2009) collected water samples at different stages of the water cycle: rainfall (one sample per event), ponded water, groundwater at the five observation wells at an experimental field (once per week), and the stream flow at the outlet of the catchment (time intervals: 4 h during the rising limb and shortly after the runoff peak, and 8 h during recession periods). Water samples were analyzed in the laboratory for stable oxygen (^{18}O) using a mass spectrometer. Then base flow was separated from stream flow using those tracer results and the mass balance based equation (Eq.2.8). More related research can be found in Soulsby et al. (2006), Stewart et al. (2007) and Koeniger et al. (2009).

In order to use hydrograph separation methods described in section 2.2.2.1 to 2.2.2.6, the temporal record of observed stream flow data is needed. These methods can be used for a large area if the stream flow data at the outlet is available. The main problem in these

methods is that they can only separate base flow from observed stream flow, and cannot predict future base flow. On the other hand, in order to use environmental tracer method, stream flow data and observed tracer concentrations of pre-event water (groundwater), stream and event water (surface runoff) are needed. This method's main drawbacks are that event and pre-event waters are often too similar in their isotope composition and the composition is often not constant in space or time (Genereux et al., 1998). Therefore, this method is suitable for a small area in the order of 10 km^2. Moreover, this method cannot predict future groundwater component of stream flow in a watershed; it can only separate groundwater component from observed stream flow using measured tracer concentrations data with some limitations. Even this method is not suitable to use in past stream flow time series data if no tracer data of stream, pre-event and event water in the past are available.

2.2.3 Review of numerical solutions

Different types of numerical models have been used to assess GW-SW interaction at various scales of watersheds. For example, Refsgaard (1997) used the MIKE SHE model for simulations of stream discharge and groundwater head (i.e., level) in the Karup catchment (440 km^2), Denmark, with a maximum grid size of 1000 m being used. The model was calibrated and validated to observed stream flow at the catchment outlet, and observed groundwater head at different wells in the study area. Stoll et al. (2011) also used the MIKE SHE model in a small catchment in northern Switzerland to assess the impacts of climate change on groundwater related hydrological fluxes. They used eight different types of climate models, which considered SRES (Special Report on Emissions Scenarios) A1B

greenhouse gas (GHG) emission scenario of the Intergovernmental Panel on Climate Change (IPCC). With an area of approximately 9 km^2, the model domain was discretized into grid cells of 100 m by 100 m. The model was calibrated with observed groundwater levels at 10 wells in the study area for a 4-year time period (1999-2002). They presented their results of how the mean annual groundwater level would change with climate up to year 2100 at the selected wells in the study area. Vansteenkiste et al. (2012) did a comparison of two spatially distributed models, MIKE SHE and WetSpa (Water and Energy Transfer between Soil, Plants and Atmosphere under quasi Steady State) (developed by Liu et al., 2003), to investigate the climate change impact on the flow regime in Grote Nete catchment (385 km^2), Belgium. The WetSpa model grid resolution was 100 m by 100 m, whereas the MIKE SHE model grid resolution was 250 m by 250 m. Both models were calibrated and validated using observed discharge at the outlet of the catchment. It was found that the MIKE SHE model required more parameters to adjust than the WetSpa model during calibration period. They reported their results of how different future climate change scenarios (i.e., high (a future with wet winters), mean (a future with intermediate between wet and dry winters), and low (a future with dry winters and summers) scenarios, which were based on the A2, A1B, B1 and B2 GHG scenarios) would affect stream discharge in the study area, while both models predicted almost similar variation pattern. They also reported how the mean monthly groundwater levels at selected wells would change under different future climate change scenarios using the MIKE SHE model between years 2071-2100 and the current climate (1961-1991).

In addition to MIKE SHE, many other models were also used. Klocking et al. (2002) used the ArcEGMO (Eco-Hydrological Watershed Model) model for assessing the impacts of land use change on the overall water availability and seasonal distribution of water for two meso-scale river basins (Saale River - 24000 km^2, and Havel River - 19100 km^2) in Germany. The model grid resolution was 1 km by 1 km. The model was calibrated for two basins with observed stream discharge at the basin outlet. The results illustrated how the mean annual basin discharge (i.e., stream flow), groundwater recharge and evapotranspiration changed in both basins from 1981-1994 under different land use change scenarios.

Wilcox (2003) used a 3-D telescopic (smaller-scale) model to investigate GW-SW interaction along a 10-km reach of the river between Brown Arroyo and San Antonio, with a study area width of approximately 5 km. The horizontal model grid cell was 31 m by 31 m, and the vertical discretization was 12 m to 31 m. The model grid was generated by using Microsoft Excel and ESRI ArcView software, and the model was calibrated and validated with observed groundwater levels. The modeling results illustrated how groundwater levels changed during sensitivity analysis.

Zhang et al. (2006a) developed a rainfall-runoff model using the revised REWASH (Representative Elementary Watershed approach) code. The model was evaluated by a multi-criteria approach using both discharge and groundwater table measured at various locations. The study was conducted in the Hesperange catchment (292 km^2), Luxembourg, while a 50 m by 50 m digital elevation model was used for watershed delineation. The model was calibrated using observed stream flow at the outlet of the catchment. The modeling results

illustrated how groundwater levels changed during rainfall events. More related research can be found in Hughes (2004), and Bidwell et al. (2008).

Van Roosmalen et al. (2007) used the DK model (The National Water Resource model for Denmark) based on the MIKE SHE code to study climate change impacts on groundwater system for two study areas of 5459 km^2 and 7226 km^2 in Denmark. The model grid cell was 1 km by 1 km. The model was calibrated and validated with observed stream discharge and groundwater levels (head) at different wells. The modeling results showed how the mean annual groundwater head would change under two IPCC GHG emission scenarios (A2 and B2) in 2071-2100, while the mean monthly stream flow, base flow and overland flow under these scenarios were also examined. Van Roosmalen et al. (2009) also used the DK model to study climate and land use changes impacts on groundwater system. They developed a 3-D model for an agricultural area of 5459 km^2 with a modeling grid size of 500 m by 500 m. The model was calibrated and validated with observed stream discharge and groundwater levels at different wells. They presented their results of how the mean annual water balance would change under A2 and B2 GHG emission scenarios in 2071-2100 when comparing to current climate (1990-2004). They also reported how the mean monthly recharge and stream flow would change under those scenarios during the same time period. In terms of combined land use and climate changes impacts, they highlighted how the mean monthly and annual evapotranspiration and recharge would change.

Rihani et al. (2007) used a 3-D variably saturated subsurface flow code called Parflow (developed by Ashby et al., 1996) and a 2-D overland flow simulator (developed by Kollet et al., 2006) for assessing GW-SW interaction in the Dominguez Channel Watershed (555 km^2)

in Los Angeles County, USA. The model domain was 17.7 km by 23.9 km by 2 m, with a grid cell of 310.9 m by 310.9 m by 0.1 m. The model was calibrated using observed stream flow hydrograph from a storm event. The modeling results illustrated how stream flow changed during sensitivity analysis.

Gauthier et al. (2009) developed a numerical model using CATHY (CATchment Hydrology) that integrates 1-D land surface and 3-D subsurface flow processes for the Thomas Brook catchment (8 km^2) in Nova Scotia, Canada. The model grid cell was 60 m by 60 m by variable thickness ranging from 10 m to 200 m (top to bottom). The model was calibrated with observed stream flow at the outlet of the catchment. The modeling results reported how groundwater levels changed with time during observed rainfall events, and how yearly recharge values changed under different heterogeneity conditions.

Yimam (2010) coupled a USGS Precipitation-Runoff Modeling System (PRMS) with a USGS MODFLOW-2005 to simulate GW-SW interaction in the Grote-Nete catchment (405 km^2), Belgium. The model domain was divided into 59 HRUs (Hydrologic Response Unit) based on their hydrologic and physical characteristics. The model was calibrated and validated with observed discharge at the outlet of the catchment. The modeling results showed how the components (subsurface flow and surface runoff) of stream flow changed with time.

Jackson et al. (2011) used the ZOODRM model (developed by Mansour et al., 2004) and the ZOOMQ3D finite difference code (developed by Jackson et al., 2004) in the Chalk aquifer system (2600 km^2), England to assess the impacts of climate change on groundwater system. They used 13 different types of climate models, which considered SRES A2 GHG emission scenario of IPCC. The ZOODRM model was used to calculate recharge in the study

area, and this recharge was then used in the ZOOMQ3D code for groundwater modeling. The ZOOMQ3D model was calibrated and validated with observed groundwater levels at different wells in the study area, and the modeling results reported how the mean annual groundwater level, stream discharge and base flow would change in the study area between year 2080 and current climate (1961-1990). They also presented how the mean monthly groundwater recharge and discharge, and groundwater levels at selected wells would change under future climate change scenarios obtained from thirteen climate models.

Goderniaux (2010) examined the climate change impacts on groundwater reserve in Geer Basin catchment (480 km^2) in Belgium using a 3-D finite element model called HydroGeoSphere. The elements have lateral dimensions equal to approximately 500 m. In total, there were 9420 and 785 nodes for subsurface and surface domains, respectively. The model was calibrated with observed groundwater levels and stream flow data. The modeling results showed how the mean annual groundwater level, stream discharge, and evapotranspiration in the study area would change under A2 GHG emission scenario in three different time periods (2011-2040, 2041-2070 and 2071-2100) with respect to present climate (1961-1990). Starzyk (2012) also used the HydroGeoSphere, a fully integrated and physics-based, numerical model capable of simulating surface-subsurface flow in a 3-D framework in Bertrand Creek Watershed (46 km^2), British Columbia. The 2-D surface mesh was created using the Grid Builder (developed by McLaren, 2009) and composed of 9,827 triangular elements (5,062 nodes) draped over the surface topography. Nodal spacing of the finite-element mesh varied from 20 m along the creek to 300 m at nodes farther from the creek. The 3-D subsurface contained 196,540 prisms and had an equivalent nodal geometry to the 2-D surface mesh (i.e., subsurface nodes coincided with

nodes on the surface mesh). The model was calibrated with observed groundwater levels and stream flow data, and the modeling results were reported as how the groundwater head in the study area and GW-SW exchange flux in four reaches changed with time.

Ma et al. (2002) used the MODFLOW to simulate the transient GW-SW interaction using the HEC-2 based water surface profiles of San Joaquin River, California. The HEC-2 modeling outputs of the 150-mile stretch of San Joaquin River were used as the inputs for the MODFLOW. Over 300 wells were drilled in the upper 100 feet of the San Joaquin Valley aquifer, and were installed in-stream and on the banks of the river. Groundwater elevation data were collected from the databases of monitoring wells of the California Department of Water Resources, the city of Fresno, the US Bureau of Reclamation and several irrigation districts. The MODFLOW model in the study area was developed using these groundwater table elevations, river conditions, soil textures, and evapotranspiration data. The model grid spacing along the river averaged about 300 feet, while the grid spacing perpendicular to the river length was 50 feet. The layer thickness was 2 feet to 60 feet from the top of the layer. The developed model was calibrated to fit observed groundwater table elevation data, and the modeling results were presented as how groundwater levels would be affected by changing future river stage conditions. Kasahara et al. (2003) simulated the hyporheic exchange flow in mountainous streams using MODFLOW and MODPATH models. A stream channel length of 1750 m with approximately 50-m width of land boundary was surveyed. A 3-D MODFLOW model was developed using groundwater level data, which were collected from over one hundred wells. The model grid cell size was 0.5 m by 0.5 m by 0.3 m, and the model was calibrated using observed groundwater table elevation data. The MODPATH model was then used to estimate hyporheic exchange flow at each well network site. The

modeling results were reported as the hyporheic exchange flow and its relative proportion with respect to observed stream discharge. They also generated water table contour maps and estimated the aerial extent of hyporheic zone. Hester et al. (2008) used HEC-RAS, MODFLOW and MODPATH models to simulate the coupled surface and subsurface hydraulics in a gaining stream reach with a 3 m width and 30 m length. The grid cell of the coupled model was 3 m by 3 m by 0.25 m, and the model was calibrated and validated using observed water levels at a weir and three in-stream piezometers. They reported how hyporheic exchange changed with different types of in-stream geomorphic structures (i.e., weirs, steps, lateral structures).

Allen et al. (2004) examined climate change impacts on groundwater system in Grand Forks aquifer (34 km^2), British Columbia using the visual MODFLOW, with modeling domain being associated with variable horizontal spatial resolution (50 m to 100 m). The Hydrologic Evaluation of Landfill Performance (HELP) hydrologic model was used to simulate recharge, and this recharge was then used in the visual MODFLOW model. The MODFLOW model was calibrated with observed groundwater levels at different wells in the study area, and they reported how the groundwater head changed under different recharge conditions. Scibek et al. (2006a, b) conducted a case study of an unconfined aquifer in the Grand Forks valley in south-central British Columbia to develop a methodology for linking climate model, hydrologic model and groundwater model to investigate future impacts of climate change on groundwater resources. The aquifer is 34 km^2, located in a semi-arid area, and comprised of heterogeneous glaciofluvial/glaciolacustrine sediments in a mountainous valley. The HELP hydrologic model was used to simulate recharge, and this recharge was used in the visual MODFLOW and the 3-D MODFLOW models to simulate groundwater

flow. They presented their results of how the mean annual recharge and groundwater head in the study area would change under different climate scenarios (2010-2039, 2040-2069). Schilling et al. (2006) also used the MODFLOW to study GW-SW interaction in Walnut Creek, Iowa, with a channel of approximately 300 m length and 10 m width. The modeling domain, covering 157 m from the groundwater divide to one edge of Walnut Creek, was discretized into an irregular grid varying from a minimum cell width of 0.2 m next to the creek to a maximum of 7.0 m at the divide. The model was calibrated using observed groundwater levels at six wells, and the results were presented as how much stream water penetrated into the flood plain during high hydraulic gradient.

Batelaan et al. (2003) used MODFLOW and WetSpa models to delineate groundwater flow system under future land use change conditions in a major part (292 km^2) of the Grote-Nete basin, Belgium. Both models were calibrated with observed groundwater levels at different wells in the study area. Woldeamlak et al. (2007) also used the MODFLOW model to investigate the effects of climate change on the groundwater system in the most parts (525 km^2) of the Grote-Nete basin, Belgium. With a spatial resolution of 50 m by 50 m, the model used only one layer of 90 m thickness. The model was calibrated and validated using observed groundwater levels at 38 wells. The outputs from climate model (i.e., precipitation and temperature) and the WetSpa model (i.e., recharge) were used as inputs for the MODFLOW model. They reported how the mean annual groundwater head and discharge would change under different climate scenarios (wet and dry scenarios for 2100).

Dams et al. (2008) developed a methodology to couple land use change model (CLUE-S: Conversion of Land Use and its Effects at Small regional extent) with a water balance model (WetSpa) and a groundwater model (MODFLOW) to assess the impacts of land use changes

on groundwater quantity in the Kleine Nete basin (581 km^2), Belgium. Yearly land use maps from 2000 to 2020 were generated using the CLUE-S model considering future European land-use demands and Special Report on Emission Scenarios (SRES) (A1, A2, B1 and B2) of IPCC. These land use maps were used in the WetSpa model to calculate yearly groundwater recharge, and the calculated recharge was then used in the steady-state MOFLOW model to determine the groundwater level and flux under different future land use and climatic conditions. The model grid resolution was 50 m by 50 m, and the MODFLOW model was calibrated with observed groundwater levels at different wells. Dams et al. (2012) also used coupled WetSpa with MODFLOW model to study the impacts of climate change on the groundwater system in the Kleine Nete basin (581 km^2), Belgium, with a grid cell size of 50 m by 50 m. The WetSpa model was used to simulate river discharge and groundwater recharge, while the MODFLOW model was used to simulate the effects of climate change on groundwater level and flux. The WetSpa model was calibrated to observed river discharge at the basin outlet and the filtered base flow, while the MODFLOW model was calibrated to the filtered base flow and observed groundwater heads at different wells. The filtered base flow was calculated from observed stream flow records using an automated base flow filtering method (developed by Arnold et al., 1999). The modeling results were presented as mean monthly variation of groundwater recharge and discharge in the study area under reference climate (1960-1991), 28 climate scenarios (A2 and B2 GHG emission scenarios from 14 climate models) of 2070-2101, and the mean of those scenarios.

Lin et al. (2007) used the CLUE-S land use change model and the generalized watershed loading functions model (developed by Haith et al., 1987) to assess various land use change impacts on stream flow, surface runoff, and groundwater discharge in the Wu-Tu watershed

(204 km^2), Taiwan. With a modeling grid resolution of 50 m by 50 m, the lumped generalized watershed loading functions model was calibrated using observed stream flow data. Wijesekara et al. (2012) used coupling of land-use cellular automata (CA) model and the MIKE-SHE/MIKE-11 hydrological model to assess the impact of future land use changes on stream flow, surface runoff, and base flow in the Elbow River watershed, Canada. The CA model was calibrated using four land-use maps covering the period 1985–2001 and validated against the maps of 2006 and 2010. Based on the historical land use changes, the future land-use changes were then performed from 2006 to 2031 at a five year interval. The MIKE-SHE model was calibrated and validated to observed river discharge at the outlet of the watershed. Zhou et al. (2013) used coupling of CLUE-S and the SWAT (Soil and Water Assessment Tool) model to understand and quantify the hydrological responses (i.e., stream flow, surface runoff, and base flow) due to land use/land cover changes in the Yangtze River delta region, China, from 1985 to 2008. The SWAT model was calibrated and validated to observed river discharge at the outlet of the region. They reported that the increase of urban areas resulted in an increase of stream flow and surface runoff, and a decrease of base flow. More related research can be found in Chang (2007), Ghaffari et al. (2010), and Schilling et al. (2010).

Krause et al. (2004) used the IWAN (Integrated Water Balance and Nutrient Dynamics) model to assess the impacts of land use changes on GW-SW interaction in a 200 km^2 sub catchment of Havel River, Germany. This model coupled the WASIM-ETH-I (Water Flow and Balance Simulation Model) with the MODFLOW. The model grid resolution was 25 m by 25 m, and the model was calibrated and validated with observed groundwater levels at different wells in the study area. They reported how the groundwater recharge changed under

different land uses in 2001-2002. Krause et al. (2007) also used the IWAN model to simulate exchange fluxes between the groundwater of the floodplain and the surface water within the direct catchment of Lower (189.1 km^2) and Central (998.1 km^2) Havel River, Germany. The model grid spatial resolution was 50 m by 50 m. The IWAN model was calibrated with the observed groundwater levels at the boreholes in the study catchments. They reported how stream flow changed daily in the last 13 years (1988-2000) in two study catchments. They also presented mean monthly dynamics of simulated exchange fluxes between the groundwater of the floodplain and the surface water.

Downer et al. (2002a) used the GSSHA (Gridded Surface Subsurface Hydrologic Analysis) model to investigate GW-SW interaction in Judicial Ditch 31 watershed (23.3 km^2), Minnesota, USA. The model grid resolution was 90 m by 90 m, and the model was calibrated using observed stream flow data at the outlet of the watershed. The modeling results illustrated the impacts of tile drain removal on surface ponding. Jenkins (2006) also used the GSSHA model to simulate transient GW-SW interaction in the floodplain of the 18-mile stretch of Rio Grande River, New Mexico, USA. The model grid resolution was 35 m by 35 m, and the model was calibrated using observed stream flow data at the outlet of the study area. The modeling results showed the transient river water table during high and low flows in Rio Grande River. Downer et al. (2006) updated GSSHA model by incorporating the volume of groundwater discharge in the modeling output to estimate groundwater contribution to stream flow. Paudel (2010) used GSSHA model to simulate watershed response under different land uses scenarios in Tifton watershed (113 km^2), Georgia. The model was calibrated using observed stream flow data at the outlet of the watershed. The modeling results presented the peak flow as well as total runoff volume under various land

use conditions in Tifton watershed. Similarly, McCarty (2013) also used GSSHA model to simulate stream flow under changes in vegetation, land use and other features in Parley's Canyon, Utah. El Hassan et al. (2013) used GSSHA model to simulate stream flow caused by tropical storm which persisted for several days in a sub-watershed (538 km^2) of San Antonio river basin. The model was calibrated using observed stream flow data at the outlet of the watershed for one rainfall event in 2007, and validated for three rainfall events in 2002, 2004 and 2010. The GSSHA model was also used in hydrologic studies in different types of watersheds (Sharif et al., 2006; Sharif et al., 2010; Swain et al., 2013).

Beven et al. (1992) used the Generalized Likelihood Uncertainty Estimation (GLUE) method as an uncertainty analysis method in the Institute of Hydrology Distributed Model (IHDM) to investigate how the stream flow hydrograph responses under parameter uncertainty during a number of storms in the Gwy catchment (3.9 km^2), Wales. The GLUE is a Bayesian Monte Carlo simulation-based method. 500 realizations of the IHDM were run considering the four most sensitive parameters for 5 storms. They presented their outputs in the form of the cumulative frequency distribution. Similar related research was done by Freer et al. (1996) in a small Ringelbach research catchment, France considering 30 realizations using the TOPMODEL. Shen et al. (2012) used the GLUE method in the SWAT model to investigate the impacts of parameter uncertainty on the stream flow and sediment in the Daning River watershed (4426 km^2) of the Three Gorges Reservoir Region, China. Twenty parameters were chosen for uncertainty analysis based on sensitivity analysis, and 10,000 model runs were performed. They also presented their outputs in the form of the cumulative frequency distribution. Kuczera et al. (1998) used the multinormal approximation to investigate the multiresponse data (i.e., stream flow, stream chloride concentration,

groundwater level) in the CATPRO model due to the uncertainty of 9 parameters in the Wights catchment (94 ha) in the Western Australia. They presented their outputs in the form of response surface.

Vrugt et al. (2003) used the Markov Chain Monte Carlo (MCMC) method in the HYMOD model to conduct uncertainty analysis of stream flow due to 5 parameters' uncertainties in the Leaf River watershed (1944 km^2), Mississippi. They presented their outputs with 95% prediction uncertainty bounds. More related research can be found in Vrugt et al. (2008), and Dotto et al. (2012). Benke et al. (2008) used the Monte Carlo Simulation (MCS) method in 2C hydrological model to conduct uncertainty analysis of the prediction of stream flow under parameter uncertainty in an area of 2000 m^2 in eastern Australia. Five parameters were chosen for uncertainty analysis based on sensitivity analysis. They reported how the output uncertainty changes due to increasing parameter variation. Mishra (2009) used the first-order second–moment (FOSM) and MCS methods in the Natural Systems Regional Simulation Model (NSRSM) to compare the effects of parameter uncertainty on the prediction of stream flow in south Florida. Five parameters were chosen for uncertainty analysis, and 100 Monte Carlo realizations were considered. The final outputs using the MCS method were presented in the form of the cumulative frequency distribution. More related research can be found in Shen et al. (2013).

Based on the above review, numerical models can determine base flow, and predict future base flow trend. In order to calibrate and validate these models, field collected groundwater levels from monitoring piezometers/wells, and stream flow data are needed. As a result, these models depend on the field methods' outputs.

2.3 Summary

Based on the above detailed literature review, numerous studies have been done for investigating GW-SW interaction in different sizes of watersheds in the last several decades. However, few studies (Van Roosmalen et al., 2007; Jackson et al., 2011; Dams et al., 2012; Vansteenkiste et al., 2012) have investigated how the mean monthly groundwater recharge and discharge, stream flow, as well as groundwater level would change between current and projected future climates in the watershed. There is little knowledge regarding how the mean monthly groundwater contribution to stream flow will change under different climate change scenarios. In addition to climate change, a number of studies (Klocking et al., 2002; Batelaan et al., 2003; Krause et al., 2004; Lin et al., 2007; Dams et al., 2008; Van Roosmalen et al., 2009; Wijesekara et al., 2012; Zhou et al., 2013) have investigated the combined effects of climate and land use changes on watershed hydrology. Many of the previous studies reported how the mean annual stream flow, groundwater recharge and discharge, as well as groundwater level would change under different land use change scenarios. However, little attention was paid to investigate how the mean monthly, seasonal and annual groundwater contributions to stream flow will change under both changing land use and climatic conditions. These monthly changes could determine the monthly status of groundwater resources and site conditions for groundwater-dependent terrestrial ecosystems (Naumburg et al., 2005). They will also determine the monthly, seasonal and annual variations of stream flow dependency on groundwater, and these will provide useful information for monthly, seasonal and annual water extractions from the river, and allocation to the stakeholders for future water supply. Using the GSSHA numerical model, this study investigated monthly,

seasonal, and annual groundwater contributions to stream flow under different GHG emission scenarios (i.e., A2 and B1) of IPCC, as well as combined climate and land use changes. Furthermore, a number of studies have investigated how stream flow in a watershed responds due to parameter uncertainty using various uncertainty analysis methods in different hydrologic models (Beven et al., 1992; Kuczera et al., 1998; Vrugt et al., 2003; Benke et al., 2008; Mishra, 2009; Dotto et al., 2012; Shen et al., 2012; Shen et al., 2013). However, few studies have reported regarding the uncertainty analysis of the mean monthly, seasonal and annual groundwater contributions to stream flow in a watershed. In this study, uncertainty analysis of the mean monthly, seasonal and annual groundwater contributions to stream flow was performed under different GHG emission scenarios using 50 Monte Carlo realizations of the most sensitive modeling parameters through the GSSHA model.

CHAPTER 3

METHODOLOGY

3. 1 Overview of study area

Situated in the Peace country region, the Kiskatinaw River Watershed (KRW) is a critical area for northern British Columbia (BC)'s social, environmental, and economic development. The City of Dawson Creek has been drawing water from Kiskatinaw River for drinking purpose since the mid-1940s because the groundwater in this region contains high total hardness (Dobson Engineering Ltd. et al., 2003). The KRW is a rain dominated hydrologic system with peak flows occurring from late June to early July, but in January the flow drops to 0.052 m^3/s, which is less than 0.5% of the average annual flow rate (10 m^3/s). There is no available information about groundwater contribution to river flow in the KRW. On average, the watershed receives an annual precipitation of 499 mm, consisting of 320 mm of rainfall, and 179 mm of snow (Dobson Engineering Ltd. et al., 2003). During the last 40 years, the City of Dawson Creek has experienced steady water demand growth with an average annual growth rate of about 3.2%. In addition to providing a community water supply, the KRW has many other values, such as timber harvesting, agriculture, oil and gas, wildlife, recreation, and potential mineral resources development (Dobson Engineering Ltd. et al., 2003). In particular, a large and increasing scale of timber harvesting, oil and gas exploration/production, and agricultural activities in recent years have caused growing concerns to various water users.

The KRW, as shown in Fig. 3.1, has been divided into 5 sub-watersheds, including (a) Mainstem (433 km^2), (b) East Kiskatinaw (996 km^2), (c) West Kiskatinaw (1005 km^2), (d) Halfmoon-Oetata (194 km^2), and (e) Brassey (208 km^2) (Dobson Engineering Ltd., 2007). It has an elevation ranging from 687 m to 1354 m (Fig. 3.2). In this research, a study area along the river of the Mainstem sub-watershed was used as a case study because the yearly time-series stream flow data, as required by the GSSHA model calibration and validation, were not available at the other 4 sub-watersheds. In addition, the drinking water intake of the water supply system for Dawson Creek is situated at Arras in the study area of the Mainstem sub-watershed. The study area (213.82 km^2) has an elevation ranging from 687 m to 950 m (Fig. 3.3), and an average slope of 7.8% (Fig. 3.4). The average slope provides information about the topography of the study area which influences surface runoff. According to Canadian topographic classification, this study area is moderately sloping (Canada Department of Agriculture, 1974). This slope was calculated by ArcGIS using the elevation values of the study area (Fig. 3.3).

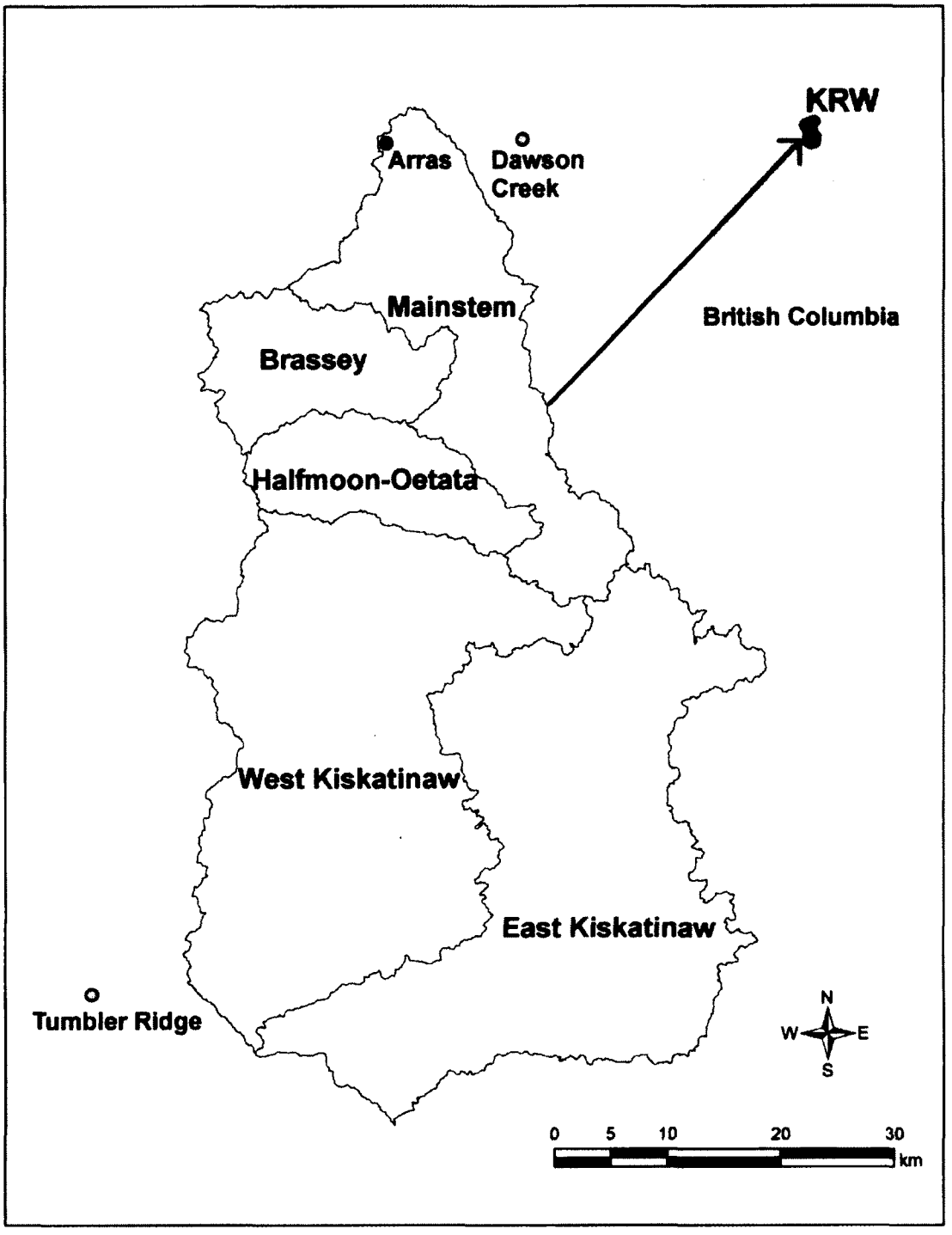

Figure 3.1 Overview of Kiskatinaw River Watershed

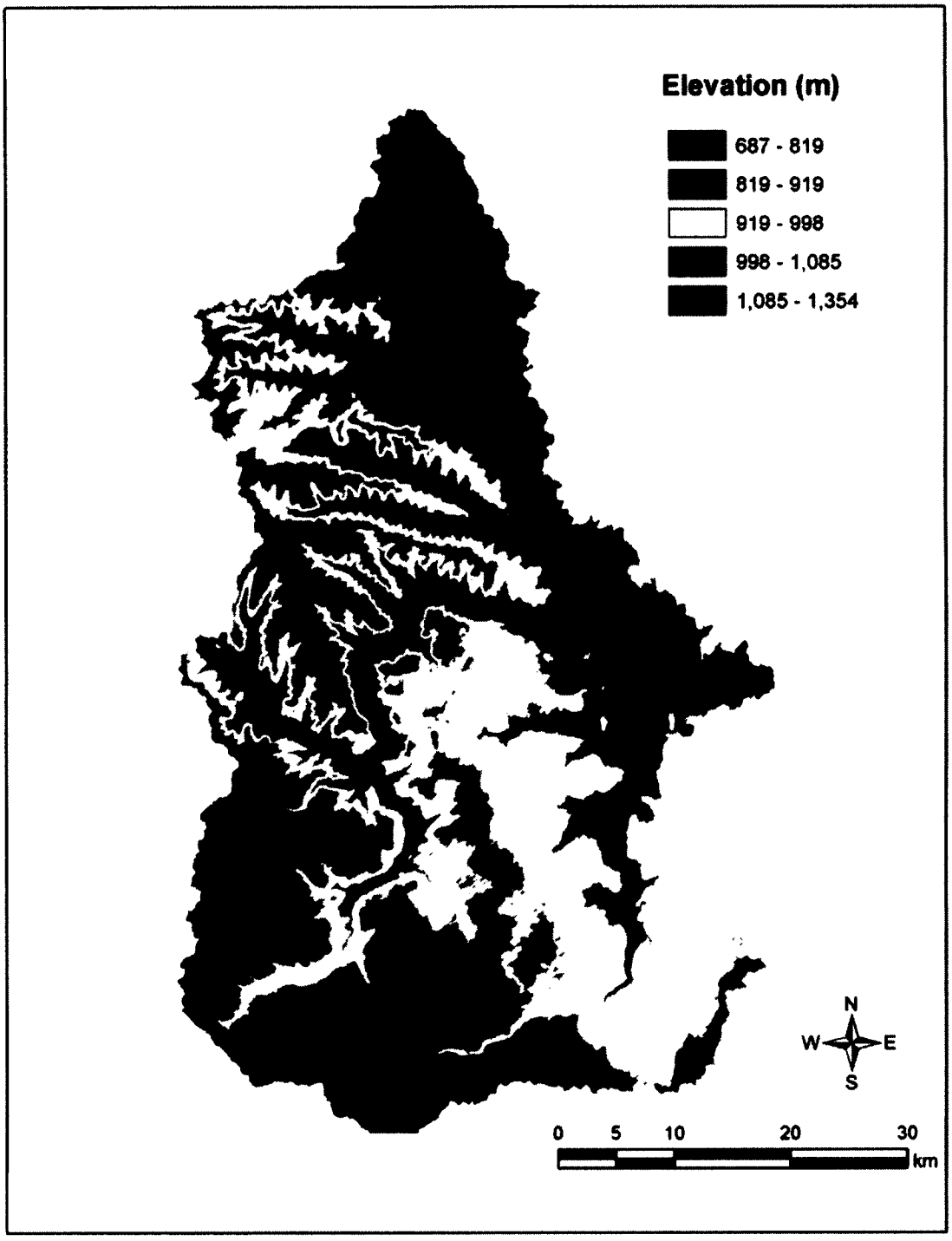

Figure 3.2 Digital elevation map of KRW

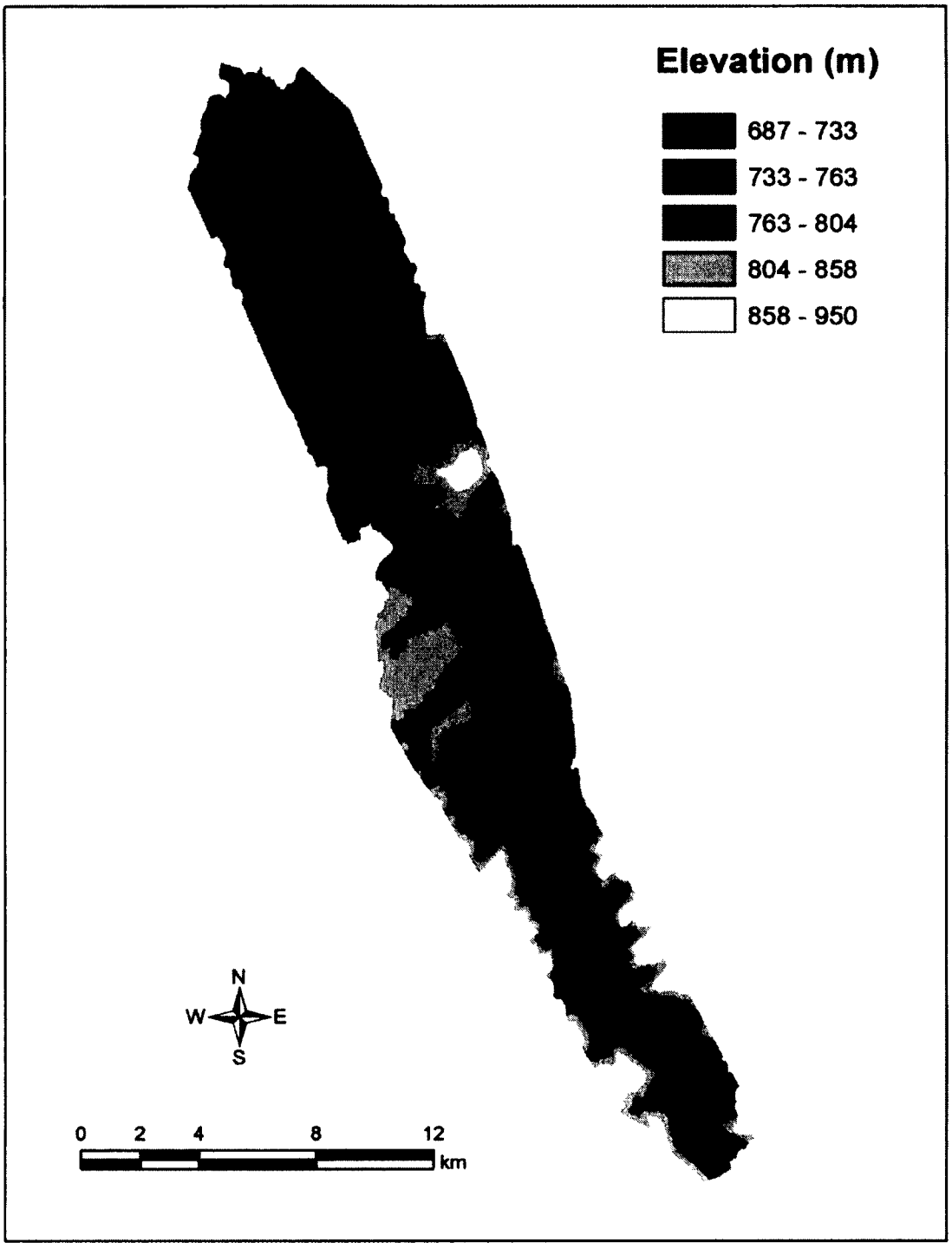

Figure 3.3 Digital elevation map of the study area

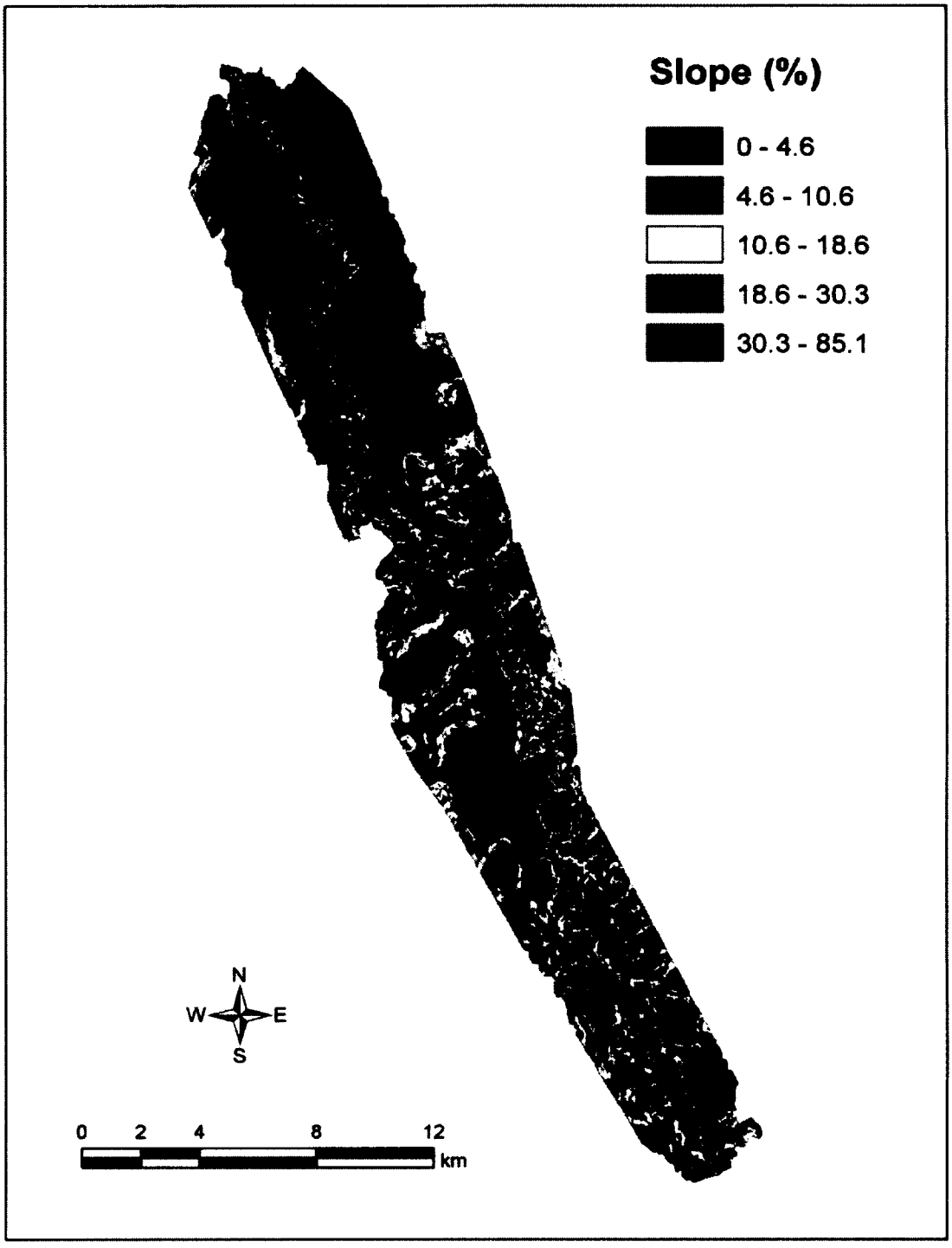

Figure 3.4 Slope patterns of the study area

3.2 Methodology

Fig. 3.5 presents the research framework of this dissertation. It includes tasks of data collection, numerical model development for investigating GW-SW interaction, generation of climate and land use/land cover changes scenarios, quantification of GW-SW interaction under various climates and land use/land cover changes scenarios, and uncertainty analysis of GW-SW interaction under climate change scenarios. The data collection was conducted through a number of ways, such as interviews with relevant stakeholders, processing of paper-based soil and land use/land cover maps, monitoring of groundwater and surface water levels, river flow data collection from Water Survey Canada, climate and meteorological data collection from neighboring weather stations, channel geometry survey, and digital elevation map (DEM) collection.

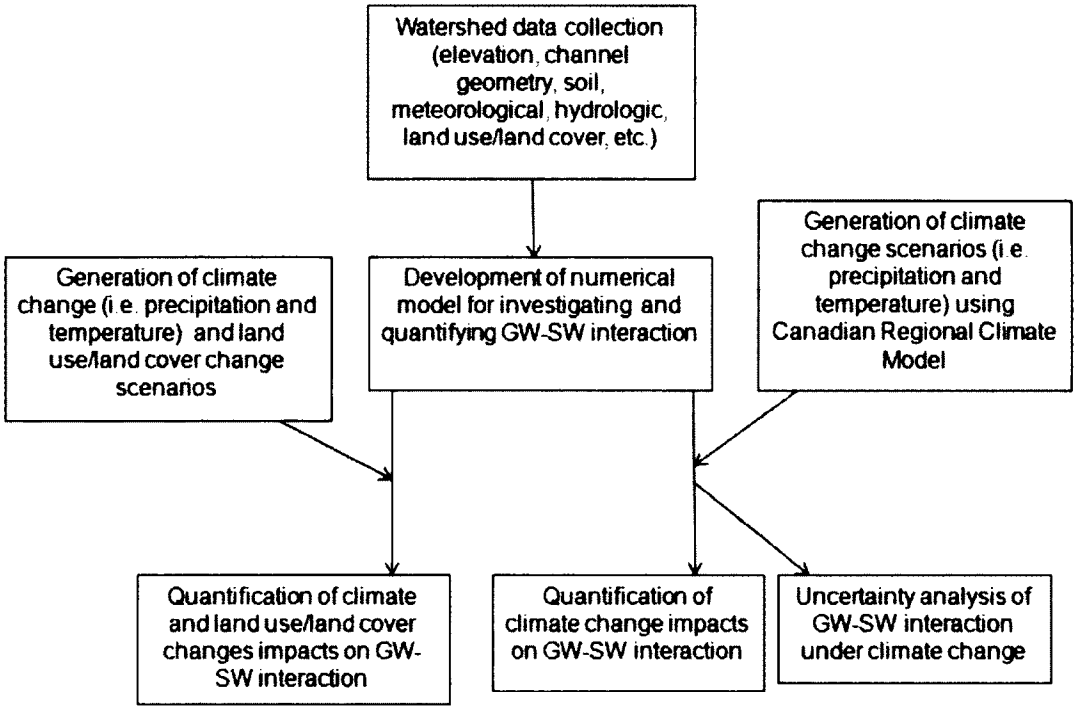

Figure 3.5 Research Framework

3.2.1 Groundwater-surface water monitoring network

In order to examine the GW-SW interaction in the KRW, a groundwater monitoring network was established in September 2010 by installing 22 piezometers equipped with Odyssey data loggers at 8 sites based on site accessibility (Fig. 3.6). At most of the sites, a bank piezometer was installed on each side of the river along with an in-stream piezometer. In addition, surface water level and discharge were measured at each of these sites using staff gauges equipped with Odyssey capacitance data loggers, and Sontek's Acoustic Doppler Flow Tracker. Cross sections were then completed using Sontek's Acoustic Doppler Flow Tracker in accordance with the BC Hydrometric Standards (British Columbia Ministry of Environment, 2009). Piezometers (¾ inch by 10 feet) with 44 holes at one end along with a welded drive tip (Fig. 3.7) were inserted at depths of between 1 m and 2.4 m at different sites using hand auger and slide hammer. In addition, one bank piezometer (1 inch by 16 feet) equipped with Odyssey data logger was installed in the study area (Fig. 3.8) in late summer 2011 due to access and logistic problems, with an insertion depth of 3.5 m using hand auger, slide hammer and high-reach iron auger with long spiral extensions. Since all the piezometers were unscreened at those holes, sediment or fines entered the piezometers during installation and after the piezometers were in place. However, the piezometers were designed in such a way that those sediments or fines entered the piezometers settled at the bottom of piezometers (just below the lower perforation of piezometer in Fig. 3.7). The sensors of the Odyssey data loggers were set up inside the piezometers after sediment or fines settled at the bottom of piezometers. In addition, the piezometers were inserted such a way that the bottom of piezometers remained at a minimum of 40 cm below the groundwater level during dry season in order to capture all seasons data, and this type of set up allowed data loggers to

record groundwater level continuously although sediment or fines entered the piezometers during the monitoring period, but they settled at the bottom of piezometers. Geist et al. (1998) also used similar unscreened piezometers for GW-SW interaction studies in the Hanford Reach of Columbia River. Since in this study pumping was not performed in those piezometers, there is no chance of clogging in those piezometers. Each Odyssey data logger was calibrated using the 3-point calibration method as outlined by Odyssey before inserting in the piezometer (www.odysseydatarecording.com). Data loggers were set for data collection of groundwater level at a 20-min interval. It is to be noted that in this study, only unconfined aquifer was considered for GW-SW interactions. Due to the lack of the stratification of soil layers of KRW, it is difficult to find out whether any confined aquifer contributes to the unconfined aquifer in KRW.

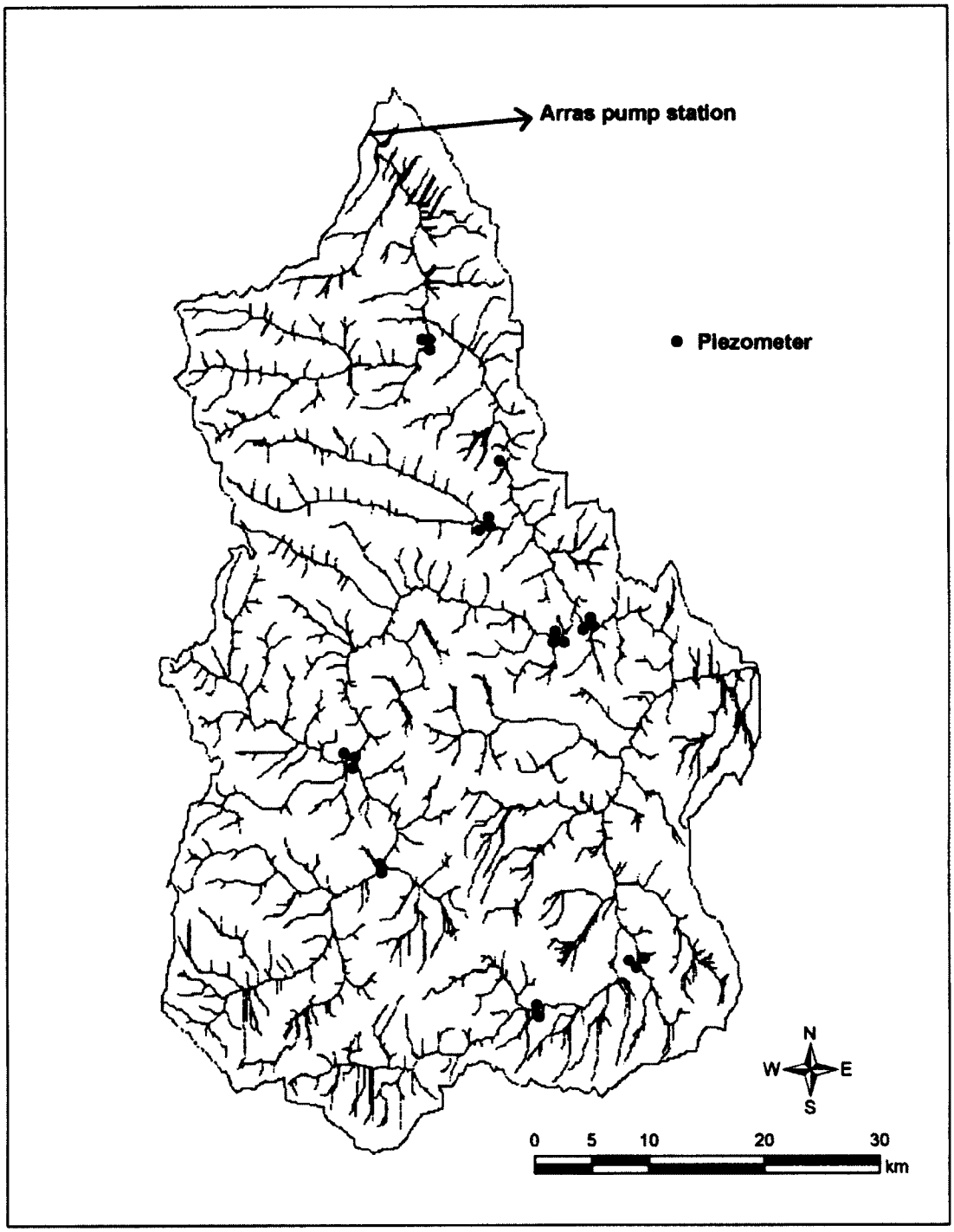

Figure 3.6 Groundwater monitoring network in the KRW

Figure 3.7 Piezometers with drilled holes and welded drive tip

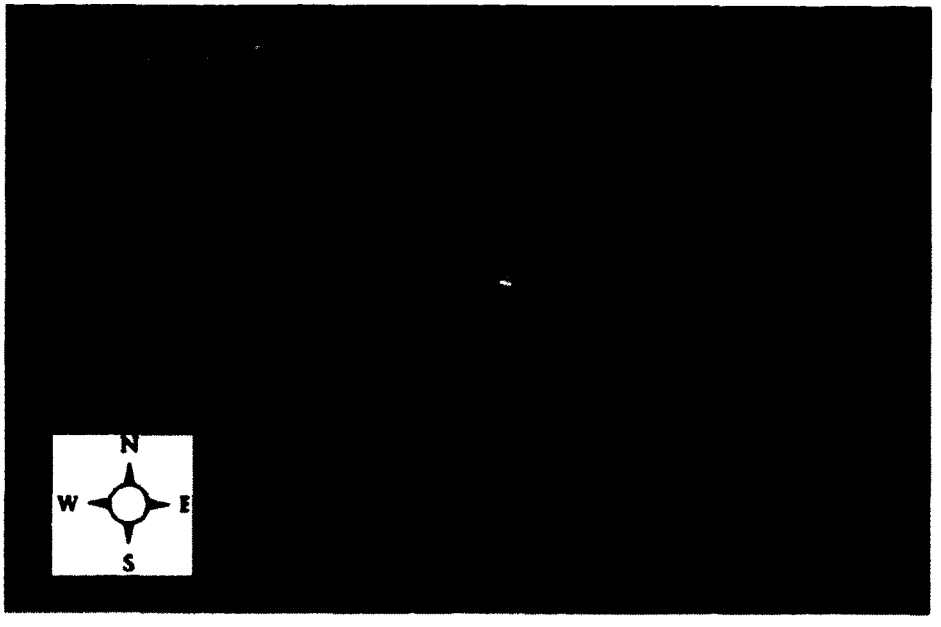

Figure 3.8 Piezometer at Mainstem area in the KRW

3.2.2 Surficial geology

Surficial geology map provides the types and distributions of unconsolidated sediments overlying bedrock, and their morphology and properties across the landscape (www.gov.bc.ca). Since the detailed soil map of KRW is not available, the surficial geology map of KRW will provide information regarding possible soil types of KRW. The surficial geology map of KRW (Fig. 3.9) was developed using Arc GIS based on data from Reimchen (1980). In KRW, there are seven types of surficial deposits, including alluvial, eolian, lacustrine, colluvial, morainal, glaciofluvial, and organic deposits. Table 3.1 lists their compositions in the KRW, and it was found that KRW is dominated by the morainal deposit.

Table 3.1 Composition of different types of surficial deposits in the KRW

Surficial deposit type	Area (km^2)	% of KRW area
Alluvial	204.35	7.09
Colluvial	47.74	1.65
Eolian	532.35	18.47
Glaciofluvial	61.92	2.15
Lacustrine	331.37	11.50
Morainal	1689.18	58.60
Organic	15.45	0.54
Total	2882.36	100

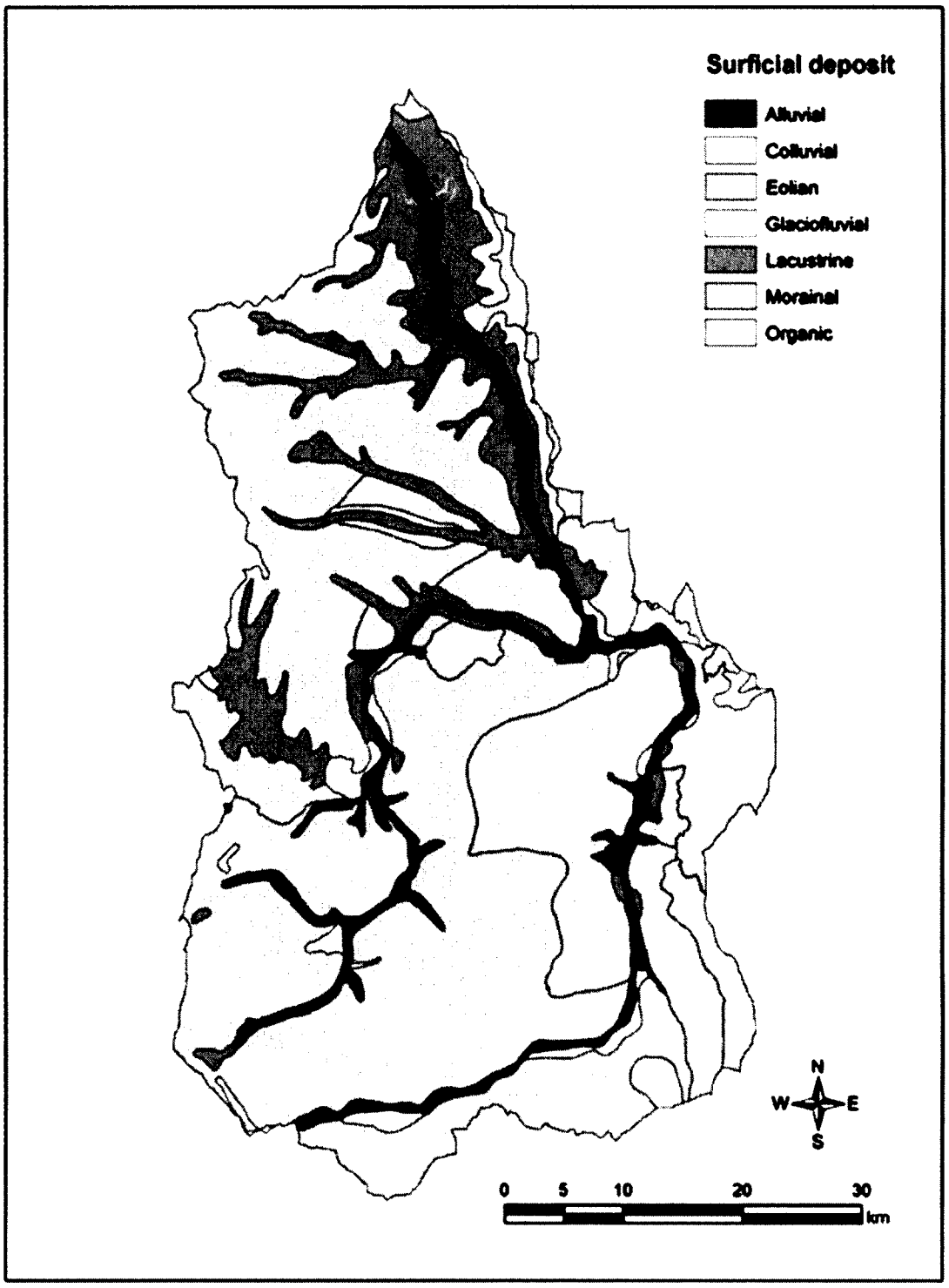

Figure 3.9 Surficial geology map of KRW

3.2.3 Soil map development

Soil map is an important input for developing the GSSHA model. Soil maps are generally available from Natural Resources Canada and Land Resource Research Institute, Canada. Unfortunately, only approximately 20% of KRW area has soil information (Fig. 3.10) from the National Topographic System map (Fig. 3.11) (Land Resource Research Institute, 1985). As a result, KRW's soil map was developed based on the surficial geology map of KRW and the land formation information of its surrounding region (i.e., Soil survey reports of the Land Resource Research Institute, Ministry of BC Environment, and Natural Resources Canada). Table 3.2 lists an example of the soil classification system in Canada (Agriculture and Agri-Food Canada, 1998), namely the Brunisolic among ten soil orders.

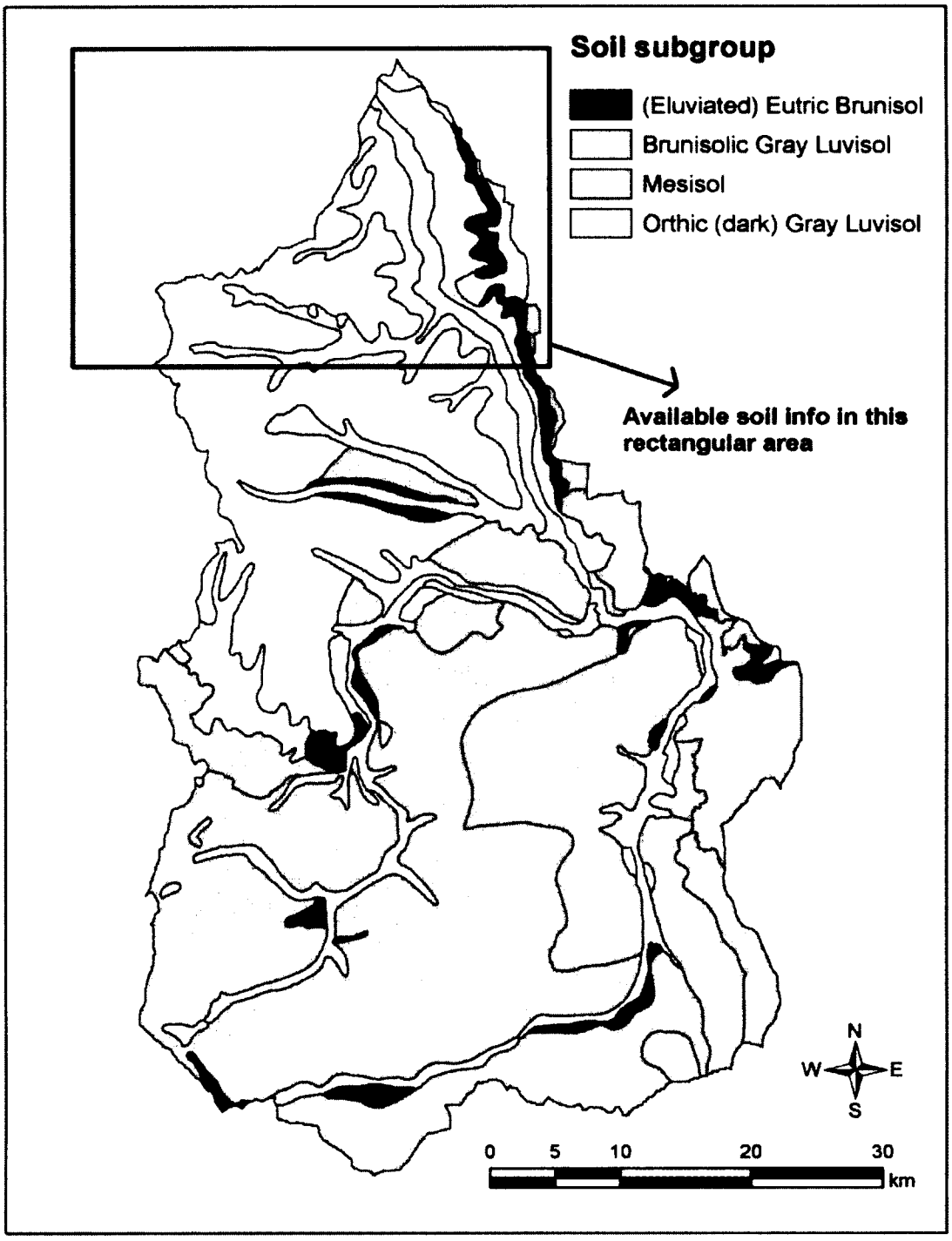

Figure 3.10 Soil (subgroup) map of KRW

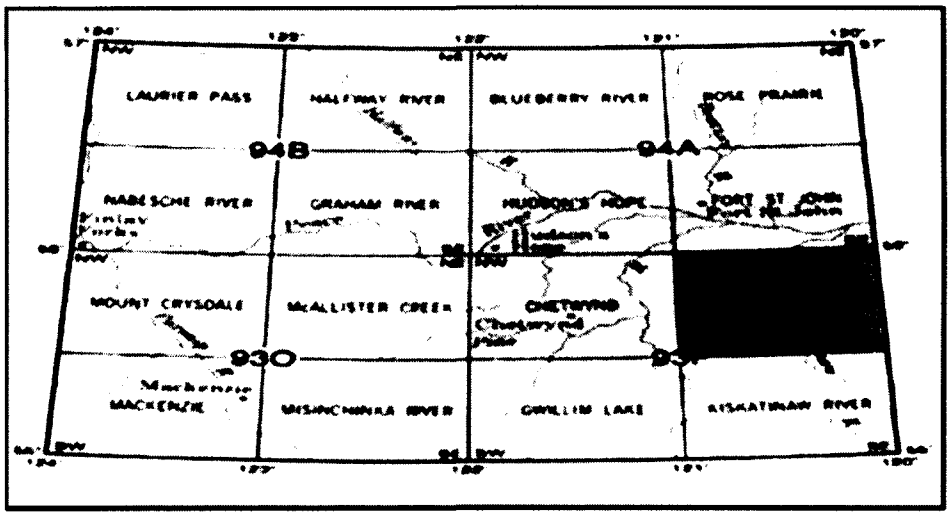

Figure 3.11 The KRW location in the NTS 93 P (Land Resource Research Institute, 1985)

Table 3.2 Canadian System of Soil Classification (Agriculture and Agri-Food Canada, 1998)

Order	Great Group	Subgroup
Brunisolic	Melanic Brunisol	Orthic Melanic Brunisol
		Eluviated Melanic Brunisol
		Gleyed Melanic Brunisol
		Gleyed Eluviated Melanic Brunisol
	Eutric Brunisol	Orthic Eutric Brunisol
		Eluviated Eutric Brunisol
		Gleyed Eutric Brunisol
		Gleyed Eluviated Eutric Brunisol

The relationship between surficial geology and soil classification in northern British Columbia can be described as follows (Land Resource Research Institute, 1985), and is shown in Table 3.3.

Table 3.3 Relationship between surficial geology and soil classification

Surficial deposit types	Surficial deposit forms to soil subgroup
Glaciofluvial	• Eluviated Eutric Brunisol (i.e., subgroup of Eutric Brunisol) landscape for elevation range of 700-1050 m • Brunisolic Gray Luvisol (i.e., subgroup of Gray Luvisol) landscape for elevation range of above 1050 m
Alluvial	Orthic Gray Luvisol (i.e., subgroup of Gray Luvisol)
Eolian	• Brunisolic Gray Luvisol when the elevation is greater than 750 m • Orthic Gray Luvisol for elevation of less than 750 m
Lacustrine	Orthic Gray Luvisol
Colluvial	Eluviated Eutric Brunisol
Morainal	• Brunisolic Gray Luvisol when the elevation is greater than 800 m • Orthic Gray Luvisol when the elevation is less than 800 m
Organic	Mesisol (i.e., Great group of Organic)

Based on the above information and the DEM, the glaciofluvial deposit information shown in the surficial geological map of KRW (Fig. 3.9) was converted into the Eluviated Eutric Brunisol and Brunisolic Gray Luvisol depending on the elevation (Table 3.3). Similarly, the alluvial, eolian, lacustrine, collovial, morainal, and organic deposits information shown in the surficial geological map were converted into the corresponding soil sub groups. After this conversion, a soil map of KRW was developed (Fig. 3.10). Luvisol is one of the mostly available soil orders in the forested region of Canada (www.SoilsofCanada.ca), and it also accounts for a major soil group in KRW, which is

dominated by forest cover (Saha et al., 2013). Each soil subgroup is associated with specific mineral contents (i.e., sand, silt and clay). Based on the percentage of mineral contents, the specific soil type (e.g., loam, clay loam, sandy loam, silt loam) was then classified using USDA (United States Department of Agriculture) soil type classification system (USDA, 1987) (Fig. 3.12). The Mesisol does not contain any sand, silt or clay, but it is considered as a loamy-skeletal family (www.SoilsofCanada.ca). As a result, it is considered as a loam. The final soil type map of KRW is shown in Fig. 3.13. This map only shows the horizontal heterogeneities of soils. Since the stratification of soil layers of KRW is not available, it was assumed that the soils in the vertical direction are same as in the horizontal direction (i.e., isotropic), for example, the area containing clay loam soil has the same soil (clay loam) in the vertical direction of that area. Therefore, in this study, the soils of KRW were assumed as isotropic. This assumption will help delineate the approximate aquifer (unconfined) bottom map using the GSSHA model. The accuracy of modeling results would improve if the detailed stratification of soil map in KRW is available because soil properties (i.e., hydraulic conductivity, porosity) greatly affect groundwater flow.

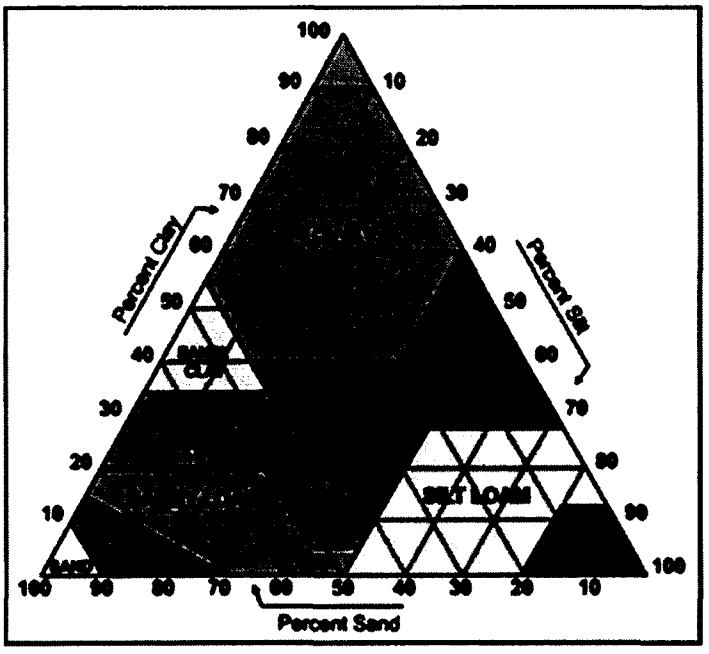

Figure 3.12 USDA Soil type classification system (USDA, 1987)

The soil type map of the study area was developed by clipping the soil type map of KRW to the study area of the Mainstem sub-watershed using Arc GIS (Fig. 3.14). Three types of soil were found, including clay loam, sandy loam, and silt loam. Clay loam covers the majority (91%) of the study area, while the silt loam and sandy loam cover 6% and 3%, respectively.

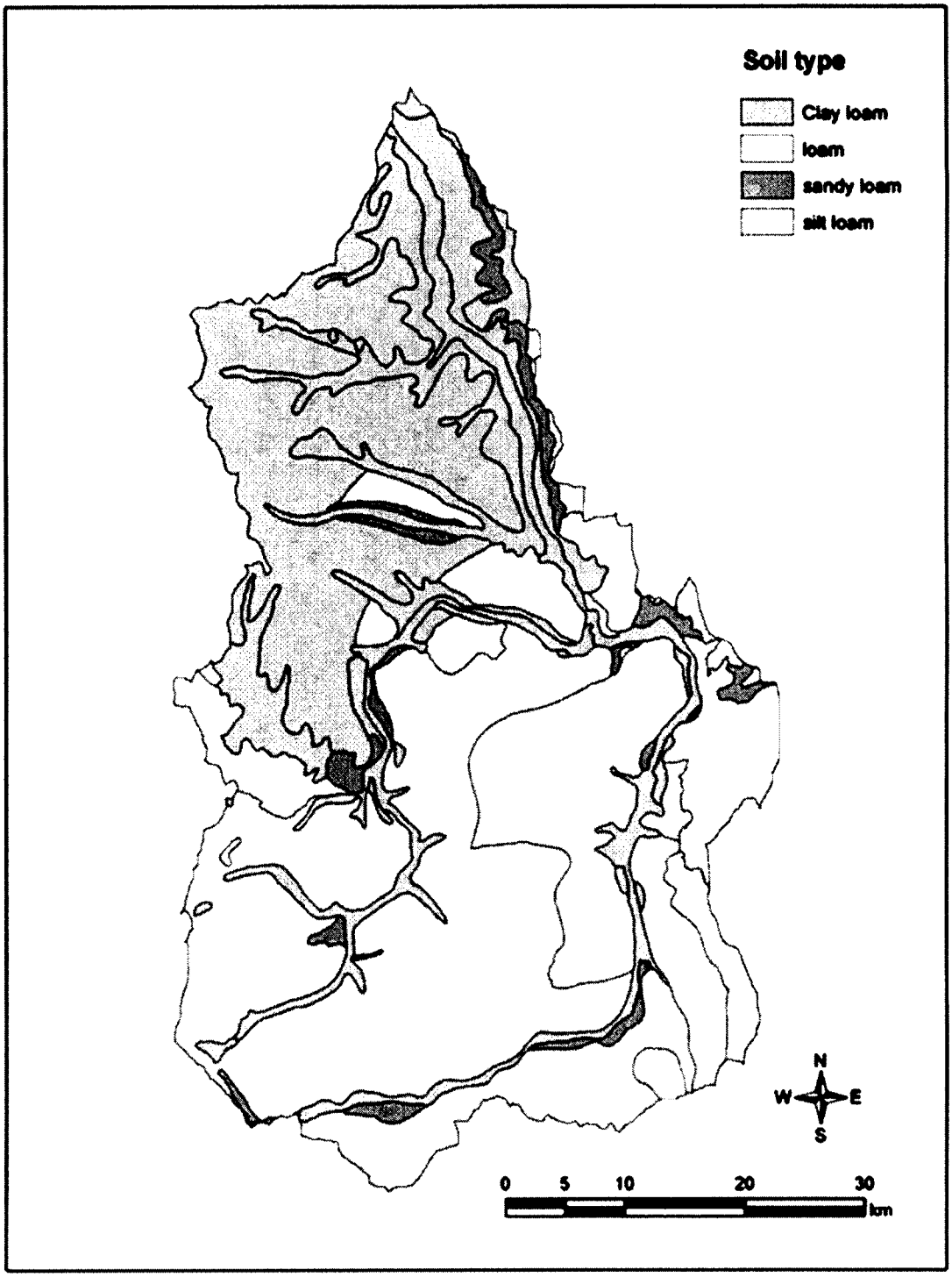

Figure 3.13 Soil type map of KRW

3.2.4 Climate and meteorological data collection

In the KRW, there is only one active weather station (i.e., Noel station). There are two other active weather stations surrounding the KRW, and they are located at Tumbler Ridge and Dawson Creek (Fig. 3.15). Holtan et al. (1962) recommended that when the watershed size is more than 20 km^2, the minimum number of weather station for watershed hydrology study will be 1 per each 8 km^2. The World Meteorological Organization (WMO) (1981) recommended using one weather station per 250 to 1000 km^2 when it is difficult to get available meteorological data. As a result, the use of data from 3 weather stations is acceptable for climate change study in KRW. In this study, observed precipitation, temperature, and other meteorological data (e.g., barometric pressure, relative humidity, wind speed, direct and global radiation) were collected from these three stations from 2000 to 2011. Since Dawson Creek and Noel weather stations did not have observed precipitation, temperature, and other meteorological data during winter and spring seasons, Tumbler Ridge weather station's data were used during those seasons. During summer and fall seasons all three weather stations' data were averaged to get their daily distribution for the study area. The arithmetic average method was used in climate data for various hydrologic studies (e.g., Fujieda et al., 1997; Anctil et al., 2004; Chenini et al., 2010; Guardiola-Claramonte et al., 2011; Wang et al., 2012).

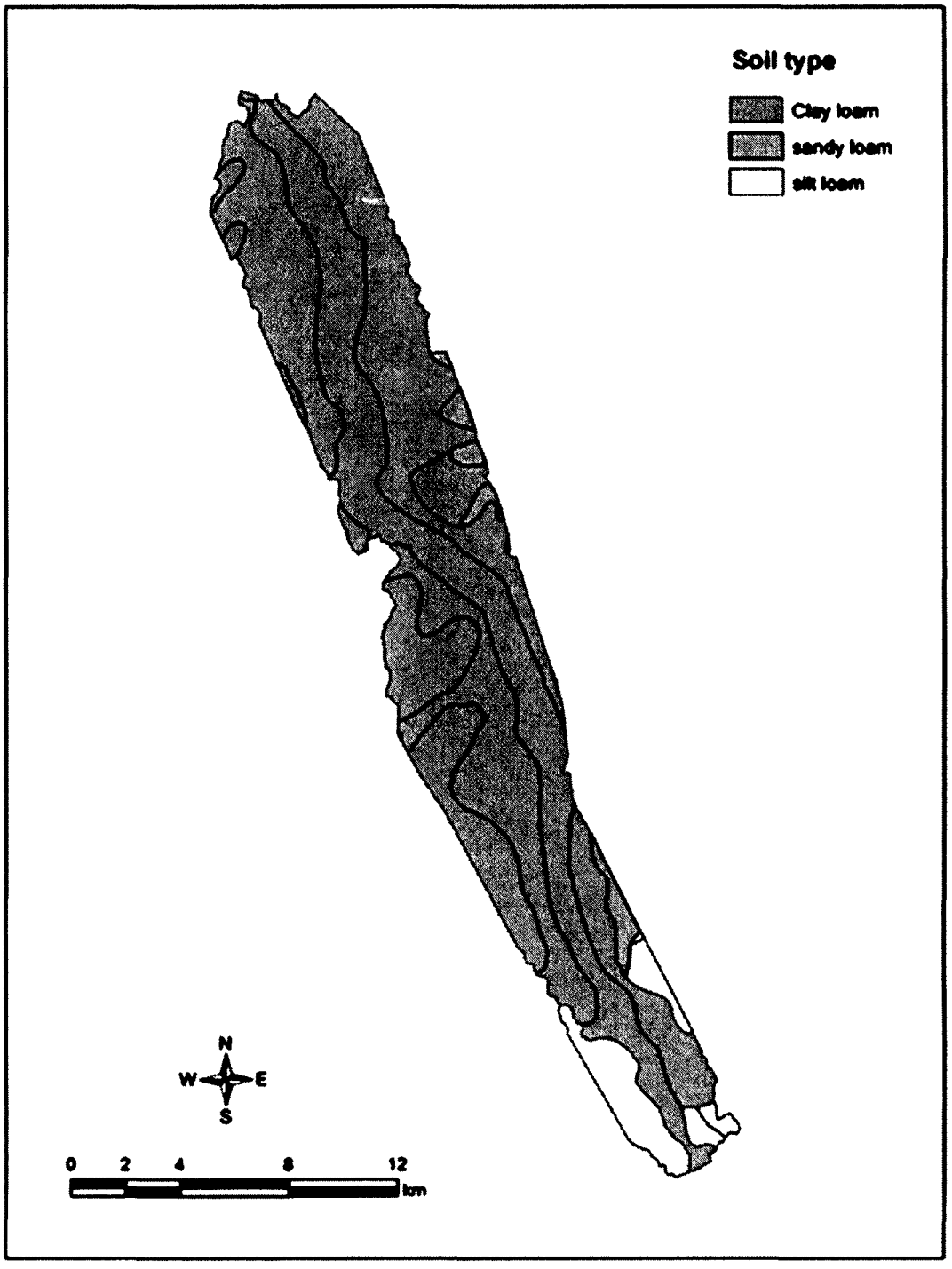

Figure 3.14 Soil type map of the study area

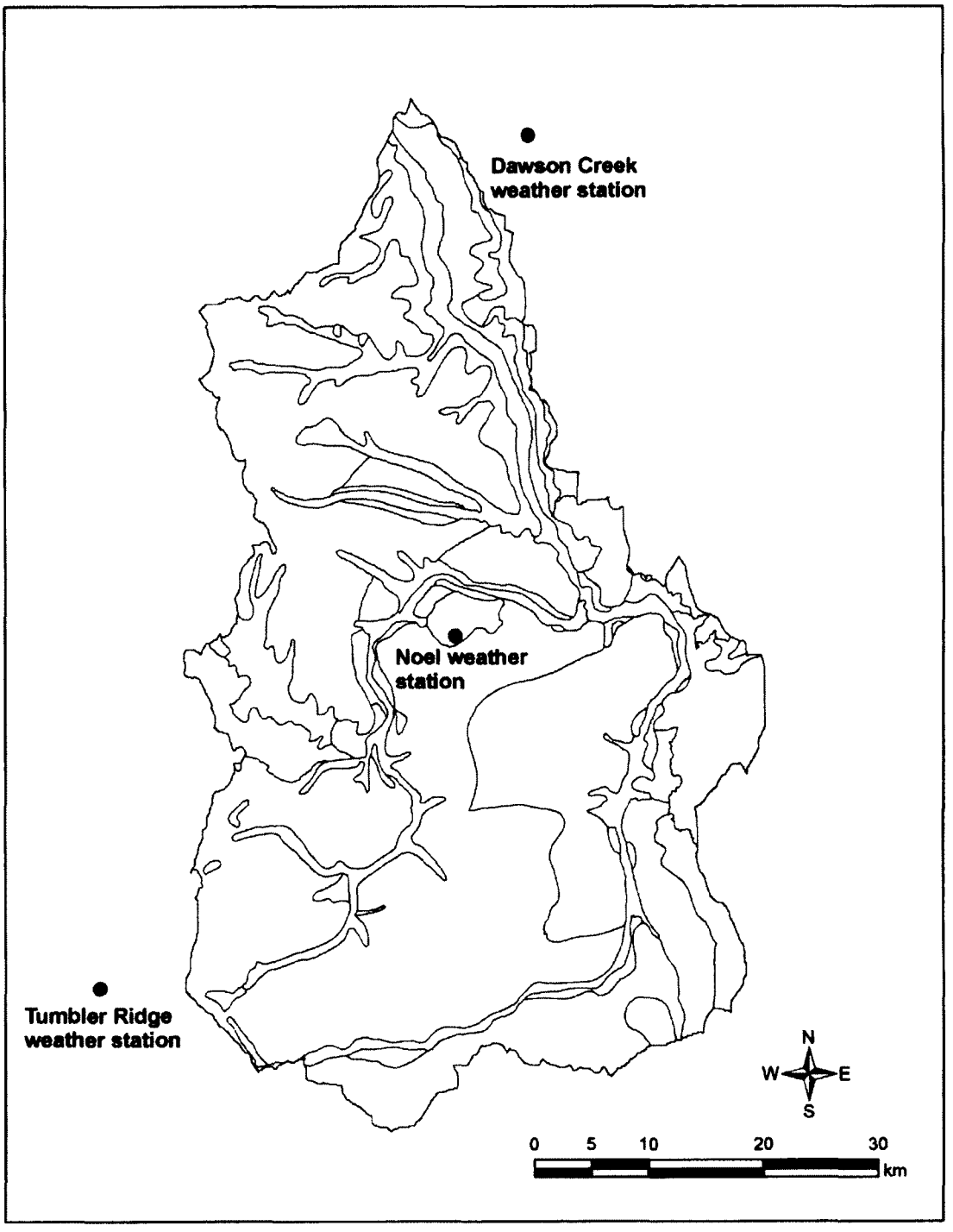

Figure 3.15 Available active weather stations in and around KRW

3.2.5 Land use/land cover map of the study area

Land use/land cover (LULC) maps for the study area of the Mainstem sub-watershed in 1999 and 2010 were generated from Saha et al.'s (2013) results using Arc GIS. The details of this LULC map generation are found in Paul (2013). The composition of different LULC in 1999 and 2010 are shown in Fig. 3.16 and 3.17, respectively. The definitions of different land use types are presented in Table 3.4. The details of LULC changes in the study area between 1999 and 2010 are shown in the next Chapter (Table 4.2).

Table 3.4 Definitions used in different land use types (Paul, 2013)

Land use types	Description
Agriculture	It includes cultivated land as well as grass land (pasture)
Built up area	It includes man-made structures e.g., houses, roads, industrial infrastructures etc.
Forest	It includes evergreen deciduous, broadleaf coniferous and mixed forests
Forest clear cut	It includes the forest cut block areas, which were cleared by the industry (e.g., oil and gas). This land use class contains most of the gas development infrastructures, including drilling pads
River	River network
Wetland	It includes non-forested and slightly forested marshes, swamps etc. where the groundwater table is at near or above the surface for significant part of the year

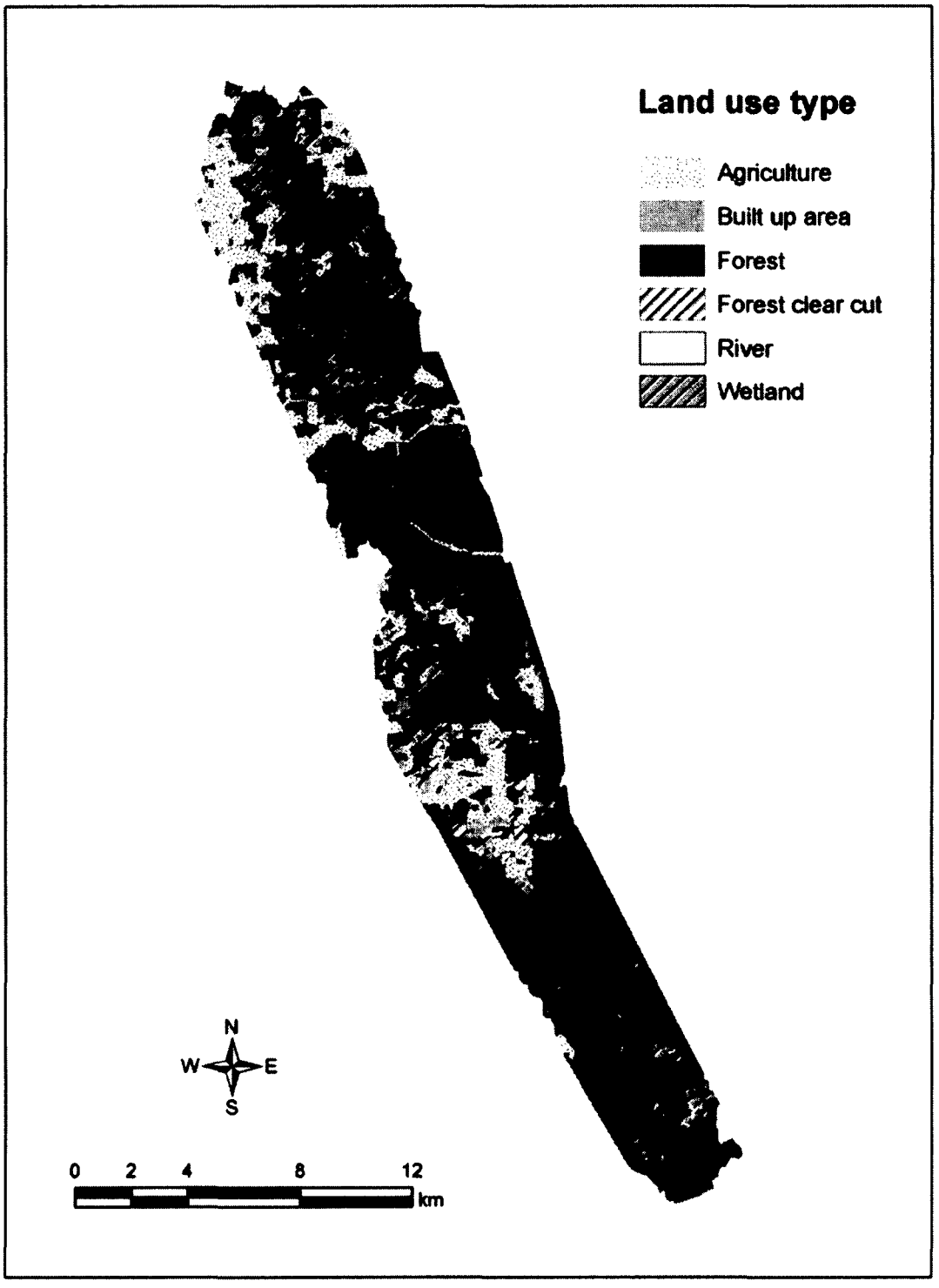

Figure 3.16 Land use/land cover map in the study area in 1999

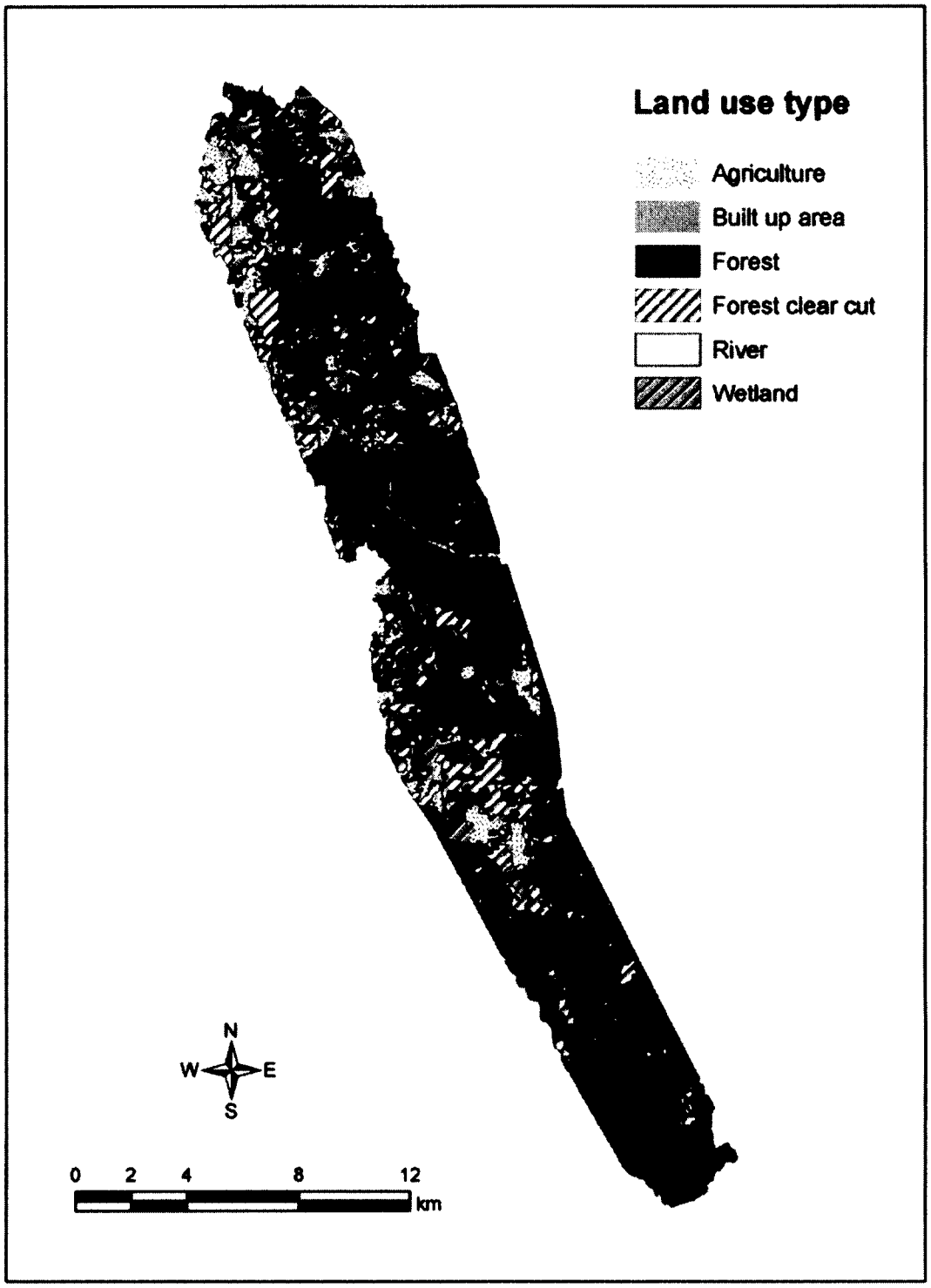

Figure 3.17 Land use/land cover map in the study area in 2010

3.3 Numerical model development

3.3.1 Model selection

The selection of numerical model for GW-SW interaction study was based on literature studies. Jenkins (2006) mentioned that groundwater flow models (e.g., Parflow, ZOOMQ3D) cannot simulate river hydraulics and evapotranspiration, and they need to be coupled with another hydrologic model for investigating stream-aquifer interaction. Some groundwater models, such as SEEP2D (Tracy, 1977) and MODFLOW (McDonald et al., 1988) can simulate the steady-state water table if the river stage is specified, but they cannot model a flood surge. In addition, the effects of water in the unsaturated zone are not considered in these groundwater flow models. GSSHA is one of the few numerical models that have the capability to incorporate the groundwater physical processes into the hydraulics. The other numerical model is MIKE SHE which was developed by DHI Water and Environment. Both models incorporate almost the same hydrologic processes, including the same unsaturated flow equation (Richard's equation). The only difference between these two models is the calculation of evapotranspiration (ET). In MIKE SHE, the Kristensen and Jensen method (Kristensen et al., 1975) is used for calculating ET based on a number of empirical equations. The required input includes time series for the reference ET, the leaf area index, the root depth, and the values for several empirical parameters that control the distribution of ET within the system (Refsgaard et al., 1995). On the other hand, in GSSHA model, the Penman-Monteith method (Monteith, 1981) is used for calculating ET by knowing the vegetation and surface characteristics based on soil and land use data. In this method, hydraulic conductivity of soils varies with the types of land uses (i.e., same soil type with different land use has

different hydraulic conductivity, and therefore, various infiltration rates). As a result, this approach is appropriate for investigating land use impacts on GW-SW interaction. Furthermore, few studies have been reported to use GSSHA model for long term simulation in GW-SW interaction studies under changing climatic and land use conditions. As a result, the GSSHA model was chosen in this study to examine GW-SW interaction.

3.3.2 Details of GSSHA

GSSHA is a physically based and distributed hydrologic model that simulates the hydrologic response of a watershed under given hydrometeorological inputs. It simulates the major hydrological processes, such as spatially and temporally varying precipitation, snowfall accumulation and melting, precipitation interception, infiltration, evapotranspiration, surface runoff routing, unsaturated zone soil moisture accounting, saturated groundwater flow, overland flow, sediment erosion and deposition, and in-stream sediment transport (Downer et al., 2002b). Each simulated process has its own time step and associated update time. During each time step, the update time is compared to the current modeling time, and when they match, the process is updated and the information is transferred to dependent processes. This formulation allows the simultaneous simulation of hydrological processes that have dissimilar response times, such as overland flow, ET, and lateral groundwater flow. In GSSHA model, snowfall accumulation is considered when precipitation occurs during air temperature of below $0^{o}C$. The details of GSSHA can be found in Downer (2002). During GSSHA model development, Watershed Modeling System (WMS) Version 8.4, a graphically-based software environment, was used in this study for

delineating watershed, importing soil and land use maps and segmentation, defining reach segment and segment cross section parameters, and providing the time series data of climate and meteorological inputs. The following modeling methods were implemented:

- Infiltration was calculated using the Green and Ampt infiltration with redistribution (GAR) method (Ogden et al., 1997).
- Overland flow routing was simulated using the alternating direction explicit (ADE) finite difference method (Saul'yev, 1957).
- Channel routing was simulated using an explicit solution of the diffusive wave equation. This method has several internal stability checks, which result in a robust solution that can be used for subcritical, supercritical, and trans-critical flows.
- Where groundwater significantly affected the surface water hydrology, saturated groundwater flow was simulated with a finite difference representation of the 2-D lateral saturated groundwater flow equations. During the simulation, the additional processes of stream-groundwater interaction and exfiltration occurred.
- When both saturated groundwater flow and channel routing are being simulated, water flux between the stream and the saturated groundwater can be simulated. By specifying that both overland flow and saturated groundwater flow grid cells containing stream network nodes be considered as river flux cells, water will move between the channel and the groundwater domain, and this water flow was calculated based on Darcy's law.
- Exfiltration is the flux of water from the saturated zone onto the overland flow plane. It is seen at a change in slope on a hillside. It occurs when the groundwater table

elevation exceeds that of the land surface. Fluxes to the land surface were computed using Darcy's law.

3.3.3 Data required

The following data are required to develop a GSSHA model:

- Watershed specific data (e.g., elevation, channel geometry, soil type, land use/land cover), which can be obtained from Geographic Information Systems (GIS) databases, satellite images, soil survey reports, and field observations.
- Precipitation and temperature data, and other meteorological data (e.g., barometric pressure, relative humidity, wind speed, direct and global radiation), which can be collected from available weather stations in the KRW.
- Stream flow data, which can be collected from Water Survey of Canada, and surface water monitoring network.
- Groundwater level data which can be collected from groundwater monitoring network.
- Channel cross section data which can be approximated based on field survey data.

3.3.4 Watershed delineation and stream network development

The Canadian Digital Elevation Data (CDED), with a resolution of 13.74 m by 23.81 m, downloaded free from Geo Base of Natural Resources Canada (www.geobase.ca) was used

for watershed delineation and stream network creation in WMS environment. The outlet location of the study area was chosen at Arras (City of Dawson Creek's water pump station), and the delineated watershed is shown in Fig. 3.18. It also shows the stream network in the study area which contains 236 segments, including segments of the main river (i.e., stream) and seasonal tributary drains. Uniform cross section of trapezoidal channel was assumed for stream segments and seasonal drains due to limited data and the infeasibility of conducting a cross sectional survey at each segment. The segments' cross section of the main river was chosen from field survey (weir's length at pump station in Arras) and Google map, while the seasonal tributary drains' cross section was chosen from field observations because these drains are very narrow. Table 3.5 lists all the defined cross sections' geometry (i.e., trapezoidal channel) for the segments. In WMS, each cross section's geometry was recorded manually.

Table 3.5 Channels' cross sections in the study area

Segment type	Channel width (m)	Channel depth (m)	Side slope (H:V)
Stream	40	1	1.5
Tributary drain	1	0.1	1.5

After the creation of stream network from DEM, 105 segments containing adverse slope were generated using the coarse grid resolution of DEM data. Such adverse slope creates backward flow from downstream to upstream which is not realistic. As a result, the streambed elevations of the adverse slope contained segments were smoothed through the interpolation of stream bed elevations manually one by one in WMS (Downer et al., 2002b).

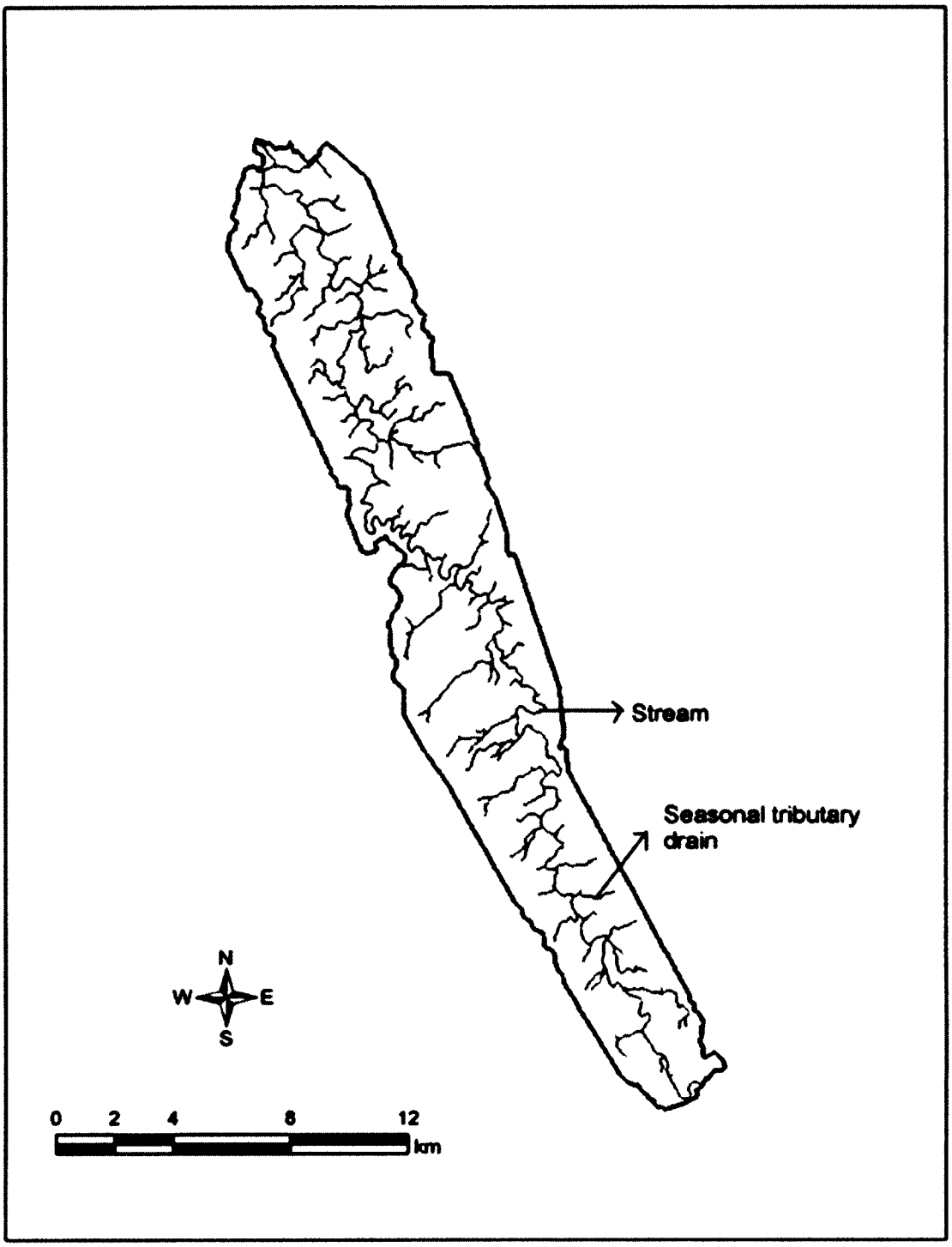

Figure 3.18 Watershed delineation and stream network development in the study area

3.3.5 Modeling grid and index map development

In this study, the Kiskatinaw River is 71.26 km long and 40 m wide. Using WMS, a 2-D GSSHA grid with a spatial resolution of 30 m by 30 m was chosen for simulation based on available digital elevation model (DEM) and land use data. The uniform grid size was selected because it is the only available option in WMS. In order to use very fine resolution grid cell (e.g., 1 m by 1 m) for simulation, DEM and land use data should be at similar scale, but the available DEM data was in a grid resolution of 13.74 m by 23.81 m, and the available land use map was in a resolution of 30 m by 30 m. In addition, the GSSHA model cannot be constructed using modeling grid below DEM cell size. As a result, the grid cell of 30 m by 30 m was chosen to maintain consistency with available DEM and land use data. A similar type of grid cell with coarse resolution was used in Ma et al. (2002) and Krause et al. (2007) for conducting GW-SW interaction studies. In a distributed model like GSSHA, the modeling parameters are assigned at the grid cell level. In GSSHA, the land use and soil type data are converted into index maps so that parameter values can be easily assigned to each grid cell. In this study, three index maps were created for parameter assignment, including a land use index map, a soil type index map, and a combined land use and soil type index map, as shown in Figs. 3.19, 3.20, and 3.21, respectively. In the land use index map, six different integer values were assigned as index ID for six types of land uses as per the guidelines of Downer et al. (2002b), for example, agriculture – 21, built up area – 16, forest – 43, forest clear cut – 83, river – 51, and wetland – 61. In the soil type index map, three different integer values were assigned as index ID for three soil types as per the guidelines of Downer et al. (2002b), such as sandy loam – 10, clay loam – 15, and silt loam – 17. In the combined

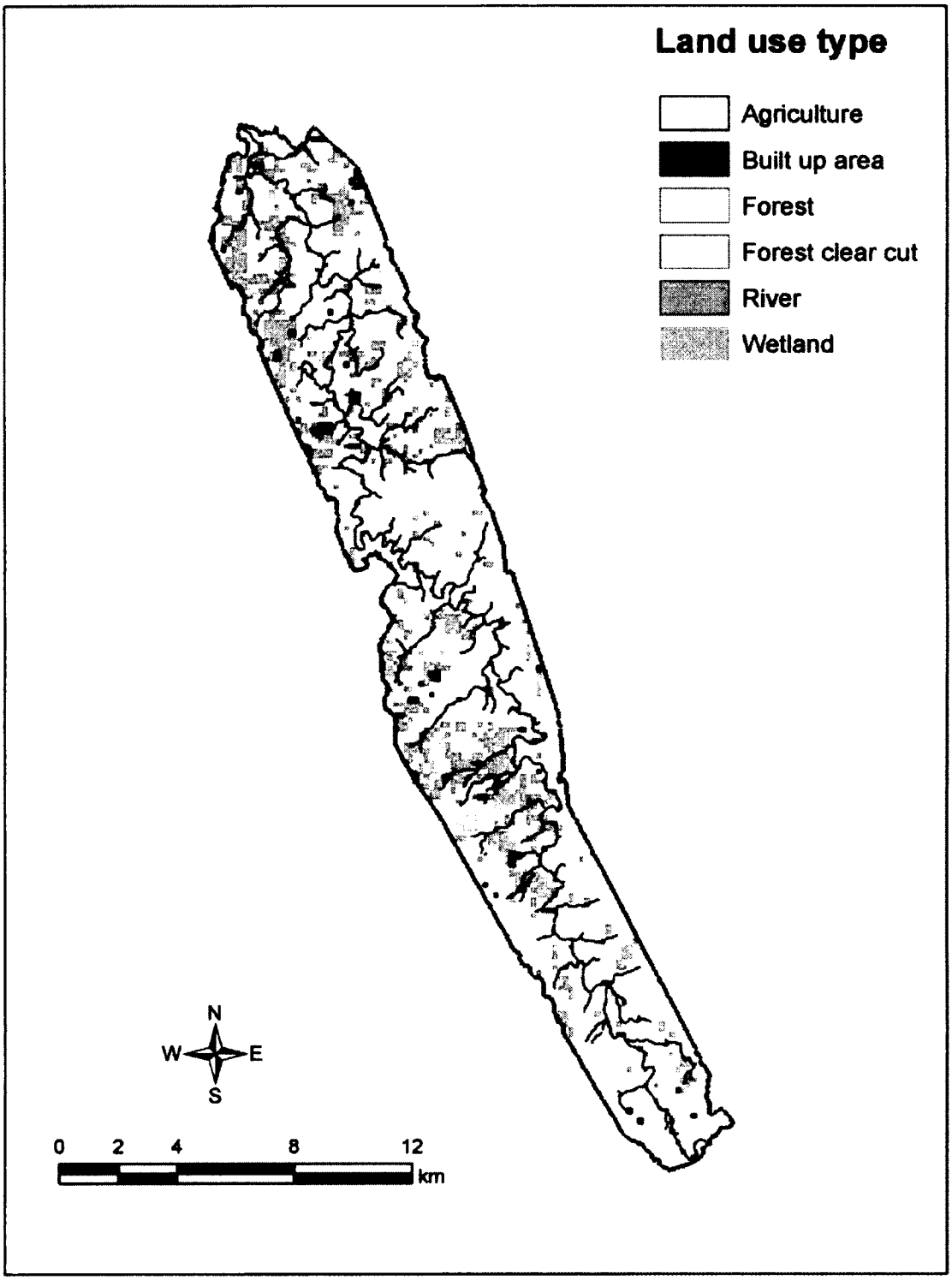

Figure 3.19 2010 land use index map.

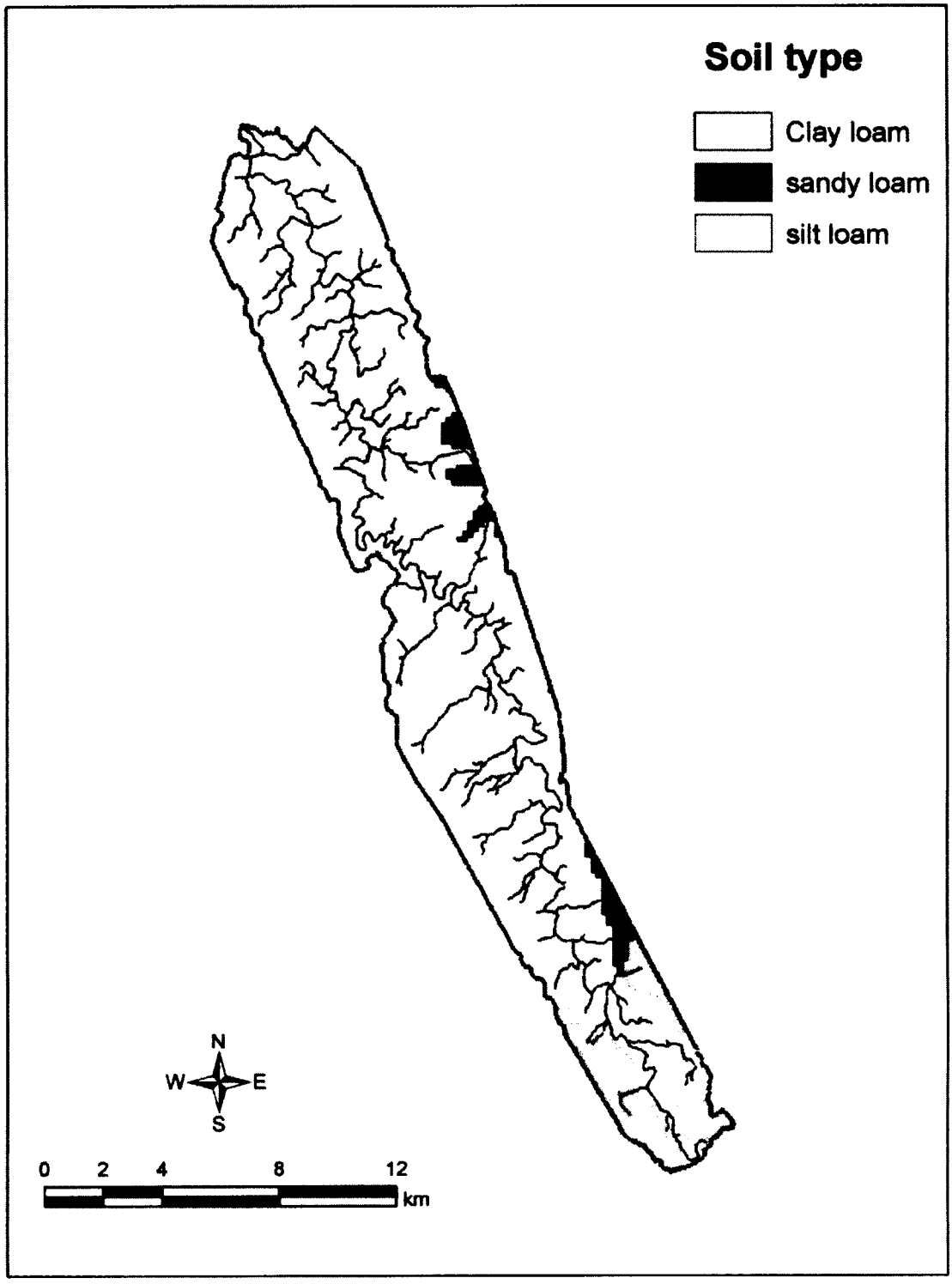

Figure 3.20 Soil type index map.

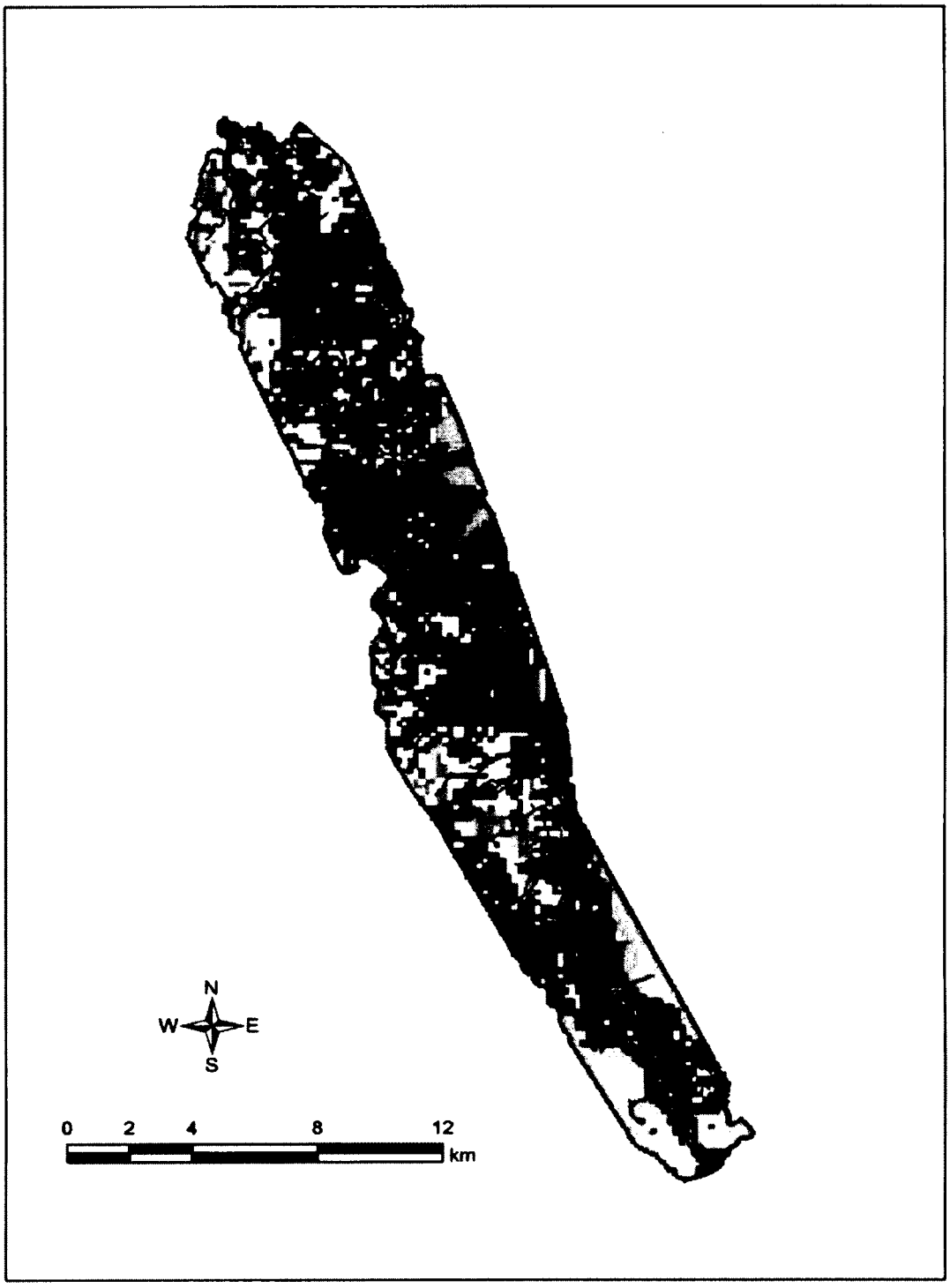

Figure 3.21 2010 combined land use and soil type index map. Here yellow, cyan, green, orange red, orange, and blue color indicates forest clear cut-clay loam, forest-silt loam, forest-sandy loam, forest-clay loam, agriculture-clay loam, and wetland-clay loam, respectively

land use and soil type index map, eleven different integer values (i.e., 1-11) were assigned as index ID for eleven different combinations of land uses and soil types for example, clay loam-forest – 1, clay loam-built up area – 2, etc.

In addition, the initial groundwater table and aquifer bottom maps were prepared for GW-SW interaction simulation. Since there is only one piezometer in the study area due to access and logistic problems, the initial groundwater table map of the study area was prepared (Fig. 3.22) using observed groundwater table data collected from the all piezometers in the groundwater monitoring network in the KRW based on the interpolation method. This map was developed by clipping the initial groundwater table map of KRW to the study area using the GIS tool in WMS. Four types of interpolation methods are available in GSSHA, including linear, inverse distance weighted (IDW), Clough-Tocher, and natural neighbor method. Linear interpolation is the simplest TIN (Triangular Irregular Network) based method, and it is suitable for huge datasets. In the IDW, all of the data points are used to calculate each interpolated value, and it is suitable for both large and scattered data (Amidror, 2002). The basic assumption of IDW is that the interpolated values should be affected more by nearby points and less by more distant points. As a result, the interpolation value at each new point is a weighted average of the values of the scattered points, while the weight of the scatter point decreases as the distance from the interpolation point to the scatter point increases (Kurtzman et al., 1999). The Clough-Tocher method is a finite element method based on TIN and suitable for both scattered and large data sets (Amidror, 2002). The natural neighbor method is area and distance weighted, and is suitable for clustered data (Connor et al., 2005). In this study, the initial groundwater table map was prepared using the IDW interpolation method because it is widely used in groundwater study (Rao et al., 2010;

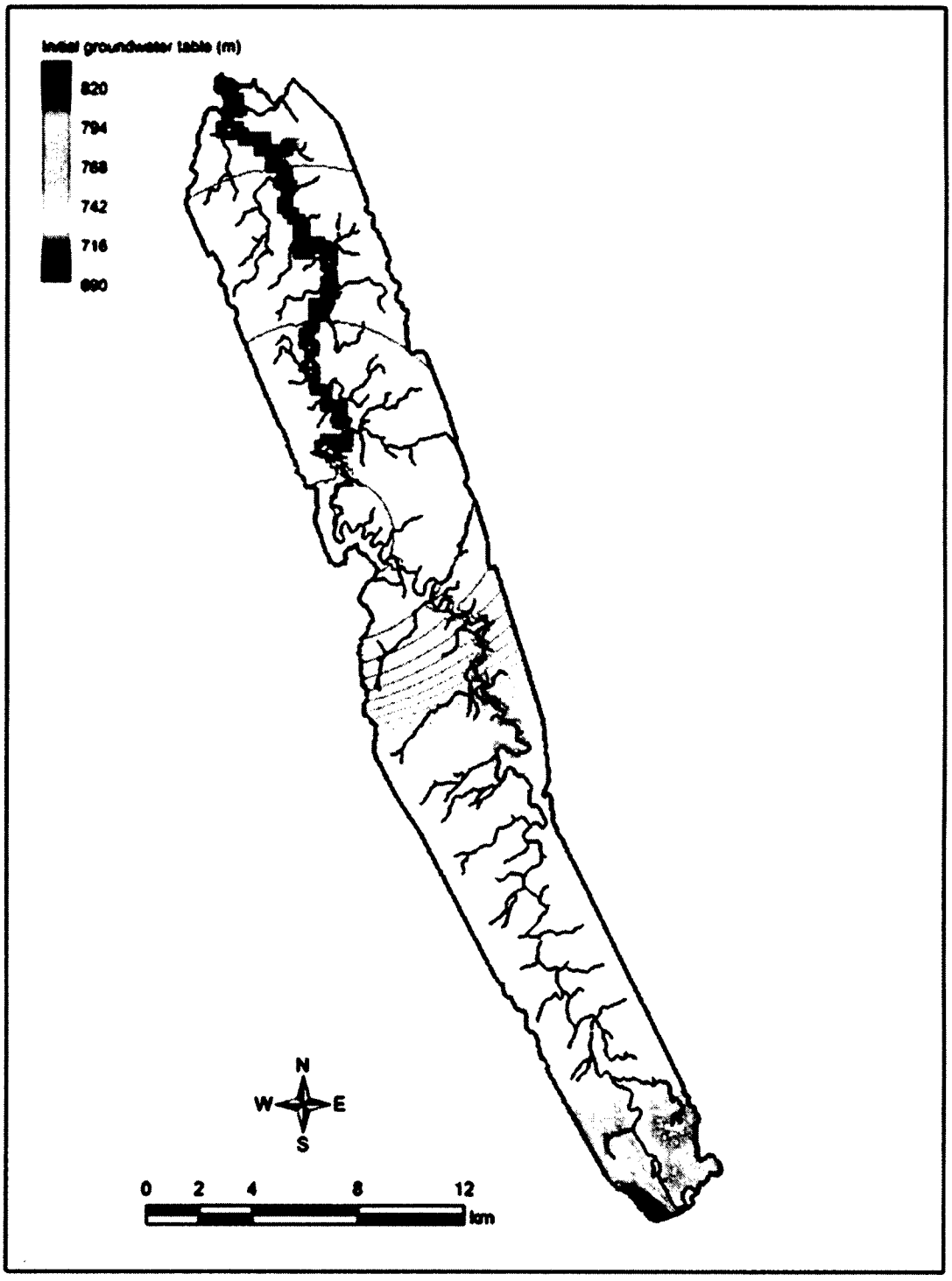

Figure 3.22 Initial groundwater table map on Oct 15th 2010. The color bar indicates groundwater table elevation above mean sea level.

Zehtabian et al., 2013). In Fig. 3.22, most interpolations were found in the south end of the study area because most of the piezometers in the groundwater monitoring network (Fig. 3.6) are located below the southern part of the study area. On the other hand, few interpolations were found in the northern half of the study area due to the presence of few piezometers around that area. All these interpolations indicate equipotential line (i.e., line with constant head or groundwater table). Groundwater flow lines are at the normal (i.e., right angle) of these equipotential lines. Based on these equipotential lines shown in Fig. 3.22, it was found that the regional groundwater flow field in the study area is a mixture of gaining and flow-through systems. The aquifer (unconfined) bottom map (Fig. 3.23) showing aquifer bottom elevation contour lines was prepared using borehole log data of a few existing wells in the upper part of KRW and its surrounding area collected from the database of British Columbia Water Resources Atlas (www.gov.bc.ca). This map was also prepared based on the IDW interpolation method. The distance between aquifer bottom elevation and ground elevation was then used to create the vertical layer of the modeling domain. For example, Woldeamlak et al. (2007) used only one layer of 90 m thickness in their developed model for investigating GW-SW interaction. Before using the collected groundwater table data, barometric pressure correction was applied because groundwater table fluctuates with atmospheric pressure change (McWhorter et al., 1977). Typically, an increase in barometric (i.e., atmospheric) pressure will cause a lower water level, and a decrease in barometric pressure will result in a higher water level. This increase in barometric pressure occurs at a location when the altitude of that location is below mean sea level, and vice versa. In the KRW, all the piezometers in the groundwater monitoring network are situated above mean sea level, and therefore,

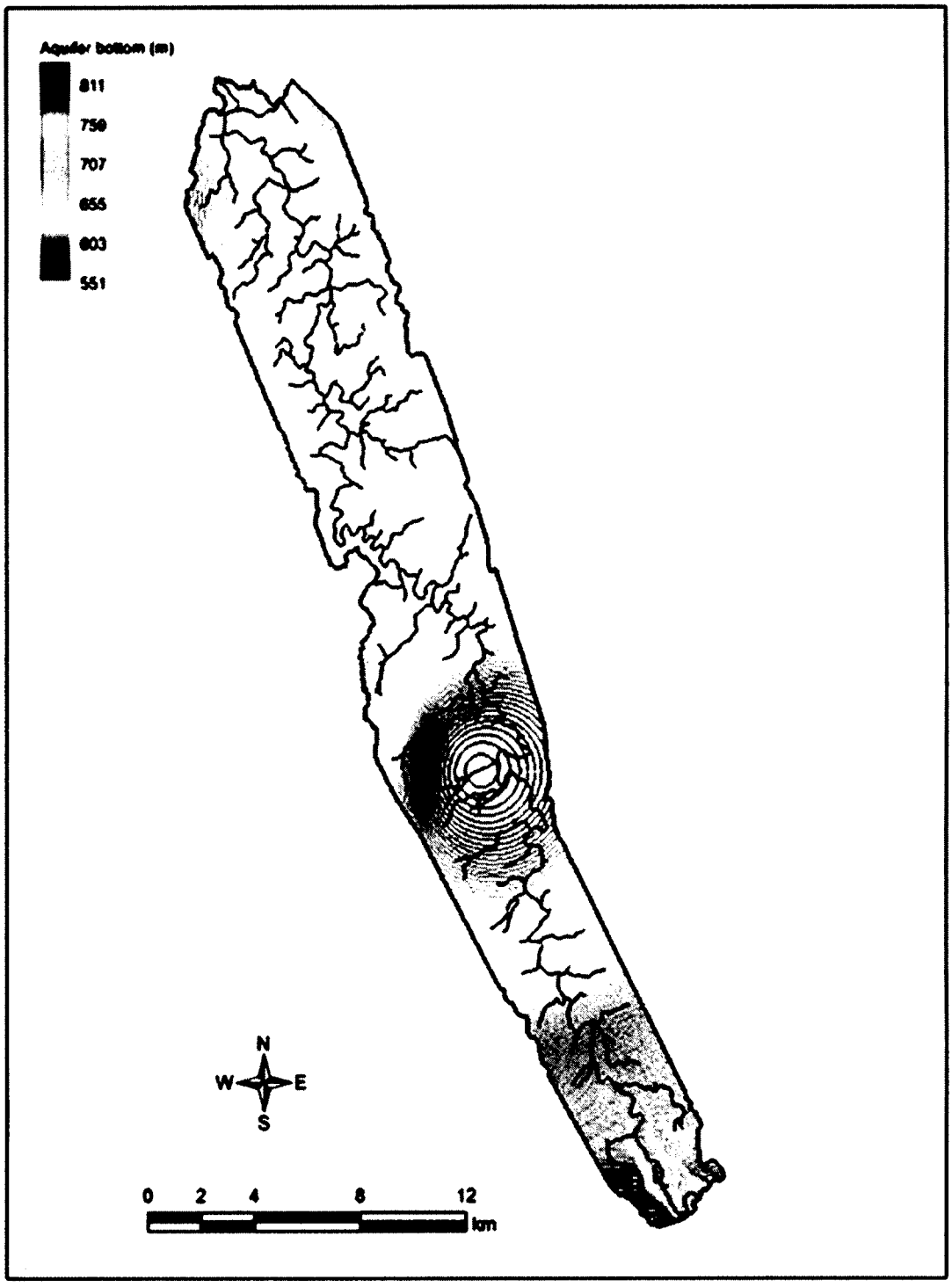

Figure 3.23 Aquifer (unconfined) bottom map. The color bar indicates aquifer bottom elevation above mean sea level.

barometric pressure decreases with increasing altitudes at those piezometers. The decrease of barometric pressure results in higher groundwater table in those piezometers because of the increase of entrapped air volume in those piezometers. Therefore, all the observed groundwater table data were subtracted by barometric pressure correction in order to get corrected groundwater table data. The barometric pressure correction was made according to the technical guidelines of Solinst (www.solinst.com). The barometric pressure data were collected from the three nearby weather stations because no barologger was used in this study to measure barometric pressure at each piezometer location. By comparing Fig. 3.22 with Fig. 3.23, the saturated thickness of unconfined aquifer in this study area ranges from about 10 m to about 140 m. This range is approximate because there are few groundwater table and aquifer bottom data available in this area. In addition, the stratification of soils in the study area is not available to firmly support this approximate range. Similar ranges were found in Ogallala (maximum thickness 366 m) and Edward Trinity (maximum thickness 243 m) aquifers in USA (Texas Water Development Board, 1995).

3.3.6 Initial and boundary conditions

In this study, the initial condition was chosen as the stream discharge (stream flow) on October 15th, 2010, at Arras (watershed outlet) because the groundwater table data collection from almost all the piezometers started on October 15th, 2010. The discharge at Arras site was determined from the summation of observed stream discharge at Farmington station (Water Survey Canada station), which is located downstream of KRW (Fig. 3.24), and the daily pumping rate from Arras. The Farmington station records stream flow in an hourly

interval. The Farmington station was chosen because it is the nearest station to Arras, and there is no observed flow data available at Arras. It is to be noted that the observed stream flow at Farmington station is the total stream flow of KRW, but the study area is only a part of KRW. Thus it is necessary to know stream flow at the inlet of the study area on October 15th, 2010 (Fig. 3.25). The flow at the inlet was determined by combining the stream flow of two confluences of Kiskatinaw River (i.e., East and West confluences in East and West Kiskatinaw sub-watersheds, respectively, in Fig. 3.24). Using Sontek's Acoustic Doppler Flow Tracker, the stream flow at both confluences was measured ten times in different months from June 2010 to February 2012. The contribution of both confluences to Kiskatinaw River flow was then calculated by dividing the measured stream flow at a particular confluence at a specific time of the particular day by the total observed flow at Farmington station at the same time on that day. In this way, the contribution of both confluences to Kiskatinaw River flow was calculated on ten occasions. Based on these contribution values, the East and West confluences contribute averagely 27% and 45%, respectively, to Kiskatinaw River flow. Tables 3.6 and 3.7 show the contribution of East and West confluences to Kiskatinaw River flow, respectively.

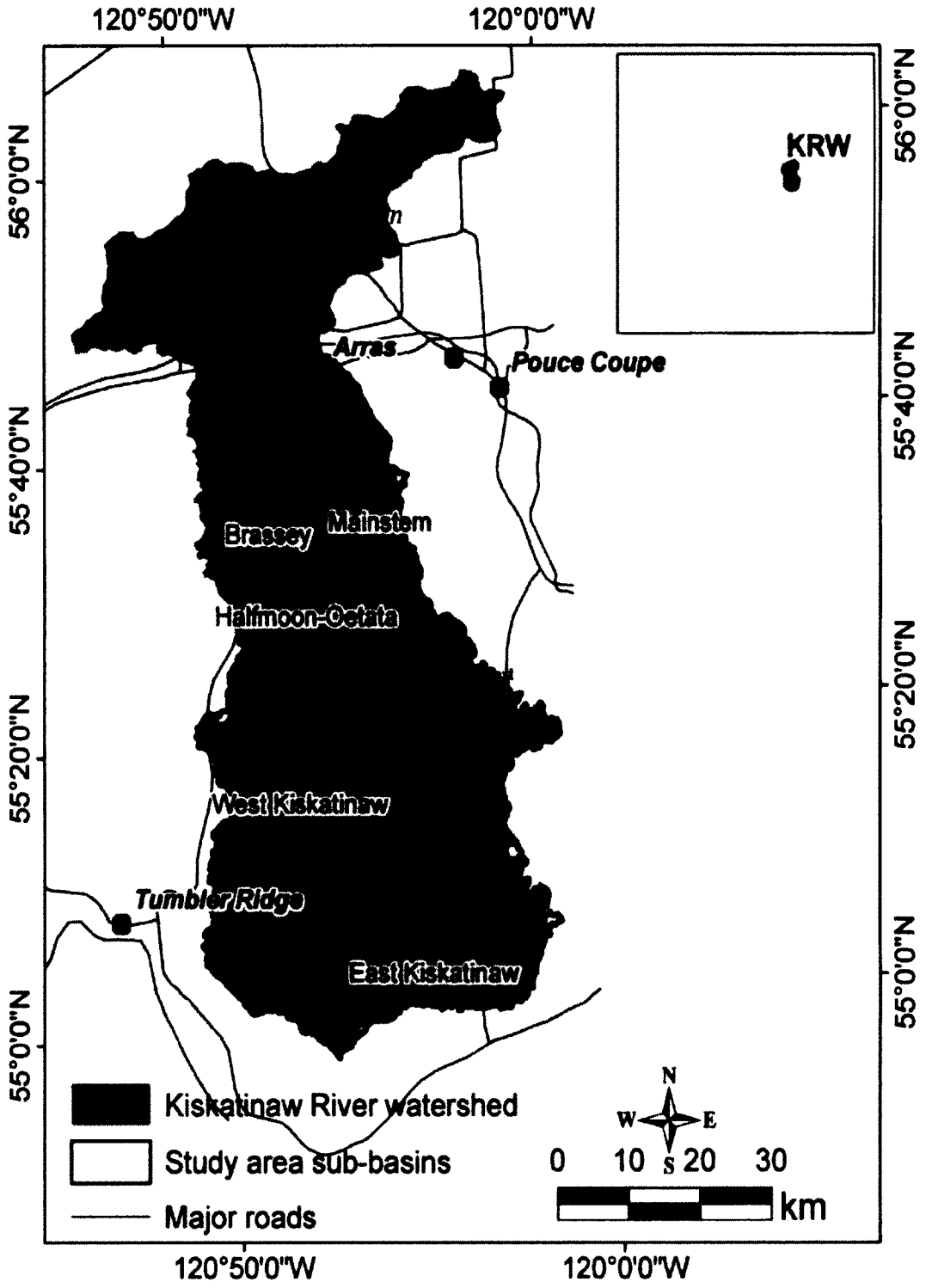

Figure 3.24 Major sub-watersheds and Water Survey Canada station at Farmington in the KRW (modified from Paul, 2013)

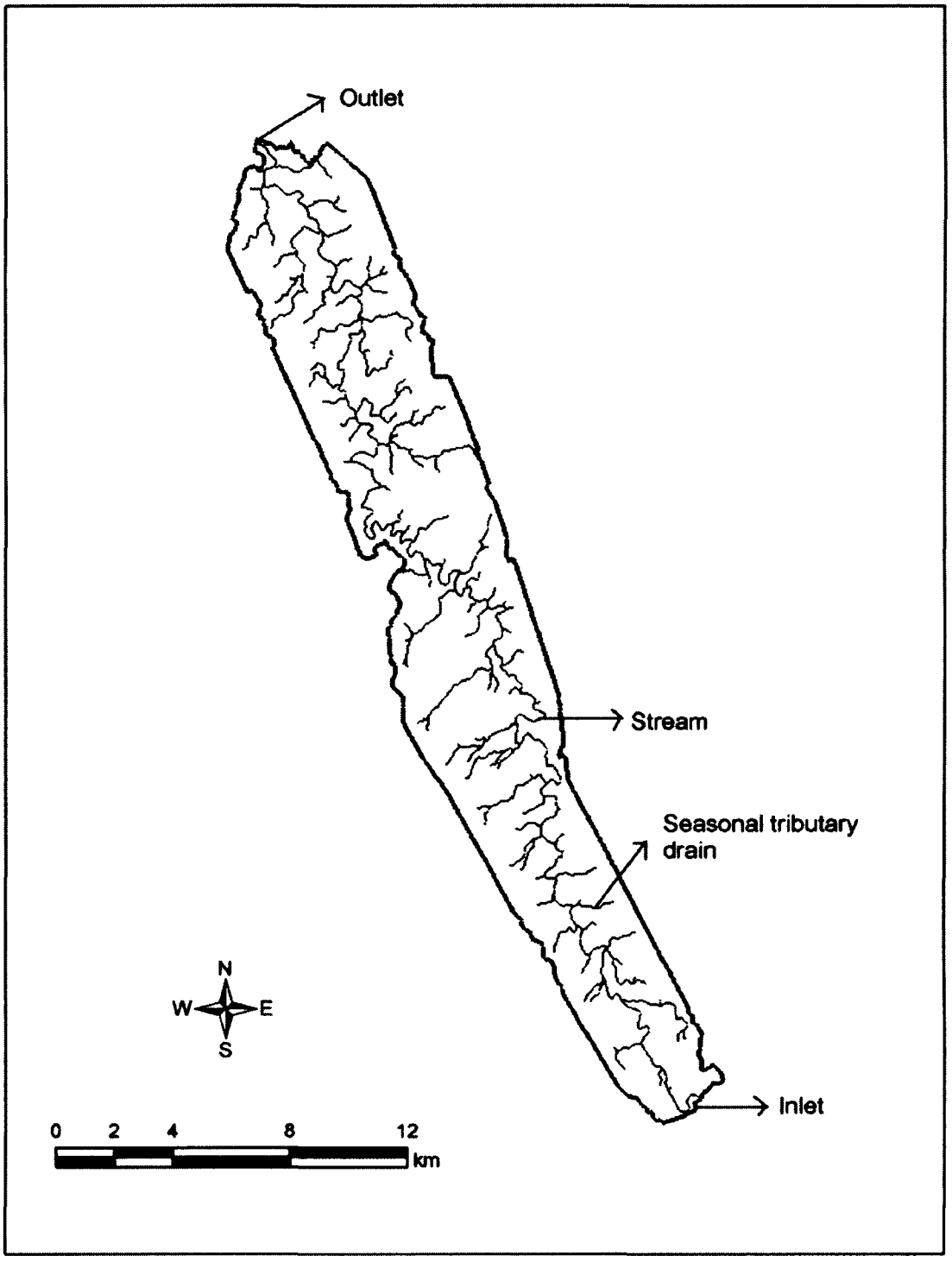

Figure 3.25 Inlet and outlet (i.e., Arras) of the study area

Table 3.6 Contribution of East confluence to Kiskatinaw River flow

Date	Time (24-hr format)	Observed stream flow at Farmington (m^3/s)	Observed stream flow at East confluence (m^3/s)	Contribution of East confluence to Kiskatinaw River flow (%)
15-Jun-2010	11:18	7.72	2.7645	35
16-Jul-2010	14:22	0.829	0.1599	19
3-Sep-2010	11:51	0.52	0.1739	33
17-Oct-2010	8:02	1.121	0.2608	23
28-Jan-2011	10:00	1.121	0.1917	17
3-Apr-2011	9:45	1.727	0.453	26
14-Jun-2011	12:37	17.93	6.0586	33
16-Aug-2011	14:53	3.5	1.4232	40
7-Sep-2011	16:48	2.1	0.6262	29
13-Feb-2012	10:46	0.9	0.1475	16
			Average	27

Table 3.7 Contribution of West confluence to Kiskatinaw River flow

Date	Time (24-hr format)	Observed stream flow at Farmington (m^3/s)	Observed stream flow at West confluence (m^3/s)	Contribution of West confluence to Kiskatinaw River flow (%)
15-Jun-2010	13:17	7.72	2.8284	36
17-Jul-2010	12:03	0.793	0.4042	51
3-Sep-2010	15:58	0.52	0.3961	76
16-Oct-2010	14:44	0.755	0.6084	80
28-Jan-2011	14:51	1.121	0.318	28
3-Apr-2011	11:33	1.727	0.2634	15
15-Jun-2011	8:09	15.93	6.0397	37
15-Aug-2011	13:38	3.65	2.0062	55
7-Sep-2011	13:19	2.1	1.0302	49
12-Feb-2012	12:04	0.9	0.2096	23
			Average	45

Hence the stream flow at the inlet of the study area is 72% of the stream flow at Farmington station, and the remaining 28% flow comes from other sub-watersheds (i.e., Mainstem, Brassey, Halfmoon-Oetata, and other areas). It is also to be noted that due to safety and logistics problems, point stream flow measurements at both confluences were not conducted during spring runoff and high flow seasons. In this study, no-flow condition was

chosen as the groundwater flow boundary condition around the perimeter of the study area for model simplicity. In fact, Kala Groundwater Consulting Ltd. (2001) found a water divide (i.e., no flow boundary condition) on the east side of the Arras area. In addition, groundwater table was not found at Arras site (east bank of Kiskatinaw River) during piezometer installation in late summer 2010, and this indicates a no-flow boundary condition at this site. For stream routing, flux river boundary condition (i.e., a boundary condition in which the cell contains a stream node allows the exchange of water between the stream and groundwater during simulation) was chosen as the groundwater flow boundary condition for stream because a significant amount of water goes into the subsurface (groundwater) flow from stream network. Two major assumptions were considered for developing the model: (1) the soils of KRW were isotropic, and (2) the stream flow at the inlet of the study area was equal to 72% of the stream flow at Farmington station. These assumptions would impact the results compared to those under using the actual information of soil layers in the study area and the temporal stream flow at the inlet.

3.3.7 Model calibration and validation

The model needs to be calibrated before being applied for prediction. The objective of calibration is to determine the parameter set which results in the best fit between the predicted and observed discharge. In this study, automated calibration was chosen, and it uses shuffled complex evolution (SCE) method (Duan et al., 1992). In this method, the minimum and maximum values (i.e., range) of each parameter are needed, and these ranges were collected from literatures and other field results obtained under similar conditions

(Gaiser, 1952; Chow, 1959; Clapp et al., 1978; Rawls et al., 1982; Rawls et al., 1983; Smedema et al., 1983; Minhas et al., 1986; Miller et al., 1998; Celik, 2005; Reynolds et al., 2007; Saskatchewan Ministry of Agriculture, 2008; Hatch et al., 2010). After calibration, the model needs to validate against another set of observed data in order to make sure that model calibration was done properly. The common goodness-of-fit statistics were used to assess the modeling performance during calibration and validation. These statistics were not used directly in the automatic calibration process, but were used after calibration as an additional method of comparison. The coefficient of determination (R^2), coefficient of efficiency (NSE: Nash-Sutcliffe efficiency), percent bias (PBIAS), and RMSE-observations standard deviation ratio (RSR) have been widely used to evaluate the goodness-of-fit of hydrologic models. The R^2 is the square of the Pearson's product moment correlation coefficient and describes the proportion of the total variance in the observed data that can be explained by the model (Legates et al., 1999). It ranges from 0 to 1, with higher values indicating better agreement. It is calculated by the following equation (Legates et al., 1999):

$$R^2 = \left\{ \frac{\sum_{i=1}^{N}\left(Q_i^{obs} - Q_{mean}^{obs}\right)\left(Q_i^{sim} - Q_{mean}^{sim}\right)}{\left[\sum_{i=1}^{N}\left(Q_i^{obs} - Q_{mean}^{obs}\right)^2\right]^{0.5}\left[\sum_{i=1}^{N}\left(Q_i^{sim} - Q_{mean}^{sim}\right)^2\right]^{0.5}} \right\}^2 \qquad (3.1)$$

Where Q_i^{obs} and Q_i^{sim} are the i^{th} observed and simulated stream flow, respectively, and Q_{mean}^{obs} and Q_{mean}^{sim} are the mean observed and simulated stream flow, respectively.

The Nash-Sutcliffe efficiency (NSE) is a normalized statistic that determines the relative magnitude of the residual variance compared to the measured data variance (Nash et al., 1970). It ranges from minus infinity to 1, with higher values indicating better agreement. If

NSE > 0, the model is considered to be a better predictor of system behavior than the mean of the observed data. NSE is calculated by the following equation (Nash et al., 1970):

$$NSE = 1 - \left[\frac{\sum_{i=1}^{N}\left(Q_i^{obs} - Q_i^{sim}\right)^2}{\sum_{i=1}^{N}\left(Q_i^{obs} - Q_{mean}^{obs}\right)^2}\right] \quad (3.2)$$

The percent bias (PBIAS) quantifies the average tendency of the simulated data to be larger or smaller than the observed data (Gupta et al., 1999). The optimal value of PBIAS is 0, with low-magnitude values indicating accurate model simulation. Positive value of PBIAS indicates model underestimation bias, while negative value indicates model overestimation bias. PBIAS is calculated by the following equation (Gupta et al., 1999):

$$PBIAS = \left[\frac{\sum_{i=1}^{N}\left(Q_i^{obs} - Q_i^{sim}\right)*100}{\sum_{i=1}^{N}\left(Q_i^{obs}\right)}\right] \quad (3.3)$$

RMSE-observations standard deviation ratio (RSR) standardizes RMSE (root mean square error) using the standard deviation of observations (Singh et al., 2004), and it combines both an error index and the additional information recommended by Legates et al. (1999). It is calculated by the following equation (Legates et al., 1999):

$$RSR = \frac{RMSE}{\sigma_{obs}} = \frac{\sqrt{\sum_{i=1}^{N}\left(Q_i^{obs} - Q_i^{sim}\right)^2}}{\sqrt{\sum_{i=1}^{N}\left(Q_i^{obs} - Q_{mean}^{obs}\right)^2}} \quad (3.4)$$

Where RMSE is root mean square error, and σ_{obs} is the standard deviation of observed stream flow. RSR varies from the optimal value of 0, which indicates zero RMSE or residual variation, and therefore, perfect model simulation. Lower RMSE means lower RSR, and therefore, better model simulation results.

Generally, the GSSHA model is calibrated and validated using observed stream flow. In this study, the GSSHA model was calibrated and validated using observed stream flow, groundwater table, and groundwater contribution to stream flow (i.e., base flow index).

3.3.7.1 Using stream flow

The ideal calibration needs 3 to 5 years of observation data, which consists of a sufficient range of hydrologic events to activate all model constituent processes during calibration (Gan et al., 1997). If such data is not available, Gupta et al. (1999) suggested that the available data should be separated into two data sets: "above-mean" flows (wet years) and "below-mean" flows (dry years). In this study, the land use map for year 2010, and the groundwater table elevation data from October 15th, 2010 to February 12th, 2012 were available. However, the steam flow data at Farmington Water Survey Canada station during January 2012 was not available. As a result, the calibration and validation were conducted using observed data from October 15th, 2010 to December 31st, 2011. During this period, the land use map of year 2010 was used due to the unavailability of land use map for year 2011. The difference between stream flow at Arras and the inlet of the study area (i.e., 72% of the stream flow at Farmington station) was used as observed stream flow at the outlet of the study area. From October 15th, 2010 to December 31st, 2011, the mean stream flow was 6.05 m^3/s. Based on

this number and the suggestion of Gupta et al. (1999), this observed time period was divided into two data sets: one from October 15th, 2010 to April 6th, 2011, which is below mean flow (i.e., 0.36 m^3/s) for calibration, and the another from April 7th, 2011 to December 31st, 2011, which is above mean flow (i.e., 9.74 m^3/s) for validation. A simulation time step of 1 minute was used for calibration and validation based on the temporal convergence study of observed and simulated stream flows at the outlet of the study area.

Fig. 3.26 shows the GSSHA model calibration results. The results show that there are some discrepancies between observed and simulated stream flows in terms of their trends during the periods from late Oct to late Nov, 2010, and from late Dec, 2010 to mid-Jan, 2011. The first discrepancy (from late Oct to late Nov, 2010) may have occurred because the model was at rest (stationary) before model simulation, thus producing the perturbation of outputs during the initial stage of model simulation. The second discrepancy may have occurred because of the consideration of stream flow at the inlet of the study area to be equal to 72% of the stream flow at Farmington station, which was found as a mean value of only 10 point stream flow measurements. The calibration obtained the following statistics: R^2= 0.67, NSE= 0.62, PBIAS= 9.2% and RSR= 0.54. Santhi et al. (2001) and Van Liew et al. (2003) mentioned that a R^2 value of greater than 0.5 is acceptable for model evaluation. US EPA (2007) stated that a R^2 value between 0.6 and 0.7 can show fair performance for hydrologic models. Moriasi et al. (2007) reported that numerical model simulation can be judged as satisfactory if NSE>0.5, RSR<0.7, and PBIAS<25%. Based on these evaluation statistics criteria, the GSSHA model calibration is deemed as satisfactory.

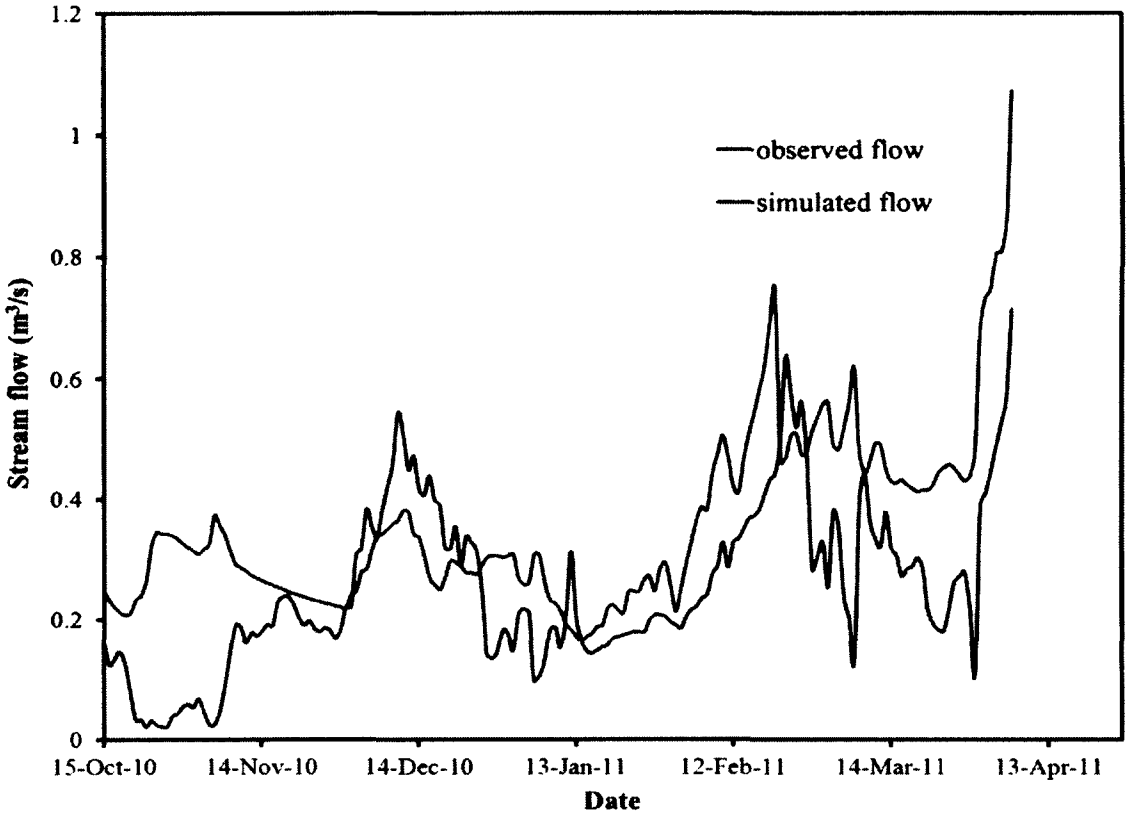

Figure 3.26 Observed and simulated stream flows at the outlet of the study area during calibration

Fig. 3.27 shows the modeling validation results, with R^2= 0.63, NSE= 0.58, PBIAS= 10.1%, and RSR= 0.6. As a result, satisfactory model validation was achieved.

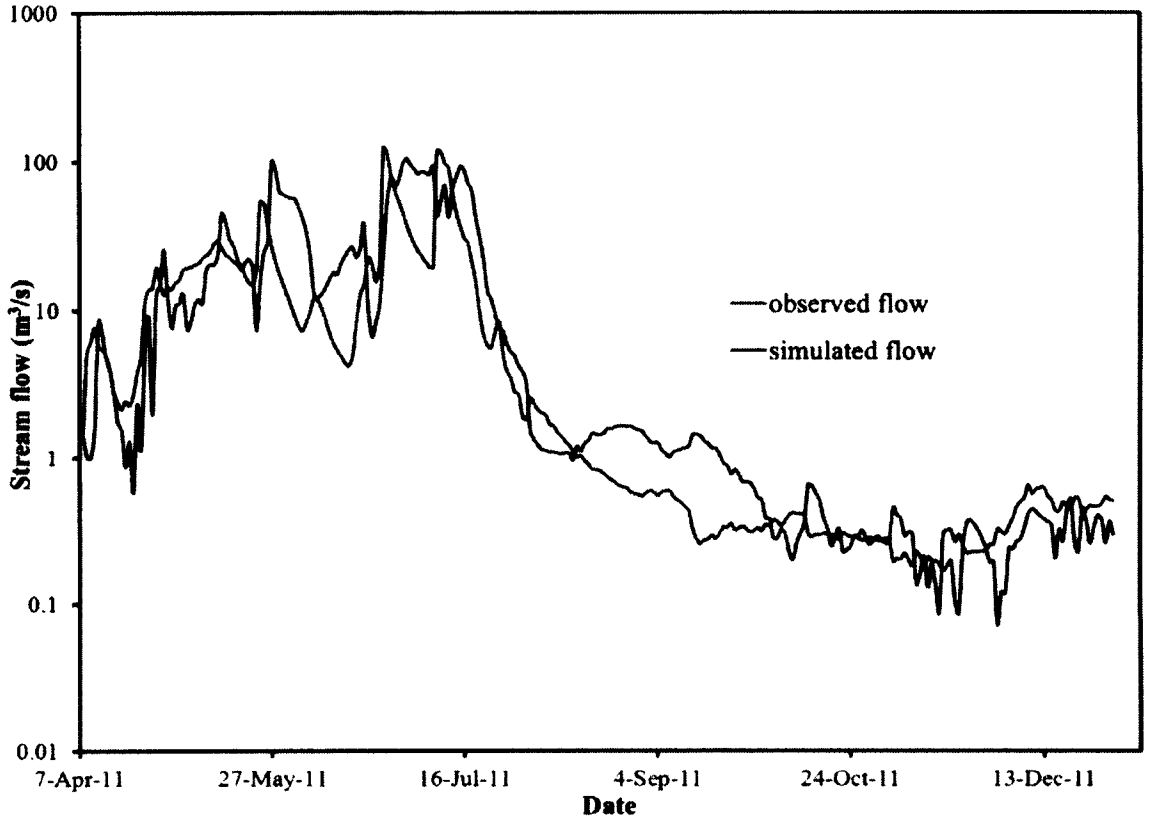

Figure 3.27 Observed and simulated stream flows at the outlet of the study area during validation

Another approach of calibration and validation was used assuming constant land use/land cover in the study area during the last several years. Similar approach was used in model calibration and validation in various GW-SW interaction studies (e.g., Krause et al., 2004; Van Roosmalen et al., 2007; Van Roosmalen et al., 2009; Jackson et al., 2011; Dams et al., 2012; Vansteenkiste et al., 2012). In this study, the calibration was conducted for the time period from October 15th, 2010 to December 31st, 2011, and the validation was performed for the time period from October 15th, 2006 to October 15th, 2010 using observed stream flow data collected from Farmington Water Survey Canada station. This validation is similar to

hindcasting, opposite of forecasting. Fig. 3.28 shows the calibration results, with R^2= 0.65, NSE= 0.61, PBIAS= 8.4 %, and RSR= 0.56, indicating satisfactory performance.

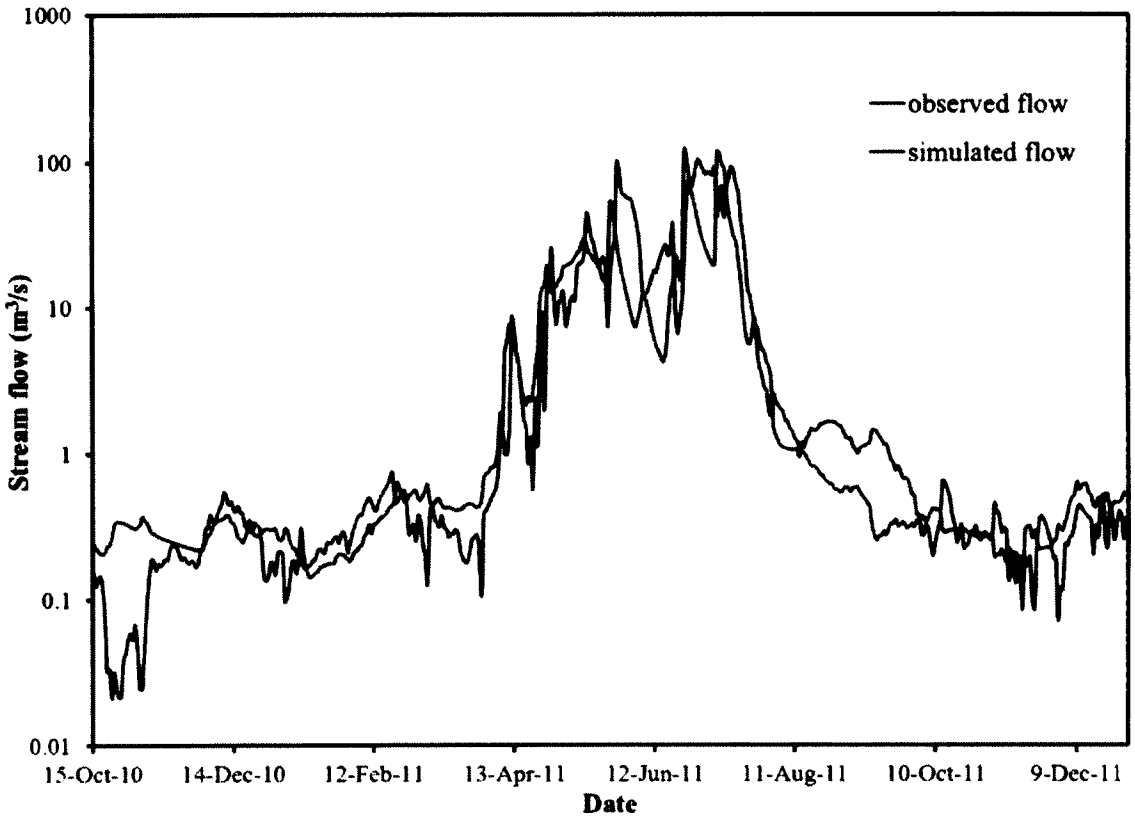

Figure 3.28 Comparison of observed and simulated stream flows at the outlet of the study area during calibration

Fig. 3.29 shows the validation results, with R^2= 0.62, NSE= 0.59, PBIAS= 13.8%, and RSR= 0.61. It also indicates satisfactory modeling performance. All the calibrated parameters in the GSSHA model and their values are listed in Table 3.8.

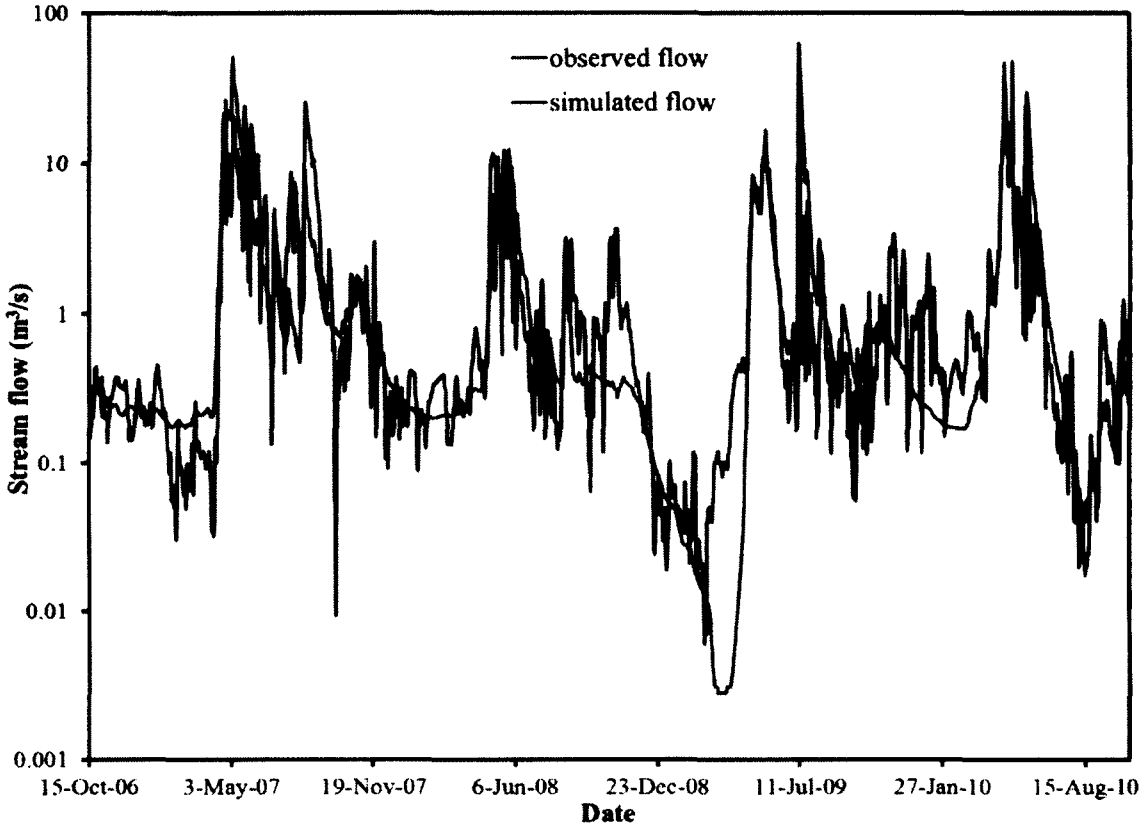

Figure 3.29 Comparison of observed and simulated stream flows at the outlet of the study area during a 4-year validation period

Table 3.8 Calibrated parameters' values used in the GSSHA model

Process	Process Parameter	Unit	Value
Infiltration	Saturated hydraulic conductivity (Ks)-clay loam/forest	cm/hr	0.15
Infiltration	Ks-clay loam/built-up area	cm/hr	0.03
Infiltration	Ks-clay loam/forest clear cut area	cm/hr	0.08
Infiltration	Ks-clay loam/agriculture	cm/hr	0.10
Infiltration	Ks-clay loam/wetland	cm/hr	0.05
Infiltration	Ks-sandy loam/forest	cm/hr	0.93

Infiltration	Ks-sandy loam/forest clear cut area	cm/hr	0.34
Infiltration	Ks-sandy loam/agriculture	cm/hr	0.42
Infiltration	Ks-silt loam/forest clear cut area	cm/hr	0.7
Infiltration	Ks-silt loam/forest	cm/hr	0.81
Infiltration	Ks-silt loam/built-up area	cm/hr	0.09
Infiltration	Initial moisture-clay loam	-	0.21
Infiltration	Initial moisture-silt loam	-	0.15
Infiltration	Initial moisture-sandy loam	-	0.11
Overland flow	Manning's n - built-up area	-	0.011
Overland flow	Manning's n-agriculture	-	0.035
Overland flow	Manning's n-forest	-	0.1
Overland flow	Manning's n-forest clear cut	-	0.03
Groundwater	Porosity-silt loam	-	0.501
Groundwater	Porosity-clay loam	-	0.464
Groundwater	Porosity-sandy loam	-	0.453
Channel flow	Manning's n - river	-	0.025
Soil moisture	Soil moisture depth	m	0.5
Groundwater-channel	Ks - stream bed material	cm/hr	1.1
Groundwater-channel	Stream bed material's thickness	cm	15
Retention	Retention depth-agriculture	mm	0.1
Retention	Retention depth-forest	mm	0.12
Retention	Retention depth-forest clear cut	mm	0.1

3.3.7.2 Using groundwater table

The GSSHA model was also calibrated and validated using observed mean daily groundwater table at one bank piezometer in the study area from September 21st, 2011 to December 31st, 2011. The comparison of mean daily measured and simulated groundwater tables at that piezometer during calibration and validation is shown in Fig. 3.30. The calibration was done from September 21st, 2011 to November 10th, 2011, with R^2= 0.59 (Fig. 3.31), NSE= 0.56, PBIAS= -16.9% and RSR= 0.66 being obtained. The validation was performed for the period from November 11th, 2011 to December 31st, 2011, with R^2= 0.91 (Fig. 3.32), NSE= 0.52, PBIAS= -23.9%, and RSR= 0.45 being found.

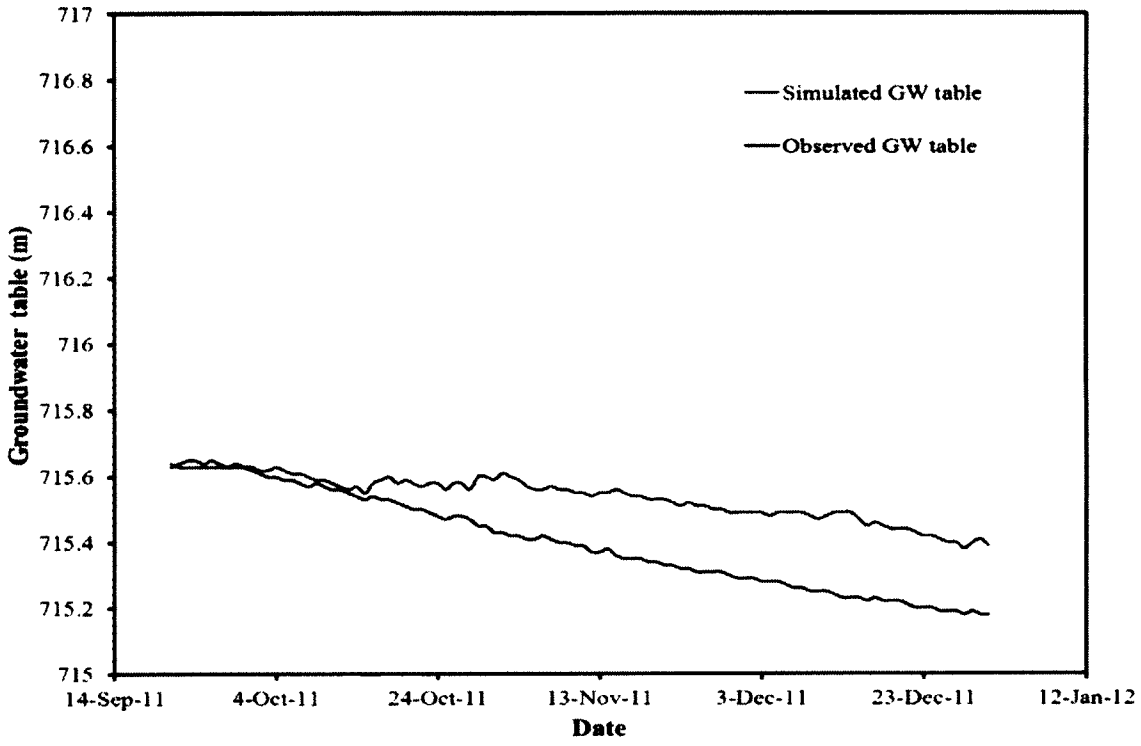

Figure 3.30 Comparison of mean daily measured and simulated groundwater tables at one piezometer in the study area during calibration and validation

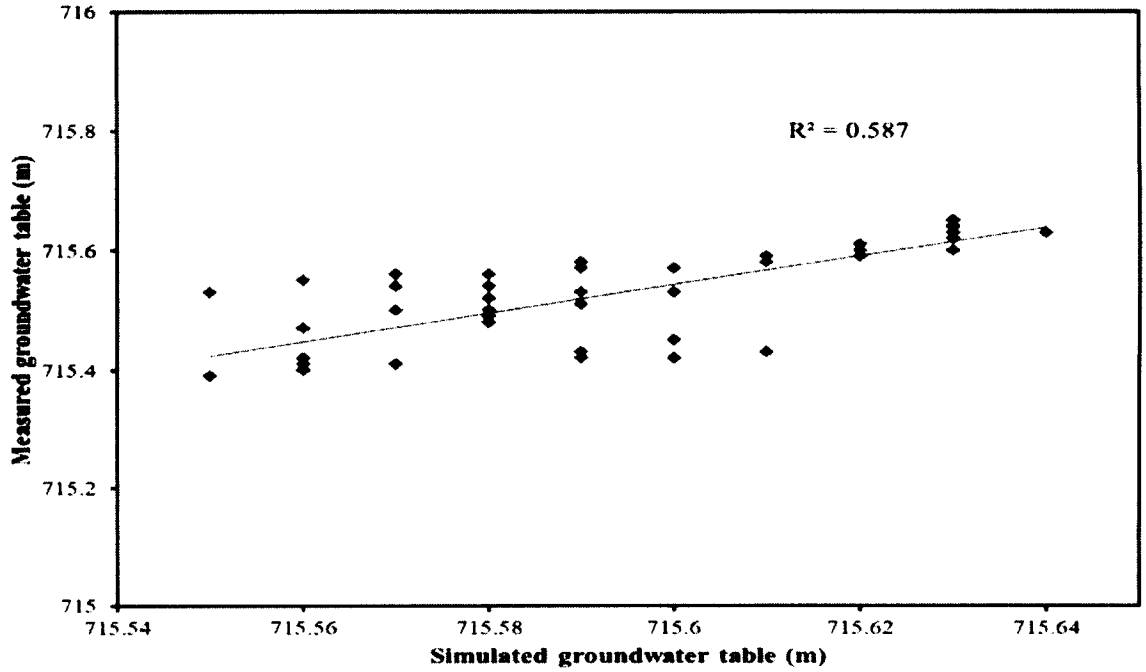

Figure 3.31 Comparison of mean daily measured and simulated groundwater tables at one piezometer in the study area during calibration

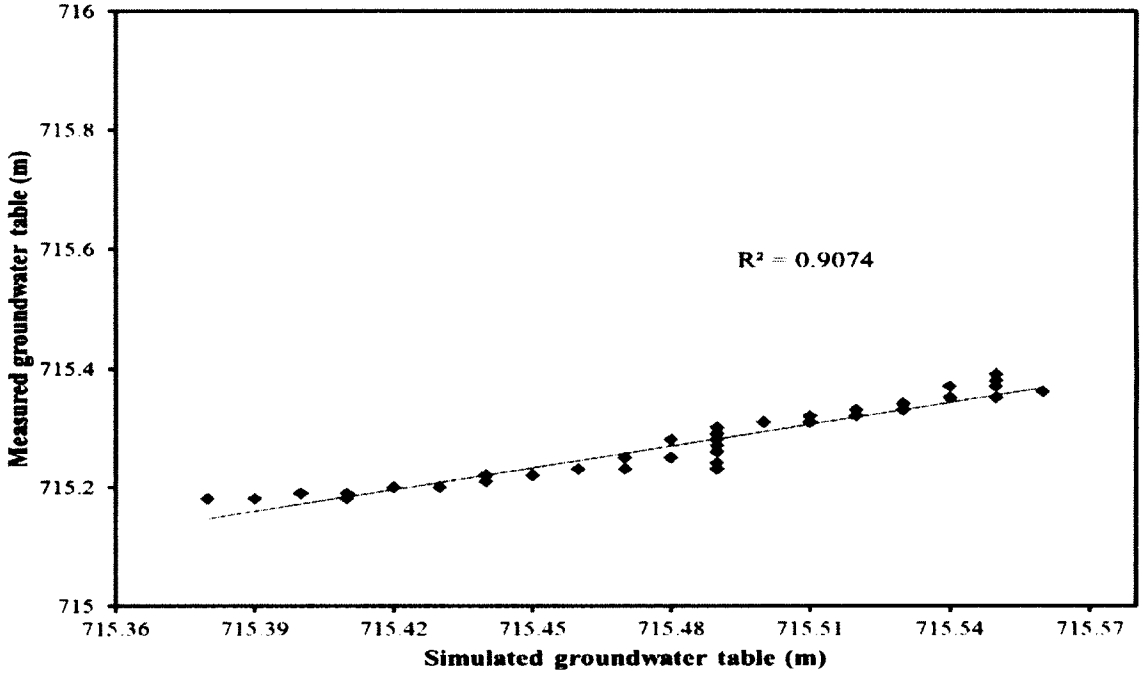

Figure 3.32 Comparison of mean daily measured and simulated groundwater tables at one piezometer in the study area during validation

3.3.7.3 Using groundwater contribution to stream flow

The GSSHA model was also calibrated and validated using the calculated mean monthly groundwater contribution to stream flow based on the PART base flow separation program of the USGS (Rutledge, 1998). In the PART program, groundwater contribution to stream flow is expressed as a base flow index. This program estimates daily base flow by considering it to be equal to stream flow on days that fit a requirement of antecedent recession, and then linearly interpolating it for other days in the stream flow record. Based on these daily values, the mean monthly groundwater contribution to stream flow was calculated. On the other hand, the GSSHA model estimates monthly total volume of stream discharge (flow) and groundwater discharge, and based on those values the mean monthly groundwater contribution to stream flow was calculated (Downer et al., 2006). The calculated groundwater contribution to stream flow in the study area by PART program for the period of January 2007 to December 2009 was used for GSSHA model calibration, with R^2= 0.92 and NSE= 0.74. The PART-calculated groundwater contribution to stream flow in the study area for the period from January 2010 to December 2011 was used for GSSHA model validation, with R^2= 0.71 and NSE= 0.55. As a result, the developed GSSHA model holds satisfactory modeling performance. The comparison of mean monthly groundwater contribution to stream flow from January 2007 to December 2011 calculated by the PART program and simulated by GSSHA model is shown in Fig. 3.33.

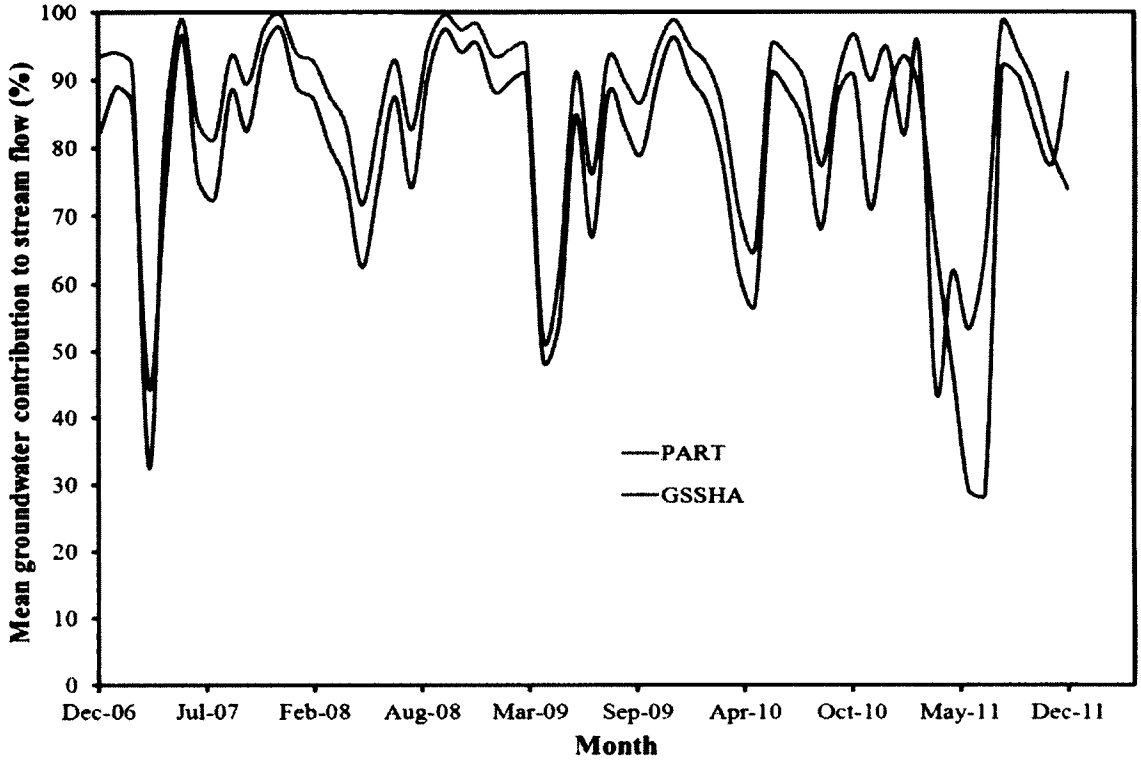

Figure 3.33 Comparison of mean monthly groundwater contribution to stream flow calculated by the PART program and simulated by the GSSHA model

CHAPTER 4

GENERATION OF CLIMATE AND LAND USE/LAND COVER CHANGE SCENARIOS

4.1 Background

In order to investigate GW-SW interaction in the study area under the impact of climate and land use changes, it is necessary to generate future climate and land use/land cover change scenarios. The climate change scenarios were generated for the KRW because of the small size of the study area compared to the grid size of the Canadian Regional Climate Model, and the lack of available climatic data in the study area. This chapter details the generation of future climate and land use/land cover change scenarios.

4.2 Generation of future climate change scenarios

In this study, future climate scenario (i.e., precipitation and temperature) data for the KRW were collected from the CRCM 4.2 (Canadian Regional Climate Model) of CCCma (Canadian Centre for Climate Modeling and Analysis) for a short-term period from 2012 to 2016 and a long-term period from 2020 to 2040. The short-term period was used to understand the annual dynamics of climate change, and to make a comparison of GW-SW interactions between the effect of climate change and the effect of combined climate and land use/land cover (LULC) changes scenarios. On the other hand, the long-term period was

chosen to provide long-term future climate prediction. The climate data from the CRCM is in the form of monthly means of climatic variables under different greenhouse gas (GHG) emission scenarios. These monthly mean values can be converted to daily values in a particular month using downscaling method. With a 45-km horizontal grid-size mesh, the CRCM is based on the MC2 (Mesoscale Compressible Community) dynamical kernel, which uses the semi-implicit and semi-Lagrangian (SISL) numerical integration scheme to solve the fully elastic and non-hydrostatic Euler field equations (Bergeron et al., 1994).

4.2.1 Downscaling of future climate data

The general circulation models (GCMs) are useful tools to explore the likelihood of plausible future climate changes. The ability of these models to provide reliable simulations of climate at a global scale is continuously increasing, and their projections of future climate conditions are becoming more consistent (van Roosmalen et al., 2010). However, due to the broad scale at which they operate, only a coarse representation of topography, land-sea contrast, and land cover is included. Their simulation ability of fine-scale atmospheric circulations is limited. Thus, a number of methods have been used to downscale the GCM data, including statistical and dynamical methods (Fowler et al., 2007). Dynamical downscaling uses regional climate models (RCMs) or limited-area models, which use lateral boundary conditions and sea surface temperatures (SSTs) from GCM as initial atmospheric conditions. The advantage of using dynamically downscaled climate data is that the variables are downscaled coherently. In addition, the dynamic downscaling is physically based, but is computationally intensive. The use of RCMs has increasingly gained interest in recent years

and the ability of RCMs to reproduce the present-day climate has substantially improved (Xu et al., 2005; van Roosmalen et al., 2010). Moreover, recent developments have resulted in RCM outputs with higher resolutions, and this is important for hydrological impact studies. The higher resolution of RCMs compared to GCMs makes it possible to realistically simulate regional climate features, such as orographic precipitation, extreme events, and regional scale climate anomalies, or non-linear effects (Fowler et al., 2007).

In statistical downscaling, the relationship between the simulated and observed climate variable is determined independently for each variable (Fowler et al., 2007). The advantage of using statistical downscaling is that it is comparatively cheap, and computationally efficient. Many statistical downscaling techniques have been developed to convert large-scale GCM and RCM outputs into results at a finer resolution. The simplest way is to apply GCM and RCM scale projections in the form of change factors (CFs) through the 'perturbation method' (Prudhomme et al., 2002) or 'delta-change' approach. Differences between the control and future GCM/RCM simulations are applied to baseline observations by simply adding or scaling the mean climatic CF to each day. As a result, it can be rapidly applied to several GCM/RCM outputs to produce a range of climate scenarios. However, this method has a number of limitations. Firstly, it assumes that GCM/RCM can simulate more accurately for the relative change than the absolute values, i.e., assuming a constant bias through time. Secondly, CFs only downscale the mean, maxima, and minima of climatic variables, ignoring change in variability and assuming a constant spatial pattern of climate (Diaz-Nieto et al., 2005). Moreover, for precipitation, the temporal sequence of wet days is assumed to be unchanged, but the variation in wet and dry spells may be an important component of climate change.

4.2.2 Delta change method

Delta change method has been commonly applied to cope with biases when using climate model outputs in hydrological impact studies (Hay et al., 2000; Xu et al., 2005). It is a simple way of transferring the change in a climatic variable simulated by climate model to an observed data set by using delta change factors. This method has been used for hydrological impact assessments in Scandinavia (e.g., Bergström et al., 2001; Andreasson et al., 2004; Graham, 2004; Graham et al., 2007; van Roosmalen et al., 2007). It consists of altering an observed database of climatic variables with delta change factors to obtain a database for the future (scenario). In this study, the monthly delta change values for precipitation and temperature were determined for the watershed scale from the CRCM 4.2 simulation outputs because these outputs are from a 45-km horizontal grid-size mesh (Bergeron et al., 1994). Absolute changes were used for temperature because it is a state variable and not a flux, whereas the relative change factors were applied for precipitation because it is a flux (van Roosmalen et al., 2010). For temperature, the procedure of delta change method is as follows:

$$T_{\Delta}(i,j) = T_{obs}(i,j) + \Delta_T(j) \quad , \ i = 1, 2 \ldots .31; j = 1, 2 \ldots 12 \qquad (4.1)$$

where T_{Δ} is the temperature input for the future hydrological scenario simulation, T_{obs} is the observed temperature in the historical period, (i, j) stand for day and month, respectively, and Δ_T is the change in temperature. This $\Delta_T$value is calculated by Eq. 4.2.

$$\Delta_T(j) = \overline{T}_{scen}(j) - \overline{T}_{ctrl}(j) \qquad j = 1, 2, 3 \ldots 12 \qquad (4.2)$$

where $\overline{T}_{ctrl}\ (j)$ is the mean daily temperature for month j and it is calculated as the mean of temperature of all days in month j for all 12 years of the reference (i.e., control) period; $\overline{T}_{scen}\ (j)$ is the mean daily temperature for month j of each particular year from 2012 to 2016 (i.e., short-term). The indices "scen" and "ctrl" stand for the scenario period (2012-2016) and the control period (2000-2011), respectively. This led to 12 monthly delta change values for each year from 2012 to 2016, and they were used to adjust the observed daily temperature within the individual months for future temperature input.

For precipitation, the delta change method can be described as follows:

$$P_{\Delta}\ (i,j) = \Delta_p\ (j) * P_{obs}(i,j) \quad , \ \text{i} = 1, 2 \ldots.31; \text{j} = 1, 2 \ldots 12 \tag{4.3}$$

where P_{Δ} is the precipitation input for the future hydrological scenario simulation, P_{obs} is the observed precipitation in the historical period, (i, j) stand for day and month, respectively, and Δ_p is the change in precipitation, which can be calculated by:

$$\Delta_p\ (j) = \frac{\overline{P}_{scen}\ (j)}{\overline{P}_{ctrl}\ (j)}, \ \text{j} = 1, 2 \ldots 12 \tag{4.4}$$

where $\overline{P}_{ctrl}\ (j)$ is the mean daily precipitation for month j and it is calculated as the mean of precipitation of all days in month j for all 12 years of the control period, and $\overline{P}_{scen}\ (j)$ is the mean daily precipitation for month j of each particular year from 2012 to 2016. The indices "scen" and "ctrl" stand for the scenario period (2012-2016) and the control period (2000-2011), respectively. Similar downscaling approaches for precipitation and temperature were used in the long-term period (2020-2040) scenarios.

One of the advantages of the delta change method is that a bias correction of the RCM data is not necessary because the change in variables between the scenario and the control

period is used, and the bias is assumed to be equal for both the control and scenario simulations. Another advantage is that an observed database is used as the baseline resulting in a consistent set of scenario data, whereas the use of climate model output directly could result in unrealistic dynamics in input variables due to climate model variance. On the other hand, the use of an observed database is also a drawback of this method because information on the changes in variability and extremes in the future climate simulated by climate model is lost. As a result, the delta change method is more applicable for impact studies on groundwater systems than surface water systems because groundwater systems are more sensitive to changes in means than to changes in extremes (van Roosmalen et al., 2010).

4.2.3 Future climate change scenarios

In this study, precipitation and temperature for the short-term (2012-2016) and long-term (2020-2040) periods were downscaled from CRCM 4.2 modeling outputs using the delta change method under two types of greenhouse gas (GHG) emission scenarios of SRES (Special Report on Emissions Scenarios) of the Intergovernmental Panel on Climate Change (IPCC) (IPCC, 2000), namely the A2 and B1 scenarios. The A2 scenario was chosen because it represents regional economic development, and in the KRW, the large-scale shale gas exploration/production activities began in 2005, and enhances regional economy (British Columbia Ministry of Energy and Mines, 2012). On the other hand, the B1 scenario was chosen because it describes a more integrated and environmental friendly world. The details of all GHG emission scenarios are presented in Table 4.1.

Table 4.1 GHG emission scenarios (IPCC, 2000)

Emission scenario	Description
A1	• The A1 scenario describes a convergent world that becomes more homogeneous with increased social and cultural interactions • Very rapid economic growth • Global population reaches peak in 2050 and then gradually decreases • Quick introduction of new and more efficient technologies • The A1 scenario is divided into 3 subsets based on their energy sources: fossil intensive (A1FI), non-fossil intensive (A1T), and balanced of all sources (A1B)
A2	• The A2 scenario describes a very heterogeneous world with self-reliance and preservation of local identities • Economic development is regionally oriented • Global population is increasing continuously • More fragmented and slower technological change than other scenarios.
B1	• The B1 scenario describes a more integrated and environmental friendly world • Rapid change in economic structures in service and information economy due to the reduction of material intensity and the introduction of clean and resource-efficient technologies • Emphasis is given on global solutions to economic, social and environmental sustainability • Global population that peaks in mid-century and thereafter declines.
B2	• The B2 scenario describes a heterogeneous world • Emphasis on local solutions to economic, social and environmental sustainability. • Global population increases continuously but at a lower rate than under the A2 scenario • Less rapid and more diverse technological changes than under the A1 and B1 scenarios.

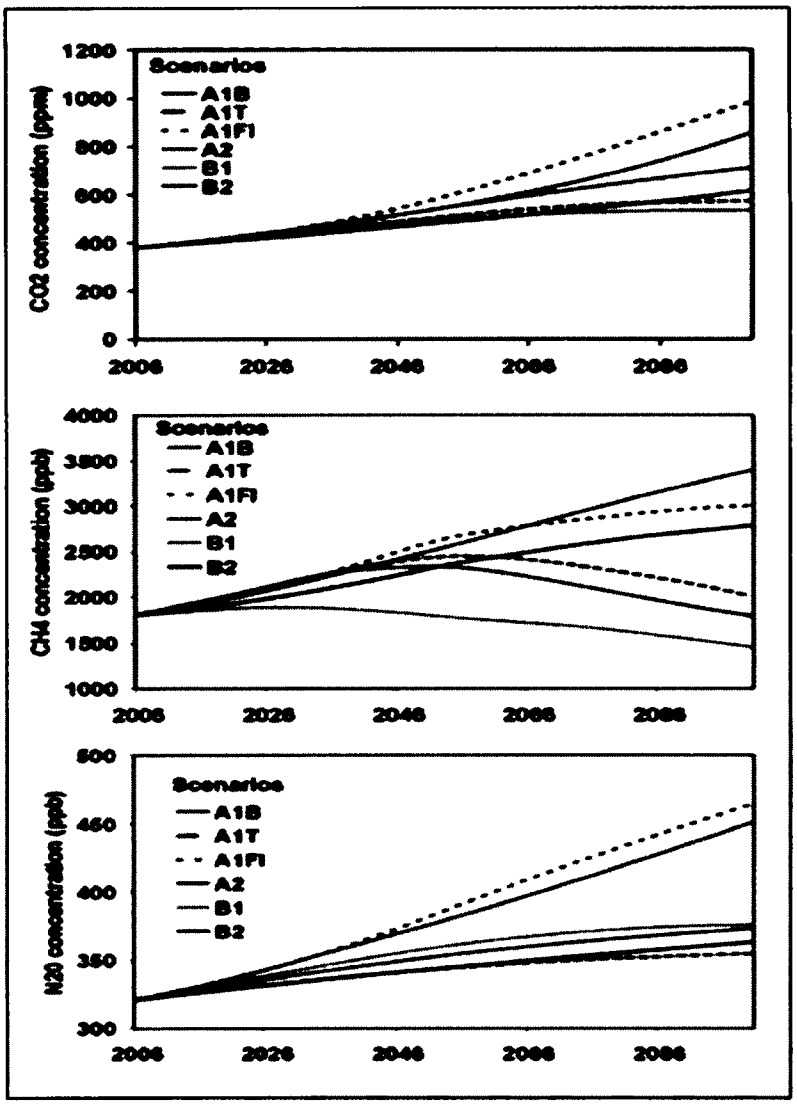

Figure 4.1 Projected trends of the atmospheric concentrations of three greenhouse gases: carbon dioxide (CO_2), methane (CH_4), and Nitrous oxide (N_2O) over the 21st century (taken from US EPA, 2011)

Emission scenarios predict future GHG emissions, which is one of the reasons for global warming (IPCC, 2007). Fig. 4.1 shows the projected trends of the atmospheric concentrations of three greenhouse gases over the 21st century: carbon dioxide (CO_2), methane (CH_4), and Nitrous oxide (N_2O). These GHG emission scenarios are used in GCMs as radiative forcing

to produce climate change scenarios for specific climate variable (e.g., precipitation, temperature). According to IPCC (2000), none of the SRES scenarios are more likely to occur than others. Hence none of the SRES scenarios represent a "best guess" for future emissions. In this study, the A2 and B1 scenarios were considered to show the variable impacts of future climate changes on GW-SW interaction.

4.2.3.1 Precipitation

4.2.3.1.1 Short-term

The future predicted monthly precipitations of KRW from 2012 to 2016 (short-term) under the A2 and B1 GHG emission scenarios using the delta change method are presented in Figs. 4.2 and 4.3, respectively. Fig. 4.2 shows that the trend of monthly precipitations is not the same in every year under the A2 scenario due to increase in the atmospheric concentrations of greenhouse gases (GHGs), especially carbon dioxide (CO_2), methane (CH_4), and Nitrous oxide (N_2O) (IPCC, 2000, 2007). The peak monthly precipitation shifts annually, and it falls between June and August, most commonly in July. Under the B1 scenario (Fig. 4.3), similar trends are found. From the comparison of projected mean monthly precipitations under both scenarios from 2012 to 2016 with respect to the mean monthly precipitations of 2000-2011 (Fig. 4.4), it is found that the peak monthly precipitation under both scenarios shifts to July rather than remaining on the trend of mean monthly precipitations of 2000-2011. It is also found that with the exception of February, May, and December, the mean monthly precipitations are higher under the A2 scenario than under the B1 scenario.

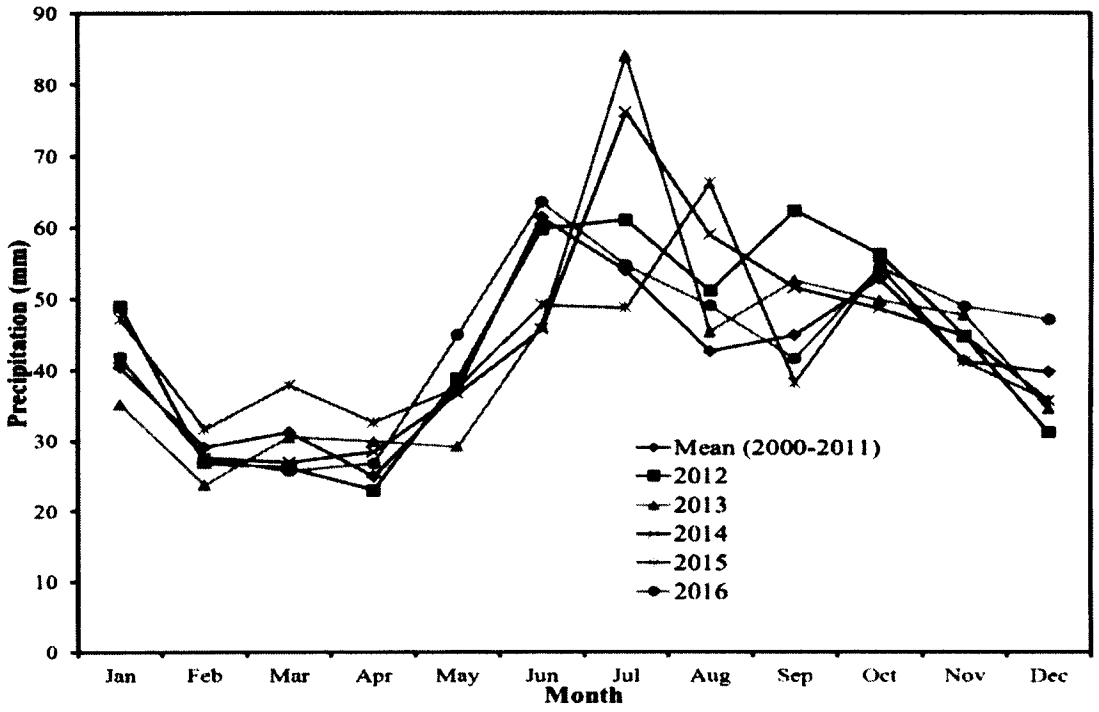

Figure 4.2 Projected monthly precipitations of KRW from 2012 to 2016 under A2 scenario

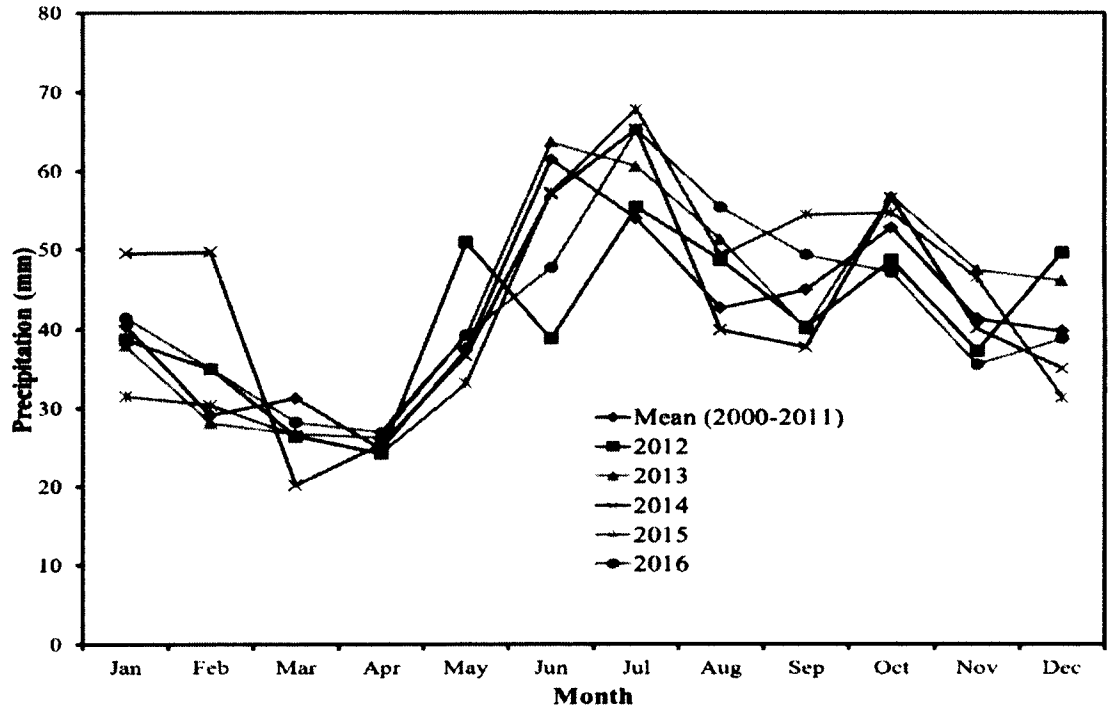

Figure 4.3 Projected monthly precipitations of KRW from 2012 to 2016 under B1 scenario

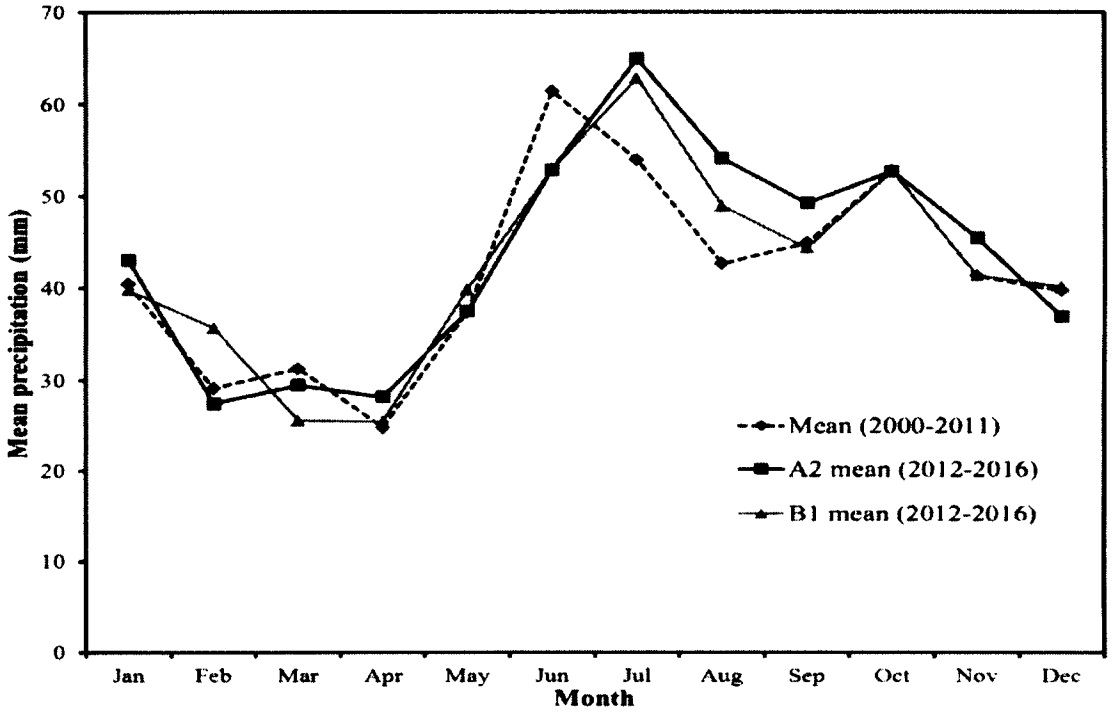

Figure 4.4 Comparison of projected mean monthly precipitations under A2 and B1 scenarios from 2012 to 2016 with respect to the mean monthly precipitations of 2000-2011

When the annual precipitations from 2012 to 2016 are compared to the mean annual precipitation of 2000-2011, it is found that precipitation increases every year under both scenarios, except in 2012 for the B1 scenario (Fig. 4.5). The increase of annual precipitation under the A2 scenario is between 2% and 6%, while the most and least increases are found in 2012 and 2013, respectively. On the other hand, under the B1 scenario, the increase of annual precipitation is between 1% and 5%, while the most and least increases are expected in 2013 and 2015, respectively. In 2012, the annual precipitation decreases by 1% as compared to the mean annual precipitation of 498 mm in 2000-2011. The mean annual precipitation of 2012-2016 under the A2 and B1 scenarios is 522 mm (standard deviation, σ=8 mm) and 510 mm (σ=11 mm), respectively, and these numbers are above the mean annual precipitation of 2000-2011 by 24 mm (5%) and 12 mm (2.5%), respectively.

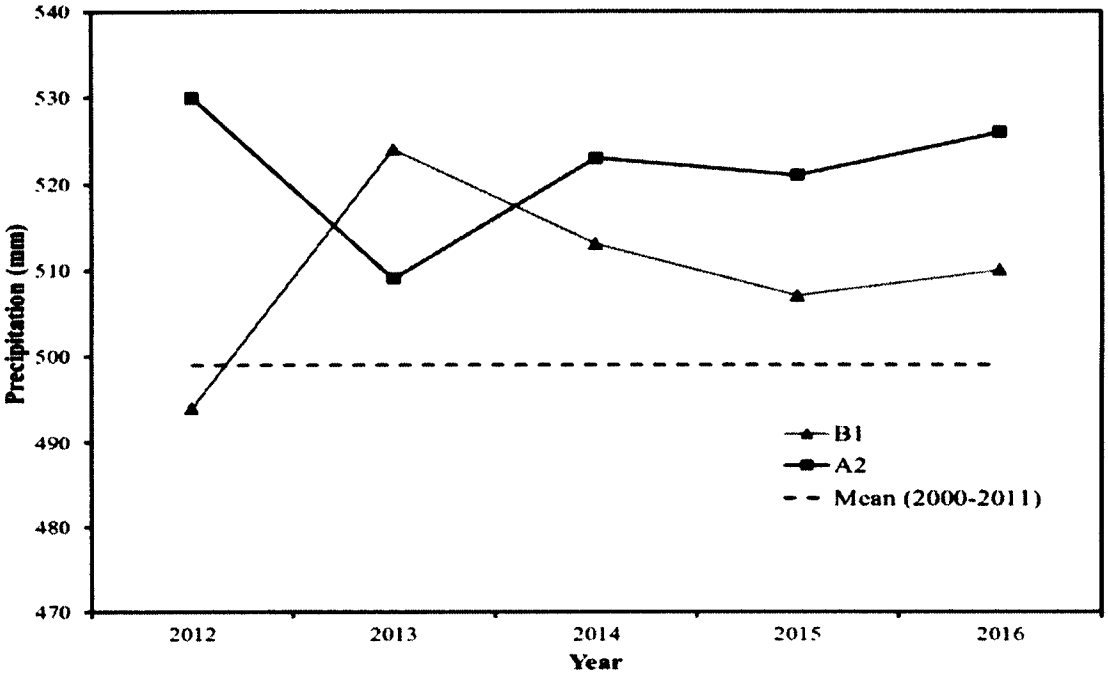

Figure 4.5 Projected annual precipitation of KRW from 2012 to 2016 under A2 and B1 scenarios

When the seasonal precipitations from 2012 to 2016 under the A2 scenario are compared to the mean seasonal precipitations of 2000-2011, it is found that summer (i.e., June to August) precipitation increases every year with a rate of 4% to 14% with respect to the mean summer precipitation of 2000-2011 (Fig. 4.6). The most and least increases are expected in 2014 and 2015, respectively. The mean precipitation from 2000 to 2011 in winter, spring, summer, and fall are 109 mm, 93 mm, 158 mm, and 138 mm, respectively. Conversely, in winter (i.e., December to February), precipitation decreases from 2012 to 2014 with a rate of 1% (i.e., in 2013) to 4% (i.e., in 2014), and then increases from 2015 (by 5%) to 2016 (by 6%). Spring (i.e., March to May) precipitation follows the similar trend of winter precipitation, with a decrease from 2012 to 2014 by a rate of 1% (i.e., in 2014) to 6% (i.e., in 2012), and then an increase from 2015 (by 15%) to 2016 (by 4%). In fall (i.e., September to November), precipitation increases from 2012 to 2014 with a rate of 2% (i.e., in 2012) to 8%

(i.e., in 2013), and then decreases in 2015 by 3%, and increases again in 2016 by 4%. On average, the mean winter, spring, summer, and fall precipitations from 2012 to 2016 under the A2 scenario are 111 mm (σ=9 mm), 95 mm (σ=8 mm), 172 mm (σ=7 mm), and 144 mm (σ=11 mm), respectively. This indicates that the mean winter, spring, summer, and fall precipitations from 2012 to 2016 under the A2 scenario increase by 2 mm (1.5%), 2 mm (2%), 14 mm (9%), and 6 mm (3.5%), respectively, with respect to the mean winter, spring, summer, and fall precipitations from 2000 to 2011. Due to the anthropogenic increases in the atmospheric concentrations of greenhouse gases, these types of variable trends are found (IPCC, 2000, 2007).

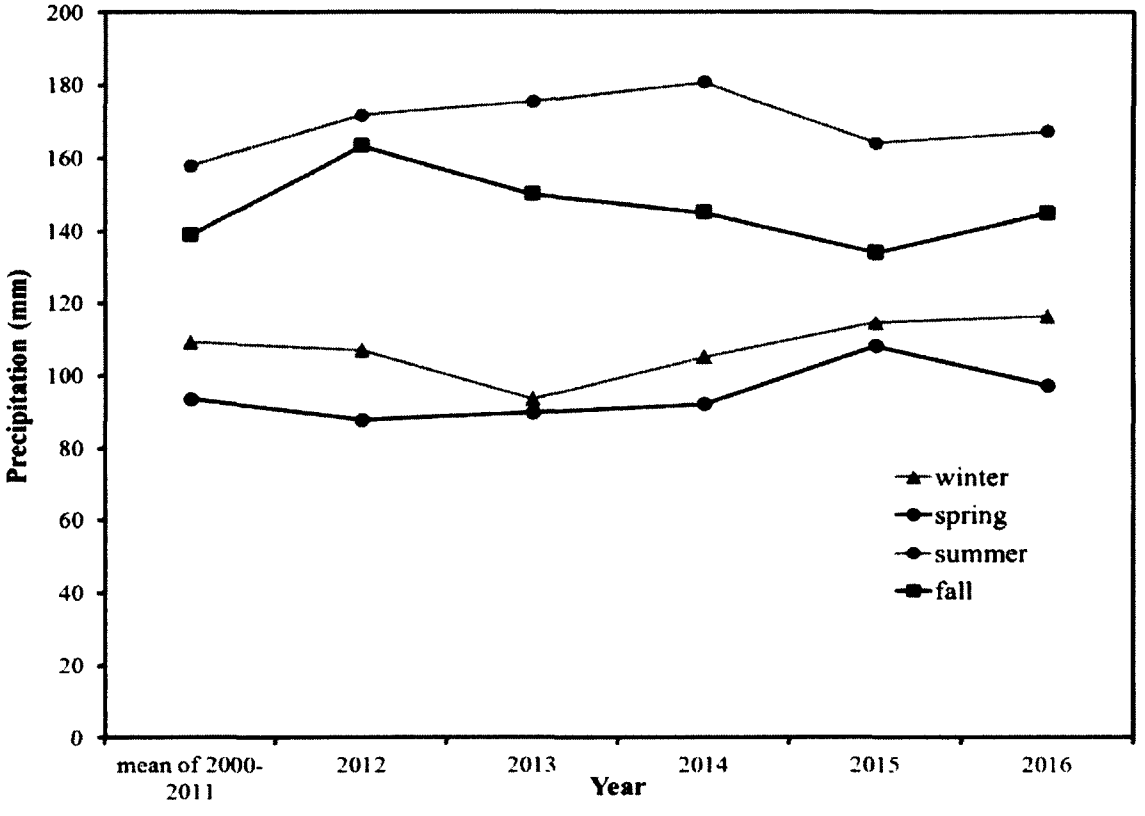

Figure 4.6 Projected seasonal precipitations of KRW from 2012 to 2016 under A2 scenario with respect to the mean seasonal precipitations of 2000-2011

When the seasonal precipitations from 2012 to 2016 under the B1 scenario are compared to the mean seasonal precipitations of 2000-2011, it is found that in winter, precipitation increases from 2012 to 2014 with a rate of 2% (i.e., in 2014) to 12% (i.e., in 2012), and then decreases in 2015 by 14%, and increases again by 5% in 2016 (Fig. 4.7). Spring precipitation increases in 2012 by 8%, and then decreases from 2013 to 2015 with a rate of 1% (i.e., in 2013) to 12% (i.e., in 2014), and then increases again in 2016 by 1%. In summer, precipitation decreases in 2012 by 9%, and then increases from 2013 to 2016 with a rate of 2% (i.e., in 2014) to 11% (i.e., in 2013). In fall, precipitation follows a decrease-increase cyclic pattern from 2012 to 2016. The most and least increases occur in 2015 (i.e., 12%) and 2013 (i.e., 4%), respectively. The most and least decreases occur in 2012 (i.e., 9%), and 2014 (i.e., 3%), respectively. On average, the mean winter, spring, summer, and fall precipitations from 2012 to 2016 under the B1 scenario are 112 mm (σ=15 mm), 94 mm (σ=8 mm), 164 mm (σ=13 mm), and 140 mm (σ=11 mm), respectively. This shows that the mean winter, spring, summer, and fall precipitations from 2012 to 2016 under the B1 scenario increase by 3 mm (2.5%), 1 mm (1%), 6 mm (4%), and 2 mm (1%), respectively, in relation to the mean winter, spring, summer, and fall precipitations from 2000 to 2011. Similarly, due to the anthropogenic increases in the atmospheric concentrations of greenhouse gases, these types of variable trends are found (IPCC, 2000, 2007).

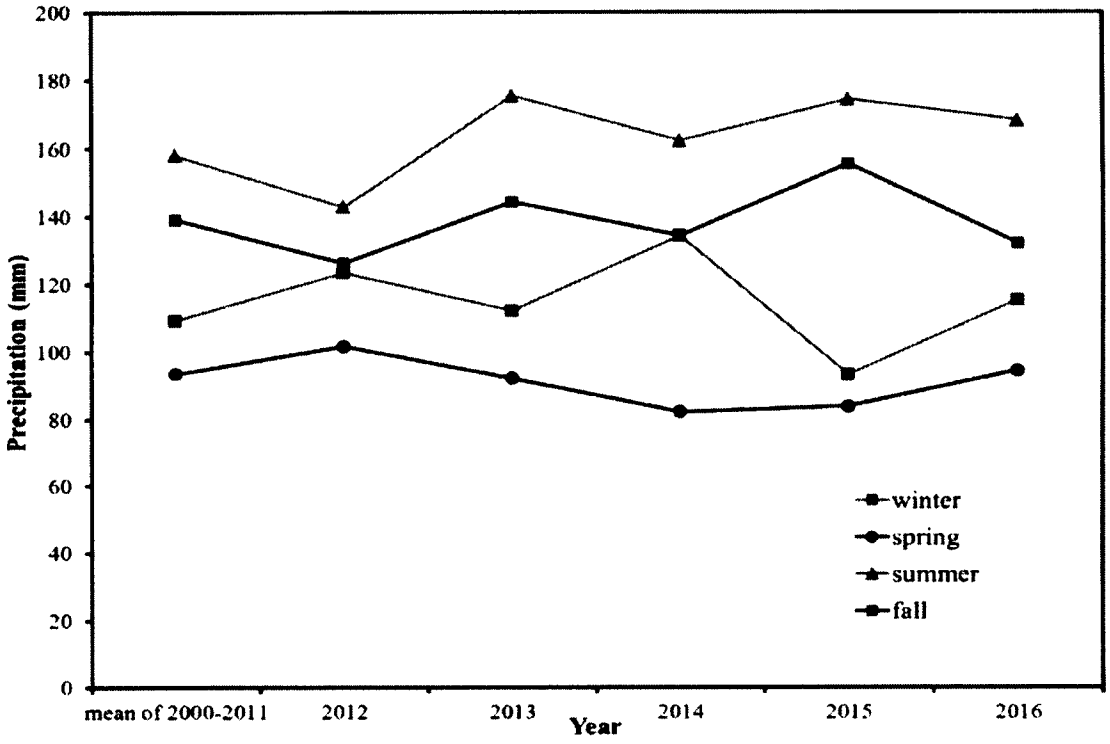

Figure 4.7 Projected seasonal precipitations of KRW from 2012 to 2016 under B1 scenario with respect to the mean seasonal precipitations of 2000-2011

Based on the above seasonal figures, it can be concluded that the mean seasonal precipitation from 2012 to 2016 increases in all seasons under both scenarios with respect to those of 2000-2011. It is also found that the increase of the mean precipitation is greater in the summer than in the winter. Similar types of precipitation increase patterns were predicted in northern British Columbia by British Columbia Ministry of Forests and Range (2008).

4.2.3.1.2 Long-term

Similar to the short-term period, the future monthly precipitations of KRW under the A2 and B1 scenarios show variable patterns in the long-term period (i.e., 2020-2040) due to the anthropogenic increases in the atmospheric concentrations of greenhouse gases (IPCC, 2000, 2007). Figs. 4.8 and 4.9 present the projected mean monthly precipitations from 2020 to 2040 under the A2 and B1 scenarios, respectively. In these figures, the error bars of one standard deviation among monthly precipitations of 2020 to 2040 are also shown. From the comparison of projected mean monthly precipitations under both scenarios from 2020 to 2040 with respect to the period of 2000-2011 (Fig. 4.10), it is found that the peak monthly precipitation under both scenarios is expected in June, and shows the similar trend of the mean monthly precipitations of 2000-2011. Similar to the short-term period, the mean monthly precipitations are higher in most of the months under the A2 scenario than under the B1 scenario.

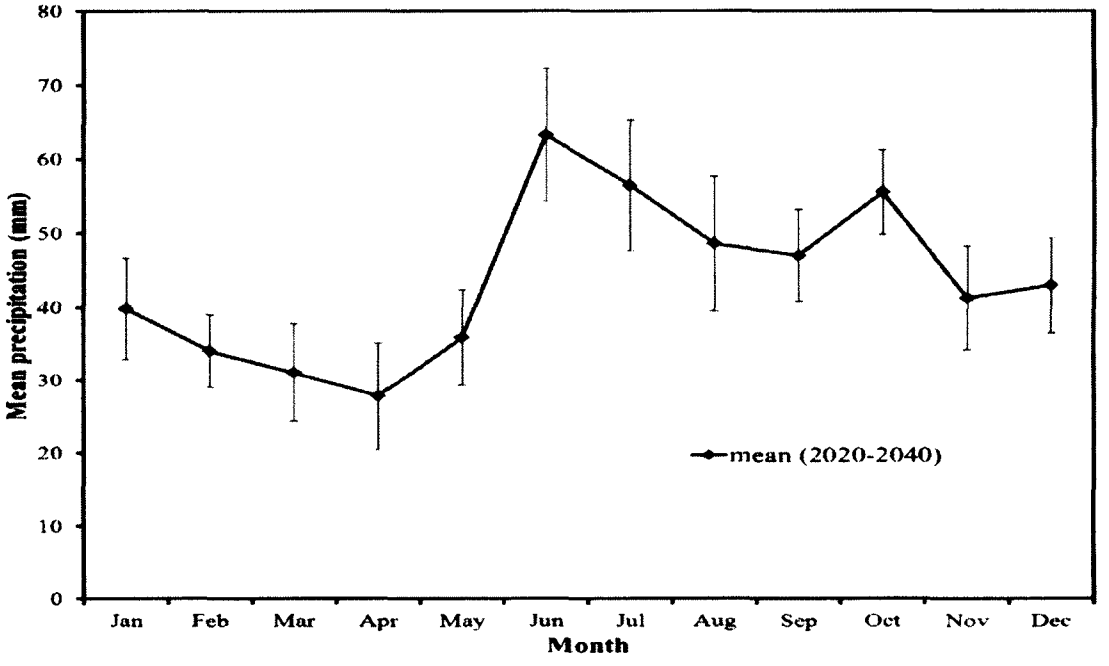

Figure 4.8 Projected mean monthly precipitations under A2 scenario from 2020 to 2040. The error bars represent one standard deviation among monthly precipitations of 2020 to 2040.

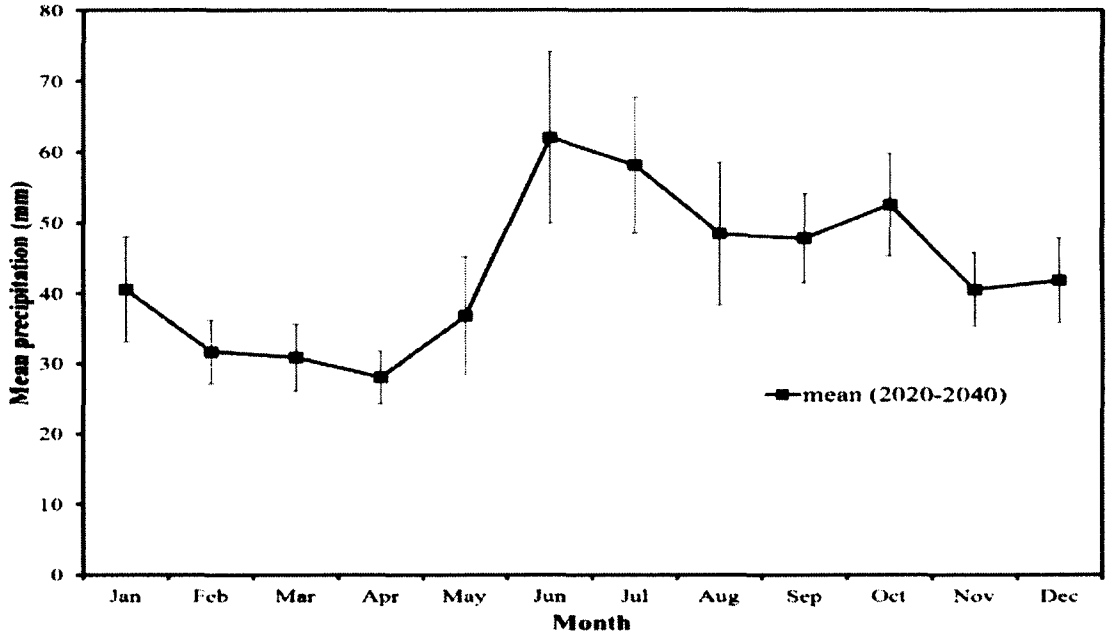

Figure 4.9 Projected mean monthly precipitations under B1 scenario from 2020 to 2040. The error bars represent one standard deviation among monthly precipitations of 2020 to 2040.

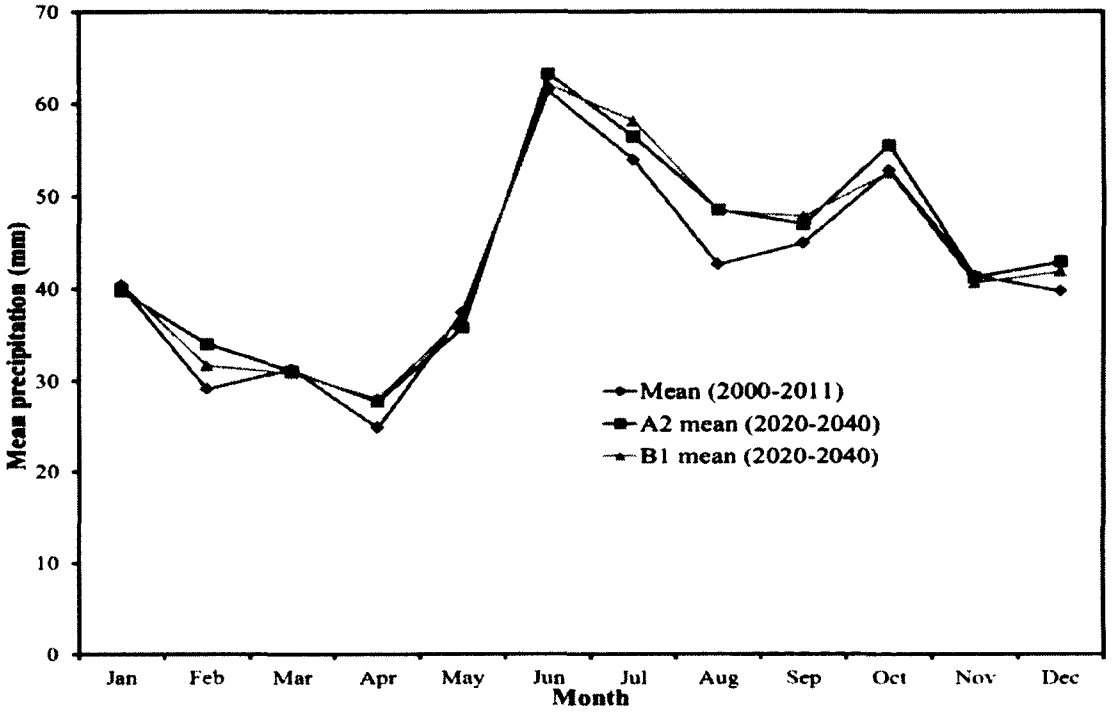

Figure 4.10 Comparison of projected mean monthly precipitations under A2 and B1 scenarios from 2020 to 2040 with respect to the mean monthly precipitations of 2000-2011

Similar to the short-term period, the mean seasonal precipitations are also expected to increase in the long-term period with respect to the mean seasonal precipitations from 2000 to 2011 due to the anthropogenic increases in the atmospheric concentrations of greenhouse gases (IPCC, 2000, 2007). On average, the mean winter, spring, summer, and fall precipitations from 2020 to 2040 under the A2 scenario will be 112 mm (σ=12 mm), 95 mm (σ=11 mm), 173 mm (σ=17 mm), and 145 mm (σ=9 mm), respectively, which is increased by 3 mm (3%), 2 mm (2%), 15 mm (9.5%), and 7 mm (5%), respectively, with respect to the period from 2000 to 2011. On the other hand, under the B1 scenario, on average, the mean winter, spring, summer, and fall precipitations from 2020 to 2040 will be 114 mm (σ=13 mm), 96 mm (σ=9 mm), 165 mm (σ=18 mm), and 141 mm (σ=13 mm), respectively, which

corresponds to an increase by 5 mm (4.5%), 3 mm (3%), 7 mm (4.5%), and 3 mm (2%), respectively, as compared to the period from 2000 to 2011. Similarly, the mean annual precipitation is expected to increase in the long-term period as compared to the period of 2000-2011. The mean annual precipitation from 2020 to 2040 under the A2 and B1 scenarios are expected to be 525 mm (σ=19 mm) and 516 mm (σ=22 mm), respectively, and these numbers are above the mean annual precipitation of 2000-2011 by 27 mm (5.5%) and 18 mm (3.5%), respectively.

4.2.3.2 Temperature

4.2.3.2.1 Short-term

The predicted mean monthly temperatures of KRW in the short-term period (2012-2016) under the A2 and B1 GHG emission scenarios using the delta change method are shown in Figs. 4.11 and 4.12, respectively. Fig. 4.11 shows that the trend of mean monthly temperatures is similar in every year under the A2 scenario, with the highest and lowest mean monthly temperatures occurring in July and January, respectively, which are similar to those of 2000-2011. Under the B1 scenario (Fig. 4.12), a similar trend of mean monthly temperatures is found. From the comparison of mean monthly temperatures under both scenarios from 2012 to 2016 with respect to those of 2000-2011 (Fig. 4.13), it is found that the A2 scenario is associated with higher values than the B1 scenario for most of the months, except in August and December.

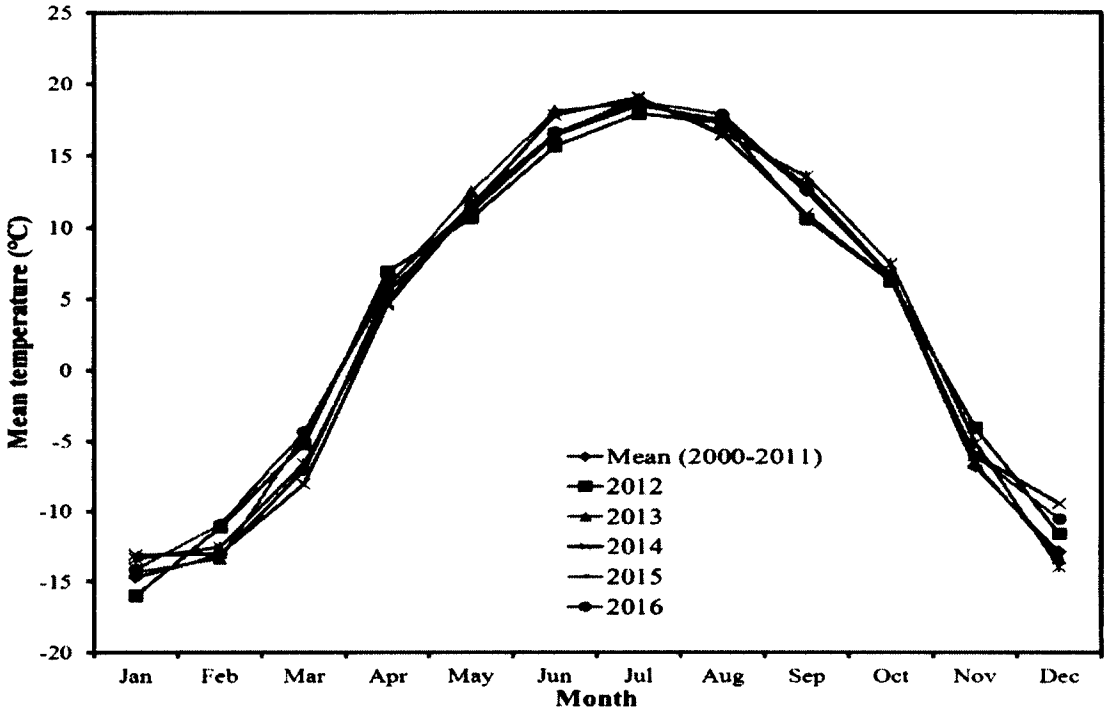

Figure 4.11 Projected mean monthly temperatures of KRW from 2012 to 2016 under A2 scenario

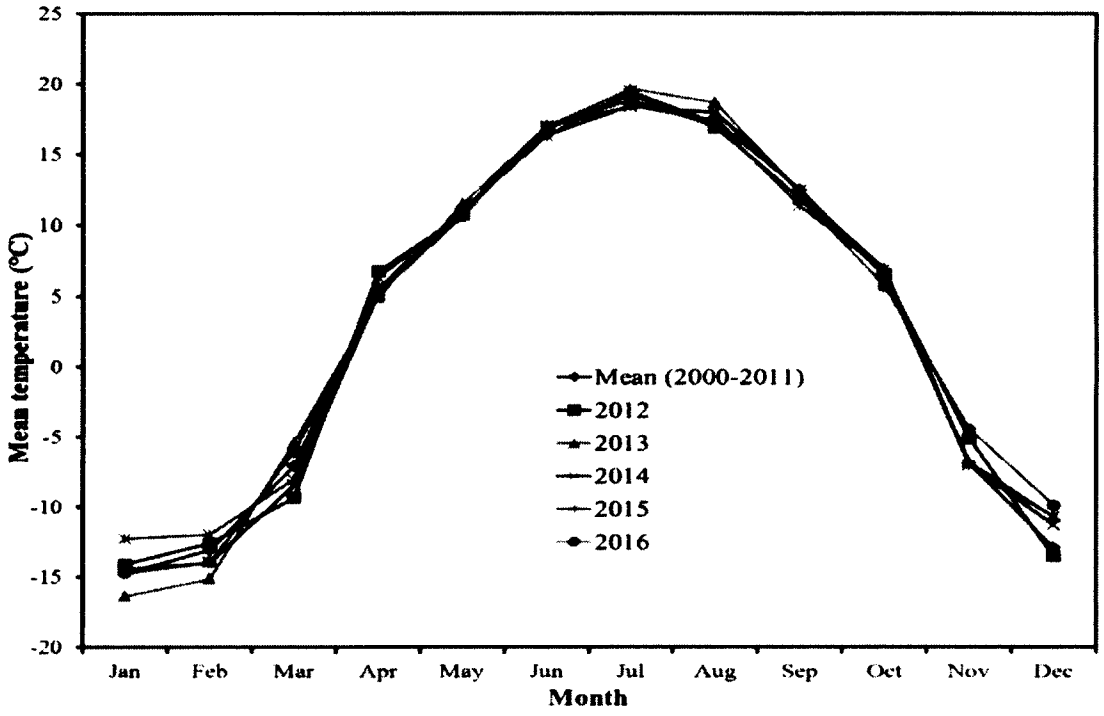

Figure 4.12 Projected mean monthly temperatures of KRW from 2012 to 2016 under B1 scenario

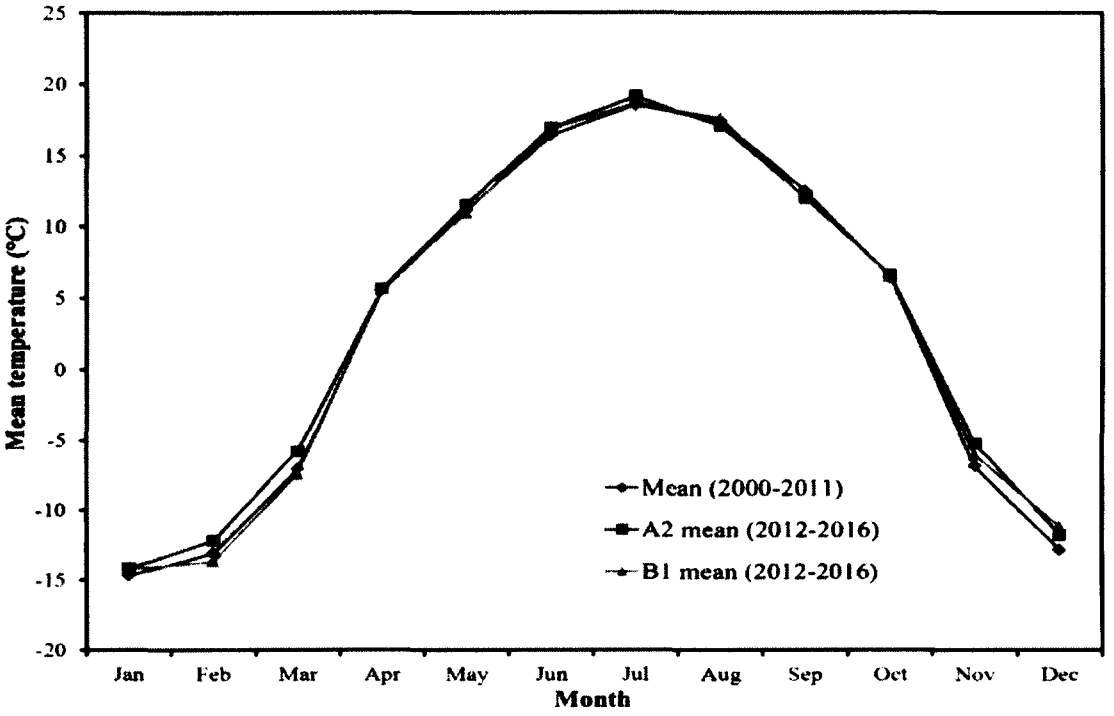

Figure 4.13 Comparison of mean monthly temperatures of 2012-2016 under A2 and B1 scenarios with respect to mean monthly temperatures of 2000-2011

It is found that the mean annual temperatures from 2012 to 2016 under both scenarios increase as compared to that of 2000-2011 (Fig. 4.14). This occurs due to the increase of the greenhouse gases concentrations in the atmosphere (IPCC, 2000, 2007). The increase of temperature under the A2 scenario is between 0.35°C and 0.92°C, while the most and least increases are expected in 2016 and 2014, respectively. On the other hand, under the B1 scenario, the increase is between 0.05°C and 0.39°C, while the most and least increases are expected in 2016 and 2014, respectively. On average, the mean annual temperature from 2012 to 2016 under the A2 and B1 scenarios are 3.27°C (σ=0.23°C) and 2.99°C (σ=0.18°C), respectively, while the mean annual temperature from 2000 to 2011 is 2.7°C.

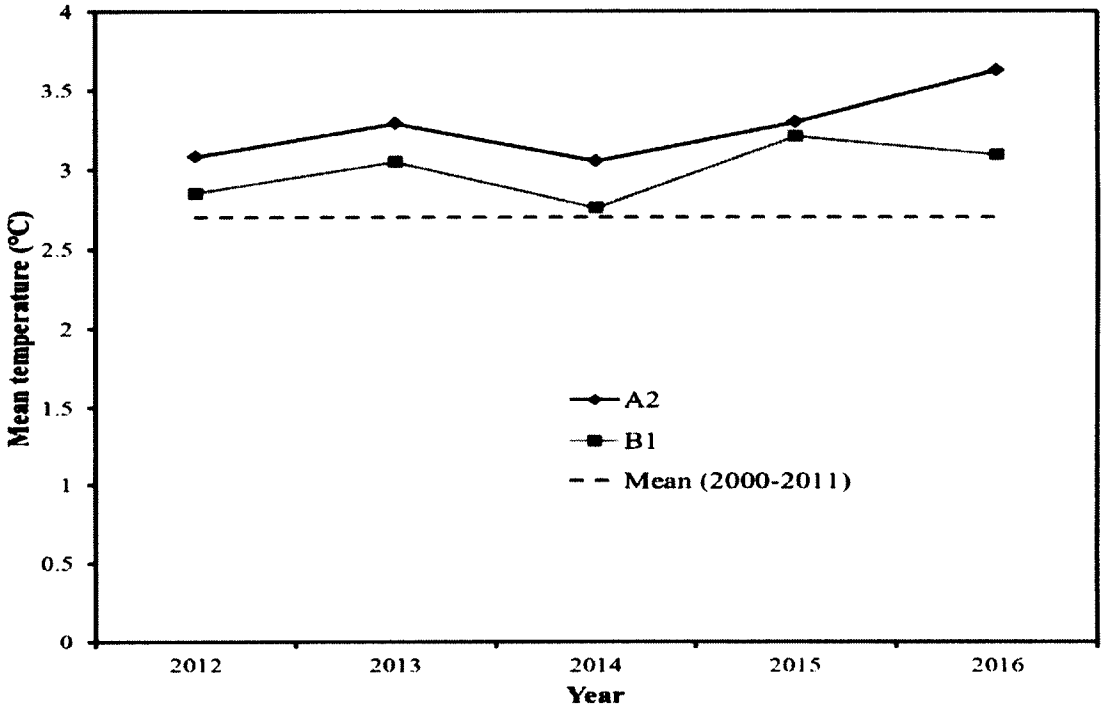

Figure 4.14 Projected mean annual temperature of KRW from 2012 to 2016 under A2 and B1 scenarios

When the mean seasonal temperatures from 2012 to 2016 under the A2 scenario are compared to those of 2000-2011, it is found that the mean summer temperature increases every year within a range of 0.18°C to 0.36°C as compared to that of 2000-2011 (Fig. 4.15). The most and least increases are expected in 2014 and 2016, respectively. The mean temperatures from 2000 to 2011 in winter, spring, summer, and fall are -13.56°C, 3.16°C, 17.43°C, and 4°C, respectively. In winter, the mean temperature increases in 2012 (by 0.64°C), and decreases in 2013 (by 0.11°C), and then increases again from 2014 to 2016 by a magnitude of 0.26°C (i.e., in 2015) to 1.71°C (i.e., in 2014). The mean spring temperature increases from 2012 (by 0.9°C) to 2013 (by 1.39°C), and then decreases in 2014 (by 0.52°C), and increases again from 2015 (by 0.1°C) to 2016 (by 1.21°C). The mean fall temperature

follows a similar trend of the mean spring temperature, with an increase from 2012 (by 0.23°C) to 2013 (by 0.3°C), and then a decrease in 2014 (by 0.3°C), and an increase again from 2015 (by 1.25°C) to 2016 (by 0.26°C). On average, the mean winter, spring, summer, and fall temperatures from 2012 to 2016 under the A2 scenario are -12.72°C (σ=0.83°C), 3.78°C (σ=0.8°C), 17.71°C (σ=0.25°C), and 4.35°C (σ=0.51°C), respectively, which corresponds to an increase by 0.84°C, 0.62°C, 0.28°C, and 0.35°C, respectively, as compared to those of 2000-2011. Due to the anthropogenic increases in the atmospheric concentrations of greenhouse gases, these types of variable trends are found (IPCC, 2000, 2007).

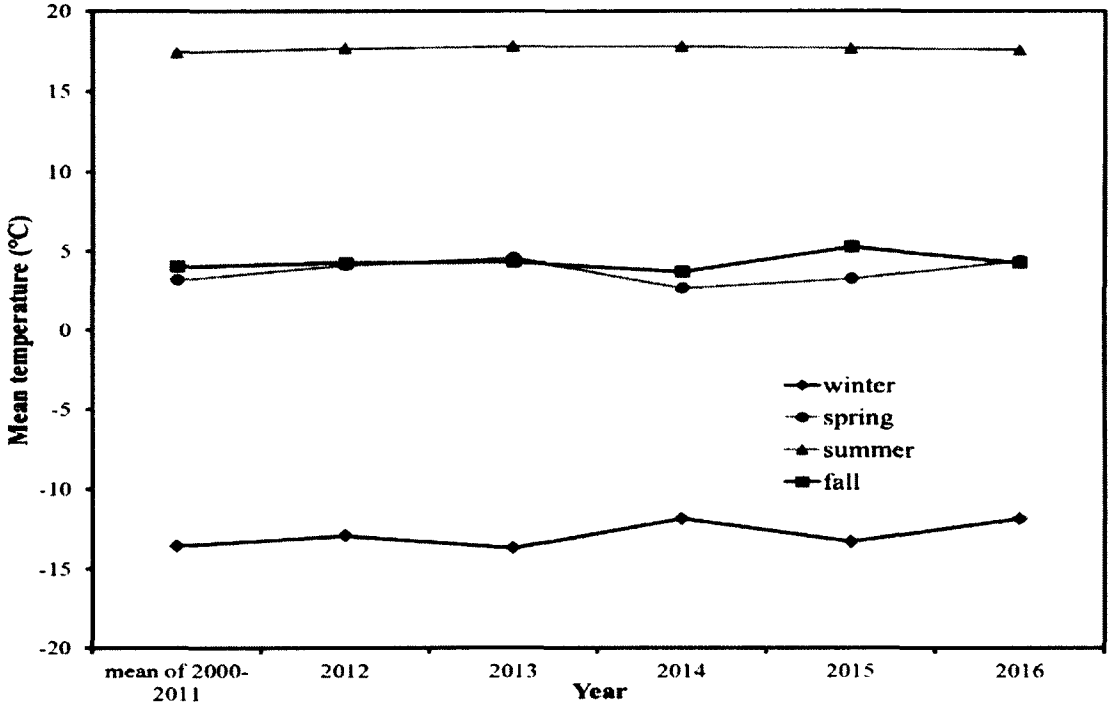

Figure 4.15 Projected mean seasonal temperatures of KRW from 2012 to 2016 under A2 scenario with respect to the mean seasonal temperatures of 2000-2011

Comparing the mean seasonal temperatures from 2012 to 2016 under the B1 scenario to those of 2000-2011 (Fig. 4.16), it is found that the mean winter temperature increases in 2012 (by 0.17°C), and decreases in 2013 (by 0.48°C), and then increases again from 2014 to 2016 with a magnitude of 0.33°C (i.e., in 2014) to 1.91°C (i.e., in 2015). The mean spring temperature decreases in 2012 (by 0.46°C), and increases in 2013 (by 0.49°C), and then decreases again from 2014 (by 0.67°C) to 2015 (by 0.1°C). In 2016, the mean spring temperature increases by 0.06°C. The mean summer temperature also follows a decrease-increase cyclic pattern from 2012 to 2016. The most and least increases are found in 2013 (i.e., 0.56°C) and 2016 (i.e., 0.29°C), respectively, while the most and least decreases are found in 2012 (i.e., 0.49°C), and 2015 (i.e., 0.11°C), respectively. The mean fall temperature increases from 2012 (by 0.42°C) to 2013 (by 0.13°C), and then decreases from 2014 (by 0.02°C) to 2015 (by 0.28°C), and finally increases in 2016 (by 0.38°C). On average, the mean winter, spring, summer, and fall temperatures from 2012 to 2016 under the B1 scenario are -13.03°C (σ=0.89°C), 3.19°C (σ=0.45°C), 17.54°C (σ=0.42°C), and 4.12°C (σ=0.29°C), respectively, which are corresponding to an increase by 0.53°C, 0.03°C, 0.11°C, and 0.12°C, respectively, as compared to those of 2000-2011. Similarly, due to the anthropogenic increases in the atmospheric concentrations of greenhouse gases, these types of variable trends are found (IPCC, 2000, 2007).

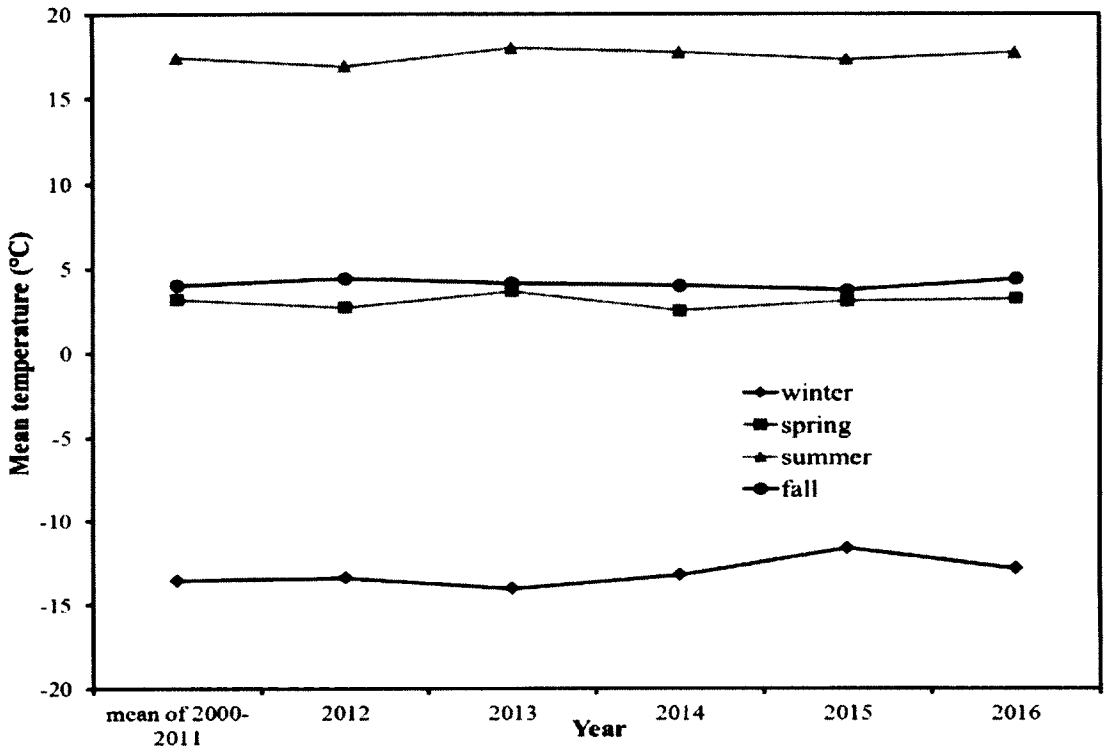

Figure 4.16 Projected mean seasonal temperatures of KRW from 2012 to 2016 under B1 scenario with respect to the mean seasonal temperatures of 2000-2011

Based on the above seasonal figures, it can be concluded that the mean seasonal temperature from 2012 to 2016 increases in all seasons under both scenarios with respect to those of 2000-2011. It is also found that the increase of the mean temperature is greater in winter than in summer. Similar predictions were obtained in northern British Columbia by British Columbia Ministry of Forests and Range (2008).

4.2.3.2.2 Long-term

The future mean monthly temperatures of KRW in the long-term period (2020-2040) under the A2 and B1 scenarios show similar patterns of the short-term period. Figs. 4.17 and 4.18 present the mean monthly temperatures from 2020 to 2040 under the A2 and B1 scenarios, respectively. Similar trends are expected in the long-term period when the projected mean monthly temperatures under both scenarios from 2020 to 2040 are compared to those of 2000-2011 (Fig. 4.19). The mean seasonal temperatures are expected to increase in the long-term period. On average, the mean winter, spring, summer, and fall temperatures from 2020 to 2040 under the A2 scenario are expected to be -12.42°C (σ=1.46°C), 3.52°C (σ=0.69°C), 18.03°C (σ=0.45°C), and 4.55°C (σ=0.66°C), respectively, which corresponds to an increase by 1.15°C, 0.36°C, 0.60°C, and 0.55°C, respectively, as compared to those of 2000-2011. On the other hand, under the B1 scenario, on average, the mean winter, spring, summer, and fall temperatures from 2020 to 2040 are expected to be -13.03°C (σ=1.15°C), 3.40°C (σ=0.55°C), 17.84°C (σ=0.62°C), and 4.32°C (σ=0.49°C), respectively, which corresponds to an increase by 0.52°C, 0.24°C, 0.40°C, and 0.32°C, respectively, as compared to those of 2000-2011. Similarly, the mean annual temperature is also expected to increase in the long-term period. On average, the mean annual temperature from 2020 to 2040 under the A2 and B1 scenarios is expected to be 3.46°C (σ=0.60°C) and 3.27°C (σ=0.41°C), respectively, which is increased by 0.76°C and 0.57°C from that of 2000-2011, respectively. This occurs due to the anthropogenic increases in the atmospheric concentrations of greenhouse gases (IPCC, 2000, 2007).

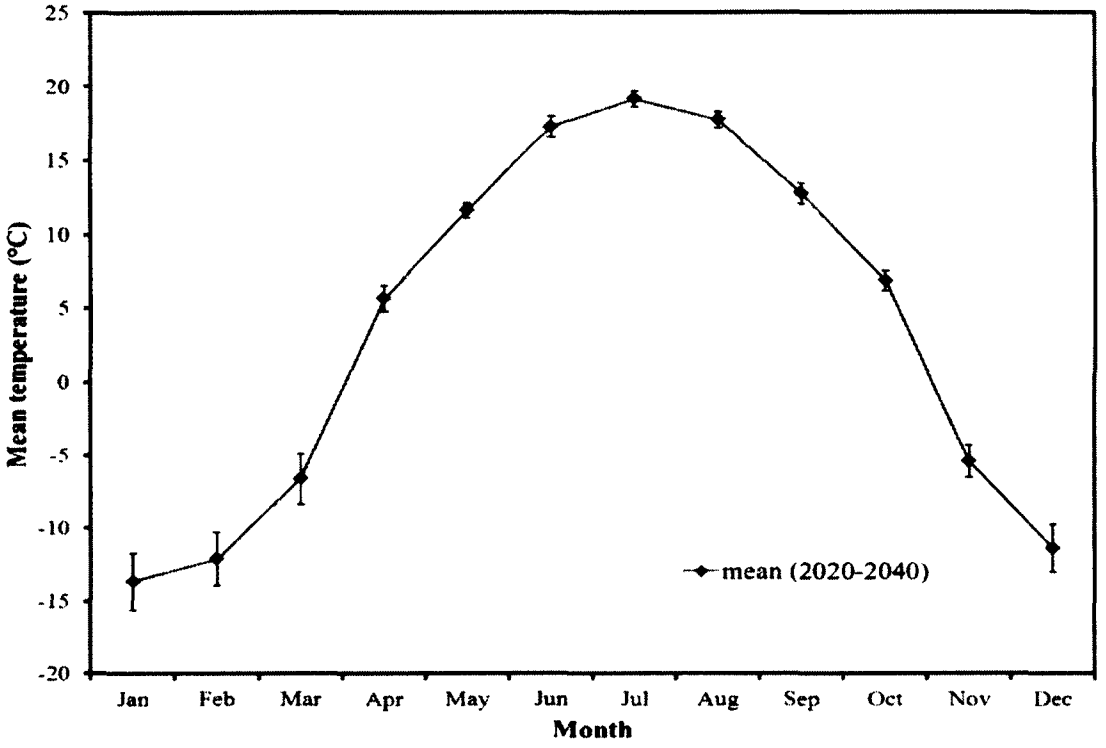

Figure 4.17 Projected mean monthly temperatures from 2020 to 2040 under A2 scenario. The error bars represent one standard deviation among mean monthly temperatures of 2020 to 2040.

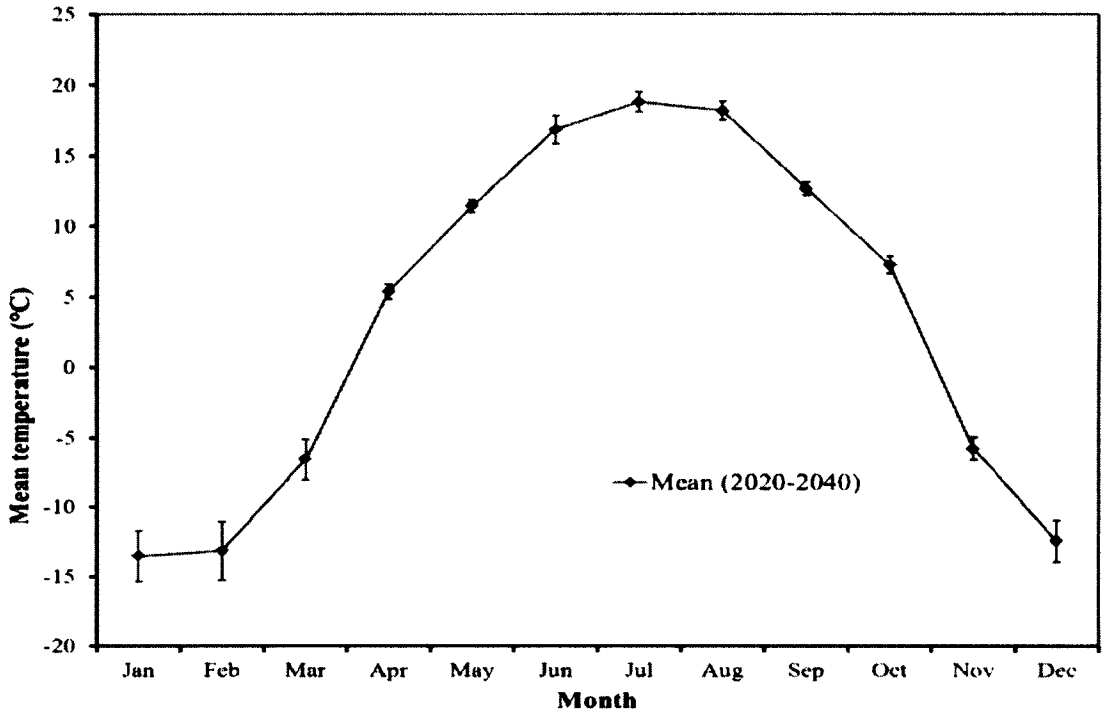

Figure 4.18 Projected mean monthly temperatures from 2020 to 2040 under B1 scenario. The error bars represent one standard deviation among mean monthly temperatures of 2020 to 2040.

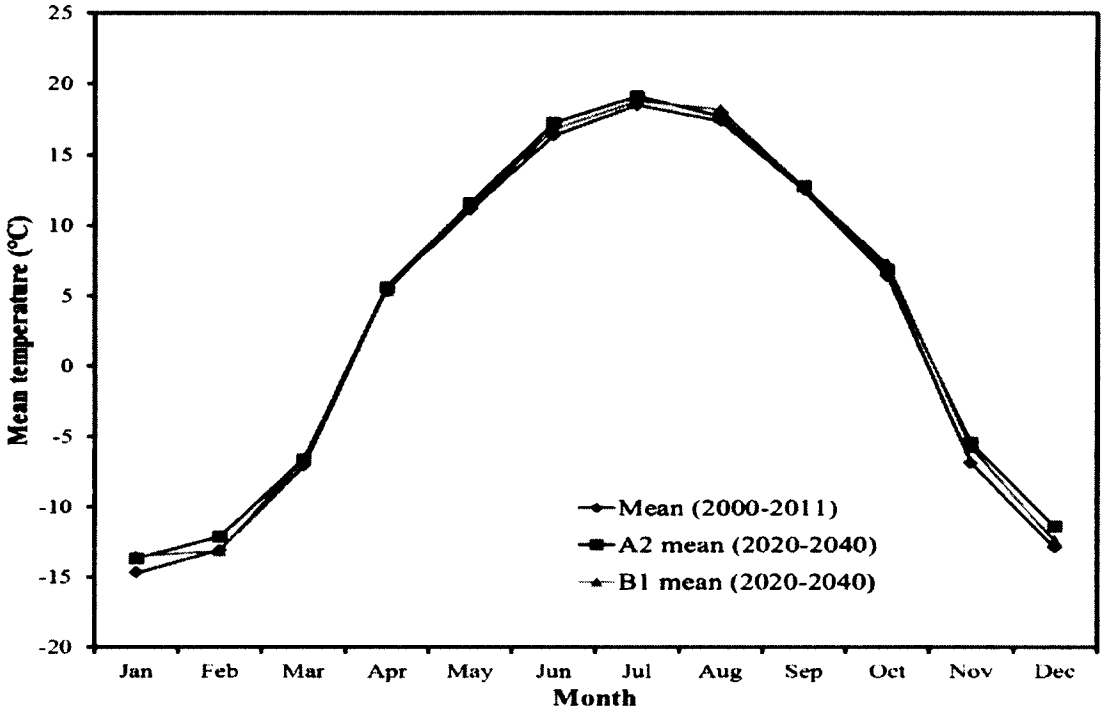

Figure 4.19 Comparison of projected mean monthly temperatures under A2 and B1 scenarios from 2020 to 2040 with respect to those of 2000-2011

4.3 Generation of future land use/land cover scenarios

4.3.1 Land use/land cover change analysis

The land use/land cover changes in the study area between 1999 and 2010 are shown in Table 4.2. In this table, land use change per year was calculated considering linear land use change in every year due to limited information available. The results show that the major land use changes occurred in forest clear cut and wetland. As compared to that in 1999, forest clear cut area increased by about 735% in 2010, while wetland area decreased by about 59%. The rapid change in forest clear cut area was due to a large scale of oil/gas exploration and production, while the rapid change in wetland area may have occurred due to the shift of vegetation and oil/gas exploration/production in the study area. It is also found that river (including small channels) and built up area (e.g., road, house, industrial infrastructures) increased by about 20% and 96%, respectively, from 1999 to 2010, while agriculture (e.g., cropland and pasture) and forest decreased by 44% and 11%, respectively. The decrease in agriculture area did not impact the local economy and population because large-scale shale gas exploration/production activities started in the KRW since 2005 and have enhanced the local economy. However, due to limited available information, the verification of these land use types changes was not possible. It is to be noted that pasture occupies the major part of the agricultural area in this study area of the Mainstem sub-watershed, while cropland occupies the major part of the agricultural area in the Brassey sub-watershed, which is not included in this study.

Table 4.2 Land use changes from 1999 to 2010 in the study area. Change (%) = [(Area of 2010 land use - Area of 1999 land use)/ Area of 1999 land use] × 100 (taken from Paul, 2013)

Land use type	Area (km^2) in 1999	Area (km^2) in 2010	Change (km^2)	Change (%)	Change/year (km^2/year)
Forest	163.36	145.35	-18.01	-11	-1.64
Agriculture	31.42	17.74	-13.68	-44	-1.24
Forest clear cut	4.78	39.89	35.11	735	3.19
Wetland	9.58	3.94	-5.64	-59	-0.51
River	3	3.6	0.6	20	0.05
Built up area	1.68	3.3	1.62	96	0.15
Total	213.82				

4.3.2 Future land use/land cover scenarios

Based on land use/land cover change analysis between 1999 and 2010, future annual land use index maps from 2012 to 2016 were generated using Arc GIS and GSSHA through the following considerations:

- Future annual land use index map considers the annual change of only forest clear cut, forest and agriculture areas because they cover 18%, 68%, and 8% of the study area, respectively, based on the 2010 land use map. It is to be noted that large-scale shale gas exploration/production activities have started in the KRW since 2005 (British Columbia Ministry of Energy and Mines, 2012). In addition, Forest Practices Board (2011) also predicted an increase of forest clear cut area in the KRW until 2017.

- Due to limited data availability, the future annual land use index map was developed by assuming that the forest and agriculture areas are converted into forest clear cut area at the conversion rate shown in Table 4.2 (i.e., forest and agricultural area will be reduced by 1.64 km^2 and 1.24 km^2 annually, respectively). The summation of annual forest and agricultural areas reduction was added to the annual increase of forest clear cut area. Drohan et al. (2012) also found a similar conversion of agricultural and forest areas in Pennsylvania into gas well pads, which is a part of forest clear cut area in this study. Typically, gas companies prefer to secure land for gas well development in agricultural areas because agricultural land is less expensive and relatively easy to clear for gas well development (Kubach et al., 2011). The projected land use types from 2012 to 2016 are then presented in Table 4.3. A similar rate of linear land use changes from 2000 to 2020 was also used in Dams et al. (2008).
- In this study, the annual conversion of forest and agriculture areas into forest clear cut area was assumed in May of every year since in the study area, most of the snowmelt occurs in April. In addition, temporal land use changes during the year are difficult to detect due to lack of proper information (e.g., clear monthly satellite images).
- The spatial allocation of future land use changes was determined based on the change of a particular land use type and how much of that particular land use type has changed spatially between 1999 and 2010. For example, the reduced agriculture area at a particular site between 1999 and 2010 was used to calculate the future annual agriculture area reduction around that site. Special attentions were paid to allocate future land use types as per the guidelines of Kiskatinaw River Watershed Management Plan by Dobson Engineering Ltd. et al. (2003), especially in the areas

that are close to Kiskatinaw River. In addition, the major land use changes occurred in 0 – 4.6% slope areas in the study area because topography also plays a major role in soil erosion, for example, steeper slope area is more susceptible to higher soil erosion during heavy rainfall events than milder slope area (Whisenant, 2008; Blanco et al., 2010). The future annual land use index maps (Fig. 4.20-4.24) considering seasonal tributary drains of the study area were generated in GSSHA based on its digital elevation map and the above considerations. In these land use index maps, different types of land uses overlap river networks, especially seasonal tributary drains. This occurs because only the main river was considered in the original land use map (Fig. 3.16-3.17) due to the resolution of remote sensing images (i.e., 30 m by 30 m), and the seasonal tributary drains are very narrow compared to Kiskatinaw river.

Table 4.3 Projected land use types from 2012 to 2016 with respect to base line of 2011. Due to the unavailability of land use map for year 2011, year 2010 land use data were assumed for year 2011.

Year	Forest (km^2)	Agriculture (km^2)	Forest Clear cut (km^2)
2011	145.35	17.74	39.89
2012	143.71	16.5	42.77
2013	142.07	15.26	45.65
2014	140.43	14.02	48.53
2015	138.79	12.78	51.41
2016	137.15	11.54	54.29

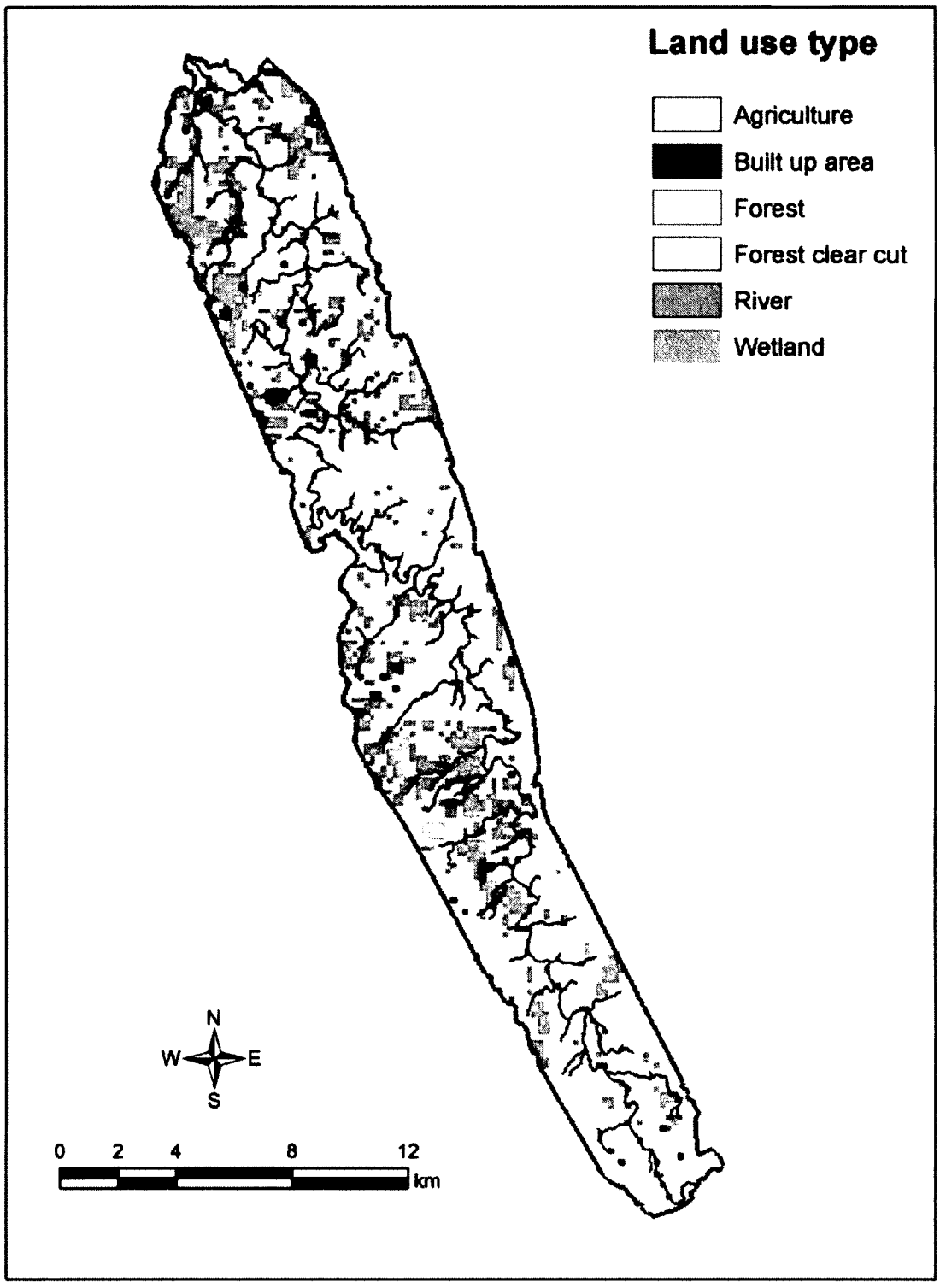

Figure 4.20 Land use index map of 2012

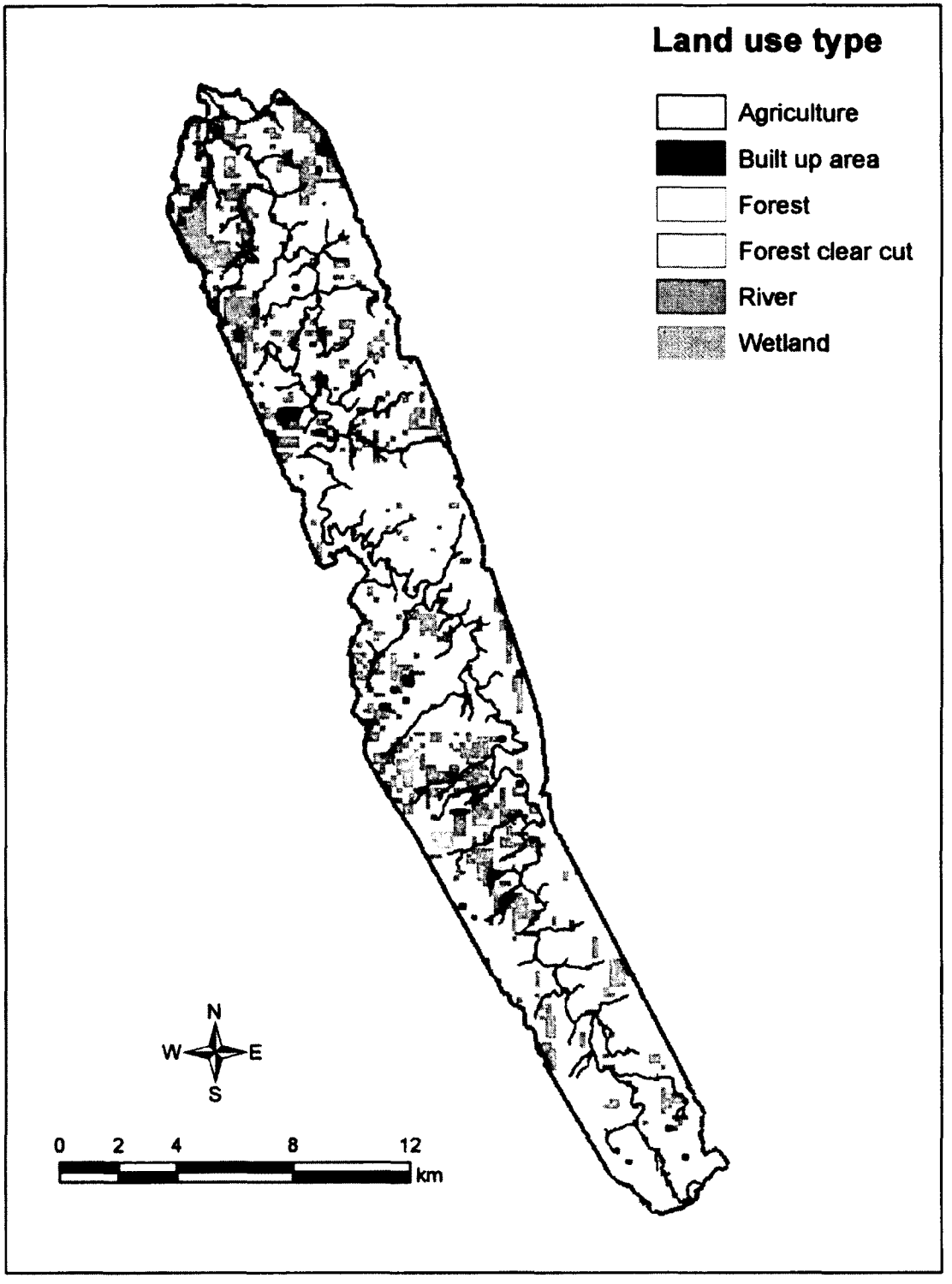

Figure 4.21 Land use index map of 2013

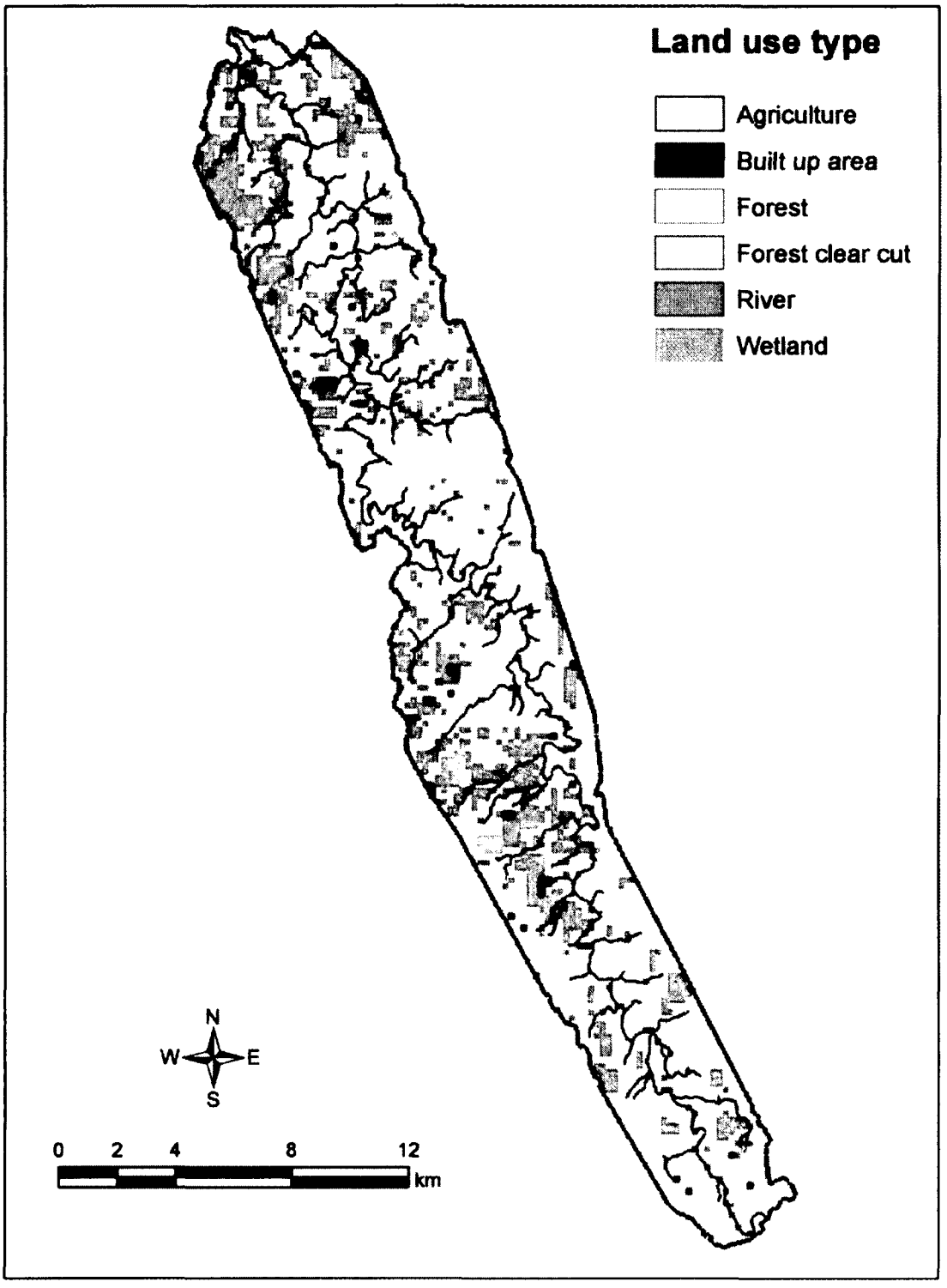

Figure 4.22 Land use index map of 2014

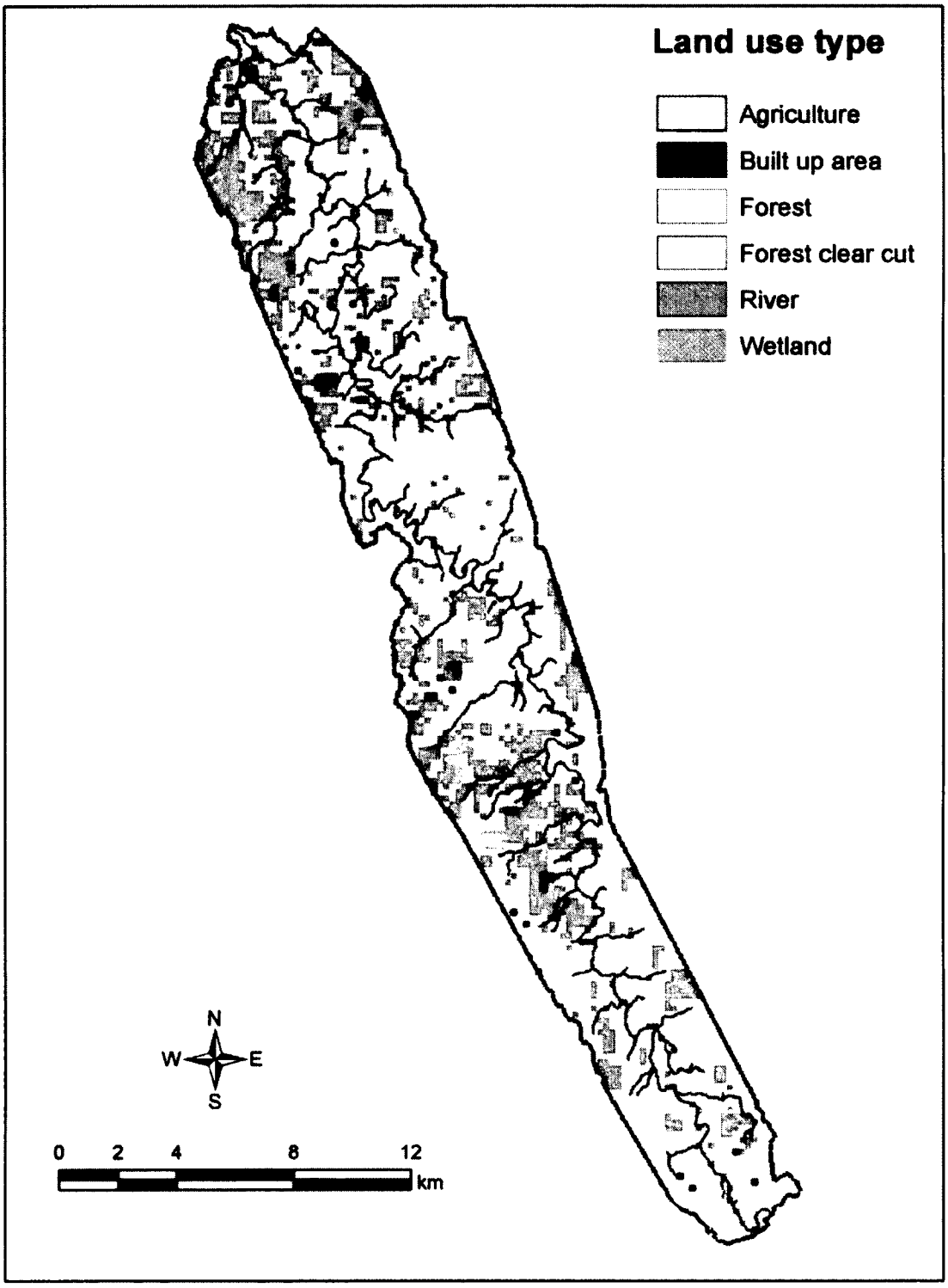

Figure 4.23 Land use index map of 2015

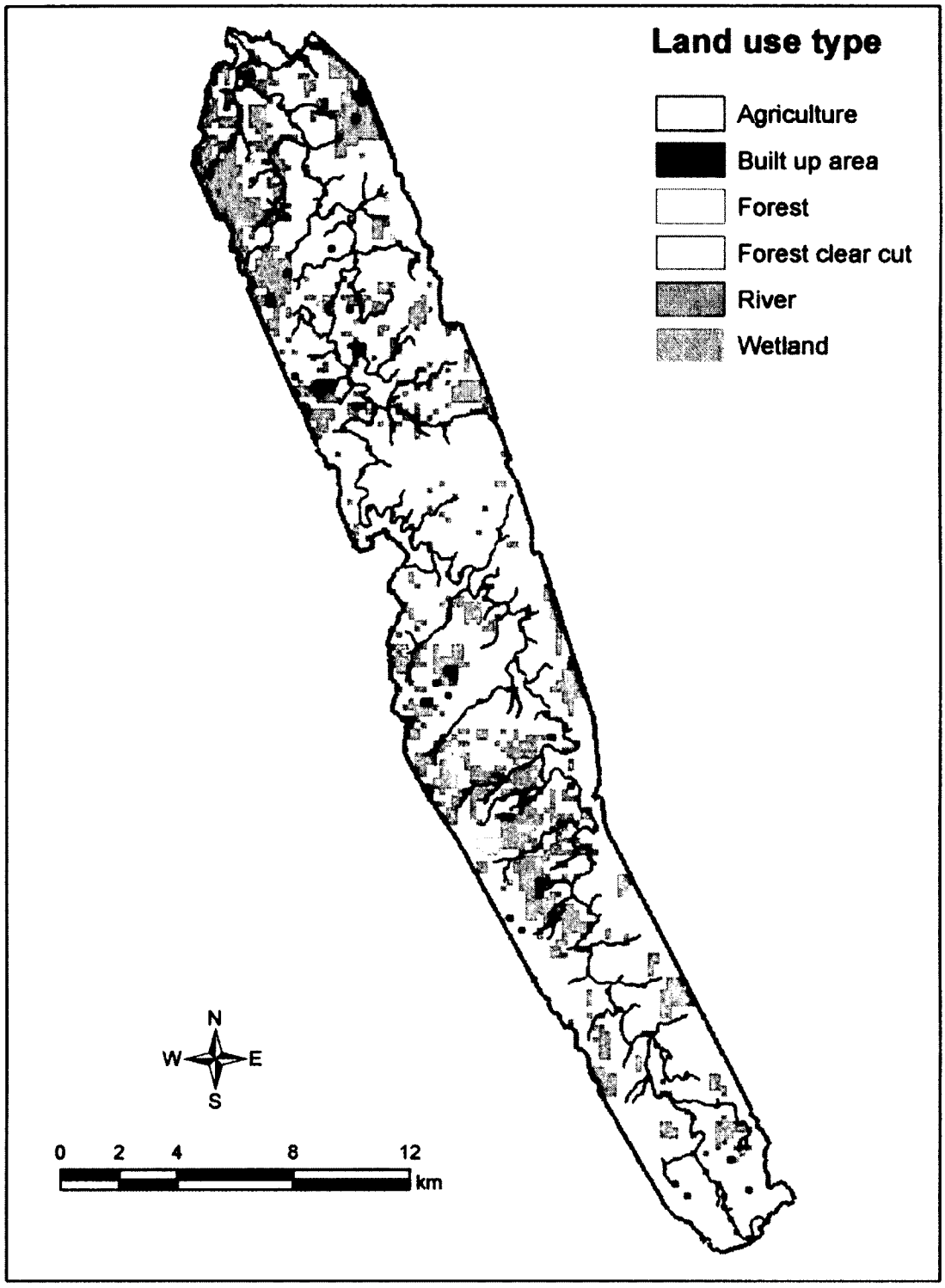

Figure 4.24 Land use index map of 2016

CHAPTER 5

CLIMATE CHANGE EFFECTS ON GW-SW INTERACTION

5.1 Background

This research attempts to investigate GW-SW interaction under climate change effects in the study area through the developed GSSHA model using the future climate scenarios that were presented in Chapter 4 of this dissertation. The monthly, seasonal and annual groundwater contributions to surface water flow under the A2 and B1 GHG emission scenarios were investigated for a short-term period of 5 years (2012 to 2016) and a long-term period of 21 years (2020-2040). During the study of climate change effects on GW-SW interaction, land use/land cover of the study area was kept constant, and the land use map of year 2010 was used.

5.2 GW-SW interaction under A2 scenario

Fig. 5.1 shows the mean monthly groundwater contributions to stream flow under climate change condition of A2 GHG emission scenario using the developed GW-SW interaction model (i.e., GSSHA) for 2012-2016 (short-term period). In the GSSHA model, the mean monthly groundwater contribution to stream flow was calculated based on the estimated monthly total volume of stream flow and groundwater discharge (Downer et al., 2006). A sample calculation of mean monthly groundwater contribution to stream flow in 2012 under

the A2 scenario using the GSSHA model is presented in Table 5.1. It is shown that the mean monthly groundwater contribution patterns vary annually due to monthly precipitation fluctuations, which result in variable monthly stream and groundwater discharges (Cannon et al., 2002; Van Roosmalen et al., 2007; Xu et al., 2008a, b; Xu et al., 2009; Xu et al., 2011). Therefore, climate change significantly affects stream and groundwater discharges, as well as the patterns of mean monthly groundwater contribution to stream flow.

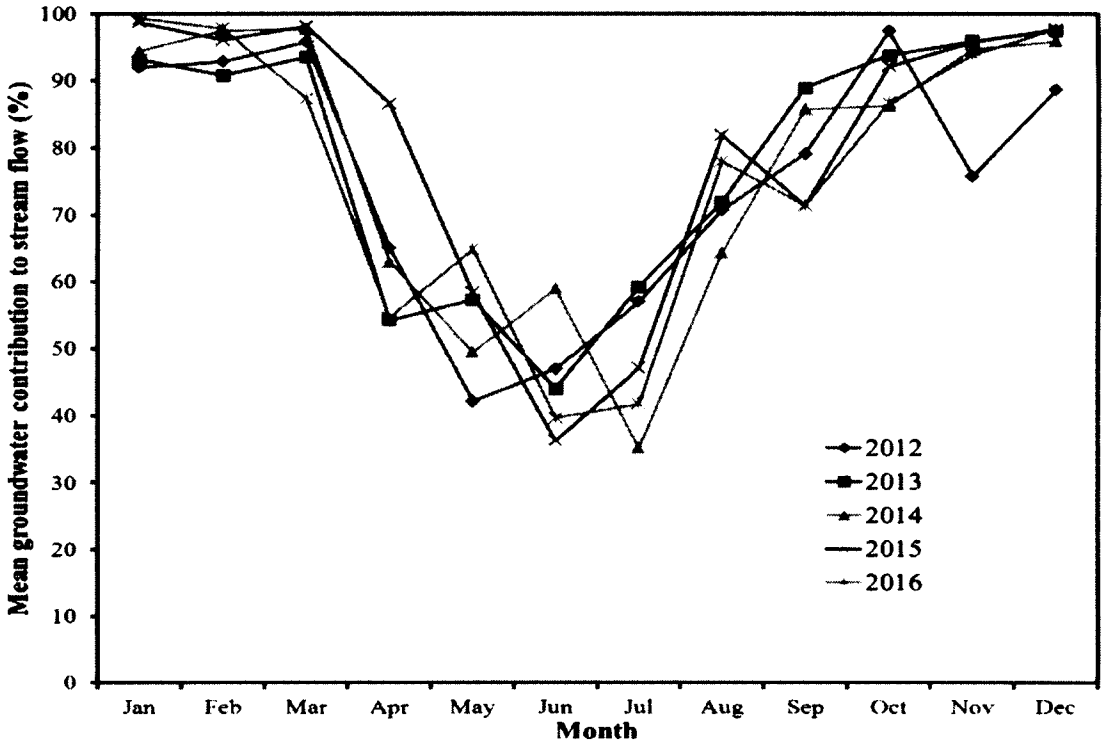

Figure 5.1 Mean monthly groundwater contributions to stream flow under climate change of A2 GHG emission scenario for 2012-2016 simulated by the GSSHA model

Table 5.1 Mean monthly groundwater contribution to stream flow in 2012 under the A2 scenario using the GSSHA model

Month	Total volume of stream flow (m^3)	Total volume of groundwater discharge (m^3)	Mean monthly groundwater contribution to stream flow (%)
Jan	496250.5	456351.9	91.96
Feb	524647.6	487292.7	92.88
Mar	680312.9	651807.8	95.81
Apr	9991218.6	6494292.1	65.02
May	37010227.9	15607213.1	42.17
Jun	17583374.6	8255394.4	46.95
Jul	23691273.9	13494549.7	56.96
Aug	3175509.6	2245402.9	70.71
Sep	1365986.8	1079539.3	79.03
Oct	1479021.5	1441010.6	97.43
Nov	1123999.0	850754.9	75.69
Dec	838180.2	743382.1	88.69

The 2012 mean monthly groundwater contribution to stream flow ranges between 42% in May and 98% in October. The remaining portion comes from surface runoff. Table 5.2 shows the detailed list of the mean monthly contribution of groundwater and surface runoff to stream flow in 2012 under the A2 scenario as an illustrative example. Similar trends are expected for years 2013 to 2016. These results demonstrate that stream flow depends mostly on groundwater flow in those months when there is highest groundwater contribution to stream flow, and vice versa (Washington State Department of Ecology, 1999). Since the regional groundwater flow field in the study area is a mixture of gaining and flow-through systems (Fig. 3.22), the river gets water from groundwater at both sides of the river bank where the groundwater flow field is a gaining system, whereas the river gets water from

groundwater at one side of the river bank, and recharges groundwater aquifer at the other side of the river bank where the groundwater flow field is a flow-through system. However, overall groundwater contributes a major portion to the stream flow in the study area.

Table 5.2 Mean monthly stream flow, groundwater discharge and surface runoff, and their contributions to stream flow in 2012 under the A2 scenario

Month	Mean stream flow (m^3/s)	Mean groundwater discharge (m^3/s)	Mean surface runoff (m^3/s)	Mean groundwater contribution to stream flow (%)	Mean surface runoff contribution to stream flow (%)
Jan	0.185	0.170	0.015	91.96	8.04
Feb	0.209	0.194	0.015	92.88	7.12
Mar	0.254	0.243	0.011	95.81	4.19
Apr	3.854	2.505	1.349	65.02	34.98
May	13.818	5.827	7.991	42.17	57.83
Jun	6.783	3.184	3.599	46.95	53.05
Jul	8.845	5.038	3.807	56.96	43.04
Aug	1.185	0.837	0.348	70.71	29.29
Sep	0.527	0.416	0.111	79.03	20.97
Oct	0.552	0.537	0.015	97.43	2.57
Nov	0.433	0.327	0.106	75.69	24.31
Dec	0.312	0.276	0.036	88.69	11.31

The comparison of mean groundwater contributions to stream flow during different seasons under the A2 scenario for 2012-2016 is presented in Fig. 5.2. From Fig. 5.2 and projected seasonal precipitation under the A2 scenario (Fig. 4.6), it can be concluded that the mean groundwater contribution to stream flow decreases when the seasonal precipitation increases, and vice versa during summer and fall seasons, because increasing precipitation results in greater increase of surface runoff (Clow et al., 2003; Van Roosmalen et al., 2007; Koeniger et al., 2009) compared to that of groundwater discharge. However, in the winter and spring seasons, the mean groundwater contribution to stream flow does not increase when the seasonal precipitation only decreases because in these seasons, the precipitation occurs mainly as snow. This snow accumulates, and results in low surface runoff before complete snow melt, and therefore, the trend of mean groundwater contribution to stream flow increases or decreases regardless of precipitation during these seasons (Covert, 1999; Walvoord et al., 2007). On average, the mean groundwater contribution to stream flow during winter, spring, summer, and fall from 2012 to 2016 is 95% (σ=2.9%), 71% (σ=2.8%), 55% (σ=2.7%), and 86% (σ=3.3%), respectively. These results demonstrate that the mean groundwater contribution to stream flow is the lowest and highest during summer and winter, respectively. Hence, stream flow depends mostly on groundwater flow during winter, but at a lesser extent during summer. Consequently, the highest and lowest water extraction from the river, and allocation to the stakeholders for future water supply could be possible during summer and winter, respectively, due to the highest (i.e., on average 6.26 m^3/s) and lowest (i.e., on average 0.25 m^3/s) mean stream flow rates during summer and winter, respectively. Similar seasonal variations of mean groundwater contribution to stream flow were found in other studies (Clow et al., 2003; Welderufael et al., 2010). However, these variations differ

from area to area depending on the type and temporal pattern of precipitation around the year. For example, in western and northern Europe (e.g., United Kingdom, Belgium, Denmark) more precipitation occurs during winter as rainfall, and therefore, results in higher surface runoff compared to groundwater discharge (Van Roosmalen et al., 2007; Dams et al., 2012), and lower groundwater contribution to stream flow during winter than other seasons, which is opposite to the finding of this study. Therefore, the seasonal variations of mean groundwater contribution to stream flow depend on the type and temporal pattern of annual precipitation in the particular area.

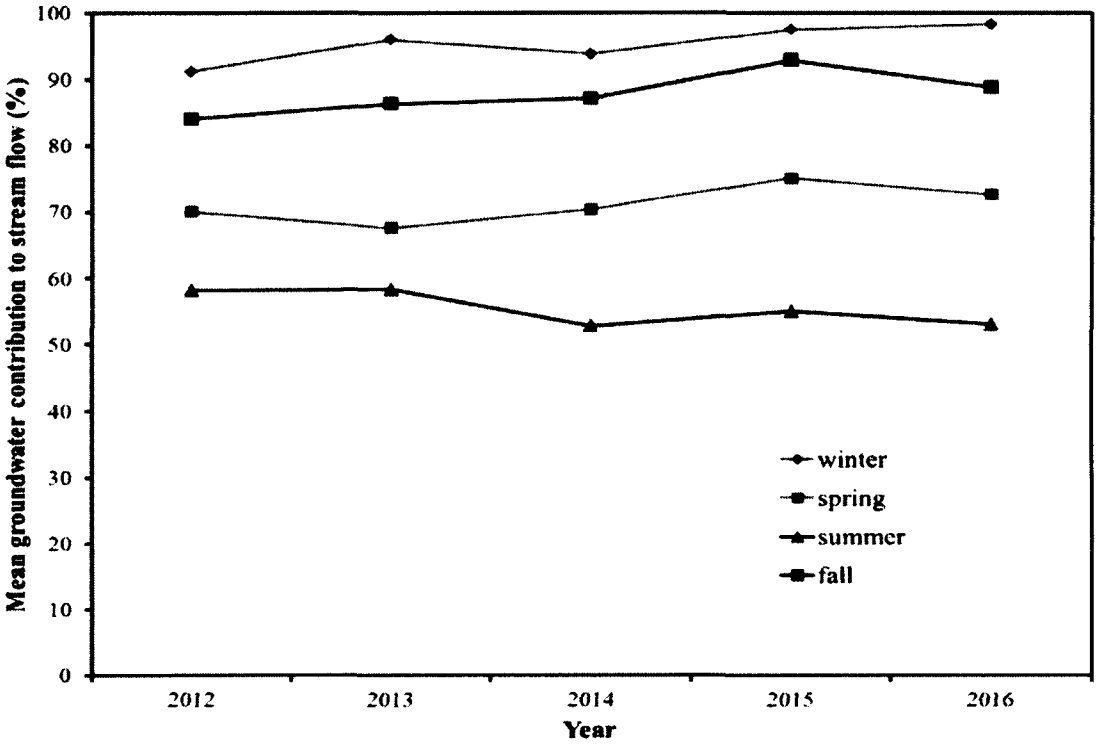

Figure 5.2 Comparison of mean groundwater contributions to stream flow during different seasons under A2 GHG emission scenario for 2012-2016

Fig. 5.3 shows the comparison of the mean daily groundwater levels for year 2011 and climate change of A2 GHG emission scenario for 2012-2016 simulated by the GSSHA model. Here, mean daily groundwater levels of the study area was analyzed, and the year 2011 (annual precipitation 552 mm) was of mild winter and flooding summer in the study area. The mean daily groundwater levels of the study area were calculated using the simulated daily groundwater levels at each grid cell of the study area. Since the GSSHA model has no provision to show the spatial difference of daily groundwater level changes, the mean daily groundwater levels of the study area were considered to show the way in which the mean daily groundwater level responds yearly. However, the patterns would be spatially different in the study area. It is found that the mean daily groundwater levels in the study area show almost similar profiles in every year due to the almost similar temporal pattern of annual precipitation. Due to high infiltration rate during snow melting and heavy rainfall events in the summer, the mean daily groundwater levels increase the most, but this high groundwater level does not increase groundwater contribution to stream flow during those times because of high stream flow generated by high surface runoff during snowmelt and heavy rainfall (Covert, 1999; Clow et al., 2003), as well as the steep topography of the study area (Vivoni et al., 2007). The peak of mean daily groundwater level hydrograph varies depending on the amount of rainfall. The mean daily groundwater levels gradually decrease during the end of summer and continue until the winter and before snow melting (i.e., before April) due to less infiltration rate, and this lower groundwater level results in lower groundwater discharge, and higher groundwater contribution to stream flow because of low stream flow during those times. However, these temporal variations of mean daily groundwater levels also differ from area to area depending on the type and temporal pattern

of precipitation around the year. For example, in western and northern Europe (e.g., United Kingdom, Belgium, Denmark) more precipitation occurs during winter as rainfall, and results in higher groundwater levels during winter than other seasons (Van Roosmalen et al., 2007; Goderniaux, 2010; Dams et al., 2012), which is opposite to the finding of this study. Therefore, similar to the seasonal variations of mean groundwater contribution to stream flow, the temporal variations of mean daily groundwater levels also depend on the type and temporal pattern of annual precipitation in the particular area.

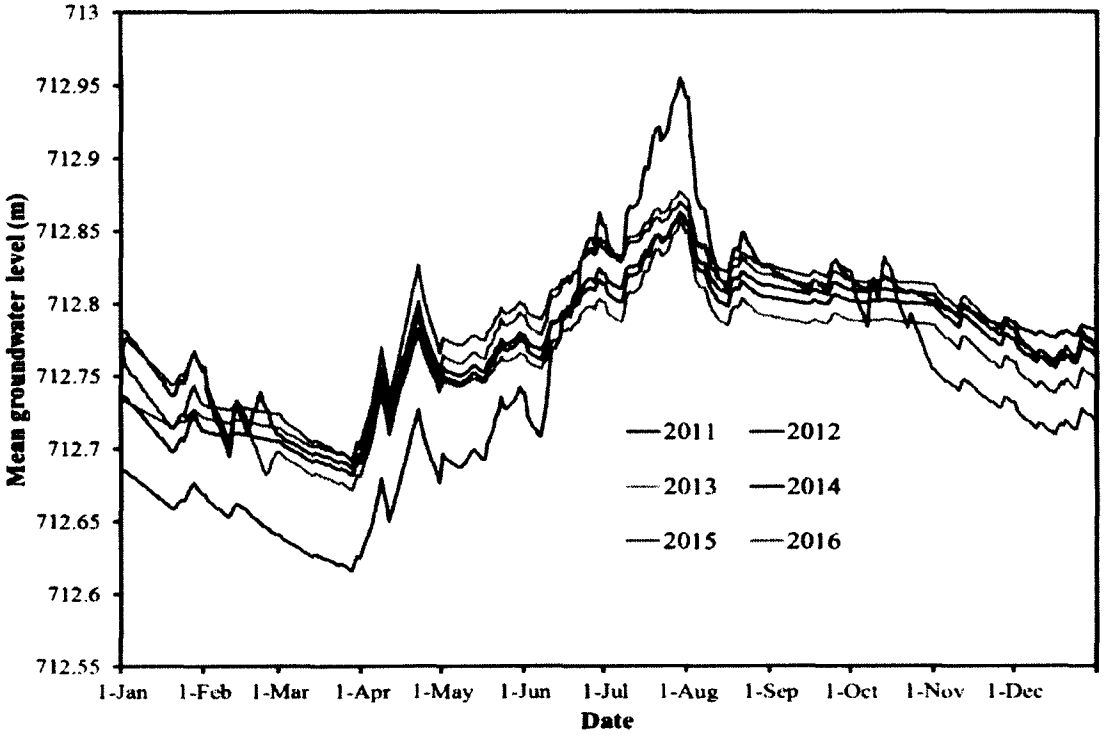

Figure 5.3 Comparison of mean daily groundwater levels of the study area for year 2011 and climate change of A2 GHG emission scenario for 2012-2016 simulated by the GSSHA model

Fig. 5.4 shows the temporal variation of the mean daily groundwater levels of the study area for year 2011 and climate change of A2 GHG emission scenario for 2012-2016. It is found that the mean daily groundwater levels are expected to increase at the end of year 2016 due to increased precipitation under the A2 scenario. Overall, the mean annual groundwater level of the study area is expected to increase by 2 cm, 1.2 cm, 2 cm, 2.4 cm, and 3 cm in 2012, 2013, 2014, 2015, and 2016, respectively, compared to the mean annual groundwater level in 2011. The mean annual groundwater level increases yearly due to consecutive years of above-normal precipitation of the study area. Therefore, climate change has a significant impact on the mean daily and annual groundwater levels. Scibek et al. (2006b) and Van Roosmalen et al. (2007) also found increased mean annual groundwater levels due to increased precipitation. However, the increase of mean annual groundwater levels varies from area to area depending on the amount of increased annual precipitation. Therefore, the increased mean annual groundwater levels in the study area will provide more groundwater discharge to stream flow for future water supply in the study area compared to year 2011.

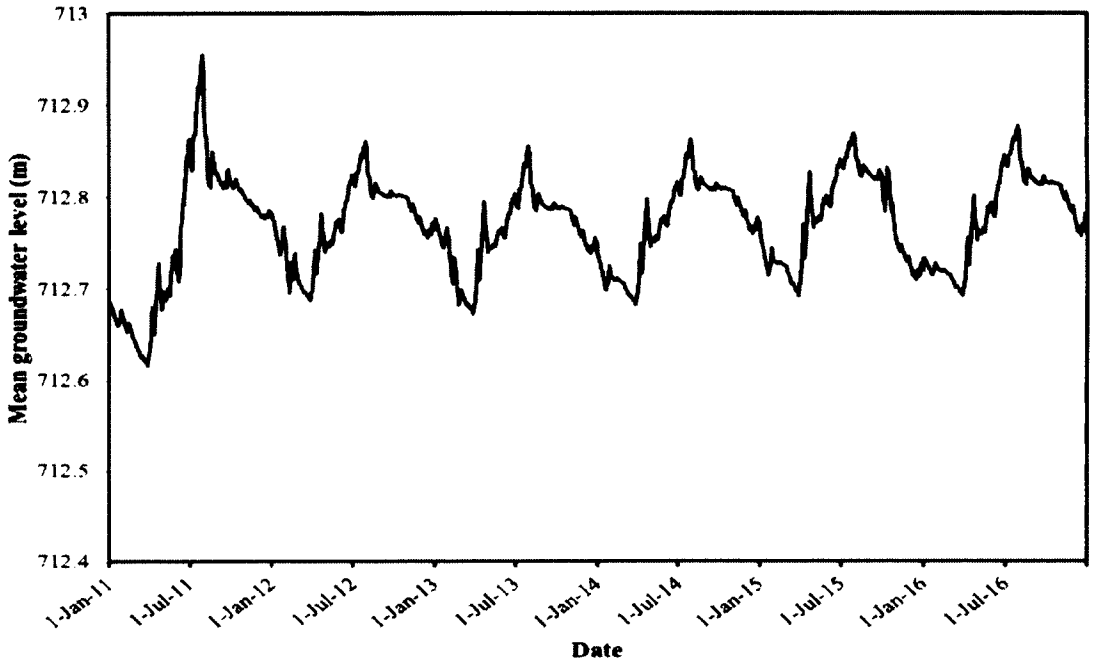

Figure 5.4 Mean daily groundwater levels of the study area for year 2011 and climate change of A2 GHG emission scenario for 2012-2016 simulated by the GSSHA model

Similar to the short-term period, the mean monthly groundwater contributions to stream flow under the A2 scenario will show variable annual patterns in the long-term period (2020-2040) due to monthly precipitation fluctuations. Fig 5.5 shows the mean monthly groundwater contributions to stream flow from 2020 to 2040 under the A2 scenario. The results also indicate the significant influences of climate change on the patterns of mean monthly groundwater contribution to stream flow.

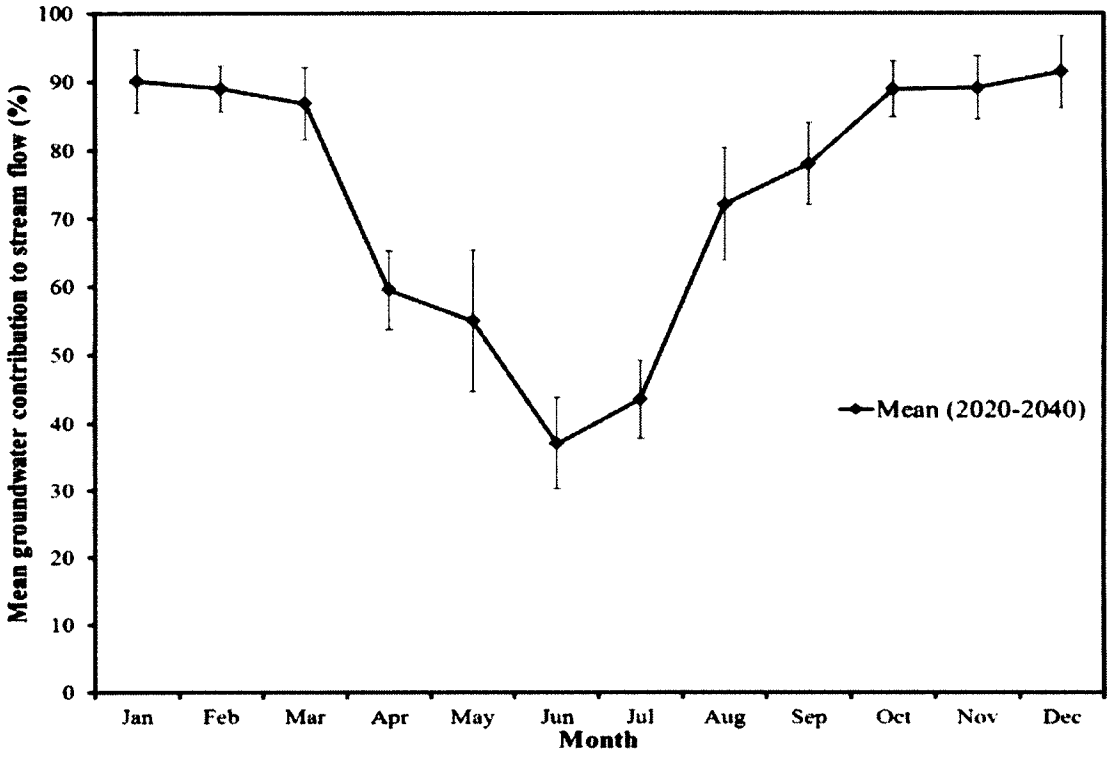

Figure 5.5 Mean monthly groundwater contributions to stream flow under A2 scenario from 2020 to 2040. The error bars represent one standard deviation among mean monthly groundwater contributions to stream flow of 2020 to 2040.

As in the short-term period, the mean groundwater contributions to stream flow during different seasons under the A2 scenario will show similar trends in the long-term period. On average, the mean groundwater contribution to stream flow during winter, spring, summer, and fall from 2020 to 2040 under the A2 scenario will be 93% (σ=3%), 69% (σ=4.5%), 50% (σ=3.5%), and 85% (σ=2.5%), respectively. Similarly, the mean daily groundwater levels in the study area will show almost identical responses annually in the long-term period due to the similar temporal pattern of annual precipitation. Fig 5.6 shows the mean daily groundwater levels of the study area of 2020-2040 under the A2 scenario.

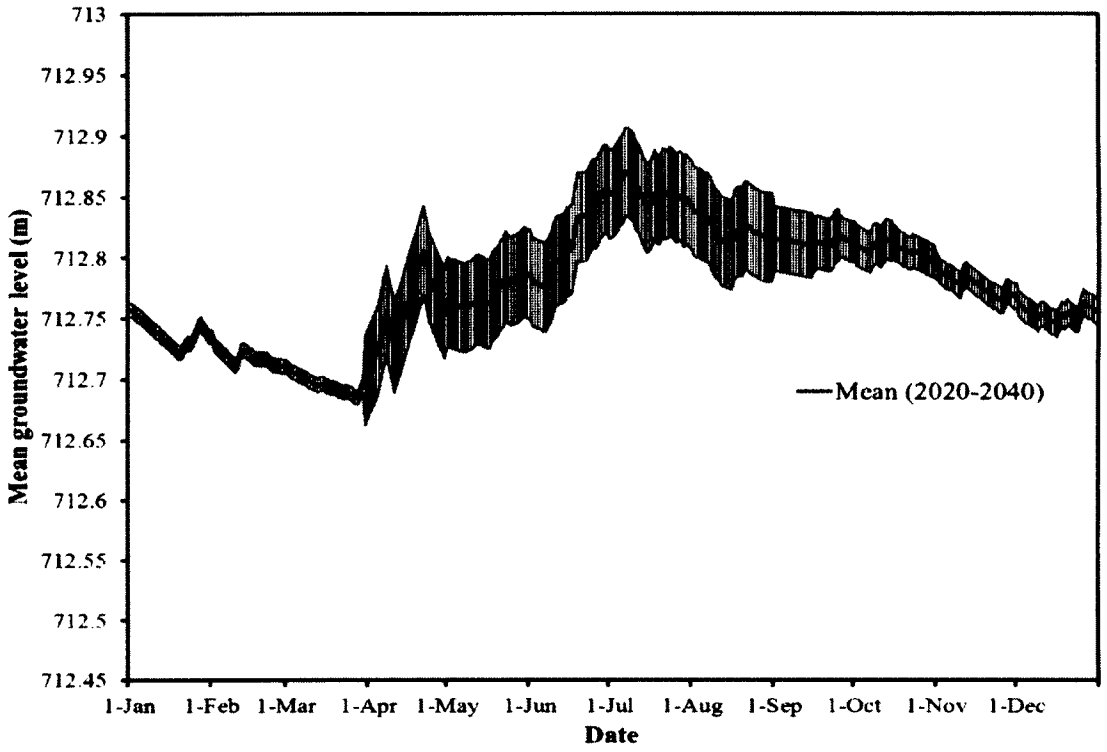

Figure 5.6 Mean daily groundwater levels of the study area under A2 scenario from 2020 to 2040. The error bars represent one standard deviation among mean daily groundwater levels of 2020 to 2040.

5.3 GW-SW interaction under B1 scenario

Fig. 5.7 illustrates the mean monthly groundwater contributions to stream flow under climate change condition of B1 GHG emission scenario for 2012-2016. Similar to those under the A2 scenario, the mean monthly groundwater contributions to stream flow under the B1 scenario also demonstrate variable annual patterns.

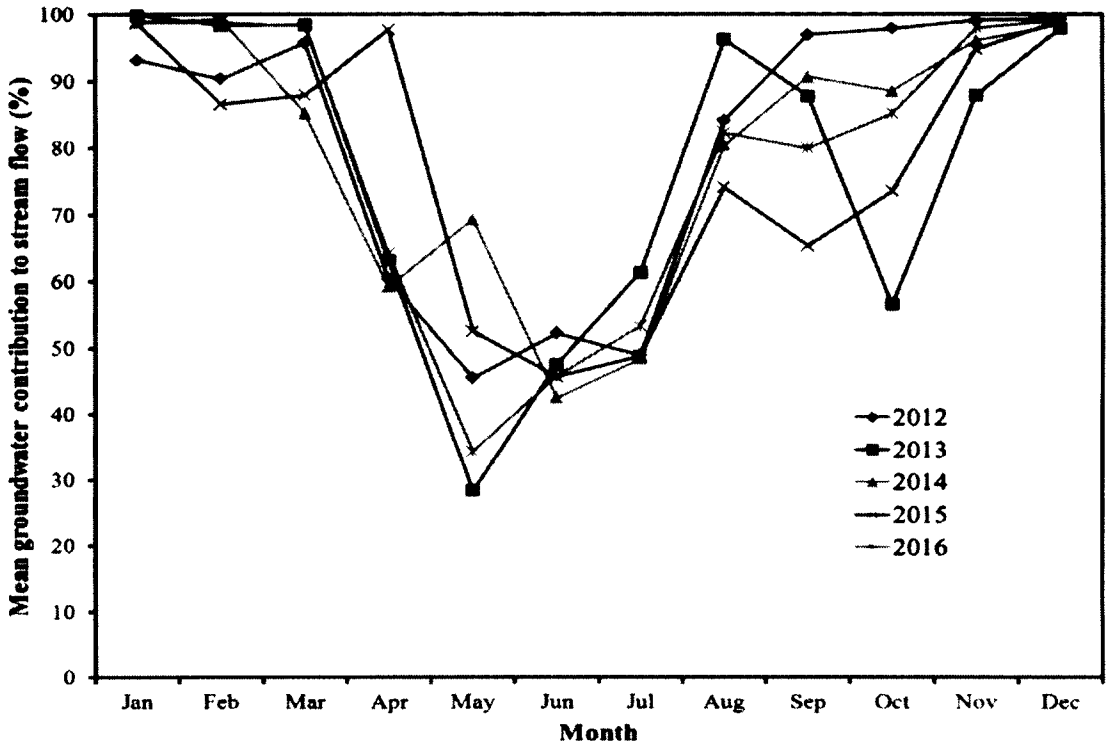

Figure 5.7 Mean monthly groundwater contributions to stream flow under climate change of B1 GHG emission scenario for 2012-2016 simulated by the GSSHA model

The comparison of mean groundwater contributions to stream flow during different seasons under the B1 GHG emission scenario for 2012-2016 is illustrated in Fig. 5.8. From this figure and projected seasonal precipitation under the B1 scenario (Fig. 4.7), it can be concluded that the mean groundwater contribution to stream flow decreases when the seasonal precipitation increases, and vice versa during the fall season only. Similar to the A2 scenario, during winter and spring seasons, the mean groundwater contribution to stream flow increases or decreases regardless of precipitation. During summer, the mean groundwater contribution to stream flow decreases when the seasonal precipitation increases, and vice versa for most of the years between 2012 and 2016. The discrepancy occurs because

under the B1 scenario, most of the summer precipitation occurs in June and July with low precipitation occurring in August, which results in higher groundwater contribution to stream flow in August than that of June and July. Consequently, this high groundwater contribution to stream flow (i.e., 84%) in August results in high mean groundwater contribution to stream flow during summer even though there is high precipitation in the summer. On average, the mean groundwater contribution to stream flow during winter, spring, summer, and fall from 2012 to 2016 is 97% (σ=2.4%), 70% (σ=4.3%), 61% (σ=4.8%), and 88% (σ=5.1%), respectively. These results also demonstrate that the mean groundwater contribution to stream flow is the lowest and highest during summer and winter, respectively. Hence, similar to the A2 scenario, stream flow depends mostly on groundwater flow during winter, but at a lesser extent during summer. Consequently, the highest and lowest water extraction from the river for future water supply could be possible during summer and winter, respectively, due to the highest (i.e., on average 6.06 m^3/s) and lowest (i.e., on average 0.23 m^3/s) mean stream flow rates during summer and winter, respectively.

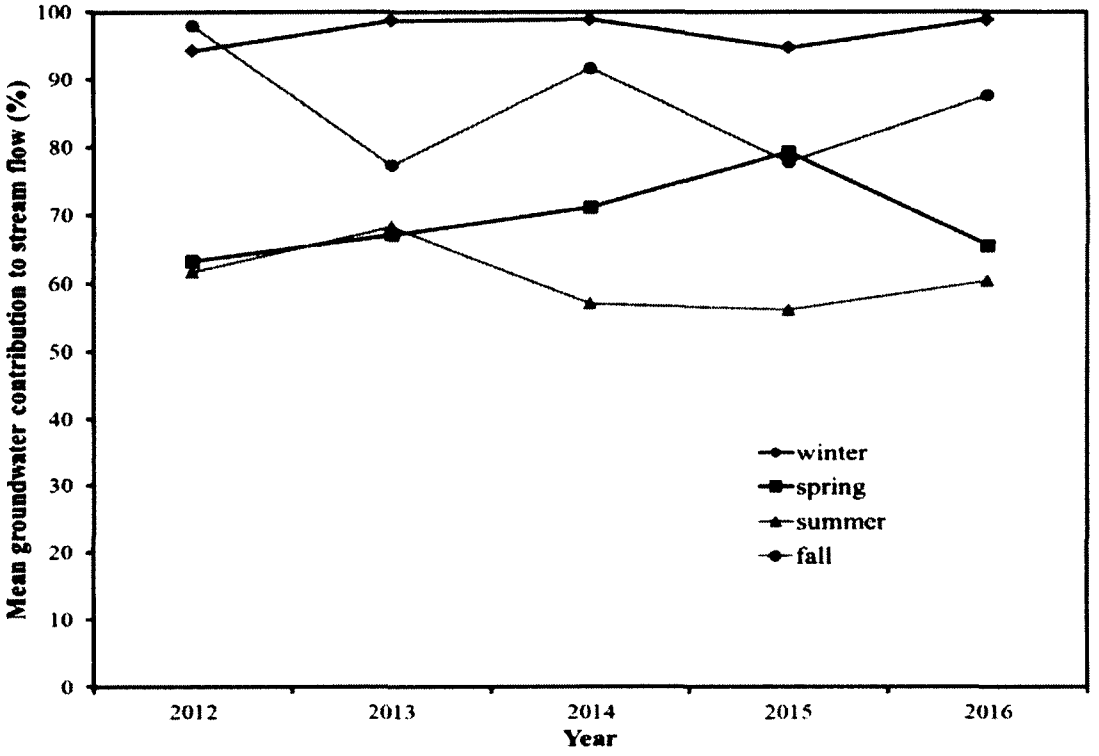

Figure 5.8 Comparison of mean groundwater contributions to stream flow during different seasons under B1 GHG emission scenario for 2012-2016

Fig. 5.9 compares the mean daily groundwater levels of the study area for year 2011 and those under climate change of B1 GHG emission scenario for 2012-2016. The results illustrate that the mean daily groundwater levels in the study area show almost similar profiles annually as those under the A2 GHG emission scenario due to the almost similar temporal pattern of annual precipitation. The mean daily groundwater levels, however, do increase at a lesser rate due to less infiltration resulting from less precipitation predicted under the B1 scenario in comparison to the A2 scenario. Fig. 5.10 illustrates the temporal variation of the mean daily groundwater levels of the study area for year 2011 and under the climate change of B1 GHG emission scenario for 2012-2016. It is also found that in comparison to 2011, the mean daily groundwater levels are expected to increase at the end of

2016 by a lesser amount than under the A2 scenario since there is less precipitation predicted under the B1 scenario. Overall, the mean annual groundwater level is expected to increase by 1 cm, 1.2 cm, 1.5 cm, and 2 cm in 2013, 2014, 2015, and 2016, respectively, compared to the mean annual groundwater level in 2011. In 2012, this water level was expected to decrease by 0.6 cm compared to the 2011 condition. Therefore, the increased mean annual groundwater levels in the study area will provide more groundwater discharge to stream flow for future water supply in the study area, except 2012, compared to year 2011. However, less groundwater discharge to stream flow will occur in the study area under the B1 scenario compared to the A2 scenario.

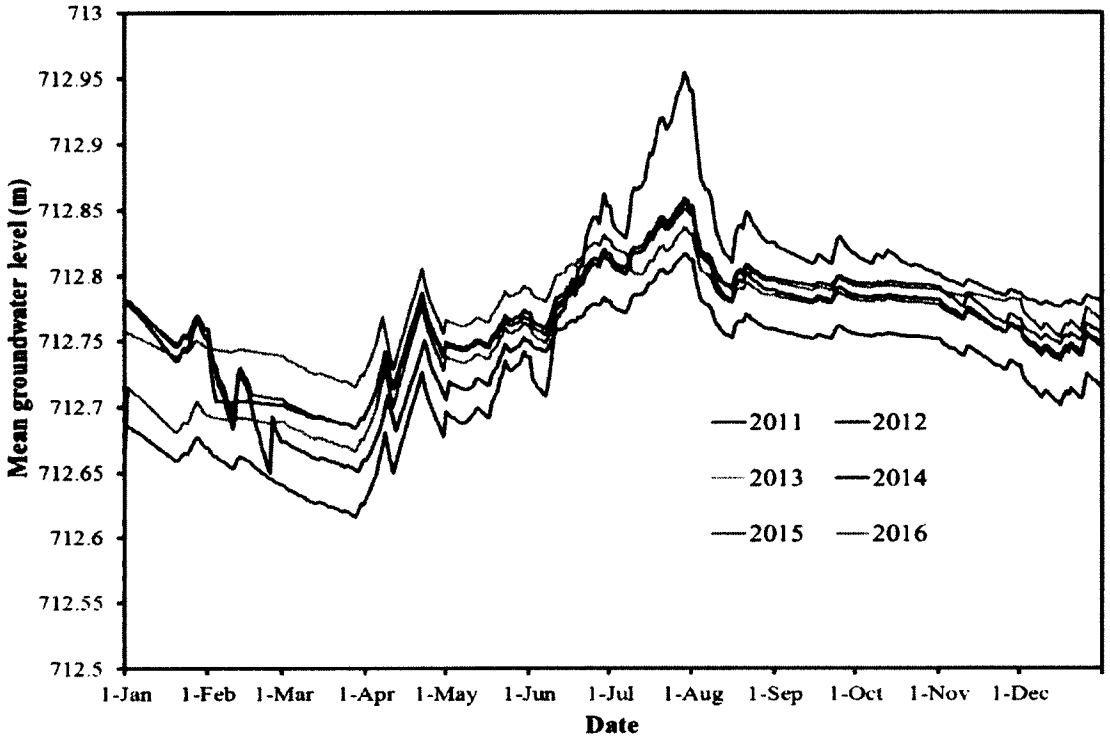

Figure 5.9 Comparison of mean daily groundwater levels of the study area for year 2011 and climate change of B1 GHG emission scenario for 2012-2016 simulated by the GSSHA model

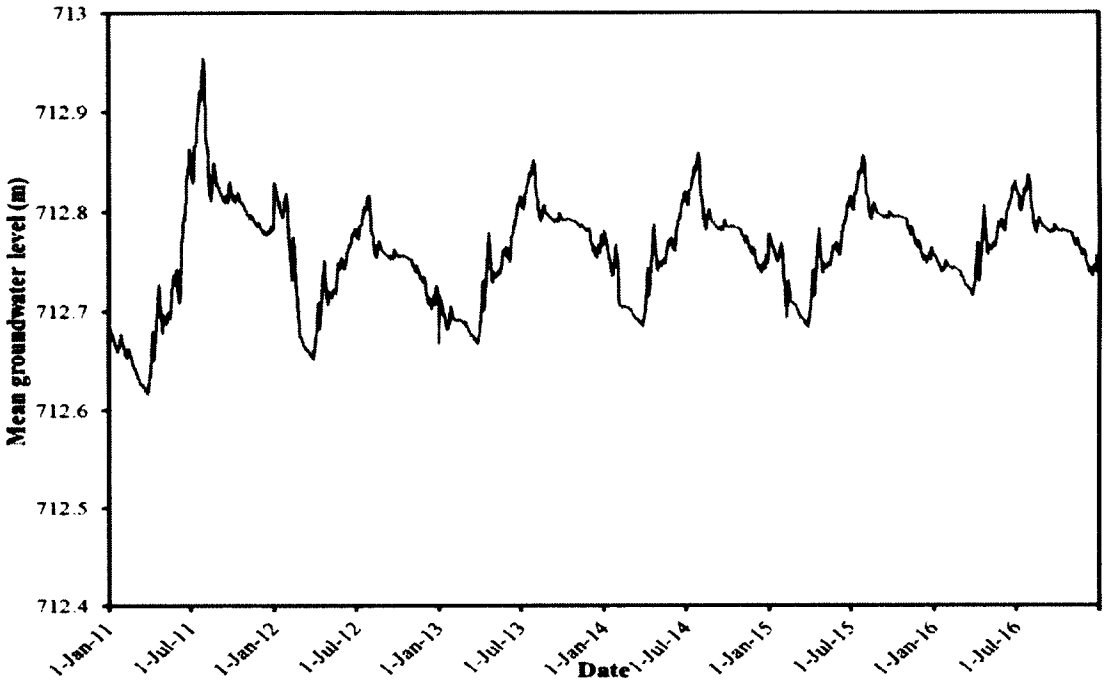

Figure 5.10 Mean daily groundwater levels of the study area for year 2011 and climate change of B1 GHG emission scenario for 2012-2016 simulated by the GSSHA model

Similar to the short-term period, the mean monthly groundwater contributions to stream flow under the B1 scenario will show variable annual patterns in the long-term period (Fig 5.11).

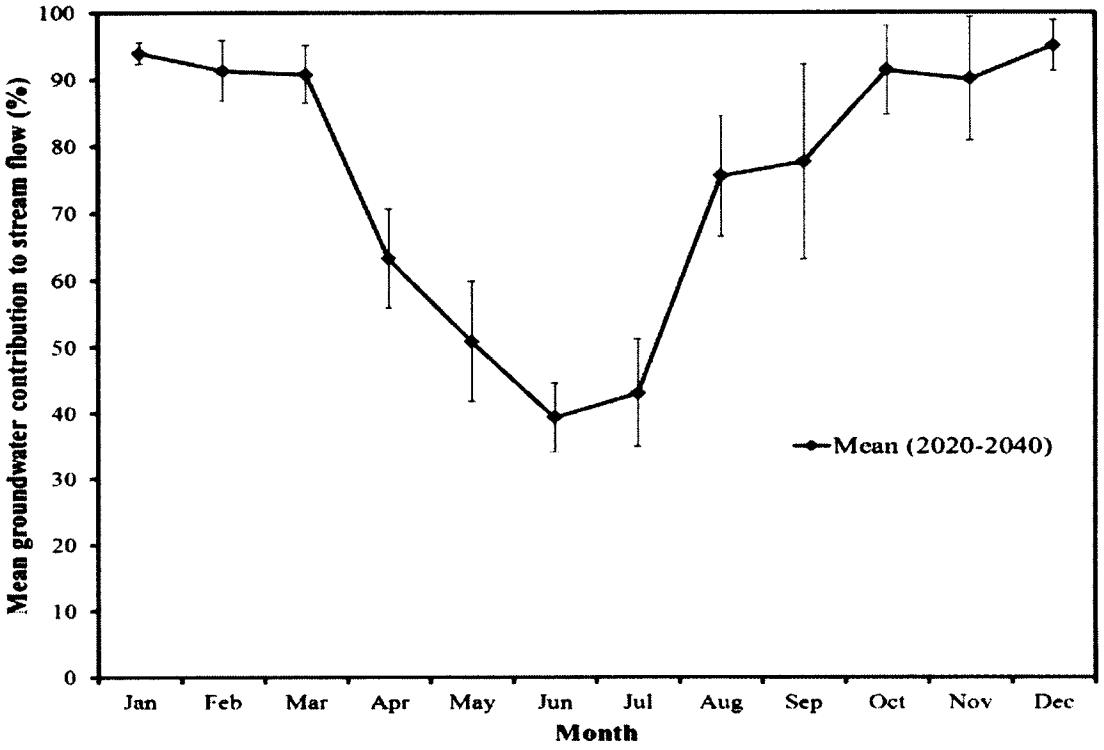

Figure 5.11 Mean monthly groundwater contributions to stream flow under B1 scenario from 2020 to 2040. The error bars represent one standard deviation among mean monthly groundwater contributions to stream flow of 2020 to 2040.

As in the short-term period, the mean groundwater contributions to stream flow during different seasons under the B1 scenario will show similar trends in the long-term period. On average, this number during winter, spring, summer, and fall from 2020 to 2040 under the B1 scenario will be 94% (σ=2%), 68% (σ=5%), 54% (σ=4%), and 86% (σ=7%), respectively. Similarly, the mean daily groundwater levels in the study area under the B1 scenario will show almost identical responses in the long-term period (Fig 5.12).

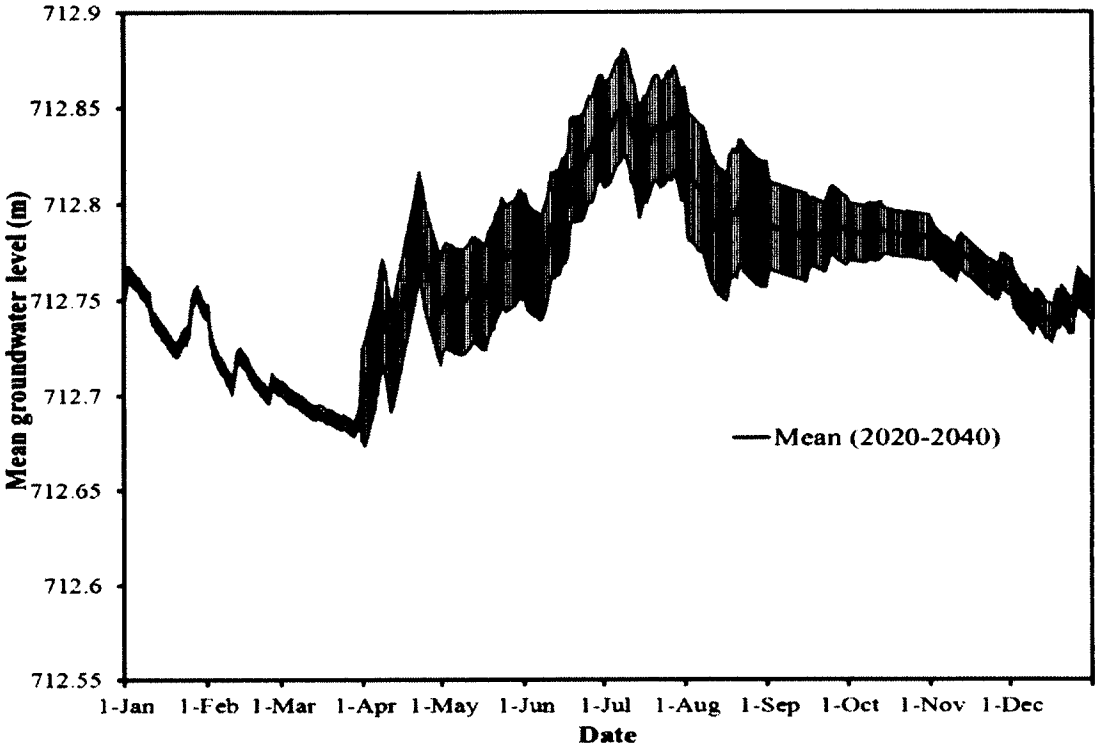

Figure 5.12 Mean daily groundwater levels of the study area under B1 scenario from 2020 to 2040. The error bars represent one standard deviation among mean daily groundwater levels of 2020 to 2040.

5.4 Comparison of GW-SW interaction between A2 and B1 scenarios

Fig. 5.13 shows the comparison of mean monthly groundwater contributions to stream flow of 2012-2016 under climate change of A2 and B1 GHG emission scenarios with respect to the reference period (2007-2011). Here, the period of 2007-2011 was used as reference period because the calibration and validation of the model was done during that time period. The results illustrate that the mean monthly groundwater contributions to stream flow of 2012-2016 are lower during most of the months under the A2 scenario than under the B1 scenario due to a higher amount of precipitation and temperature increase predicted

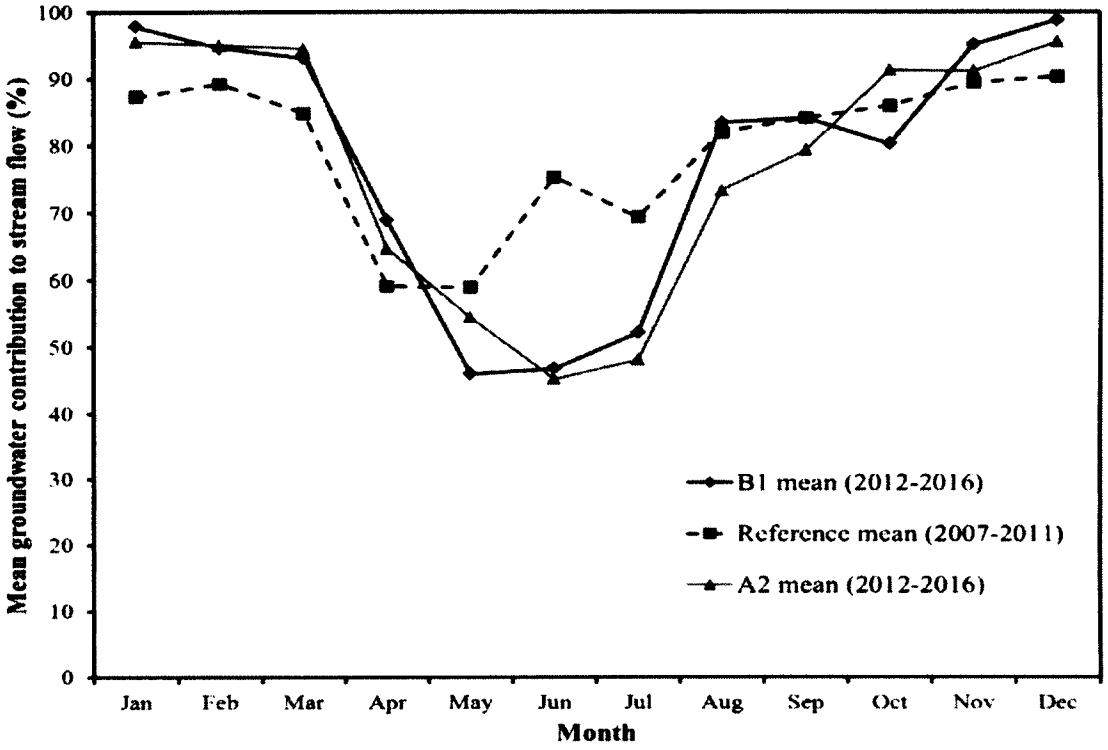

Figure 5.13 Comparison of mean monthly groundwater contributions to stream flow of 2012-2016 under climate change of A2 and B1 GHG emission scenarios with respect to reference period (2007-2011)

under the A2 scenario. The lowest and highest mean monthly groundwater contributions to stream flow of 2012-2016 under the A2 scenario are found in June (i.e., 45%), and January and December (i.e., 96%), respectively. On the other hand, under the B1 scenario, the lowest and highest mean monthly groundwater contributions to stream flow of 2012-2016 are found in May (i.e., 46%) and December (i.e., 99%), respectively. On average, stream flow is mostly dependent on groundwater flow during December under both scenarios. On the other hand, stream flow is least dependent on groundwater flow during May and June under the B1 and A2 scenarios, respectively. The results also show that the mean monthly groundwater contributions to stream flow of 2012-2016 under the A2 and B1 scenarios are lower in late

spring and summer than under the reference period (2007-2011) due to increased precipitation and temperature predicted under those scenarios during those seasons with respect to the reference period. During other months, especially in winter and early spring, however, the mean monthly groundwater contributions to stream flow of 2012-2016 under both scenarios are almost higher than that under the reference period due to variable precipitation observed in those months of reference period. Therefore, climate change influences the patterns of mean monthly groundwater contribution to stream flow significantly.

The comparison of the mean annual groundwater contributions to stream flow from 2012 to 2016 under climate change of the A2 and B1 scenarios with respect to year 2011 is presented in Fig. 5.14. The results illustrate that the A2 scenario shows an increase-decrease cyclic pattern of mean annual groundwater contribution to stream flow from 2012 to 2016. On the other hand, the B1 scenario shows a decrease-increase cyclic pattern of mean annual groundwater contribution to stream flow from 2012 to 2016. The highest and lowest mean annual groundwater contributions during 2012-2016 under the A2 scenario are found in 2013 (i.e., 78.1%) and 2012 (i.e., 75.2%), respectively, due to the lowest (i.e., 509 mm) and highest (i.e., 530 mm) precipitation predicted in those years between 2012 and 2016. On the other hand, under the B1 scenario, the highest and lowest mean annual groundwater contributions during 2012-2016 are found in 2012 (i.e., 80.2%) and 2013 (i.e., 77%), respectively, due to the lowest (i.e., 494 mm) and highest (i.e., 524 mm) precipitation predicted in those years. On average, the mean annual groundwater contribution to stream flow of 2012-2016 under the A2 and B1 scenarios is 76.7% (σ=1.1%) and 78.2% (σ=1.25%), respectively. This variation occurs due to a higher precipitation and temperature increase

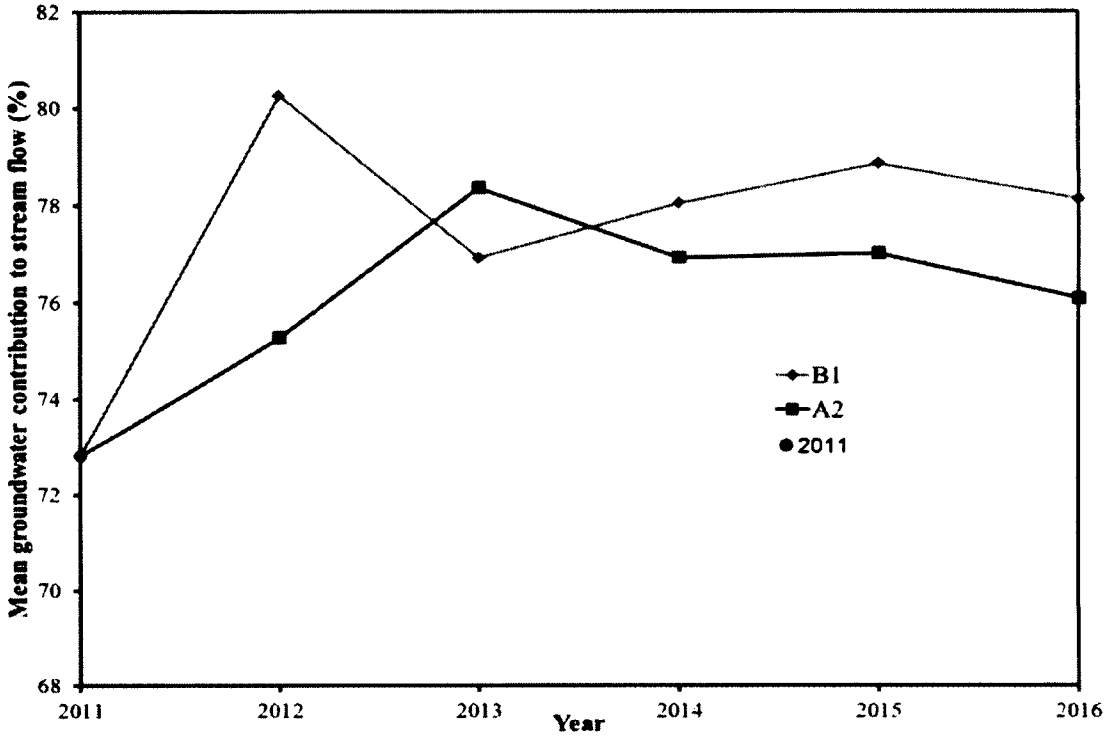

Figure 5.14 Comparison of mean annual groundwater contributions to stream flow from 2012 to 2016 under climate change of A2 and B1 GHG emission scenarios with respect to year 2011

predicted under the A2 scenario than under the B1 scenario during 2012 to 2016. On average, it was found that the mean annual groundwater contribution to stream flow during the reference period (2007-2011) is approximately 80%. These results also correspond to the finding in other studies of similar mean annual groundwater contribution to stream flow (Clow et al., 2003 (75%); Hughes, 2004 (74-80%); Hood et al., 2006 (67-74%); Hannah et al., 2007 (70%); Stewart et al., 2007 (87%); Bidwell et al., 2008 (78-93%); Koeniger et al., 2009 (60-70%); Yimam, 2010 (71.9%)). In general, surface runoff and base flow, which determine groundwater contribution to stream flow, are influenced by geographic environment, catchment geology, topography, soils and vegetation (Soulsby et al., 2006;

Price, 2011). In addition, climate also influences the groundwater contribution to stream flow (Price, 2011). For example, in Arctic and subarctic watersheds, where permafrost is the main characteristic of climate, the mean annual groundwater contribution to stream flow ranges from 31% to 38% (Walvoord et al., 2007); in western and northern Europe (e.g., United Kingdom, Germany, Belgium), where more precipitation occurs during winter as rainfall, the mean annual groundwater contribution to stream flow is 30% - 40% (Soulsby et al., 2006), 30% (Krause et al., 2007), 60% - 70% (Koeniger et al., 2009), and 71.9% Yimam (2010); in the mountainous region, where snowmelt and glacier melt provide a significant surface runoff, the mean annual groundwater contribution to stream flow is 75% (Clow et al., 2003), and 67% - 74% (Hood et al., 2006), 70% (Hannah et al., 2007); in Cuito River watershed in Angola, where the terrain is hilly and the climate is arid, the mean annual groundwater contribution to stream flow ranges from 74% to 80% (Hughes, 2004); in a steep headwater catchment in New Zealand in humid climate, the mean annual groundwater contribution to stream flow is 87% (Stewart et al., 2007), and 78% - 93% (Bidwell et al., 2008). With respect to the mean annual groundwater contribution to stream flow during the reference period, the mean annual groundwater contribution to stream flow from 2012 to 2016 under the A2 and B1 scenarios is expected to decrease by 3.3% and 1.8%, respectively, due to the increased precipitation (on average 6.1% under the A2 and 3.6% under the B1 scenarios) and temperature (on average 0.64°C under the A2 and 0.36°C under the B1 scenarios) predicted, with respect to that under the reference period. This would result in increased stream flow (on average 6.7% under the A2 and 3% under the B1 scenarios) and groundwater discharge (on average 2.8% under the A2 and 1.2% under the B1 scenarios), but the major increases occurred in surface runoff (on average 22.5% under the A2 and 11.2% under the B1

scenarios). Therefore, climate change significantly affects stream and groundwater discharges, and surface runoff, as well as the mean annual groundwater contribution to stream flow. Table 5.3 presents a summary of mean annual stream flow, surface runoff, and groundwater discharge under the reference period and both scenarios for the short-term period. Walvoord et al. (2007) also found similar type of change in the mean annual groundwater contribution to stream flow in the Yukon River basin. This decreased groundwater contribution to stream flow under both scenarios may result in warmer stream temperature, lower dissolved oxygen in stream, and increased nutrient concentrations in stream (e.g., Dissolved organic carbon (DOC) and nitrogen (DON)) that may promote excessive growth of habitat-choking algae by increasing surface runoff and soil erosion (Price et al., 2006; Leigh, 2010). These results demonstrate that under the B1 scenario those above mentioned impacts will be lower as compared to the A2 scenario due to higher annual groundwater contribution to stream flow under the B1 scenario. These results also demonstrate that stream flow is more dependent on groundwater flow under the B1 scenario than under the A2 scenario. Therefore, more annual water extraction from the river, and allocation to the stakeholders for future water supply could be possible under the A2 scenario than under the B1 scenario without causing a negative impact on regional groundwater level.

Table 5.3 Mean annual precipitation, temperature, stream flow, surface runoff, and groundwater discharge under the reference period (2007-2011) and A2 and B1 scenarios for the short-term period (2012-2016). The values within the parentheses are relative changes except for temperature, where absolute changes were calculated.

Scenario	Mean annual precipitation (mm)	Mean annual temperature (°C)	Mean annual stream flow (m^3/s)	Mean annual groundwater discharge (m^3/s)	Mean annual surface runoff (m^3/s)
Reference period	492	2.63	3.08	2.46	0.62
A2	522 (6.1%)	3.27 (0.64)	3.29 (6.7%)	2.53 (2.8%)	0.76 (22.5%)
B1	510 (3.6%)	2.99 (0.36)	3.18 (3%)	2.49 (1.2%)	0.69 (11.2%)

When the mean monthly groundwater contributions to stream flow of 2020-2040 (long-term period) under the A2 and B1 scenarios are compared to that under the reference period (2007-2011), results similar to the short term period are found (Fig. 5.15). The lowest and highest mean monthly groundwater contributions to stream flow of 2020-2040 are expected in June (i.e., 37%) and December (i.e., 92%) under the A2 scenario, and also in June (i.e., 46%) and December (i.e., 95%) under the B1 scenario, respectively. On average, stream flow is expected to be mostly dependent on groundwater flow during December, but least dependent during June under both scenarios.

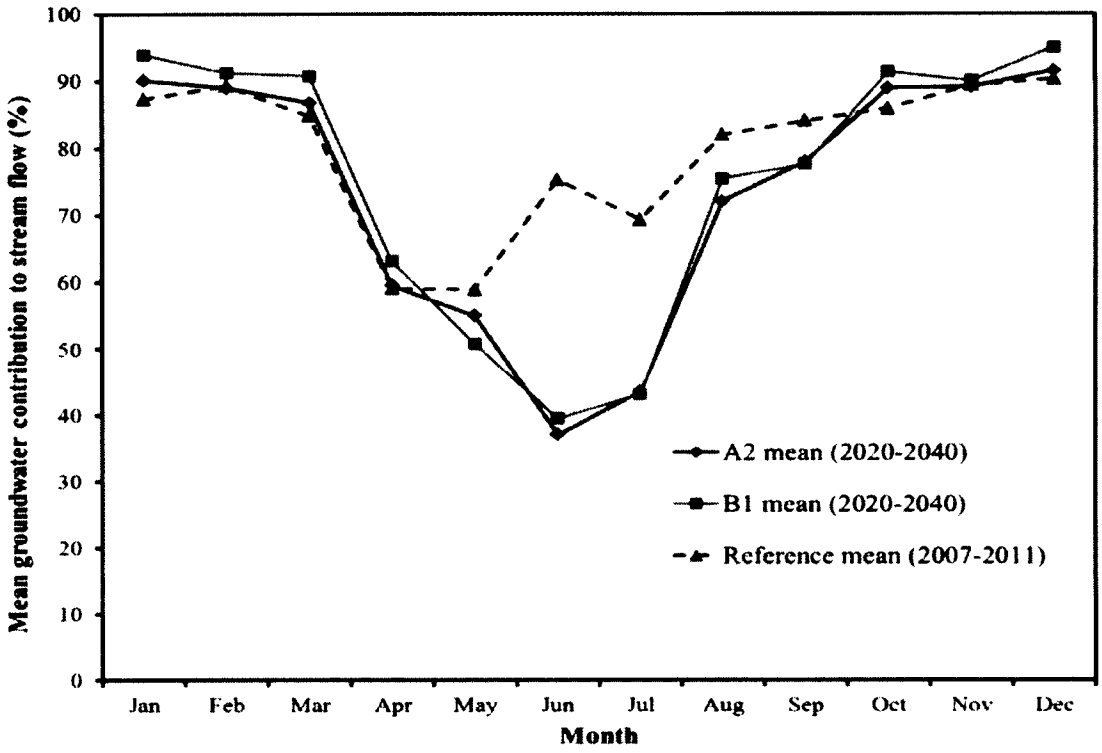

Figure 5.15 Comparison of mean monthly groundwater contributions to stream flow of 2020-2040 under climate change of A2 and B1 GHG emission scenarios with respect to reference period (2007-2011)

The mean annual groundwater contribution to stream flow, on average, during 2020-2040 under the A2 and B1 scenarios is expected to be 74.5% (σ=2%), and 75.6% (σ=3%), respectively, representing a decrease by 5.5% and 4.4%, respectively, with respect to that under the reference period (2007-2011). This variation occurs due to the increased precipitation (on average 6.7% under the A2 and 4.8% under the B1 scenarios) and temperature (on average 0.83°C under the A2 and 0.64°C under the B1 scenarios) predicted, with respect to that under the reference period. The climate change would result in increased stream flow (on average 10.9% under the A2 and 7.9% under the B1 scenarios), groundwater discharge (on average 3.7% under the A2 and 2.3% under the B1 scenarios), and surface

runoff (on average 40.3% under the A2 and 30.5% under the B1 scenarios). Table 5.4 shows a summary of mean annual stream flow, surface runoff, and groundwater discharge under the reference period and both scenarios for the long-term period.

Table 5.4 Mean annual precipitation, temperature, stream flow, surface runoff, and groundwater discharge under the reference period (2007-2011) and A2 and B1 scenarios for the long-term period (2020-2040). The values within the parentheses are relative changes except for temperature, where absolute changes were calculated.

Scenario	Mean annual precipitation (mm)	Mean annual temperature (°C)	Mean annual stream flow (m^3/s)	Mean annual groundwater discharge (m^3/s)	Mean annual surface runoff (m^3/s)
Reference period	492	2.63	3.08	2.46	0.62
A2	525 (6.7%)	3.46 (0.83)	3.42 (10.9%)	2.55 (3.7%)	0.87 (40.3%)
B1	516 (4.8%)	3.27 (0.64)	3.32 (7.9%)	2.51 (2.3%)	0.81 (30.5%)

Fig. 5.16 shows the comparison of mean daily groundwater levels of the study area between A2 and B1 GHG emission scenarios for 2012-2016. The results show that during most of the time, the mean daily groundwater levels under the A2 scenario are higher than those under the B1 scenario due to an increased infiltration resulting from a higher amount of precipitation and temperature increase predicted to occur under the A2 scenario. As a result, for most of the years between 2012 and 2016, except 2013, more groundwater discharge to stream flow occurs in the A2 scenario in the study area. When the precipitation under the B1

scenario is higher than that under the A2 scenario (e.g., in 2013), the mean daily groundwater levels under the B1 scenario are higher than those under the A2 scenario.

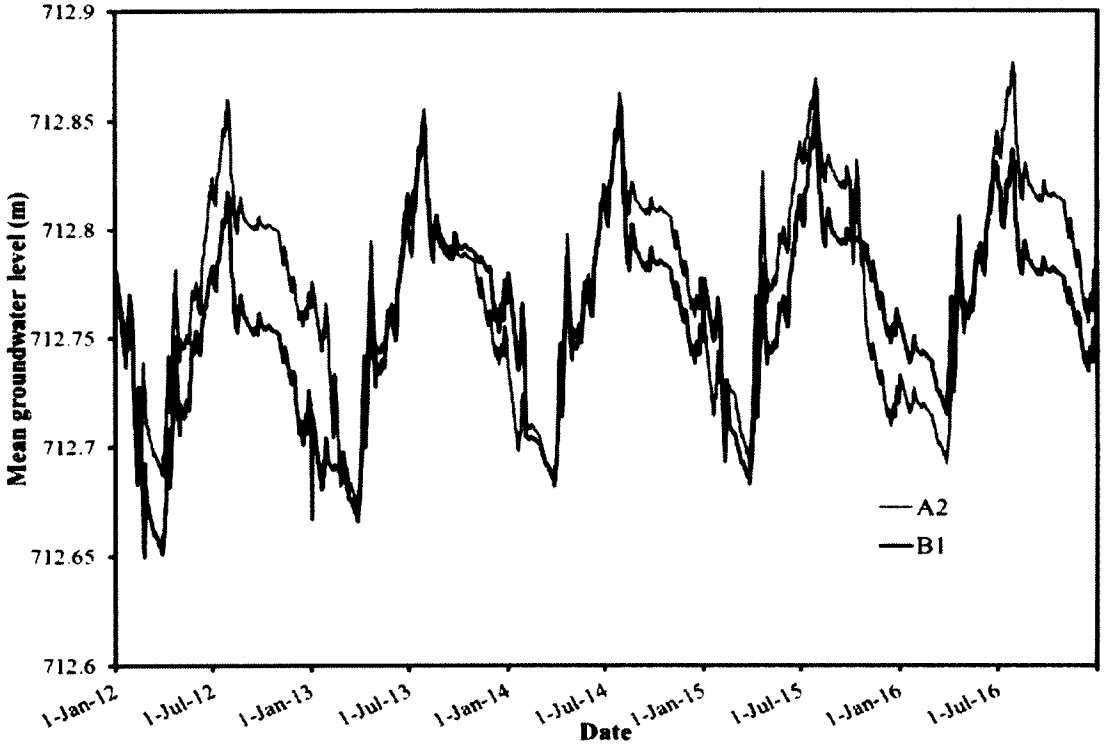

Figure 5.16 Comparison of mean daily groundwater levels of the study area between A2 and B1 GHG emission scenarios for 2012-2016 simulated by the GSSHA model

Fig. 5.17 presents the comparison of 2012-2016's mean daily groundwater levels of the study area under climate change of A2 and B1 GHG emission scenarios with respect to the reference period (2007-2011). Similar to the results obtained from Fig. 5.16, the mean daily groundwater levels of 2012-2016 are higher during most of the months under the A2 scenario than under the B1 scenario, with the highest and lowest mean daily groundwater levels under both scenarios occurring in July and March, respectively. Under both scenarios, however, the

mean daily groundwater levels are higher than those under the reference period (2007-2011) due to increased precipitation and temperature predicted. On average, the mean annual groundwater level under the A2 and B1 scenarios is expected to increase by 4.5 cm (σ=1.9 cm) and 3.5 cm (σ=1.5 cm), respectively, compared to that under the reference period. These results indicate that climate change has a significant impact on the mean daily and annual groundwater levels. Therefore, the increased mean annual groundwater levels in the study area will provide more groundwater discharge to stream flow (on average 2.8% in the A2 and 1.2% in the B1 scenarios) under both scenarios in the study area. However, less groundwater discharge will be available under the B1 scenario compared to the A2 scenario due to low groundwater levels under the B1 scenario. These high groundwater levels under the A2 scenario also support the more annual water extraction from the river, and allocation to the stakeholders for future water supply under the A2 scenario than under the B1 scenario without causing a negative impact on regional groundwater level, compared to the reference period.

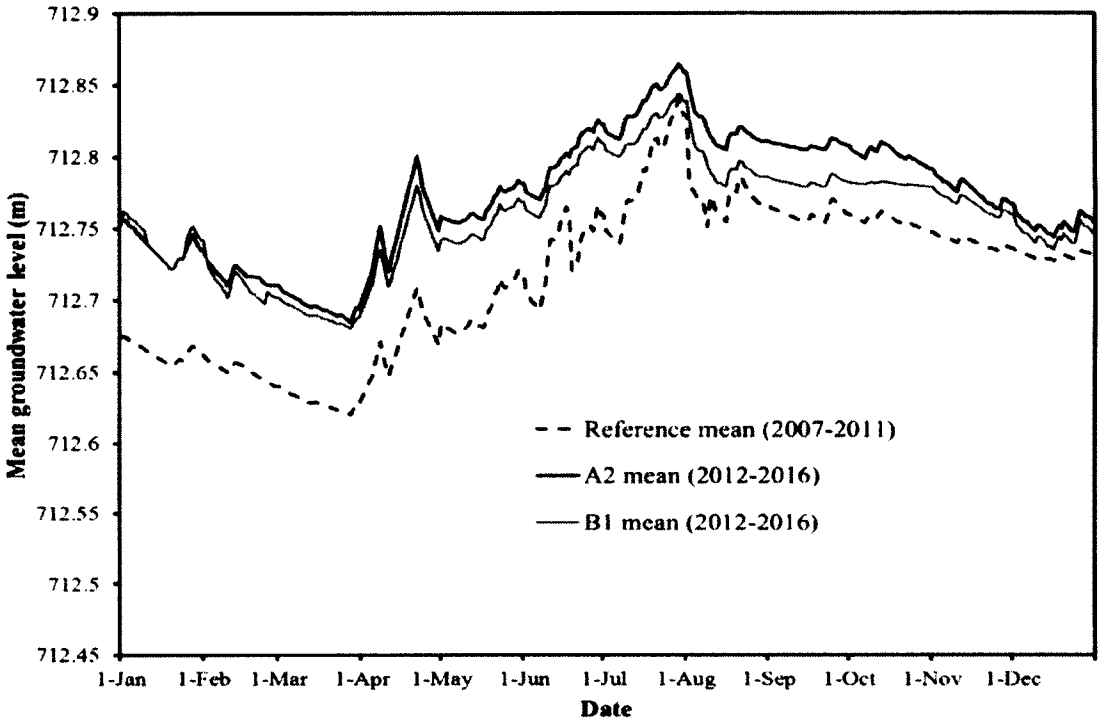

Figure 5.17 Comparison of mean daily groundwater levels of the study area of 2012-2016 under A2 and B1 GHG emission scenarios with respect to the reference period (2007-2011)

When the mean daily groundwater levels of the study area of 2020-2040 under climate change of both emission scenarios are compared to those during the reference period (2007-2011), results almost similar to those during the short-term period are found, except for the peak groundwater levels due to the shift of peak monthly precipitation (Fig. 5.18). Compared to the mean annual groundwater level under the reference period, the mean annual groundwater level under the A2 and B1 scenarios during 2020-2040 is expected to increase, on average, by 5.5 cm (σ=2.5 cm) and 4.3 cm (σ=2 cm), respectively. Therefore, these increased mean annual groundwater levels in the study area under both scenarios in the long-term period will result in similar impacts as in the short-term period.

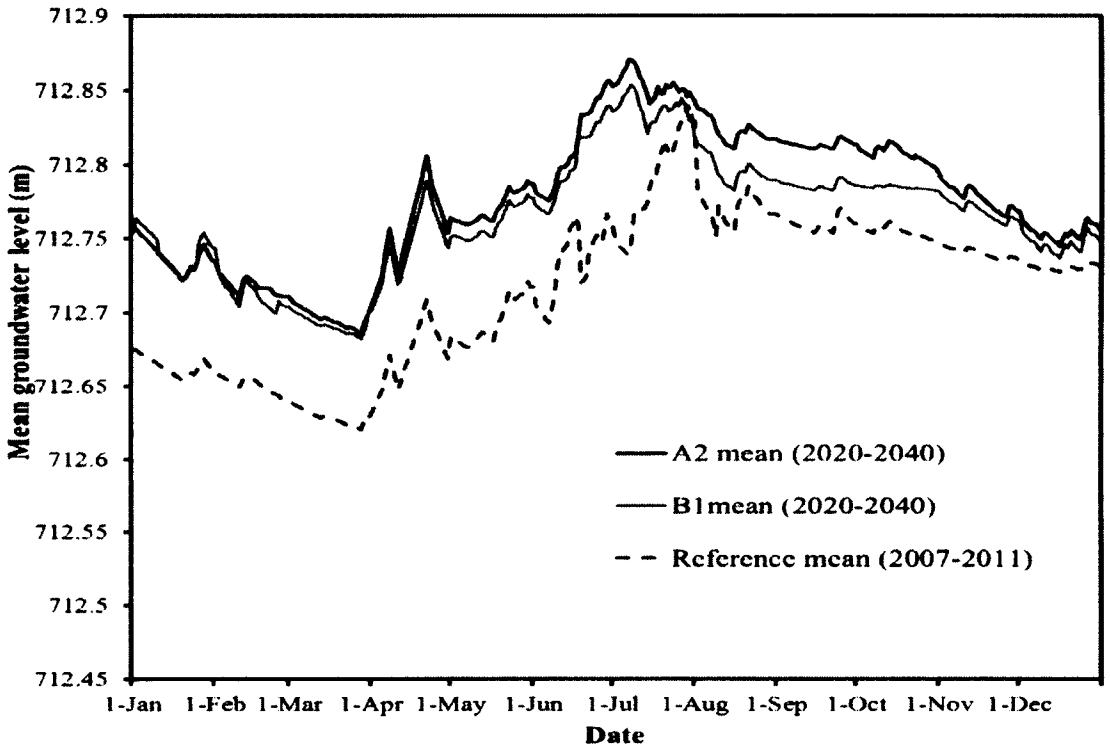

Figure 5.18 Comparison of mean daily groundwater levels of the study area of 2020-2040 under A2 and B1 GHG emission scenarios with respect to the reference period (2007-2011)

Figs. 5.19-5.22 illustrate the comparison of mean groundwater contributions to stream flow between A2 and B1 GHG emission scenarios during different seasons from 2012 to 2016 with respect to year 2011. It can be found that during winter, the mean groundwater contributions are lower for most of the years under the A2 scenario than under the B1 scenario (Fig. 5.19). This variation occurs because more precipitation is predicted during fall under the A2 scenario which results in higher groundwater levels and stream flow. In addition, during winter, precipitation occurs as snow which cannot completely infiltrate, but having higher groundwater levels resulting from fall season under the A2 scenario generates

higher groundwater discharge as well as stream flow in winter than under the B1 scenario. As a result, the mean groundwater contributions to stream flow during winter under the A2 scenario are lower than under the B1 scenario. These results also demonstrate that the mean groundwater contribution to stream flow during winter depends on the antecedent season's precipitation amount. On average, the mean groundwater contribution to stream flow during 2012-2016 winters under the A2 and B1 scenarios is 95% and 97%, respectively. During the spring of most of the years between 2012 and 2016, the mean groundwater contributions to stream flow are lower under the B1 scenario than under the A2 scenario (Fig. 5.20). This discrepancy may occur due to the fact that more precipitation is predicted during winter under the B1 scenario than under the A2 scenario, and during spring, almost equal precipitation is predicted under both scenarios. When snow melts in April, higher surface runoff occurs under the B1 scenario which results in lower mean groundwater contribution to stream flow. These results also indicate that the mean groundwater contribution to stream flow during spring depends on the amount of the antecedent season's precipitation. On average, the mean groundwater contribution to stream flow during spring under the A2 and B1 scenarios of 2012-2016 is 71% and 70%, respectively. During summer, the contributions are lower under the A2 scenario than under the B1 scenario due to more precipitation increase being predicted under this scenario (Fig. 5.21). On average, the mean groundwater contribution to stream flow during summer under 2012-2016's A2 and B1 scenarios is 55% and 61%, respectively. During fall, the contributions under both scenarios show variable patterns annually because variable annual precipitation patterns are predicted during fall under both scenarios (Fig. 5.22). On average, the contribution during fall under the A2 and B1 scenarios of 2012-2016 is 86% and 88%, respectively.

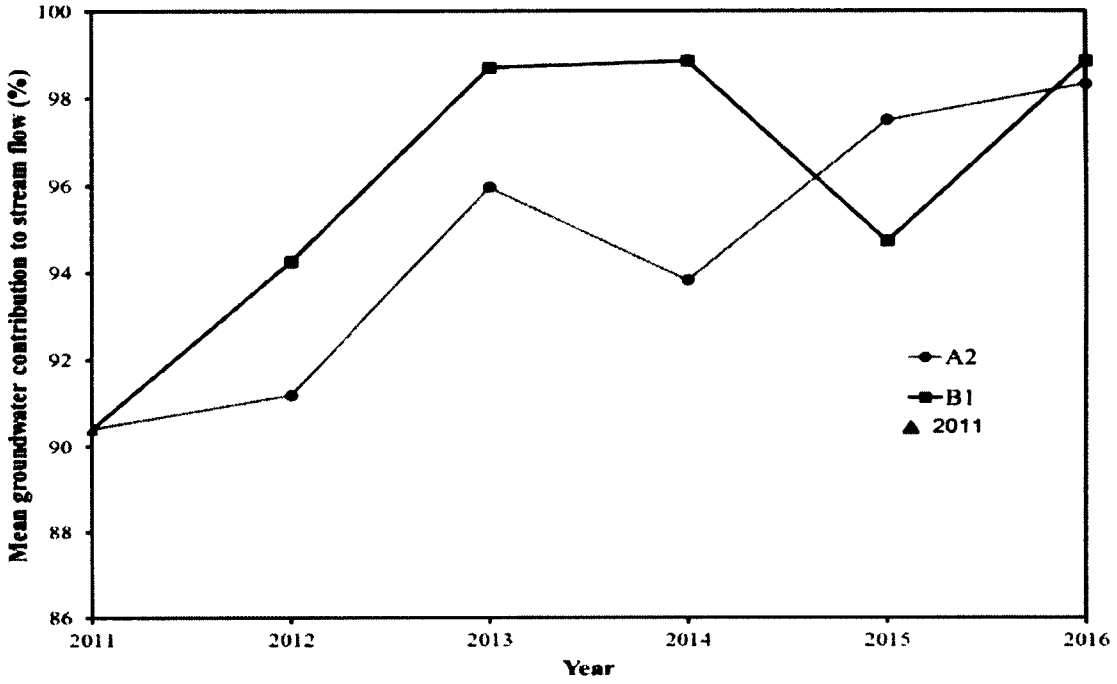

Figure 5.19 Comparison of mean groundwater contributions to stream flow between A2 and B1 scenarios during winter from 2012 to 2016 with respect to year 2011

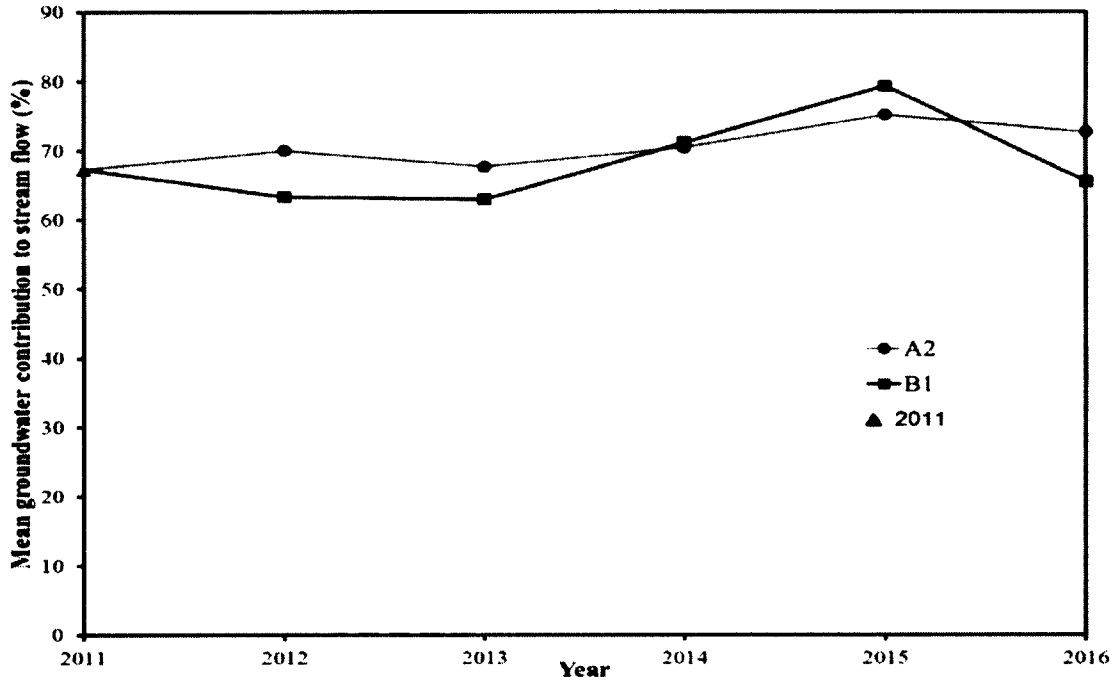

Figure 5.20 Comparison of mean groundwater contributions to stream flow between A2 and B1 scenarios during spring from 2012 to 2016 with respect to year 2011

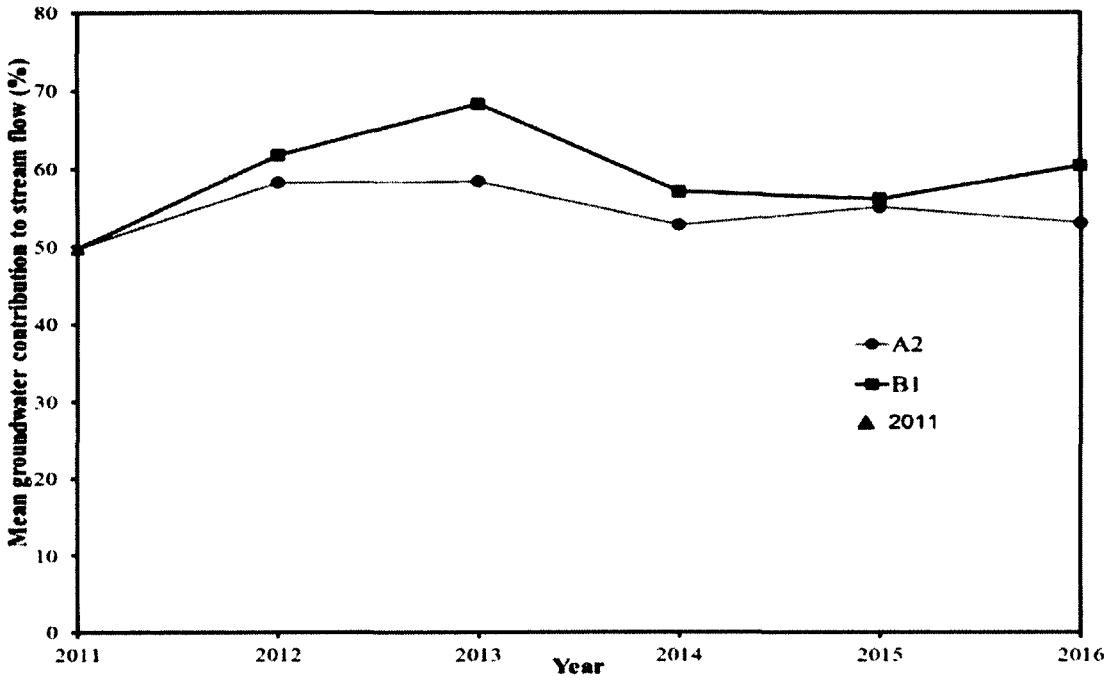

Figure 5.21 Comparison of mean groundwater contributions to stream flow between A2 and B1 scenarios during summer from 2012 to 2016 with respect to year 2011

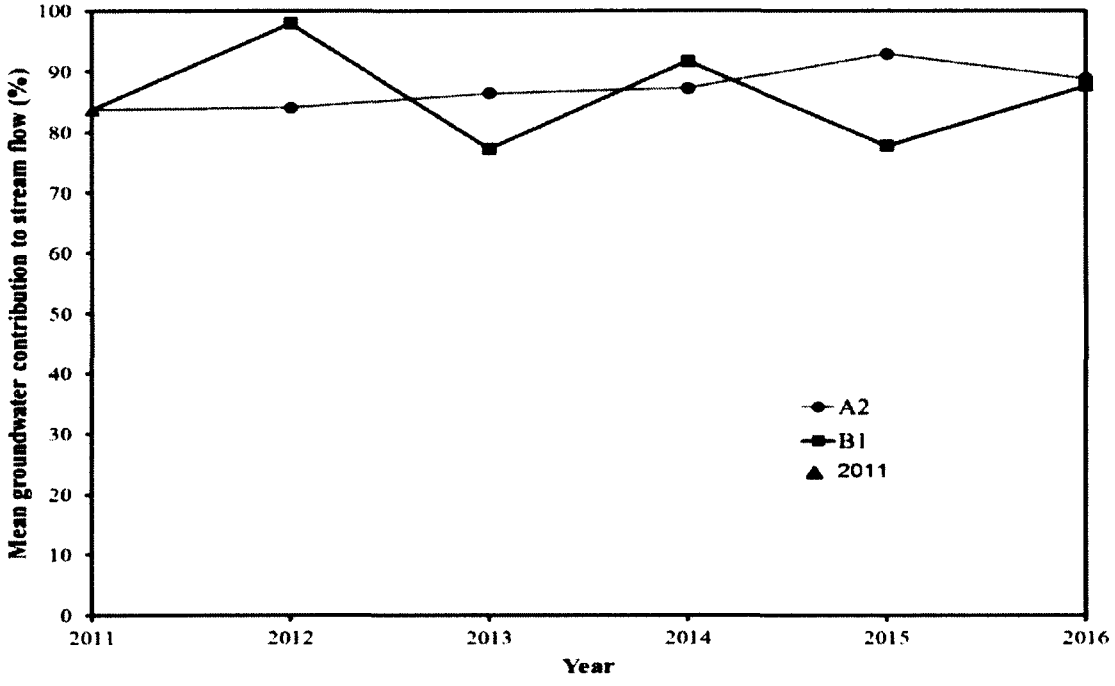

Figure 5.22 Comparison of mean groundwater contributions to stream flow between A2 and B1 scenarios during fall from 2012 to 2016 with respect to year 2011

Similar to the short-term period, the mean groundwater contributions to stream flow during various seasons follow similar trends in the long-term period. On average, under the A2 scenario, this contribution during winter, spring, summer, and fall from 2020 to 2040 will be 93% (σ=3%), 69% (σ=4.5%), 50% (σ=3.5%), and 85% (σ=2.5%), respectively. On the other hand, under the B1 scenario, this contribution will be 94% (σ=2%), 68% (σ=5%), 54% (σ=4%), and 86% (σ=7%), respectively. On average, the corresponding contribution during 2007-2011 (reference period) is 98% (σ=2.6%), 72% (σ=2.9%), 62% (σ=5.9%), and 89% (σ=4.2%), respectively. As compared to the period of 2007 to 2011, the mean groundwater contribution to stream flow during winter, spring, summer, and fall from 2020 to 2040 is expected to decrease by 5%, 3%, 12%, and 4% under the A2 scenario, respectively, and decrease by 4%, 4%, 8%, and 3% under the B1 scenario, respectively. This is due to increased precipitation and temperature predicted under both scenarios as compared to the reference period. Therefore, the effect of climate change on the mean seasonal groundwater contributions to stream flow is significant.

These decreased seasonal groundwater contributions to stream flow under both scenarios will result in seasonal warmer stream temperature, lower dissolved oxygen in stream, and increased nutrient concentrations in stream. These impacts will be expected more during summer among other seasons due to higher decrease of groundwater contribution to stream flow during summer. These results also demonstrate that under the B1 scenario these impacts will be expected less, except in spring, as compared to that under the A2 scenario due to higher groundwater contribution to stream flow in the B1 scenario.

5.5 Summary

In this study, the impacts of climate change on GW-SW interaction were investigated using a study area along the river of the Mainstem sub-watershed of KRW as a case study for a short-term period (2012-2016) and a long-term period (2020-2040) by using the developed GW-SW interaction model (i.e., GSSHA). Two types of IPCC climate change scenarios (A2: heterogeneous world with self-reliance and preservation of local identities, and B1: more integrated and environmental friendly world) were chosen. Based on the simulation results for the short-term period, it was found that groundwater contributes significantly to stream flow in the study area under both climate change scenarios. These contributions showed monthly, seasonal, and annual variations due to precipitation variability. On average, stream flow is mostly dependent on groundwater flow during December under both scenarios, while least dependent on groundwater flow during May and June under the B1 and A2 scenarios, respectively. The mean annual groundwater contribution to stream flow during 2012-2016 under both scenarios is 76.7% (σ=1.1%) and 78.2% (σ=1.25%), respectively. This contribution is lower under the A2 scenario because of higher annual precipitation and temperature increase predicted under the A2 scenario. As compared to that during the reference period (2007-2011), the mean annual groundwater contribution to stream flow during 2012-2016 under the A2 and B1 scenarios is expected to decrease by 3.3% and 1.8%, respectively, due to increased precipitation (on average 6.1% under A2 and 3.6% under B1 scenarios) and temperature (on average 0.64°C under A2 and 0.36°C under B1 scenarios). From the seasonal point of view, the mean groundwater contribution to stream flow under both scenarios is the lowest and highest during summer and winter, respectively. In addition, the mean daily groundwater levels were analyzed in this study. Under both scenarios, the

mean daily groundwater level increases the most due to high infiltration rate during snow melt and high rainfall events in summer, but it gradually decreases during the end of summer until winter and before snow melting due to less infiltration rate. The highest and lowest mean daily groundwater levels during 2012-2016 under both scenarios were found in July and March, respectively. It was also found that the groundwater levels are generally higher under the A2 scenario than under the B1 scenario. The results for the long-term period (2020-2040) are similar to those for the short-term period. On average, the mean annual groundwater contribution to stream flow during 2020-2040 under the A2 and B1 scenarios is expected to be 74.5% (σ=2%) and 75.6% (σ=3%), respectively. As compared to the reference period (2007-2011), the groundwater contribution during 2020-2040 under the A2 and B1 scenarios is expected to decrease by 5.5% and 4.4%, respectively, due to the increased precipitation (on average 6.7% under the A2 and 4.8% under the B1 scenarios) and temperature (on average 0.83°C under the A2 and 0.64°C under the B1 scenarios). Therefore, climate change influences significantly the temporal patterns of mean groundwater contribution to stream flow. In general, the modeling results represent a new way to understand the temporal dynamics of GW-SW interaction under climate change. The results obtained from this study will provide useful information for effective short-term and long-term water resources decision making in terms of monthly, seasonal and annual water extractions from the river. The US Army Corps of Engineers and the Bureau of Reclamation have also used short-term water management strategies in the last few decades to solve numerous constraints before making long-term management decisions, which always requires more resources and are therefore, more expensive (USACE et al., 2013). The results

will also provide ecological conditions of the stream, which will be beneficial to aquatic ecosystems. They will be useful for the planning of regional water resources management.

CHAPTER 6

EFFECTS OF CLIMATE AND LAND USE CHANGES ON GW-SW INTERACTION

6.1 Background

It has been known that ongoing climate change will significantly impact the hydrologic cycle (Kundzewicz et al., 2008). Due to the importance of groundwater resources in the hydrologic cycle, climate change impact studies on groundwater have received increasing attention during the last decade. Most of the previous studies reported how the mean annual groundwater level and groundwater recharge or discharge (i.e., mean of 20 to 40 years) would change under different climate change scenarios. Only a few studies (Van Roosmalen et al., 2007; Jackson et al., 2011; Dams et al., 2012; Vansteenkiste et al., 2012) reported how these variables show monthly variation between current and projected future climates. There is little knowledge regarding how the mean monthly groundwater contribution to stream flow will change under different climate change scenarios. In addition, land use changes can also significantly affect groundwater recharge and discharge, and surface water flow patterns by altering soils' infiltration rate (Jinno et al., 2009). For example, increasing urban area resulted in decreasing groundwater discharge, and increasing stream flow and surface runoff (Klocking et al., 2002; Chang, 2007; Lin et al., 2007; Dams et al., 2008; Zhou et al., 2013); the conversion of perennial vegetation to seasonal growing crops in the Mississippi River Basin resulted in increased groundwater discharge and stream flow, and decreased surface runoff (Zhang et al., 2006b; Schilling et al., 2010); changing agricultural area into grasslands

in a sub catchment of Havel River, Germany, resulted in decreased groundwater discharge (Krause et al., 2004); the conversion of grassland into forest in the western part of Jutland, Denmark, resulted in decreased groundwater discharge (Van Roosmalen et al., 2009); a decrease of grassland area with concurrent increases of shrub land rain-fed agriculture, bare ground irrigated agriculture and urban area led to an increase in the surface runoff and a decrease in the groundwater discharge and stream flow (Ghaffari et al., 2010). A number of studies (Klocking et al., 2002; Batelaan et al., 2003; Krause et al., 2004; Dams et al., 2008; Van Roosmalen et al., 2009; Wijesekara et al., 2012; Zhou et al., 2013) have investigated watershed hydrology under the combined impacts of climate and land use changes. Many of the previous studies reported how the mean annual groundwater recharge and discharge, stream flow, as well as groundwater level would change under different land use change scenarios. However, little attention was paid to investigate how the mean monthly, seasonal and annual groundwater contributions to stream flow will change under both changing land use and climatic conditions. In fact, such information could determine the monthly status of groundwater resources and site conditions for groundwater-dependent terrestrial ecosystems (Naumburg et al., 2005). They will also determine the monthly, seasonal and annual variations of stream flow dependency on groundwater, and these will provide useful information for both short and long-term water supply decisions making.

This research attempts to investigate GW-SW interaction under combined climate and land use/land cover (LULC) changes effects in the study area through the developed GSSHA model. The monthly, seasonal and annual groundwater contributions to stream flow under the A2 and B1 GHG emission scenarios with LULC changes were investigated for a short-term

period of 5 years (2012 to 2016) due to limited future projected land uses data. The annual land use maps from 2012 to 2016 were used in the developed GSSHA model.

6.2 GW-SW interaction under A2 scenario with LULC changes

Fig. 6.1 presents the mean monthly groundwater contributions to stream flow under the A2 GHG emission scenario with land use and land cover (LULC) changes during 2012-2016. Similar to the climate change effects, the groundwater contributions under the combined effects show variable annual patterns (Cannon et al., 2002; Van Roosmalen et al., 2007; Lin et al., 2007; Xu et al., 2011). The mean monthly groundwater contribution to stream flow in 2012 ranges from 42% in May to 96% in October. Similar trends are found for years 2013 to 2016. However, this range is lower than that under the climate change effects (no land use change). This variation occurs due to land use changes, which result in increasing surface runoff and stream flow, and decreasing groundwater discharge due to increasing forest clear cut area of low hydraulic conductivity soil. Klocking et al. (2002), Chang (2007), Lin et al. (2007), Dams et al. (2008), and Zhou et al. (2013) also found decreasing groundwater discharge and increasing surface runoff and stream flow due to increasing built up area of low hydraulic conductivity soils. Therefore, combined climate and land use changes have offsetting and additive impacts on water resources systems. Similar to the climate change effects, stream flow depends mostly on groundwater flow in those months when there is the highest groundwater contribution to stream flow (Washington State Department of Ecology, 1999), but at a lesser extent during the months when there is the lowest groundwater contribution.

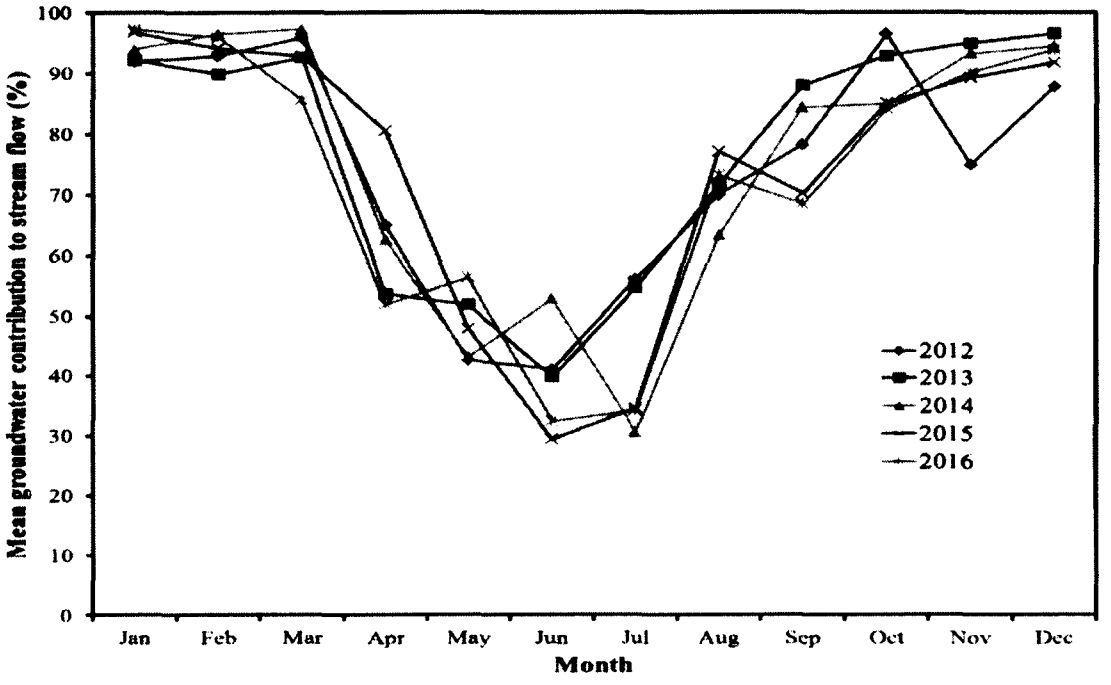

Figure 6.1 Mean monthly groundwater contributions to stream flow during 2012-2016 under the combined effects of A2 GHG emission scenario and LULC changes

Fig. 6.2 shows the comparison of mean groundwater contributions to stream flow during different seasons under the effects of A2 GHG emission scenario and LULC changes for 2012-2016. These results show similar trends that are found for the sole effects of A2 GHG emission scenario (Fig. 5.2). On average, the mean groundwater contribution to stream flow during winter, spring, summer, and fall of 2012-2016 is 93% (σ=1.9%), 68% (σ=3.5%), 50% (σ=4.5%), and 84% (σ=3.1%), respectively. Hence, stream flow depends mostly on groundwater flow during winter, while at a lesser extent during summer. Consequently, the highest and lowest water extraction from the river, and allocation to the stakeholders for future water supply could be possible during summer and winter, respectively, due to the

highest (i.e., on average 6.57 m^3/s) and lowest (i.e., on average 0.26 m^3/s) mean stream flow rates during summer and winter, respectively. Clow et al. (2003) and Welderufael et al. (2010) found similar seasonal variations of mean groundwater contribution to stream flow. Compared to only climate change effects, these contributions are lowered by 2%, 3%, 5%, and 2% during winter, spring, summer, and fall, respectively. These variations occur due to decreasing groundwater discharge and increasing stream flow and surface runoff resulted from increasing forest clear cut area. These results indicate the significant role of LULC

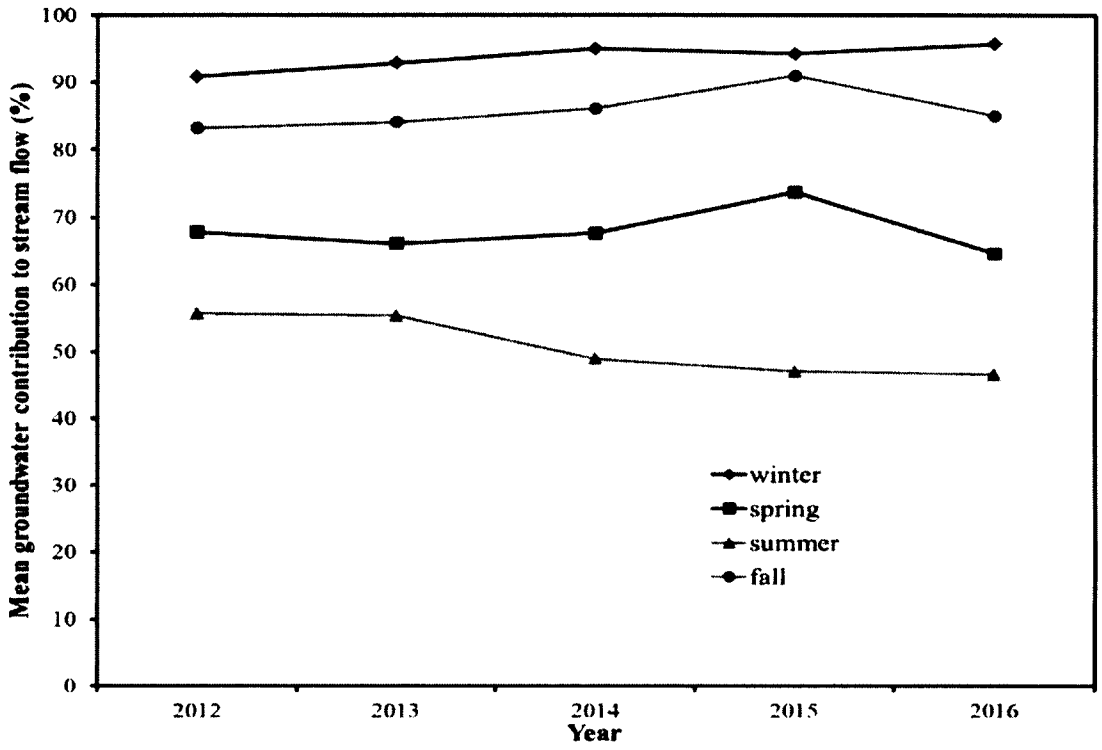

Figure 6.2 Comparison of mean groundwater contributions to stream flow during different seasons under the combined effects of A2 GHG emission scenario and LULC changes for 2012-2016

change in stream flow, surface runoff, groundwater discharge, as well as the mean seasonal groundwater contributions to stream flow. Klocking et al. (2002), Chang (2007), Lin et al. (2007), Dams et al. (2008), and Zhou et al. (2013) found similar decreasing groundwater discharge, and increasing stream flow and surface runoff due to urbanization (area of low hydraulic conductivity soils). Therefore, this decreased groundwater contribution to stream flow may result in more warmer stream temperature, lower dissolved oxygen in stream, and increased nutrient concentrations in stream (e.g., Dissolved organic carbon (DOC) and nitrogen (DON)) that may promote excessive growth of habitat-choking algae by increasing surface runoff and soil erosion (Price et al., 2006; Leigh, 2010) than those under the sole climate change effects. It should be noted that the variations differ from area to area depending on the type and temporal pattern of precipitation around the year, for example, in western and northern Europe (e.g., United Kingdom, Belgium, Denmark) more precipitation occurs during winter as rainfall, and therefore, results in higher surface runoff compared to groundwater discharge (Van Roosmalen et al., 2007; Dams et al., 2012) and lower groundwater contribution to stream flow during winter than other seasons, which is opposite to the finding of this study. In addition, different types of annual land use changes also play a vital role in these variations, for example, changing perennial vegetation into seasonal growing crops in the Mississippi River Basin increased groundwater discharge and stream flow, and decreased surface runoff (Zhang et al., 2006b; Schilling et al., 2010); altering agricultural area into grasslands in a sub catchment of Havel River, Germany, decreased groundwater discharge (Krause et al., 2004); changing grassland into forest in the western part of Jutland, Denmark, decreased groundwater discharge (Van Roosmalen et al., 2009). Therefore, the seasonal variations of mean groundwater contribution to stream flow depend

on the type and temporal pattern of annual precipitation, and the types of annual land use changes in the particular area. It is found that the groundwater contribution decreases the most in summer due to increasing forest clear cut area of low hydraulic conductivity soil and more precipitation. Zhou et al. (2013) found similar variations of surface runoff and stream flow during wet season due to urbanization.

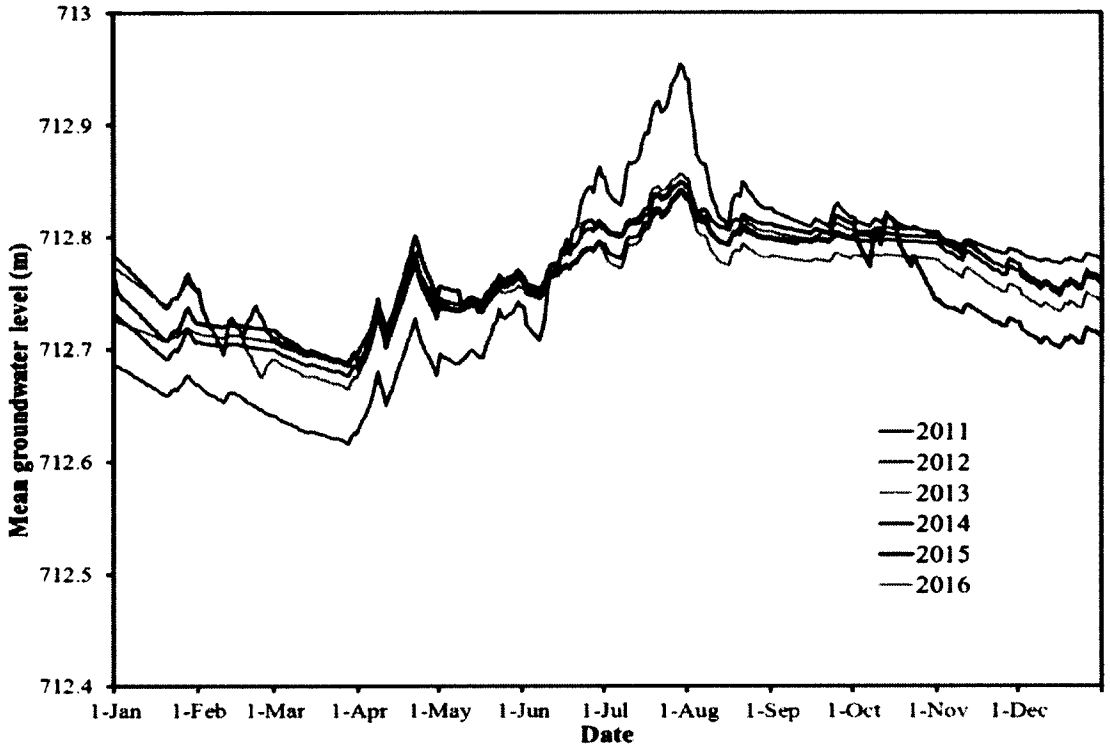

Figure 6.3 Comparison of mean daily groundwater levels of the study area for year 2011 and under the combined effects of A2 scenario and LULC changes for 2012-2016

Fig. 6.3 shows the comparison of mean daily groundwater levels of the study area in 2011 and those during 2012-2016 under the combined effects of the A2 scenario and LULC

changes. The year 2011 (with annual precipitation of 552 mm) was of mild winter and flooding summer in the study area. It is found that the mean daily groundwater levels in the study area show almost similar profiles in every year due to the almost similar temporal pattern of annual precipitation. Due to high infiltration rate during snow melting and heavy rainfall events in the summer, the mean daily groundwater levels increase the most. However, the high groundwater level does not increase groundwater contribution to stream flow during those seasons as a result of the high surface runoff caused by snowmelt, heavy rainfall, (Covert, 1999; Clow et al., 2003), steep topography (Vivoni et al., 2007) and land use changes. The mean daily groundwater levels gradually decrease during the end of summer and continue until the winter and before snow melting (i.e., before April), and this lower groundwater level results in lower groundwater discharge, and higher groundwater contribution to stream flow because of low stream flow during those times. Similar variation patterns were found for the sole climate change effects, but the mean daily groundwater levels increase at a lesser rate than the sole climate change effects due to increasing surface runoff and decreasing infiltration resulting from LULC changes. These temporal variations of mean daily groundwater levels also vary with area based on the type and temporal pattern of precipitation around the year, for example, more precipitation occurs during winter as rainfall in western and northern Europe (e.g., United Kingdom, Belgium, Denmark), and causes higher groundwater levels during winter than other seasons (Van Roosmalen et al., 2007; Goderniaux, 2010; Dams et al., 2012), which is opposite to the finding of this study. In addition, different types of annual land use changes also influence these variations for example, shifting agricultural area into grasslands in a sub catchment of Havel River, Germany, caused decreasing groundwater levels (Krause et al., 2004); the conversion of

forest to paddy field resulted in lower groundwater levels in Jambi Province, Indonesia (Furukawa et al., 2005). As discussed before, the temporal variations of groundwater levels depend on the type and temporal pattern of annual precipitation as well as the types of annual land use changes in the particular area.

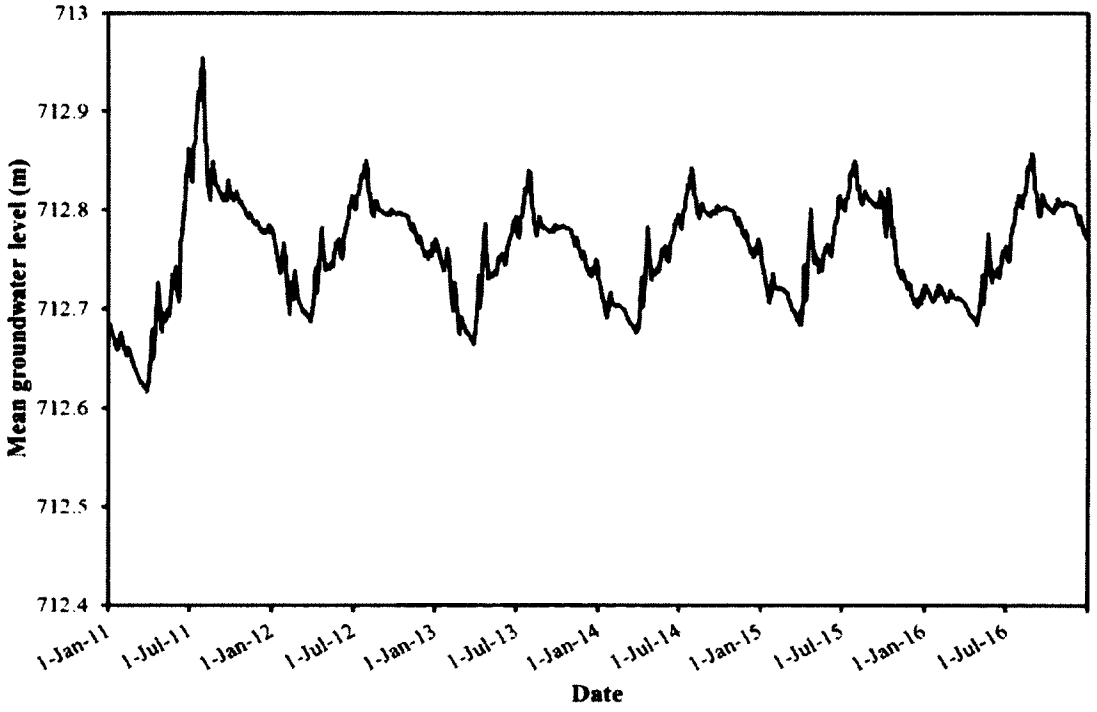

Figure 6.4 Mean daily groundwater levels of the study area for year 2011 and under the combined effects of A2 scenario and LULC changes for 2012-2016

The mean daily groundwater levels of the study area in 2011 and those during 2012-2016 under the effect of A2 scenario and LULC changes are presented in Fig. 6.4. The results show that the mean daily groundwater levels are expected to increase at the end of year 2016 due to increased precipitation under the A2 scenario. Overall, the mean annual groundwater

level is expected to increase by 1.8 cm, 0.5 cm, 1 cm, 1.2 cm, and 1.5 cm in 2012, 2013, 2014, 2015, and 2016, respectively, as compared to that in 2011. The groundwater level increases yearly due to consecutive years of above-normal precipitation in the study area. This indicates that climate change has a significant effect on the mean daily and annual groundwater levels. Scibek et al. (2006b) and Van Roosmalen et al. (2007) also found increased mean annual groundwater levels due to increased precipitation. However, the increase of mean annual groundwater levels varies from area to area depending on the amount of increased annual precipitation. It is also found that the mean annual groundwater level decreases annually as compared to that under the sole climate change (A2 scenario) effects because of increasing forest clear cut area which results in decreasing infiltration. As compared to only climate change effects, the mean annual groundwater level under the combined effects of A2 scenario and LULC changes is expected to decrease by 0.2 cm, 0.7 cm, 1 cm, 1.2 cm, and 1.5 cm in 2012, 2013, 2014, 2015, and 2016, respectively. These results indicate that land use change has an important impact on the mean daily and annual groundwater levels. Dams et al. (2008) also found similar decreasing mean annual groundwater levels due to increasing urban area. Therefore, less groundwater discharge to stream flow will occur in the study area under the combined effects of A2 scenario and LULC changes. This annual pattern of decreasing groundwater levels in the study area due to this type of land use change also indicate one of the possible reasons of depleting wetlands in the KRW due to extensive oil/gas exploration activities (Paul, 2013), along with climate change.

6.3 GW-SW interaction under B1 scenario with LULC changes

Fig. 6.5 illustrates the mean monthly groundwater contributions to stream flow during 2012-2016 under the combined effects of B1 GHG emission scenario and LULC changes. Similar to those under the effect of only climate change, the patterns also vary annually due to land use changes and monthly precipitation fluctuations (Cannon et al., 2002; Van Roosmalen et al., 2007; Lin et al., 2007). The mean monthly groundwater contribution to stream flow decreases almost every year as compared to that with only climate change effect.

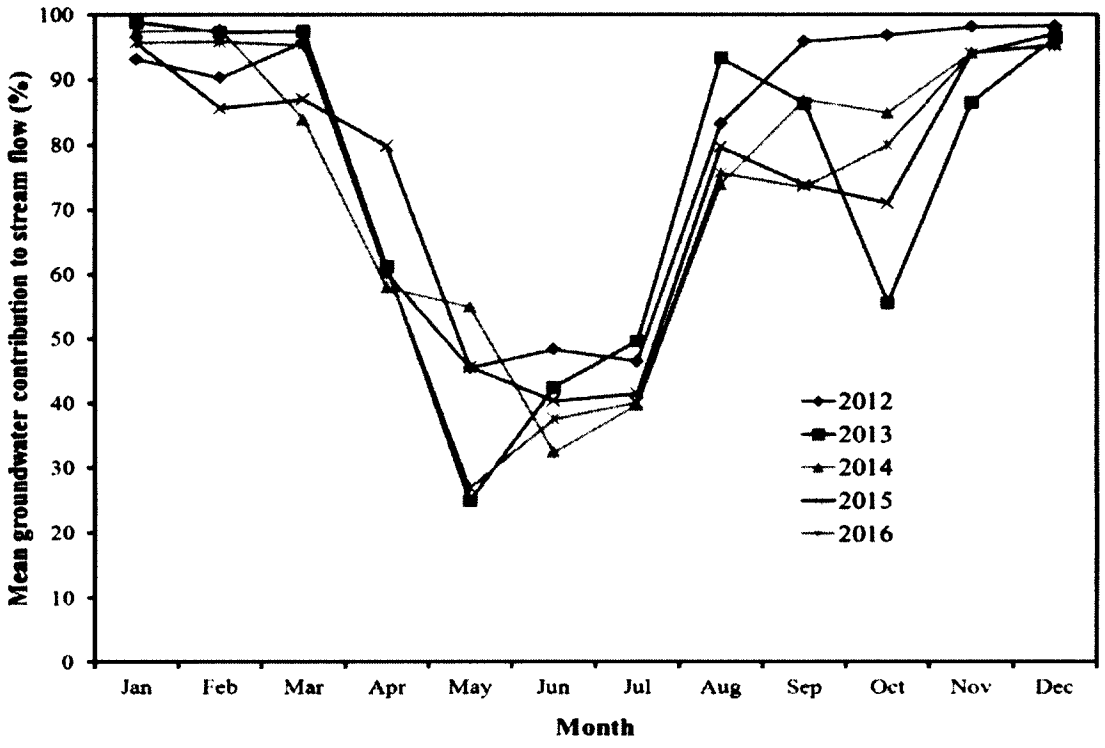

Figure 6.5 Mean monthly groundwater contributions to stream flow during 2012-2016 under the combined effects of B1 GHG emission scenario and LULC changes

Fig. 6.6 presents the comparison of mean groundwater contributions to stream flow during different seasons between 2012-2016 under the combined effects of B1 GHG emission scenario and LULC changes. Similar types of trends are found as those under the effects of B1 scenario (Fig. 5.8). On average, the mean groundwater contribution to stream flow during winter, spring, summer, and fall from 2012 to 2016 is 96% (σ=2.1%), 66% (σ=4.1%), 57% (σ=5.5%), and 86% (σ=6.5%), respectively. Hence, similar to the results under the effects of A2 scenario and LULC changes, stream flow depends mostly on groundwater flow during winter, but at a lesser extent during summer. Consequently, the highest and lowest water extraction from the river, and allocation to the stakeholders

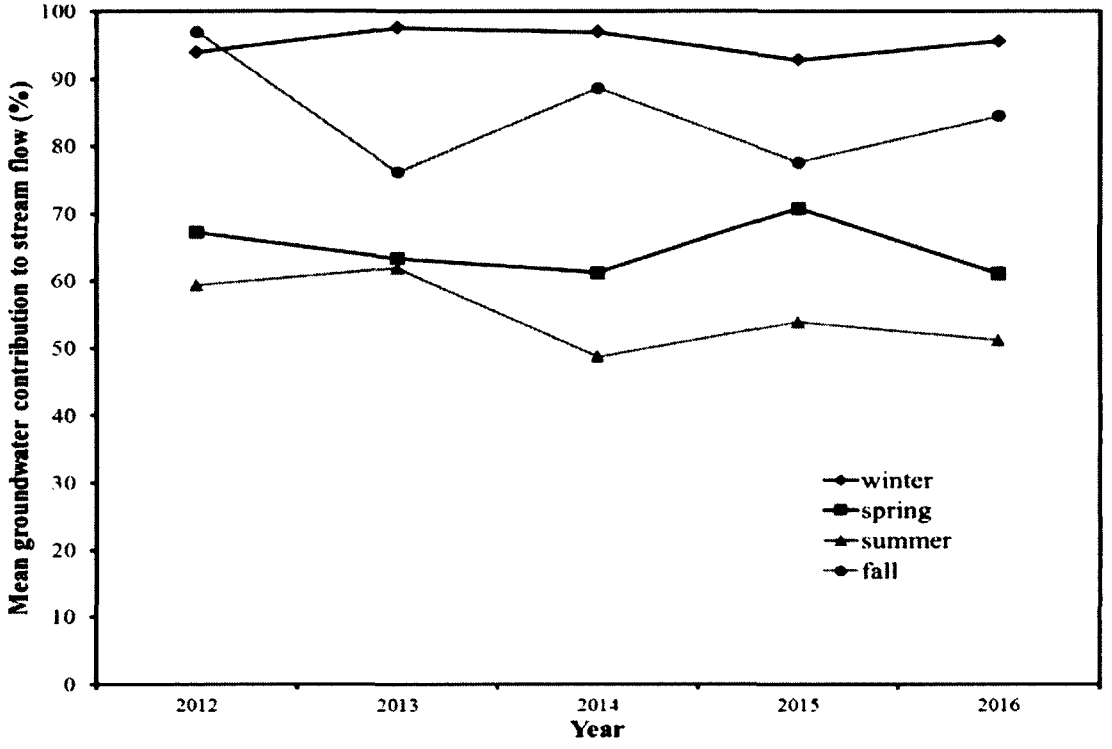

Figure 6.6 Comparison of mean groundwater contributions to stream flow during different seasons under the combined effects of B1 GHG emission scenario and LULC changes for 2012-2016

for future water supply could be possible during summer and winter, respectively, due to the highest (i.e., on average 6.30 m^3/s) and lowest (i.e., on average 0.235 m^3/s) mean stream flow rates during summer and winter, respectively. Compared to the results under the effect of only climate change, these contributions are reduced by 1%, 4%, 4%, and 2% during winter, spring, summer, and fall, respectively. The mean groundwater contribution to stream flow of 2012-2016 also decreases most during the summer due to increasing forest clear cut area of low hydraulic conductivity soil and more precipitation predicted during summer.

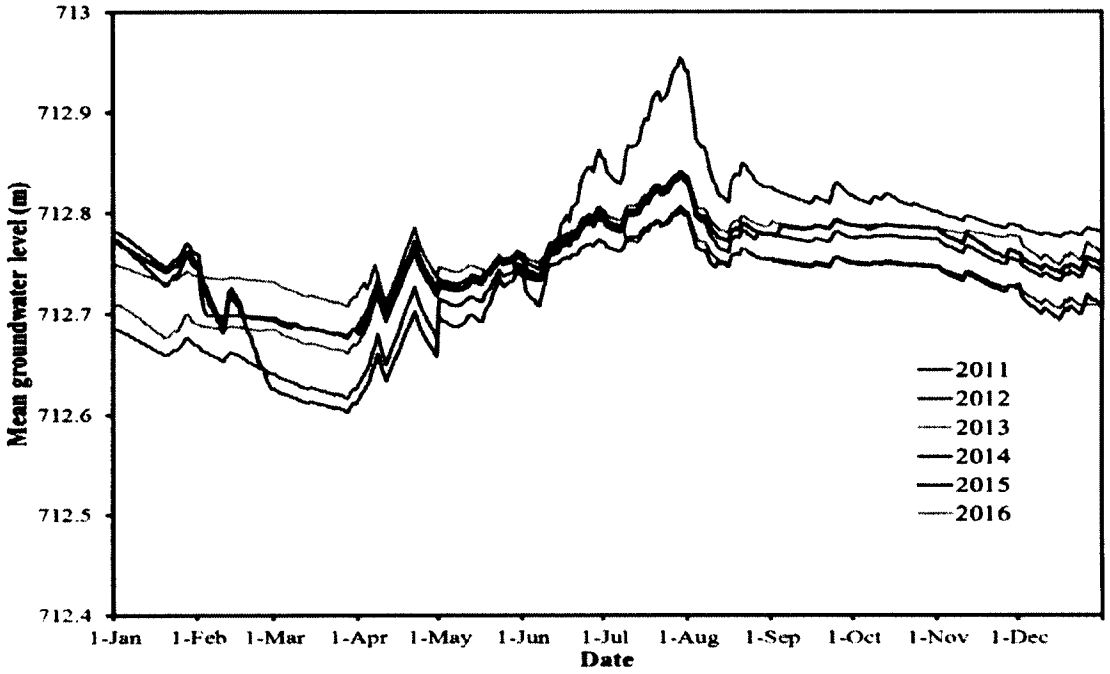

Figure 6.7 Comparison of mean daily groundwater levels of the study area for year 2011 and under the combined effects of B1 scenario and LULC changes for 2012-2016

Fig. 6.7 compares the mean daily groundwater levels of the study area in year 2011 and those in 2012-2016 under the combined effects of B1 scenario and LULC changes. Similar to those under the effect of only climate change, the mean daily groundwater levels in the study

area show almost similar profiles due to the almost similar temporal pattern of annual precipitation, but they increase at a lesser rate as compared to the results under the effects of A2 scenario and LULC changes.

Fig. 6.8 shows the temporal variation of the mean daily groundwater levels of the study area in 2011 and those in 2012-2016 under the combined effects of B1 scenario and LULC changes. It can be found that the groundwater levels are expected to increase at the end of year 2016 by a lesser amount than under the combined effects of A2 scenario and LULC changes. This occurs due to less precipitation predicted under the B1 scenario than under the A2 scenario. Overall, the mean annual groundwater level is expected to increase by 0.4 cm, 0.3 cm, 0.4 cm, and 0.7 cm in 2013, 2014, 2015, and 2016, respectively, but decrease by 1 cm in 2012, as compared to that in 2011. It is also found that the mean annual groundwater level decreases annually as compared to that under the effect of only climate change (B1 scenario), with a decrease of 0.4 cm, 0.6 cm, 0.9 cm, 1.1 cm, and 1.3 cm occurring in 2012, 2013, 2014, 2015, and 2016, respectively. Therefore, less groundwater discharge to stream flow will occur in the study area under the combined effects of B1 scenario and LULC changes. However, the decrease of mean annual groundwater level under the effect of B1 scenario and LULC changes was less than that under the effect of A2 scenario and LULC changes because less precipitation results in less surface runoff under the effect of B1 scenario and LULC changes.

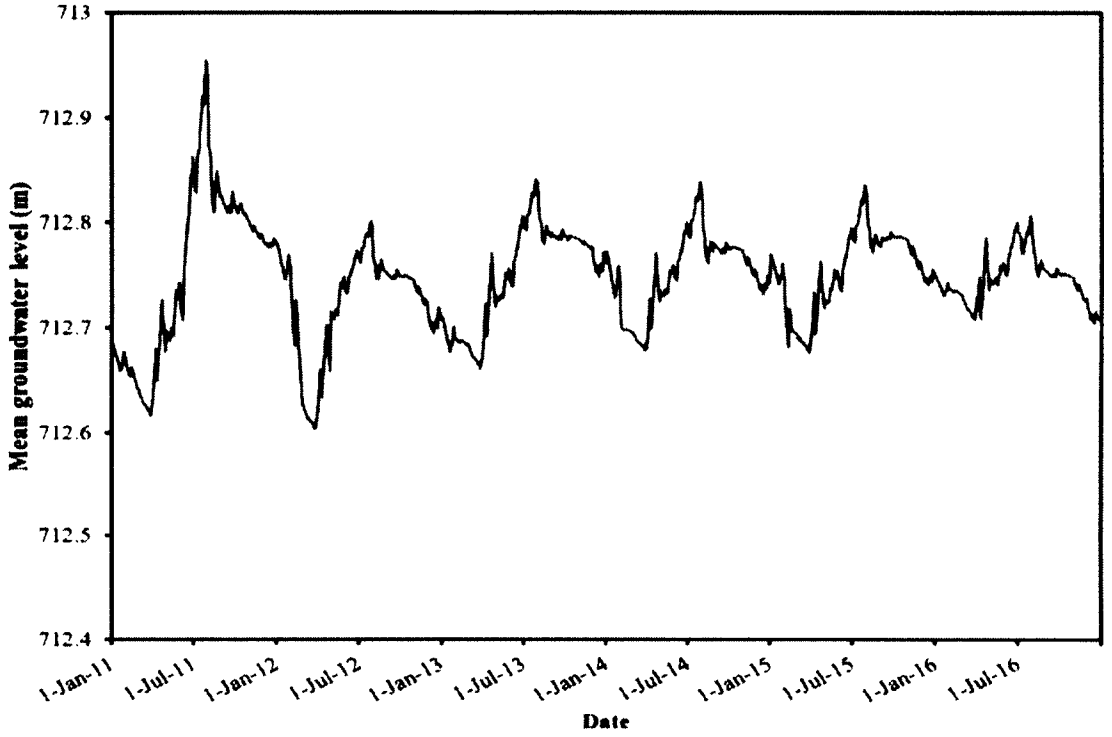

Figure 6.8 Mean daily groundwater levels of the study area for year 2011 and under the combined effects of B1 scenario and LULC changes for 2012-2016

6.4 Comparison of GW-SW interaction between A2 and B1 scenarios with LULC changes

When the mean monthly groundwater contributions to stream flow in 2012-2016 under the combined effects of A2 or B1 GHG emission scenario and LULC changes are compared to those during the reference period (2007-2011) (Fig. 6.9), similar trends are found as those under the effect of only climate change (Fig. 5.13). The lowest and highest mean monthly groundwater contributions to stream flow in 2012-2016 are found in June (i.e., 39%) and January (i.e., 95%), respectively, under the combined effects of A2 scenario and LULC

changes, but are found in May (i.e., 40%) and December (i.e., 97%), respectively, under the combined effects of B1 scenario and LULC changes.

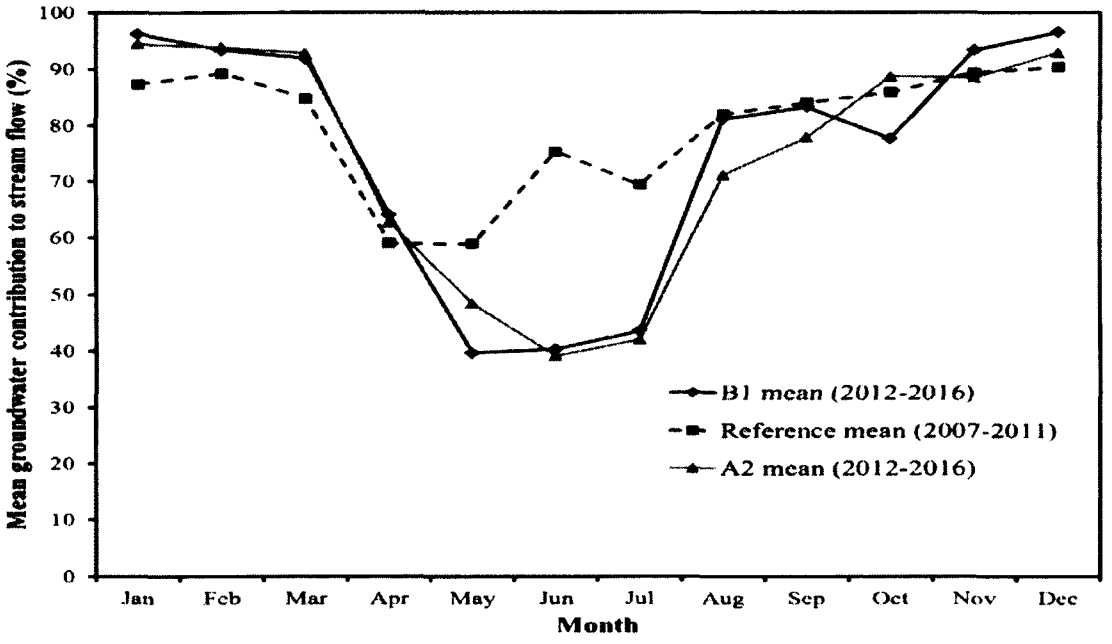

Figure 6.9 Comparison of mean monthly groundwater contributions to stream flow during 2012-2016 under the combined effects of A2 or B1 GHG emission scenario and LULC changes with respect to reference period (2007-2011)

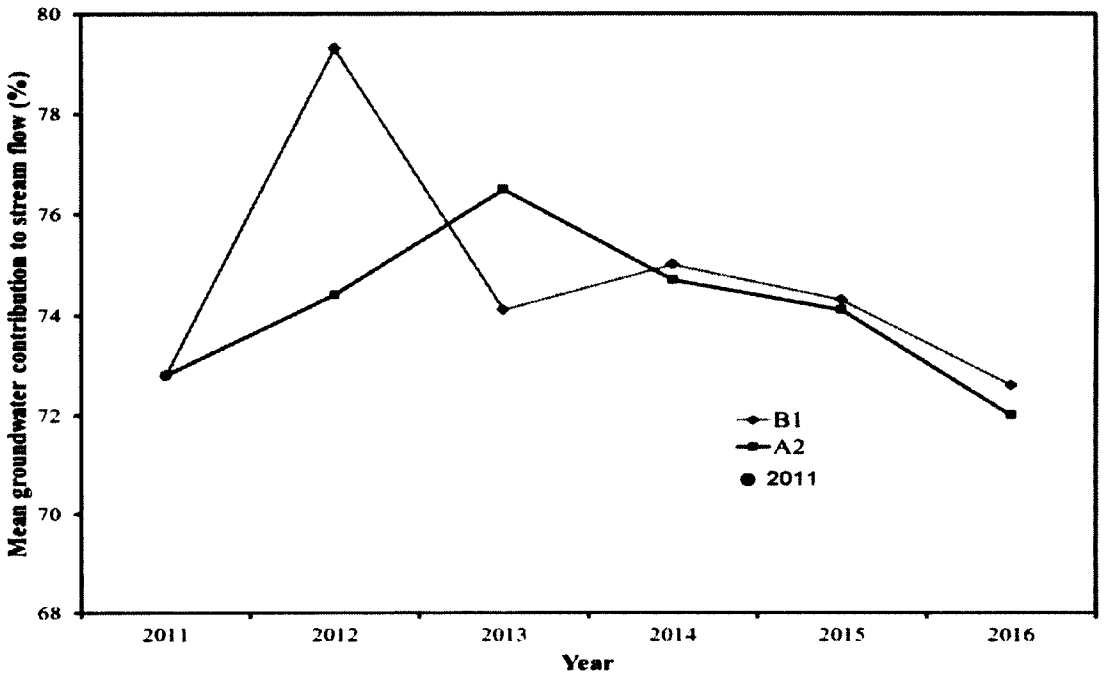

Figure 6.10 Comparison of mean annual groundwater contributions to stream flow from 2012 to 2016 under the combined effects of A2 or B1 GHG emission scenario and LULC changes with respect to year 2011

Fig. 6.10 illustrates the comparison of mean annual groundwater contributions to stream flow in 2012-2016 under the combined effects of A2 or B1 GHG emission scenario and LULC changes with respect to year 2011. It is found that both scenarios show an opposite pattern from 2012 to 2014, but a similar pattern from 2014 to 2016. The highest and lowest groundwater contributions to stream flow during 2012-2016 are found in 2013 (i.e., 76.5%), and 2016 (i.e., 72%), respectively, under the combined effects of A2 scenario and LULC changes, but are found in 2012 (i.e., 79.3%), and 2016 (i.e., 72.9%), respectively, under the combined effects of B1 scenario and LULC changes. On average, the mean annual groundwater contribution to stream flow of 2012-2016 under the effect of A2 or B1 scenario and LULC changes is 73.6% (σ=1.6%) and 75.7% (σ=2.4%), respectively. This variation

occurs due to a higher precipitation and temperature increase predicted under the A2 scenario than under the B1 scenario, which results in more surface runoff and stream flow, and less groundwater discharge. Compared to the climate change effects only, these contributions are lowered by 3.1% and 2.5% (i.e., absolute value) under the A2 and B1 scenario with LULC changes, respectively, while the stream flow increased averagely 3.4% and 2.8%, respectively. In addition, surface runoff increased averagely 19.5% and 17.8%, respectively, under the combined effects of A2 or B1 scenario and LULC changes, but groundwater discharge decreased averagely 0.7% and 0.5%, respectively, under the combined effects of A2 or B1 scenario and LULC changes. Therefore, LULC change plays a significant role in stream flow, surface runoff, groundwater discharge, as well as the mean annual groundwater contribution to stream flow. However, under the effect of B1 scenario and LULC changes, the mean annual groundwater contribution to stream flow decreases at a lesser extent as compared to that under the effect of A2 scenario and LULC changes. In addition, as compared to the reference period, the mean annual groundwater contribution to stream flow from 2012 to 2016 under the combined effects of A2 or B1 scenario and LULC changes is expected to decrease by 6.4% and 4.3%, respectively due to land use changes and increased precipitation (on average 6.1% under the A2 and 3.6% under the B1 scenarios) and temperature (on average 0.64°C under the A2 and 0.36°C under the B1 scenarios). These changes result in increased stream flow (on average 10.1% under the A2 and 5.8% under the B1 scenarios with LULC changes), groundwater discharge (on average 2.1% under the A2 and 0.7% under the B1 scenarios with LULC changes), and surface runoff (on average 42% under the A2 and 29% under the B1 scenarios with LULC changes). Table 6.1 presents a summary of mean annual stream flow, surface runoff, and groundwater discharge under the

reference period and the combined effects of A2 or B1 climate change scenario and LULC changes for the short-term period. These results demonstrate that stream flow is more dependent on groundwater flow under the effect of B1 scenario and LULC changes than under the effect of A2 scenario and LULC changes. Therefore, more annual water extraction from the river, and allocation to the stakeholders for future water supply could be possible under the effects of A2 scenario and LULC changes than under the effects of B1 scenario and LULC changes without causing a negative impact on regional groundwater level as well as aquatic ecosystems, compared to the reference period.

Table 6.1 Mean annual precipitation, temperature, stream flow, surface runoff, and groundwater discharge under the reference period (2007-2011) and the combined effects of A2 or B1 scenario and LULC changes for the short-term period (2012-2016). The values within the parentheses are relative changes except for temperature, where absolute changes were calculated.

Scenario	Mean annual precipitation (mm)	Mean annual temperature (°C)	Mean annual stream flow (m^3/s)	Mean annual groundwater discharge (m^3/s)	Mean annual surface runoff (m^3/s)
Reference period	492	2.63	3.08	2.46	0.62
A2 and LULC	522 (6.1%)	3.27 (0.64)	3.40 (10.1%)	2.51 (2.1%)	0.89 (42%)
B1 and LULC	510 (3.6%)	2.99 (0.36)	3.27 (5.8%)	2.47 (0.7%)	0.80 (29%)

The comparison of mean daily groundwater levels of the study area in 2012-2016 under the effect of A2 or B1 scenario and LULC changes is shown in Fig. 6.11. The results show that the groundwater levels under the effect of A2 scenario and LULC changes are higher most of the time than those under the effect of B1 scenario and LULC changes due to a higher amount of precipitation and temperature increase predicted under the A2 scenario.

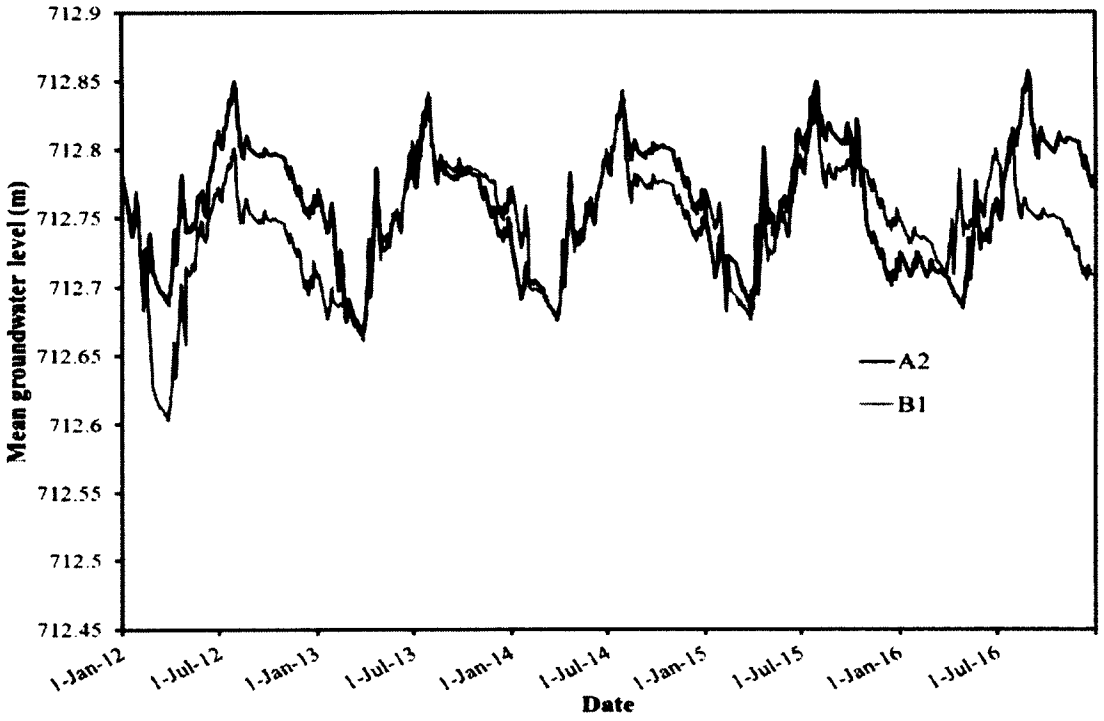

Figure 6.11 Comparison of mean daily groundwater levels of the study area between A2 and B1 GHG emission scenarios with LULC changes for 2012-2016

Fig. 6.12 demonstrates the comparison of the mean daily groundwater levels of the study area of 2012-2016 under the A2 and B1 scenarios with LULC changes with respect to the reference period (2007-2011). Similar to the results obtained from Fig. 6.11, the mean daily

groundwater levels of 2012-2016 are higher most of the months under the A2 scenario than under the B1 scenario. The highest and lowest mean daily groundwater levels of 2012-2016 under both scenarios are found in July and March, respectively. When compared to those during the reference period (2007-2011), the mean daily groundwater levels of 2012-2016 under both scenarios are higher during most of the months due to a higher amount of precipitation and temperature increase. However, the mean daily groundwater levels under the B1 scenario with LULC changes are lower in a few months of the year than those during the reference period (2007-2011) because of increasing forest clear cut area predicted to occur under the B1 scenario with LULC changes during 2012 to 2016. On average, the mean annual groundwater level under the A2 and B1 scenarios with LULC changes is expected to increase by 3.8 cm (σ=2.1 cm) and 2.9 cm (σ=1.3 cm), respectively, compared to that during the reference period. In addition to this, the mean annual groundwater level decreases by 0.7 cm and 0.6 cm (i.e., absolute value) under the A2 and B1 scenarios with LULC changes, respectively, compared to the climate change effects only (no land use change). These results indicate that LULC change has a significant impact on the mean daily and annual groundwater levels. Therefore, less groundwater discharge to stream flow (on average 0.7% and 0.5%, respectively, in the A2 and B1 scenarios with LULC changes) will be available in the study area under the A2 and B1 scenarios with LULC changes, as compared to those in climate change effects only.

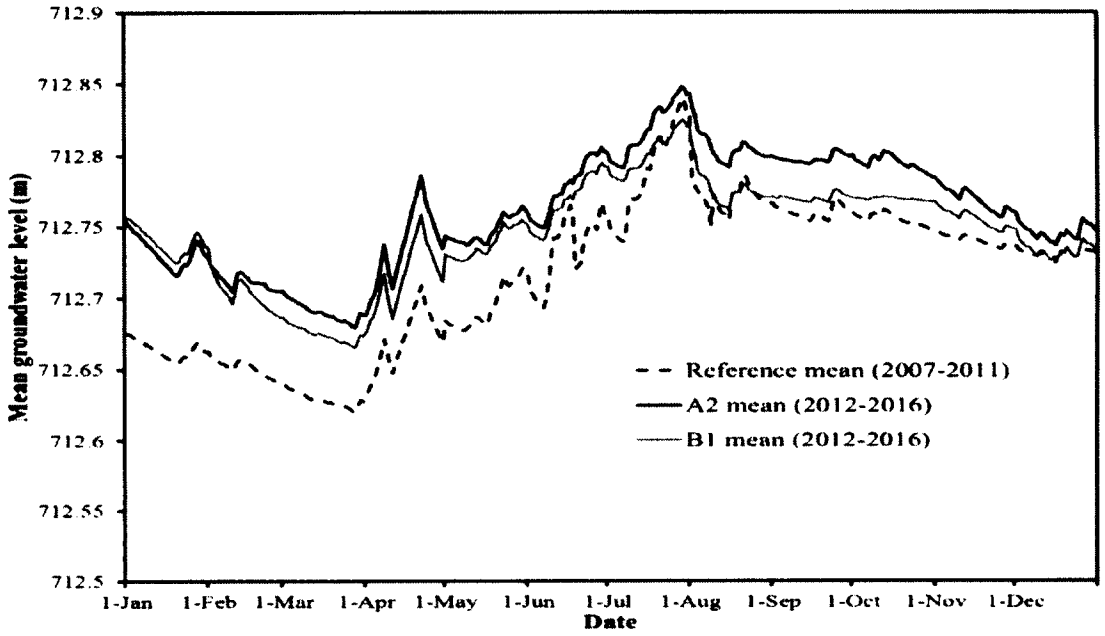

Figure 6.12 Comparison of mean daily groundwater levels of the study area of 2012-2016 under the combined effects of A2 or B1 GHG emission scenarios and LULC changes with respect to reference period (2007-2011)

Figs. 6.13-6.16 present the comparison of mean groundwater contributions to stream flow between the A2 and B1 GHG emission scenarios with LULC changes during different seasons from 2012 to 2016 with respect to year 2011. The results during various seasons follow similar trends as those under the effect of only climate change. On average, under the effect of A2 scenario and LULC changes, the mean groundwater contribution to stream flow during winter, spring, summer, and fall of 2012-2016 is 93% (σ=1.9%), 68% (σ=3.5%), 50% (σ=4.5%), and 84% (σ=3.1%), respectively. These numbers changed to 96% (σ=2.1%), 66% (σ=4.1%), 57% (σ=5.5%), and 86% (σ=6.5%), respectively, under the effect of B1 scenario and LULC changes. The mean groundwater contribution to stream flow during all seasons under the combined effects of A2 or B1 scenario and LULC changes is lower than that under the effect of only climate change by 2%-5% and 1%-4% (i.e., absolute values), respectively.

This occurs due to increasing surface runoff and stream flow, and decreasing groundwater discharge resulting from annual increasing forest clear cut area of low hydraulic conductivity soil from 2012 to 2016. The most decrease occurs in summer under the A2 scenario with LULC changes, but in spring and summer under the B1 scenario with LULC changes. The least decrease occurs in fall and winter under the A2 scenario with LULC changes, but in winter under the B1 scenario with LULC changes. Therefore, land use change has also an important impact on the mean seasonal groundwater contributions to stream flow.

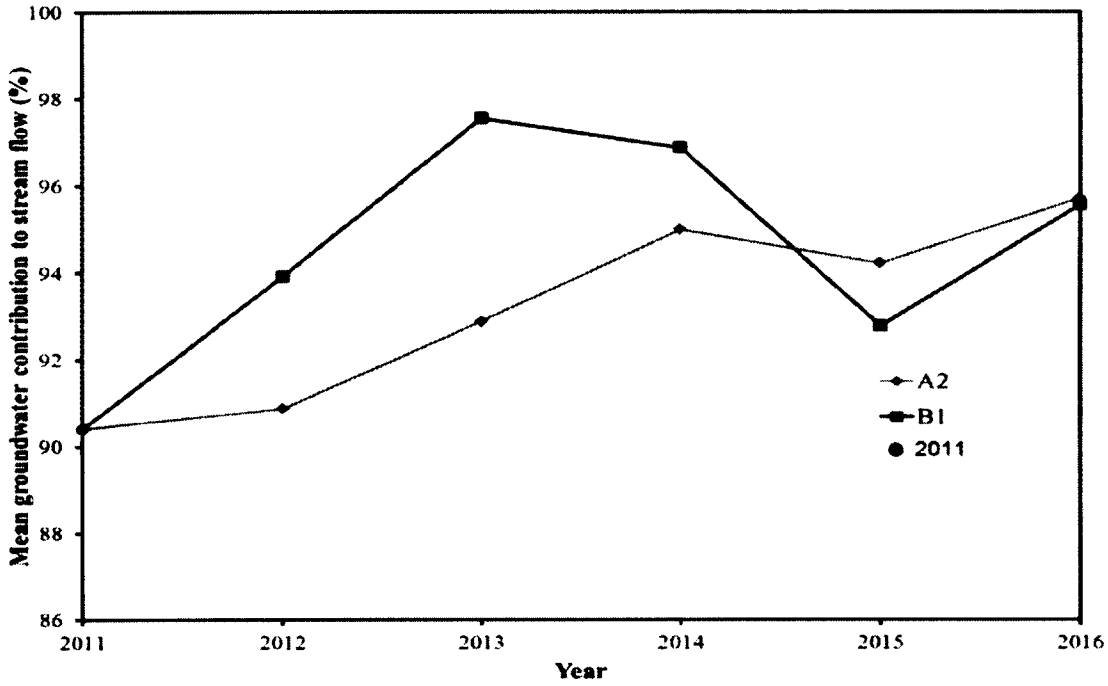

Figure 6.13 Comparison of mean groundwater contributions to stream flow between A2 and B1 scenarios with LULC changes during winter from 2012 to 2016 with respect to year 2011

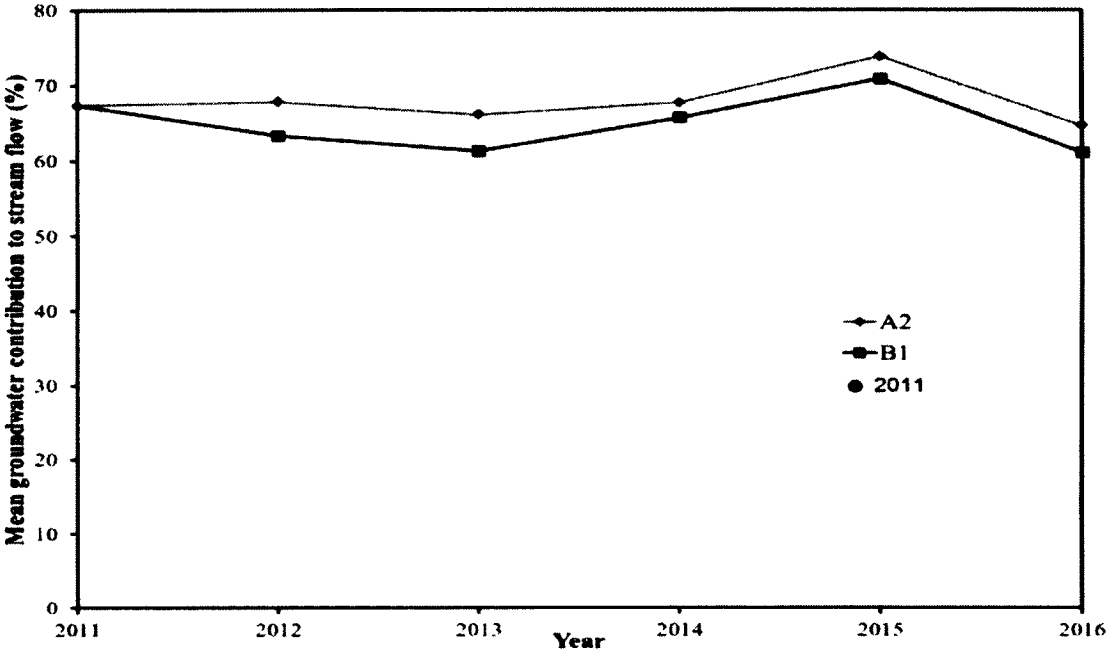

Figure 6.14 Comparison of mean groundwater contributions to stream flow between A2 and B1 scenarios with LULC changes during spring from 2012 to 2016 with respect to year 2011

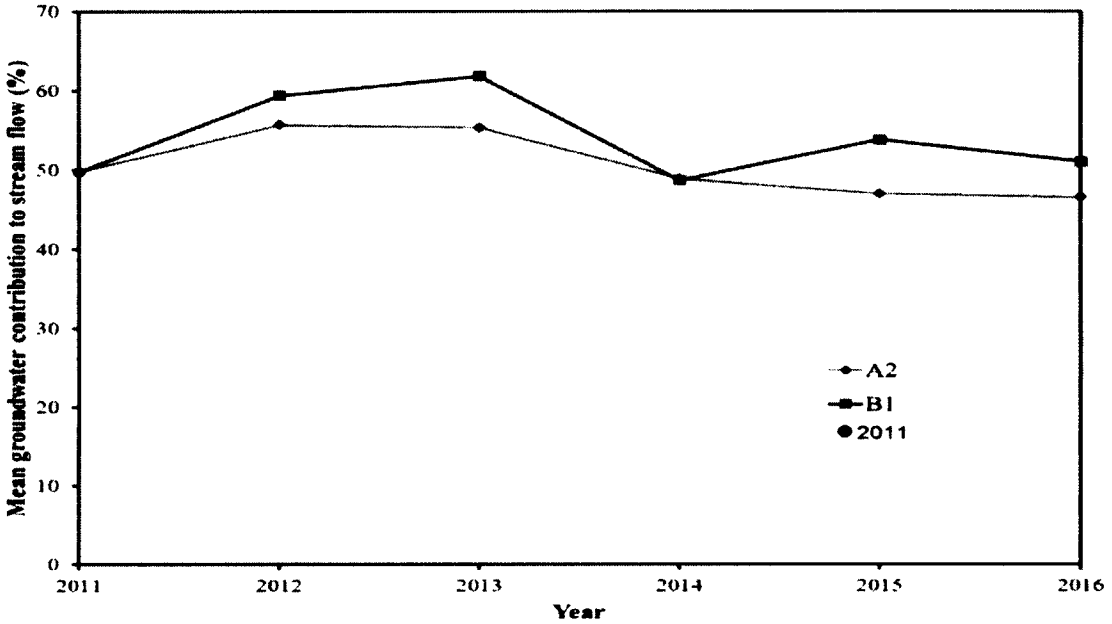

Figure 6.15 Comparison of mean groundwater contributions to stream flow between A2 and B1 scenarios with LULC changes during summer from 2012 to 2016 with respect to year 2011

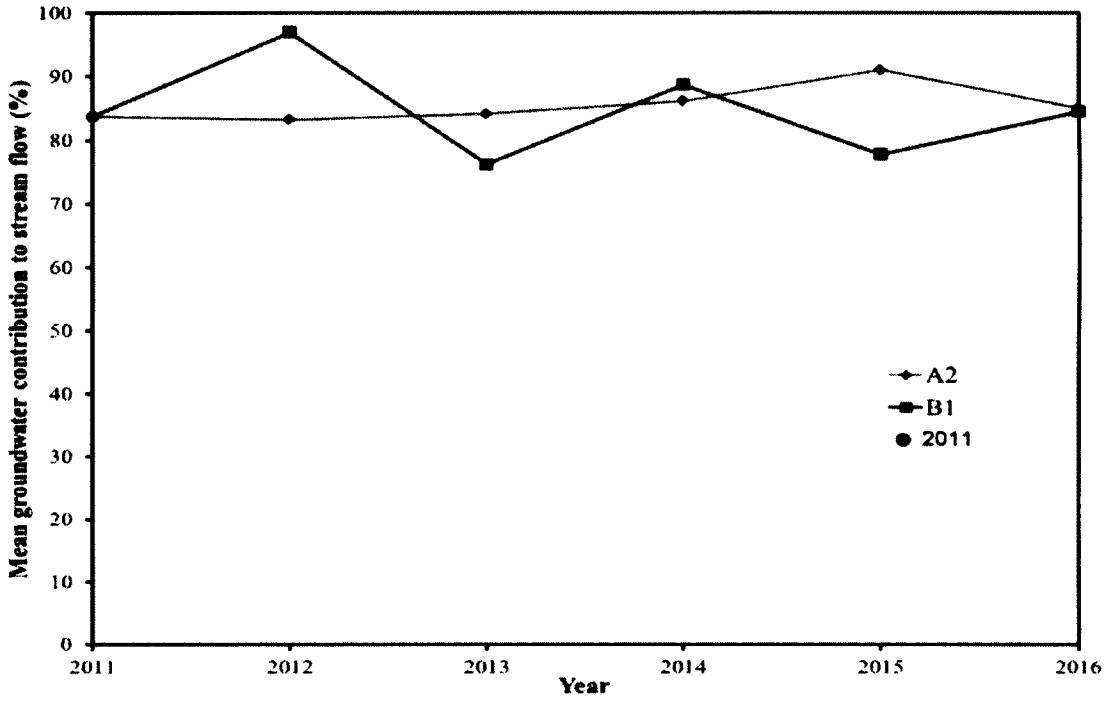

Figure 6.16 Comparison of mean groundwater contributions to stream flow between A2 and B1 scenarios with LULC changes during fall from 2012 to 2016 with respect to year 2011

6.5 Summary

The impact of combined climate and land use changes on GW-SW interaction was examined using a study area along the river of the Mainstem sub-watershed of KRW as a case study using the developed GW-SW interaction model (i.e., GSSHA) for the short-term period (2012 to 2016). The future land use conditions were generated based on the changes of land use types between 1999 and 2010, and two types of climate change scenarios (A2: heterogeneous world with self-reliance and preservation of local identities, and B1: more integrated and environmental friendly world) were chosen. Under the combined effects of climate and land use changes, similar results to those under the effect of only climate change

were found, but with a decreasing rate in the mean groundwater contribution to stream flow and mean groundwater levels. On average, the mean annual groundwater contribution to stream flow of 2012-2016 under the A2 and B1 scenarios with LULC changes is 73.6% (σ=1.6%) and 75.7% (σ=2.4%), respectively. As compared to climate change effects only, these contributions were lowered by 3.1% and 2.5%, respectively. This indicates that land use change has an important role in the groundwater contribution to stream flow by shifting the flow patterns to the regime with more surface runoff and stream flow, but less groundwater discharge. The mean daily groundwater levels increase under both scenarios in every year during snow melt and high rainfall events in summer, but at a lesser rate than those under the effect of only climate change due to increasing surface runoff and decreasing infiltration resulted from LULC changes. It was also found that the mean annual groundwater level under the combined effects of climate and land use changes decreases every year compared to only climate change effects. These results also indicate that land use change has an important impact on the mean daily and annual groundwater levels. In general, the inclusion of annual climate and LULC changes scenarios in the developed model represents a new attempt to assess GW-SW interaction under combined climate and LULC changes. In addition, the modeling results also represent a new way to understand the temporal dynamics of GW-SW interaction under combined climate and LULC changes. The results obtained from this study will provide useful information for seasonal and annual water extractions from the river and allocation to the stakeholders for future water supply, as well as ecological conditions of the stream, which will be beneficial to aquatic ecosystems. They will also provide how LULC changes can impact the groundwater contribution to stream flow and regional groundwater levels, which will be useful for planning of regional groundwater

resource management, as well as water resources management considering future climate and land use changes.

CHAPTER 7

UNCERTAINTY ANALYSIS OF GW-SW INTERACTION

7.1 Background

Groundwater-surface water (GW-SW) interaction plays a vital role in the functioning of riparian ecosystem (Kalbus et al., 2006). During flooding season, surface water can recharge groundwater, but during drought season groundwater acts as an important source to feed the surface water flow. As a result, groundwater and surface water are closely linked components of the hydrologic system due to their interdependency to each other. The development and exploitation of any one component can affect the other component. Therefore, for sustainable water resources management, it is crucial to quantify the exchange processes between these two components (Sophocleous, 2002). During the last decade, many researchers used different hydrologic models to quantify these exchange processes. Most of the parameters (e.g., precipitation, soil properties, surface roughness) in hydrologic models used for GW-SW interaction simulation require intensive field measurements (Benke et al., 2008), and they are always associated with uncertainty. Such uncertainty would also lead to uncertainty in modeling outputs (Muleta et al., 2004), which would jeopardize decision making of water resource management. This uncertainty analysis results could provide a range of outputs instead of one output, and enable the watershed manager to take proper action about water withdrawal from the river, and allocation to the stakeholders for future water supply depending on month and season.

Due to the importance of parameter uncertainty in hydrologic models, many researchers used different uncertainty analysis methods in different hydrologic models to conduct uncertainty analysis of modeling outputs during the last several decades. For example, Beven et al. (1992) used Generalized Likelihood Uncertainty Estimation (GLUE) method in the Institute of Hydrology Distributed Model (IHDM) to investigate how the stream flow hydrograph varies under the parameter uncertainty during a number of storms in the Gwy catchment, Wales. Kuczera et al. (1998) assessed the use of multinormal approximation to parameter uncertainty for the exploration of multiresponse data (i.e., stream flow, stream chloride concentration, groundwater level) in the CATPRO model in the Wights catchment in the Western Australia. Vrugt et al. (2003) used Markov Chain Monte Carlo (MCMC) method in the HYMOD model to find out the variation of stream flow under the parameter uncertainty in the Leaf River watershed, Mississippi. Benke et al. (2008) used the Monte Carlo simulation (MCS) method as an uncertainty analysis method in 2C hydrological model to investigate the impacts of parameter uncertainty on the prediction of stream flow in eastern Australia. Mishra (2009) used first-order second–moment (FOSM) and MCS methods in the Natural Systems Regional Simulation Model (NSRSM) to compare the impacts of parameter uncertainty on stream flow prediction in south Florida. Shen et al. (2012, 2013) used GLUE and MCS methods, respectively, in the SWAT model to quantify the effects of parameter uncertainty on the stream flow and sediment in the Daning River watershed of the Three Gorges Reservoir Region, China. However, few studies have reported regarding the uncertainty analysis of the mean monthly, seasonal and annual groundwater contributions to stream flow in a watershed. These contributions information could determine the temporal

variations of stream flow dependency on groundwater, and these will provide useful information for both short and long-term water supply decisions making.

This study attempts to conduct uncertainty analysis of GW-SW interaction under the A2 and B1 GHG emission scenarios to find out the variation of mean monthly, seasonal and annual groundwater contributions to stream flow with respect to the parameter uncertainty. Year 2013 was chosen as a case study because in 2013, the mean annual groundwater contribution to stream flow is lower under the B1 scenario than under the A2 scenario. Before conducting uncertainty analysis, sensitivity analysis was performed to find out the most sensitive parameters to the model output. Then 50 Monte Carlo realizations of the most sensitive modeling parameters were generated for the GSSHA model to conduct uncertainty analysis of GW-SW interaction.

7.2 Sensitivity analysis

Before conducting uncertainty analysis of any hydrological model, it is important to do sensitivity analysis of the modeling input parameters because sensitivity analysis indicates the assessment of uncertainty importance (Mishra, 2009). Sensitivity analysis is an important tool for identifying the important modeling input parameters, testing the model conceptualization, and improving the model structure (Sieber et al., 2005). Modeling input parameters always contain some degree of uncertainty because of spatial variability, budget constraints, and access difficulties. A modeler, however, has to assign values to each input parameter to run the model. Then the model is calibrated against the limited measured data by adjusting the modeling parameters' values based on certain criteria. Therefore, the modeler has to have a clear understanding of all the input parameters and of the processes

represented in the model. Without knowing the sensitivity of parameters of the model could results in wastage of time for further research using the same model. Therefore, sensitive analysis is a useful tool for better understanding the impact of the modeling input parameters on the model output, and thus, reduced uncertainty (Hamby 1994; Lenhart et al. 2002). It also helps to enable a focused planning of future research and field measurements.

7.3 Sensitivity analysis of GW-SW interaction

In this study, sensitivity analysis was conducted using the OAT (One-factor-At-a-Time) method (Saltelli et al., 2000). The OAT method is chosen because it is the simplest method for conducting sensitivity analysis (Hamby, 1994), and three are 28 calibrated parameters in the developed GSSHA model which requires lots of runs for conducting sensitivity analysis using other methods (e.g., factorial design). Using the OAT method, each calibrated parameter was changed by a small amount at a time from a reference (i.e., base) value while keeping the remaining parameters constant, and then the corresponding change in the modeling output (i.e., mean monthly groundwater contributions to stream flow) was computed. This procedure was repeated for three times, and every time the calibrated parameter was increased and decreased by a factor of 20% of the reference value. Based on these computed changes, relative sensitivity of each parameter was determined by calculating the normalized sensitivity coefficient (NSC) or relative sensitivity coefficient. This sensitivity coefficient is dimensionless and calculated using the following formula (Hamby, 1994).

$$NSC = \frac{(R_a - R_n)/R_n}{(P_a - P_n)/P_n} \qquad (7.1)$$

Where NSC is the normalized sensitivity coefficient, R_a and P_a are the model output and parameter values after a particular model run using the changing parameter's value, respectively, and R_n and P_n are the model output and parameter nominal values, respectively. Table 7.1 lists all the parameters' relative sensitivities, as well as their sensitivity rankings. Here, relative sensitivity and ranking were evaluated based on the change of mean monthly groundwater contributions to stream flow.

Table 7.1 Calibrated parameters' relative sensitivities and their sensitivity rankings

Parameter	Unit	Relative sensitivity	Rank
Manning's n (river)	-	0.39	1
Soil moisture depth	m	0.32	2
Initial soil moisture (clay loam)	-	0.29	3
Ks (clay loam-forest)	cm/hr	0.24	4
Porosity (clay loam)	-	0.12	5
Ks (clay loam-forest clear cut area)	cm/hr	0.08	6
Ks (clay loam-agriculture)	cm/hr	0.006	7
Ks (sandy loam-forest)	cm/hr	0.0052	8
Ks (clay loam-built up area)	cm/hr	0.005	9
Ks (clay loam-wetland)	cm/hr	0.003	10
porosity (silt loam)	-	0.002	11
Ks (silt loam-forest)	cm/hr	0.0001	12

Table 7.1 shows that 12 parameters out of 28 calibrated parameters of the developed model, as shown in Table 3.8, have little to large impacts on the modeling output. 11 of these 12 parameters control infiltration and soil moisture, which, in turn, control groundwater flow, whereas the other parameter controls stream (i.e., channel) flow routing. Manning's n (river), which controls stream flow routing, has the highest relative sensitivity. Two criteria (mean and standard deviation) of the normalized sensitivity coefficients were selected to identify the most sensitive parameters, which influence the modeling output (Nejadhashemi et al., 2011). Mean and standard deviation were calculated based on the estimated NSC values of the four runs in the OAT method. Soil moisture depth, initial soil moisture (clay loam), Ks (clay loam-forest), porosity (clay loam), and Ks (clay loam-forest clear cut area) ranked second, third, fourth, fifth, and sixth, respectively, based on their relative sensitivities' values. The parameters (i.e., Ks (clay loam-agriculture), Ks (sandy loam-forest), Ks (clay loam-built up area), Ks (clay loam-wetland), porosity (silt loam), and Ks (silt loam-forest)), ranked from seventh to twelfth, and their changes had very little impact on the change of mean monthly groundwater contributions to stream flow as well as relative sensitivity because clay loam-agriculture, sandy loam- forest, clay loam-built up area, clay loam-wetland, silt loam, and silt loam-forest cover 8%, 2%, 1%, 2%, 6%, and 6% of the study area, respectively. As a result, these six parameters (i.e., ranked seventh to twelfth) were not considered for uncertainty analysis in this study. Benke et al. (2008) also noted that when parameters have little impact on the modeling output value, they can be easily ignored for simplification of the model structure.

7.4 Uncertainty analysis of GW-SW interaction

Uncertainty analysis of GW-SW interaction was conducted using the six most sensitive calibrated parameters. These input parameters' values were obtained from text books, journals, and other field collected results conducted by scientific institutes under similar conditions (Gaiser, 1952; Chow, 1959; Clapp et al., 1978; Rawls et al., 1982; Rawls et al., 1983; Smedema et al., 1983; Minhas et al., 1986; Miller et al., 1998; Western et al., 2002; Bora et al., 2003; Celik, 2005; Choi et al., 2007; Reynolds et al., 2007; Saskatchewan Ministry of Agriculture, 2008; Hatch et al., 2010). The values of these parameters were assumed to be normally distributed. Table 7.2 lists all these parameters' mean and standard deviation values which were used for generating 50 Monte Carlo realizations of these parameters based on the assumed probabilistic distributions. In this study, the Monte Carlo simulation was used as the uncertainty analysis method because it is the most popular reliability-analysis-based stochastic method for evaluating uncertainties in hydrology studies (Lahkim et al., 1999). In this method a number of realizations of the uncertain parameters are generated and using those realizations same numbers of final outputs are produced. The final outputs are generally presented in the form of a probability distribution or a cumulative frequency distribution. 50 realizations of the most sensitive parameters were selected because of computational constraint. Using these realizations, uncertainty analysis of GW-SW interaction was conducted for the A2 and B1 GHG emission scenarios for year 2013. In this study, year 2013 was chosen as a case study to see the variation of GW-SW interactions with respect to parameter uncertainty due to lower mean annual groundwater contribution to stream flow under the B1 scenario than under the A2 scenario in 2013.

Table 7.2 Mean and standard deviation values of the most sensitive parameters used for uncertainty analysis

Parameter	Unit	Mean	Standard deviation
Manning's n (river)	-	0.032	0.01
Soil moisture depth	m	0.60	0.125
Initial soil moisture (clay loam)	-	0.18	0.04
Ks (clay loam-forest)	cm/hr	0.20	0.08
Porosity (clay loam)	-	0.45	0.02
Ks (clay loam-forest clear cut area)	cm/hr	0.12	0.05

7.4.1 Uncertainty analysis of GW-SW interaction under A2 scenario

The uncertainty analysis results of GW-SW interaction under the A2 GHG emission scenario in different months of 2013 are shown in Fig. 7.1. The cumulative relative frequency distribution of the mean monthly groundwater contributions to stream flow is presented. The results show that the patterns of mean monthly groundwater contributions to stream flow vary monthly due to the model nonlinearity to input data (i.e., precipitation amount, and temperature), and the modeling parameter uncertainty. Table 7.3 lists the detailed uncertainty analysis results (i.e., range, mean and standard deviation) of the mean monthly groundwater contributions to stream flow in different months of 2013 under the A2 scenario against the simulated value for the corresponding month using the calibrated parameters' values that were used in model calibration and validation. These results indicate the necessity of using uncertainty analysis in modeling parameters rather than point

estimates. The results also illustrate that the output generated by the calibrated model using the calibrated parameters' values, falls within the range of modeling outputs from uncertainty analysis. It is also found that the calculated highest range of mean monthly groundwater contributions to stream flow occurs during low flow months in fall, winter, and early spring.

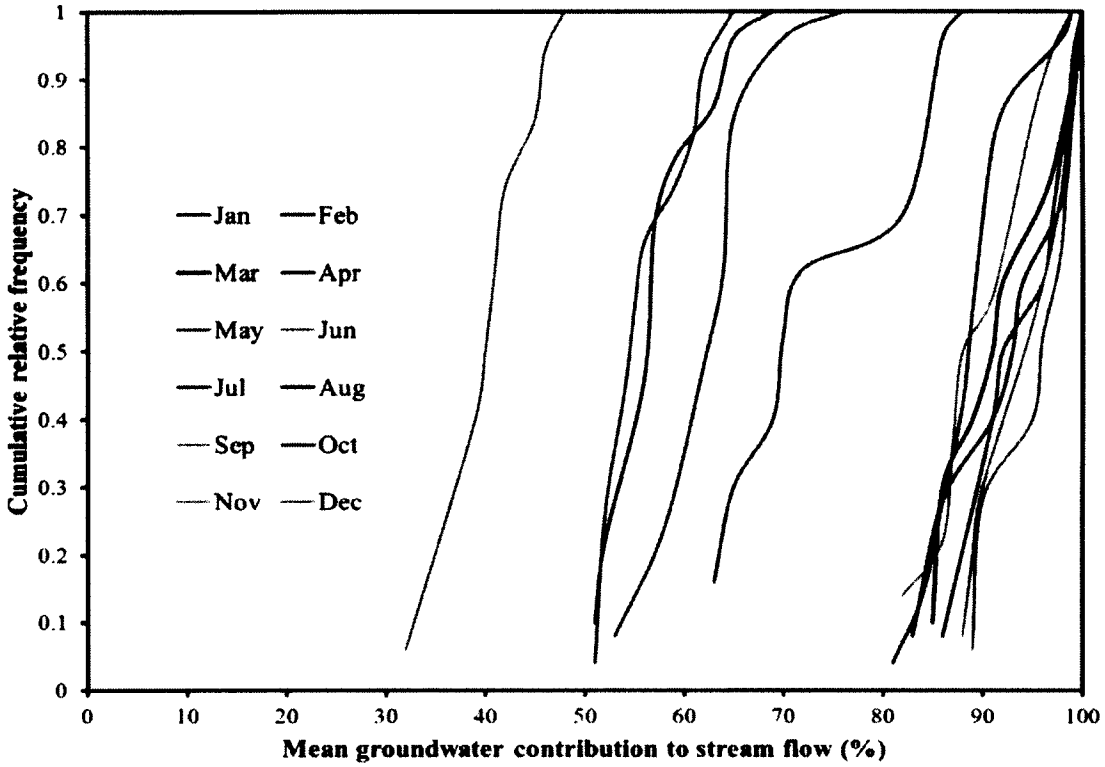

Figure 7.1 Cumulative relative frequency distribution of mean groundwater contributions to stream flow in different months of 2013 under A2 GHG emission scenario

Table 7.3 Uncertainty analysis results of mean monthly groundwater contributions to stream flow under A2 GHG emission scenario in 2013 against the simulated value for corresponding month using the calibrated parameters' values

Month	Range of mean groundwater contribution to stream flow (%)	Mean (%)	Standard deviation (%)	Output using the calibrated parameters' values (%)
Jan	86-100	94.19	5.74	93.16
Feb	83-100	93.22	6.32	90.79
Mar	85-100	92.44	5.63	93.53
Apr	51-69	58.19	6.08	54.26
May	51-65	56.78	4.71	57.23
Jun	32-48	41.10	4.45	44.04
Jul	53-76	64.40	5.55	59.20
Aug	63-88	76.76	10.0	71.89
Sep	82-99	90.41	6.33	88.94
Oct	81-99	90.06	5.53	93.81
Nov	89-100	94.73	4.35	95.90
Dec	88-100	95.23	4.55	97.50

Fig. 7.2 shows the cumulative relative frequency distribution of the mean groundwater contributions to stream flow in different seasons of 2013 under the A2 scenario. Similar to the monthly variations, the mean groundwater contributions to stream flow also show the seasonal variation patterns. Table 7.4 lists the detailed uncertainty analysis results for different seasons of 2013. The maximum and minimum ranges are found in winter and summer, respectively.

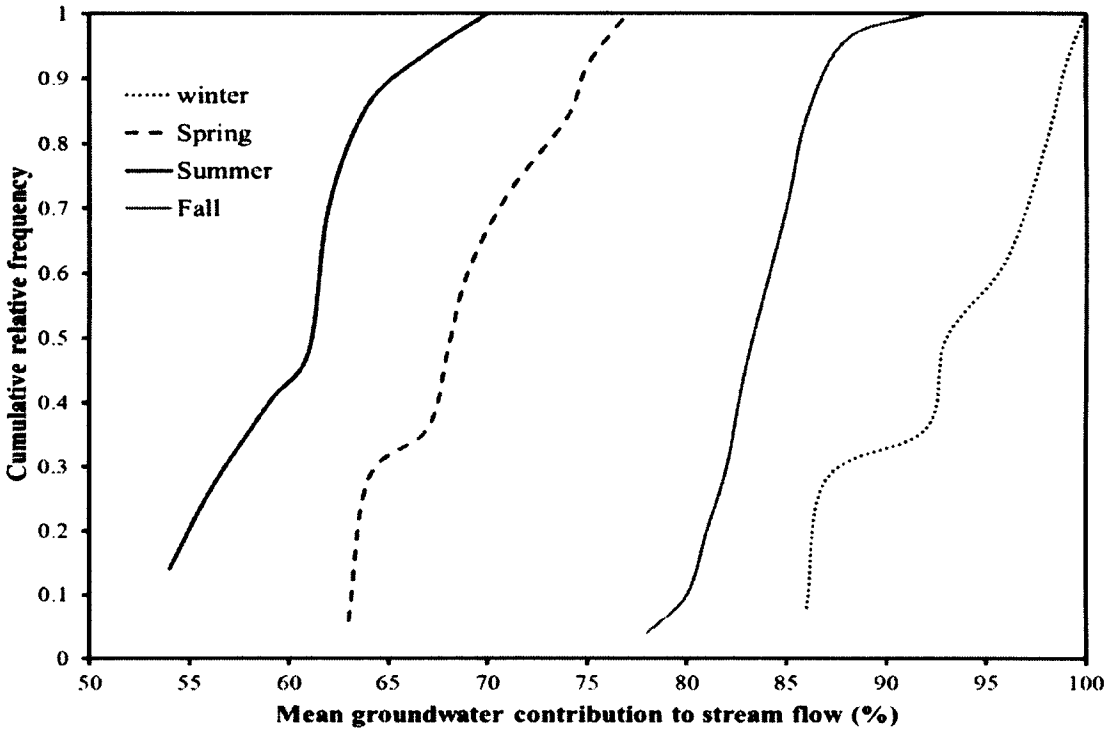

Figure 7.2 Cumulative relative frequency distribution of mean groundwater contributions to stream flow in different seasons of 2013 under A2 GHG emission scenario

Table 7.4 Uncertainty analysis results of mean groundwater contributions to stream flow under A2 GHG emission scenario in different seasons of 2013 against the simulated value for corresponding season using the calibrated parameters' values

Season	Range of mean groundwater contribution to stream flow (%)	Mean (%)	Standard deviation (%)	Output using the calibrated parameters' values (%)
Winter	86-100	93.88	5.47	96.78
Spring	63-77	69.14	5.32	68.61
Summer	54-70	60.82	6.28	59.16
Fall	78-94	88.04	4.08	87.36

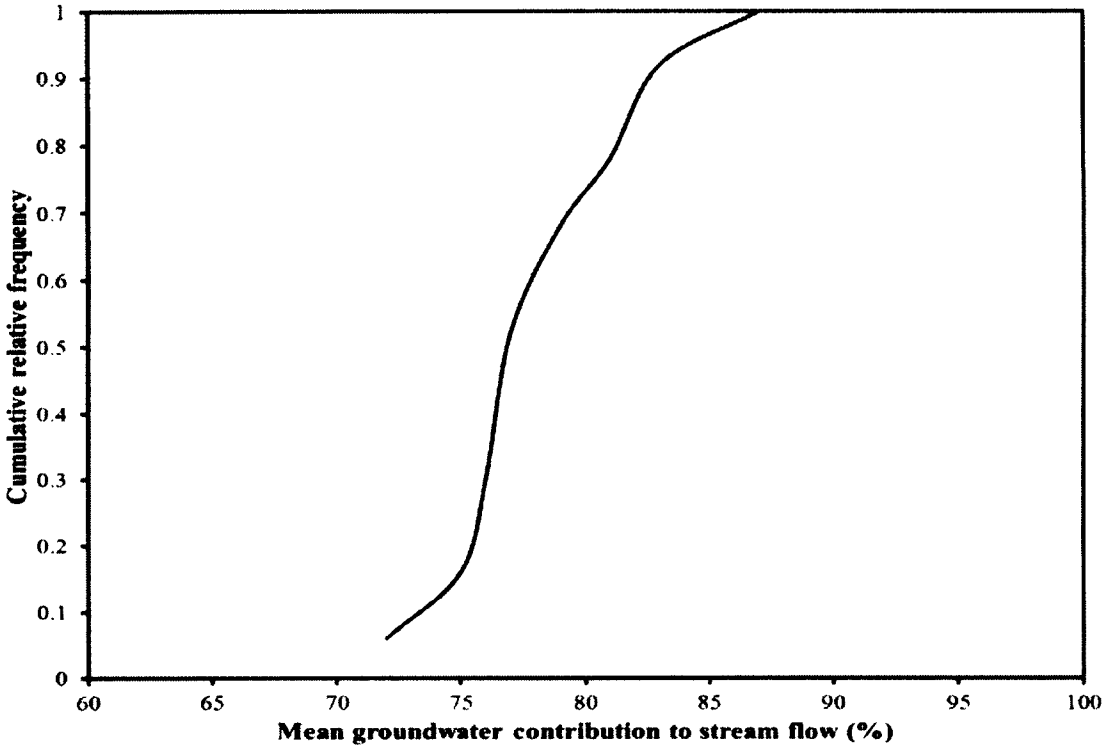

Figure 7.3 Cumulative relative frequency distribution of mean annual groundwater contributions to stream flow in 2013 under A2 GHG emission scenario.

Fig. 7.3 illustrates the cumulative relative frequency distribution of the mean annual groundwater contributions to stream flow in 2013 under the A2 scenario. The mean annual groundwater contributions to stream flow range from 72% to 87%, with a mean of 79% and a standard deviation of 4%. On the other hand, the mean annual groundwater contribution to stream flow in 2013 is 78%, using the calibrated parameters' values. Therefore, these uncertainty analysis results will provide a range of outputs instead of one output, and using a specific confidence interval (e.g., 95%) with this range of outputs would provide more information to the watershed manager to take particular action with certain degree of risks regarding water withdrawal from the river and allocation to stakeholder for future water

supply. However, the range of outputs and predication will differ from year to year depending on the patterns of annual precipitation and temperature.

7.4.2 Uncertainty analysis of GW-SW interaction under B1 scenario

Fig. 7.4 demonstrates the uncertainty analysis results of GW-SW interaction under the B1 GHG emission scenario in different months of 2013. Table 7.5 lists the detailed uncertainty analysis results (i.e., range, mean and standard deviation) of the mean monthly groundwater contributions to stream flow under the B1 scenario in 2013 against the simulated value for the corresponding month using the calibrated parameters' values. Similar to the A2 scenario, the output of a particular month, generated using the calibrated parameters' values, falls within the range of the modeling outputs from uncertainty analysis. It is also found that the calculated highest range of mean monthly groundwater contribution to stream flow occurs during low flow months in winter and early spring.

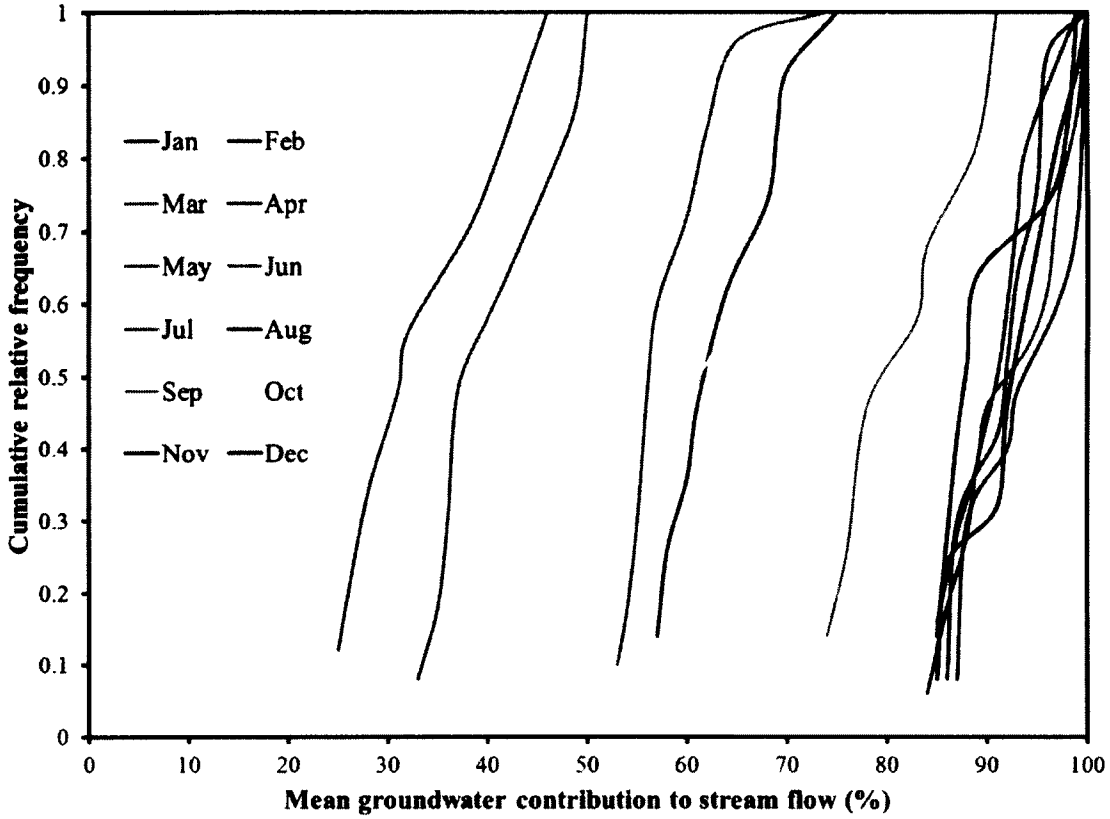

Figure 7.4 Cumulative relative frequency distribution of mean groundwater contributions to stream flow in different months of 2013 under B1 GHG emission scenario

Table 7.5 Uncertainty analysis results of mean monthly groundwater contributions to stream flow under B1 GHG emission scenario in 2013 against simulated value for corresponding month by using the calibrated parameters' values

Month	Range of mean groundwater contribution to stream flow (%)	Mean (%)	Standard deviation (%)	Output using the calibrated parameters' values (%)
Jan	87-100	94.29	5.56	99.79
Feb	86-100	93.53	4.94	98.32
Mar	85-100	93.27	5.82	98.46
Apr	57-75	64.15	6.35	63.16
May	25-46	35.67	7.97	28.30
Jun	33-50	41.35	6.36	47.21
Jul	53-74	60.53	6.43	61.30
Aug	84-99	91.64	5.19	96.20
Sep	74-91	81.99	6.91	87.70
Oct	53-80	66.02	10.10	56.48
Nov	85-99	91.15	5.49	87.82
Dec	85-100	92.65	5.64	97.89

Fig. 7.5 presents the cumulative relative frequency distribution of the mean groundwater contributions to stream flow in different seasons of 2013 under the B1 GHG emission scenario. Table 7.6 lists the detailed uncertainty analysis results. Similar to the A2 scenario, the maximum and minimum ranges under the B1 scenario are found in winter and summer, respectively. Fig. 7.6 shows the cumulative relative frequency distribution of the mean annual groundwater contributions to stream flow in 2013 under the B1 scenario. The mean annual groundwater contributions to stream flow range from 70% to 82%, with a mean of

75% and a standard deviation of 3.5%. On the other hand, the mean annual groundwater contribution to stream flow in 2013 is close to 77%, using the calibrated parameters' values. Compared to the A2 scenario, the range of mean annual groundwater contributions to stream flow under the B1 scenario is lower because more precipitation predicted under the B1 scenario than under the A2 scenario in 2013.

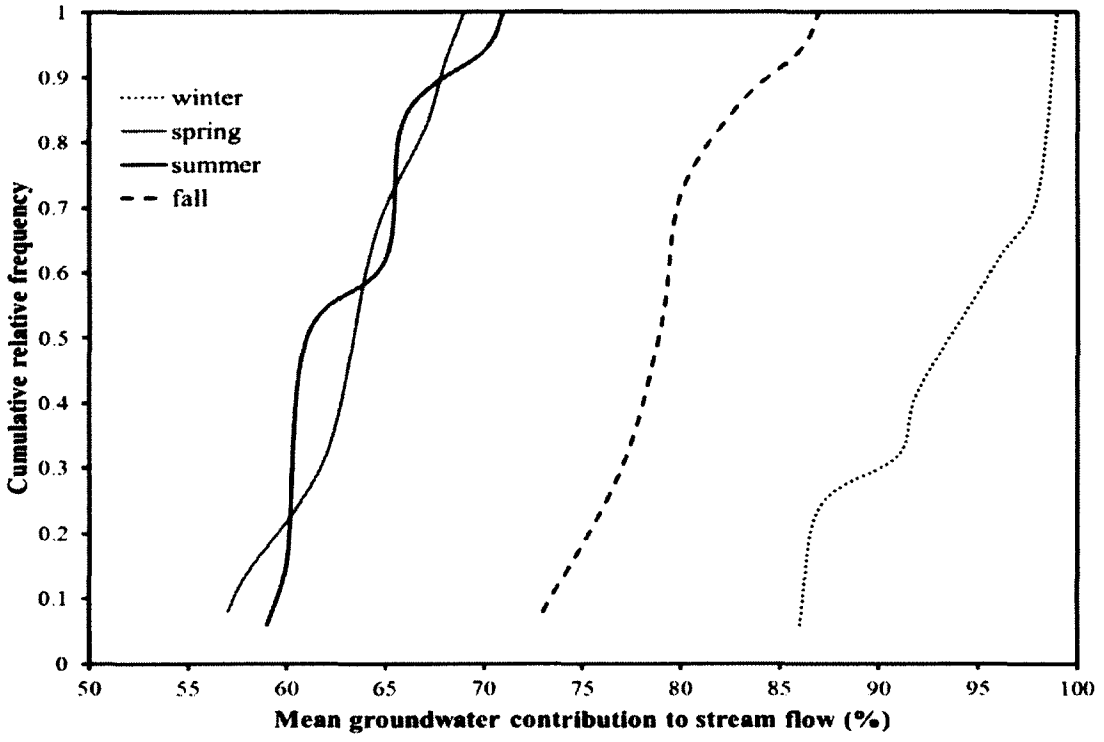

Figure 7.5 Cumulative relative frequency distribution of mean groundwater contributions to stream flow in different seasons of 2013 under B1 GHG emission scenario

Table 7.6 Uncertainty analysis results of mean groundwater contributions to stream flow under B1 GHG emission scenario in different seasons of 2013 against simulated value for corresponding season using the calibrated parameters' values

Season	Range of mean groundwater contribution to stream flow (%)	Mean (%)	Standard deviation (%)	Output using the calibrated parameters' values (%)
Winter	86-99	94.10	4.82	98.70
Spring	59-72	65.26	3.81	63.31
Summer	57-69	64.03	4.45	68.33
Fall	73-87	80.19	4.31	77.33

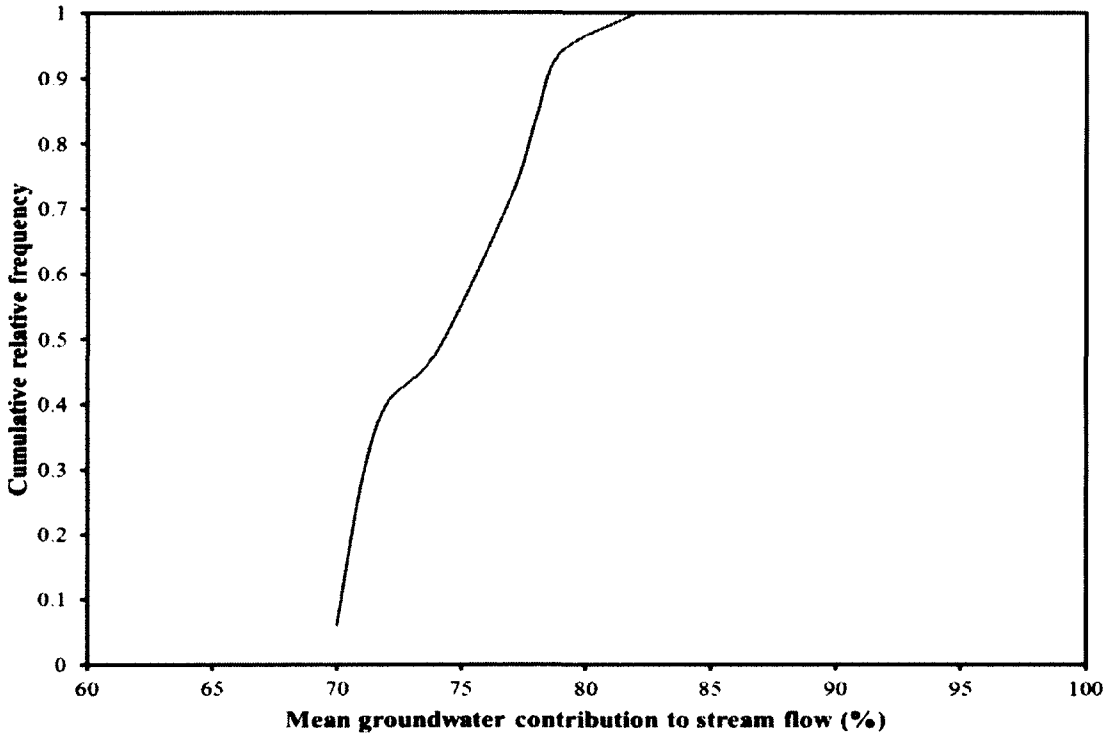

Figure 7.6 Cumulative relative frequency distribution of mean annual groundwater contributions to stream flow in 2013 under B1 GHG emission scenario

7.5 Summary

The uncertainty analysis of GW-SW interaction was conducted in a study area along the river of the Mainstem sub-watershed of KRW for the A2 and B1 GHG emission scenarios for year 2013 as a case study to show the variation of output (i.e., mean groundwater contribution to stream flow) with respect to the parameter uncertainty. Before conducting uncertainty analysis, sensitivity analysis was performed to find out the most sensitive modeling parameters. It was found that Manning's n (river), soil moisture depth, initial soil moisture (clay loam), Ks (clay loam-forest), porosity (clay loam), and Ks (clay loam-forest clear cut area) ranked as the top six sensitive modeling parameters based on their relative sensitivities. The values of these six parameters were assumed to be normally distributed, and their mean and standard deviation values were used for generating 50 Monte Carlo realizations to perform the uncertainty analysis. Based on the uncertainty analysis results, it was found that the mean monthly, seasonal and annual groundwater contributions to stream flow patterns under both scenarios showed different variation patterns due to the model nonlinearity and input parameter uncertainty. The results indicate that uncertainties in the six identified sensitive parameters have significant effects on the predicted mean groundwater contribution to stream flow. In general, these uncertainty analysis results represent a new attempt to indicate the complexities and uncertainties in GW-SW interaction system. Therefore, it is of necessity to use the uncertainty analysis results rather than the point estimates for better water resources management decision making. The uncertainty analysis results combined with a specific confidence interval could provide the watershed manager more information to take particular action with certain degree of risks regarding water

withdrawal from the river and allocation to stakeholder for future water supply depending on month and season.

CHAPTER 8

CONCLUSIONS

8.1 Summary

In this dissertation research, a GW-SW interaction model was developed through the Gridded Surface Subsurface Hydrologic Analysis (GSSHA) modeling system, and applied to a study area (213.82 km^2) along the river in the Mainstem sub-watershed of KRW to (1) investigate climate change impacts on GW-SW interaction under different GHG emission scenarios (i.e., A2 and B1 scenarios of IPCC), (2) examine the combined impacts of land use/land cover (LULC) and climate changes on GW-SW interaction, and (3) conduct uncertainty analysis of GW-SW interaction under different GHG emission scenarios. A brief summary of this dissertation is given as follows:

In Chapter 2, a detailed literature review of GW-SW interaction in the watershed was discussed. In Chapter 3, a GW-SW interaction model for the study area of the Mainstem sub-watershed of KRW was developed through the GSSHA modeling system using the field data (i.e., elevation, channel geometry, surficial geology, soils, land use and land cover, groundwater level, etc.) collected from the watershed. The model was calibrated and validated using observed stream flow data and climate data (i.e., precipitation and temperature) in the KRW by changing soil parameters (i.e., hydraulic conductivity and porosity), overland surface roughness, channel roughness, overland retention depth, initial soil moisture and soil moisture depth. In addition to stream flow, the developed model was also calibrated and validated using observed groundwater level data and the calculated mean

monthly groundwater contribution to stream flow (i.e., base flow index) using the PART base flow separation program of the USGS. In Chapter 4, future climate scenarios (i.e., precipitation and temperature) data, both short-term (2012-2016) and long-term (2020-2040) periods, for the KRW under the A2 (heterogeneous world with self-reliance and preservation of local identities), and B1 (more integrated and environmental friendly world) GHG emission scenarios of the Intergovernmental Panel on Climate Change (IPCC) were downscaled by the delta change method using the CRCM 4.2 (Canadian Regional Climate Model) of CCCma (Canadian Centre for Climate Modeling and Analysis) output data. The short-term period was chosen to understand the annual dynamics of climate change, and to make a comparison of GW-SW interactions between the effect of climate change and the effect of combined climate and land use/land cover (LULC) changes, and the long-term period was chosen to provide long-term future climate prediction. In addition, the future land use/land covers scenarios in the short-term (2012-2016) period were generated using the Arc GIS and GSSHA based on land use/land cover change analysis between 1999 and 2010.

In Chapter 5, the impact of climate changes on GW-SW interaction was investigated for a short-term period of 5 years (2012 to 2016) and a long-term period of 21 years (2020-2040) using the developed GW-SW interaction model. The simulation results indicated that the mean annual groundwater contribution to stream flow during the short-term period (2012-2016) under the A2 and B1 greenhouse emission scenarios is expected to decrease by 3.3% and 1.8%, respectively, as compared to that during the reference period (2007-2011), due to increased precipitation (on average 6.1% under the A2 and 3.6% under the B1 scenarios) and temperature (on average 0.64°C under the A2 and 0.36°C under the B1 scenarios). These climate changes would result in increased stream flow (on average 6.7% under the A2 and

3% under the B1 scenarios), groundwater discharge (on average 2.8% under the A2 and 1.2% under the B1 scenarios), and surface runoff (on average 22.5% under the A2 and 11.2% under the B1 scenarios). However, the major increase would occur in surface runoff compared to stream flow and groundwater discharge. Therefore, climate change significantly affects stream flow, groundwater discharge and surface runoff, as well as the annual dynamics of GW-SW interaction. It was also found that the mean groundwater contribution to stream flow varied monthly, seasonally, and annually due to monthly, seasonal, and annual precipitation variability, respectively. From the seasonal point of view, the mean groundwater contribution to stream flow under both scenarios is the lowest and highest during summer and winter, respectively. In addition, climate change has also a significant effect on the mean daily and annual groundwater levels. Results similar to the short-term period were found for the long-term period (2020-2040). The results obtained from this study will provide useful information in the short-term and long-term periods for seasonal and annual water extractions from the river and allocation to the stakeholders for future water supply, as well as for evaluating the ecological conditions of the stream, which will be beneficial to aquatic ecosystems. They will be useful for the planning of regional water resources management.

In Chapter 6, the impact of combined land use (i.e., increasing forest clear cut area, and decreasing forest and agricultural areas) and climate changes on GW-SW interaction was examined using the developed GW-SW interaction model for the short-term period (2012-2016) due to limited future projected land uses data. It was found that the mean annual groundwater contribution to stream flow during the short-term period under the combined effects of A2 or B1 climate change scenario and LULC changes is expected to decrease by

6.4% and 4.3%, respectively, with respect to that under the reference period (2007-2011), due to land use changes and increased precipitation (on average 6.1% under the A2 and 3.6% under the B1 scenarios) and temperature (on average 0.64°C under the A2 and 0.36°C under the B1 scenarios). These changes would result in increased stream flow (on average 10.1% under the A2 and 5.8% under the B1 scenarios with LULC changes), groundwater discharge (on average 2.1% under the A2 and 0.7% under the B1 scenarios with LULC changes), and surface runoff (on average 42% under the A2 and 29% under the B1 scenarios with LULC changes). Therefore, combined climate and land use changes provide additive impacts on hydrological fluxes (e.g., stream flow, groundwater discharge). As compared to climate change effects only, these groundwater contributions to stream flow were lowered by 3.1% and 2.5% under the A2 and B1 scenario with LULC changes, respectively. This result also demonstrates that land use change has an important role in the groundwater contribution to stream flow by shifting the flow patterns to the regime with more surface runoff and stream flow, but less groundwater discharge. In addition, land use change has also a significant influence on the mean daily and annual groundwater levels. The results obtained from this study will provide useful information for seasonal and annual water extractions from the river and allocation to the stakeholders for future water supply, as well as for evaluating the ecological conditions of the stream, which will be beneficial to aquatic ecosystems. They will also provide how LULC changes can impact the groundwater contribution to stream flow and regional groundwater levels. Therefore, they will be useful for planning of regional groundwater resource management, as well as water resources management considering future climate and land use changes.

In Chapter 7, uncertainty analysis of GW-SW interaction was conducted under the A2 and B1 scenarios for year 2013 as a case study to show the variation of output (i.e., mean groundwater contribution to stream flow) with respect to the parameter uncertainty. Before conducting uncertainty analysis, sensitivity analysis was performed to find out the most sensitive parameters to the model output. The uncertainty analysis results under both scenarios revealed that the mean monthly, seasonal, and annual groundwater contributions to stream flow patterns vary monthly, seasonally, and annually, respectively, due to the model nonlinearity to input data (precipitation amount, and temperature), and uncertainty of the sensitive model parameters. In addition, the uncertainty analysis results showed that uncertainties in the most sensitive parameters have significant effects on the predicted mean groundwater contribution to stream flow, and indicate the complexities and uncertainties in GW-SW interaction system. Therefore, it is of necessity to use such uncertainty analysis results rather than the point estimates for better water resources management decision making.

8.2 Research Achievements

In this dissertation research, a GW-SW interaction model was developed through the Gridded Surface Subsurface Hydrologic Analysis (GSSHA) modeling system to investigate GW-SW interaction under the effects of climate and land use changes, where the key contribution was the inclusion of climate and LULC changes scenarios in the developed model to assess GW-SW interaction. The modeling results in this study represent a new way

to understand the temporal dynamics of GW-SW interaction under climate change, as well as combined climate and LULC changes. In addition, the uncertainty analysis results indicate the complexities and uncertainties in this interaction system. The developed model, based on very limited data, was used to understand GW-SW interaction in a study area (213.82 km^2) along the river of the Mainstem sub-watershed of KRW. The modeling results will provide useful decision support for water resources management considering climate and land use changes.

8.3 Recommendations

Although this GW-SW interaction model was developed based on very limited data, it predicts future scenarios of groundwater contribution to stream flow under climate change and combined climate and LULC changes for both a short term and a long-term period. The following recommendations are suggested for further studies on GW-SW interaction studies in this study area:

1. A detailed soil map for the study area, as well as for the entire KRW, which includes different soil types, needs to be prepared.
2. More bank piezometers in the study area as well as the entire KRW need to be installed in order to get better regional groundwater flow field.
3. Stream flow at the East and West confluences during spring runoff and high flow during summer need to be measured so that there can be complete data sets of stream flow available throughout the year. In addition, cross sections of the river in the

Mainstem area need to be measured. It could be done using tape measurement and boat.

4. More weather stations in the study area need to be set up so that Thiessen polygon method can be used for getting accurate observed precipitation.
5. Soil moisture and soil moisture depth under different land use/land covers need to be measured because these two parameters are very sensitive to the model output. These could be measured using tensiometer, electrical resistance blocks, and time domain reflectometer (TDR) depending on budget and accuracy. For cost and ease of use, tensiometer and electrical resistance blocks are effective practical devices, whereas TDR is very expensive but it provides accurate and more reliable data compared to other methods.
6. Manning's n for river channel during different seasons of the river stage should be calculated because n value changes seasonally and this parameter is very sensitive to the model output. It could be done by measuring river depth and width using a tape, water-surface profile using a clinometer, and flow velocity using a velocity meter at a large number of river sections during different seasons, and putting those values in the Manning's equation. The details of these methods can be found in Acrement et al. (1984). The average of the calculated manning's n values would provide the actual manning's n value of a particular season. However, it would cost a lot since extensive field measurement in a long river (i.e., 71.26 km long) requires time and resources. Therefore, the number of sections of the river needs to be determined for these measurements based on budget.

7. Since future climate change scenarios are full of uncertainty (Christensen et al., 2007), uncertainty analysis of climate change should be incorporated to assess the average impact of climate change scenarios on GW-SW interaction.
8. The results obtained from this study may be different in another region which has similar monthly precipitation trends to this study area, but different geological, land uses and topography conditions. In addition, the results obtained from this study also may be different in another region where monthly precipitation trends are different in comparison to this study area. Therefore, the results obtained in this study should be compared to another climatic and geological region in order to gain better understanding of the impacts of climate and land use change on GW-SW interactions under different climatic and watershed conditions.
9. Different climate models may give different scenarios of future precipitation and temperature trends under the A2 and B1 GHG emission scenarios, and therefore, precipitation and temperature predicted from other climate models (e.g., NCARPCM developed by National Center for Atmospheric Research (NCAR), USA; HADCM3 developed by UK Meteorological Office, United Kingdom; ECHAM50M developed by Max Planck Institute for Meteorology, Germany) should be used for comparing the results obtained from this study. In addition, different downscaling method (e.g., dynamic downscaling) could also be used to compare the results.
10. More land use maps of the study area, as well as the whole KRW need to be prepared annually between 1999 and 2010 so that the change of land use type can be determined accurately. However, for accurate future land use projections, the land use

change model (e.g., CLUE-S, Land use change modeling kit (LUCK)), along with economic model (e.g., Wonderland model, World3), should be used.

11. Due to limited available data, the understanding of complex GW-SW interaction processes in a large-scale area is always limited. Therefore, multiple techniques need to be used to assess GW-SW interaction in a large-scale area. For example, another watershed model (e.g., MIKE SHE) could be used to compare the findings of this study. In addition to piezometer studies, environmental tracer method (i.e., stable isotopic tracers, such as stable oxygen and hydrogen isotopes) could be used to find out groundwater contribution to stream flow. Since this method is applicable for small scale area, therefore a number of water samples need to be collected at a number of locations during different seasons for isotope analysis. The average of the isotope results would provide the seasonal and annual groundwater contributions to stream flow in the study area.
12. Fine resolution of DEM and LULC maps could be used for better understanding of GW-SW interaction in the watershed. In addition, more Monte Carlo simulations should be used for better results of uncertainty. However, High Performance Computing (HPC) as well as higher budget would be needed to achieve those goals.

REFERENCES

Acrement, G.J., and Schneider, V.R. (1984). Guide for Selecting Manning's Roughness Coefficients for Natural Channels and flood plains. Federal Highways Administration, US Department of Transportation, Report No. FHWA-TS-84-204, Washington, 62 pp.

Agriculture and Agri-Food Canada. (1998). The Canadian system of soil classification. 3rd ed, publication no. 1646, 187 pp.

Allen, D.M., and Scibek, J. (2004). Climate change and groundwater: A modeling approach for identifying impacts and resource sustainability in the Central Interior of British Columbia. Summary report for Climate Change Action Fund, Natural Resources Canada.

Amidror, I. (2002). Scattered data interpolation methods for electronic imaging systems: a survey. *Journal of Electronic Imaging*, 11(2),157-176.

Anctil, F., Perrin, C., and Andreassian, V. (2004). Impact of the length of observed records on the performance of ANN and of conceptual parsimonious rainfall-runoff forecasting models. *Environmental Modeling & Software*, 19, 357-368.

Anderson, M.G., and Burt, T.P. (1980). Interpretation of recession flow. *Journal of Hydrology,* 46, 89–101.

Andreasson, J., Bergström, S., Carlsson, B., Graham, L.P., and Lindström, G. (2004). Hydrological Change - Climate change impact simulation for Sweden. *A Journal of the Human Environment*, 33(4–5), 228–234.

Anibas, C., Buis, K., Verhoeven, R., Meire, P., and Batelaan, O. (2011). A simple thermal mapping method for seasonal spatial patterns of groundwater-surface water interaction. *Journal of Hydrology*, 397(1–2), 93– 104.

Arnold, J.G., and Allen, P.M. (1999). Automated methods for estimating baseflow and ground water recharge from stream flow records. *Journal of American Water Resource Association*, 35, 411–424.

Ashby, S.F., and Falgout, R.D. (1996). A parallel multigrid preconditioned conjugate gradient Algorithm for groundwater flow simulations. *Nuclear Science and Engineering*, 124(1), 145-159.

Batelaan, O., De Smedt, F., and Triest, L. (2003). Regional groundwater discharge: phreatophyte mapping, groundwater modeling and impact analysis of land-use change. *Journal of Hydrology*, 275, 86-108.

Becker, M.W., Georgian, T., Ambrose, H., Siniscalchi, J., and Fredrick, K. (2004). Estimating flow and flux of ground water discharge using water temperature and velocity. *Journal of Hydrology*, 296(1–4), 221– 233.

Benke, K.K., Lowell, K.E., and Hamilton, A.J. (2008). Parameter uncertainty, sensitivity analysis and prediction error in a water-balance hydrological model. *Mathematical and Computer Modelling*, 47, 1134-1149.

Bergeron, G., Laprise, L., and Caya, D. (1994). Formulation of the Mesoscale Compressible Community (MC2) Model. Internal Report from Cooperative Centre for Research in Mesometeorology. Montréal, Canada, 165 pp.

Bergström, S., Carlsson, B., Gardelin, M., Lindström, G., Pettersson, A., and Rummukainen, M. (2001).Climate change impacts on runoff in Sweden – assessments by global climate models, dynamical downscaling and hydrological modeling. *Climate Research,* 16, 101–112.

Beven, K.J., and Binley, A.M. (1992). The future of distributed models: Model calibration and uncertainty prediction. *Hydrological Processes*, 6, 279– 298.

Bidwell, V.J., Stenger, R., and Barkle, G.F. (2008). Dynamic analysis of groundwater discharge and partial are contribution to Pukemanga stream, New Zealand. *Hydrology and Earth System Sciences*, 12, 975-987.

Blanco, H., and Lal, R. (2010). Water erosion. Principles of Soil Conservation and Management. Springer, p. 28–30. ISBN 978-90-481-8529-0

Blume, T., Zehe, E., and Bronstert, A. (2007). Rainfall—runoff response, event-based runoff coefficients and hydrograph separation. *Hydrological Sciences Journal*, 52(5), 843-862. DOI: 10.1623/hysj.52.5.843

Bora, P.K., and Rajput, T.B.S. (2003). Spatial and temporal variability of manning's n in irrigation furrows. *Journal of Agricultural Engineering*, 40 (3), 53-61.

British Columbia Ministry of Energy and Mines. (2012). The status of exploration and development activities in the Montney Play region of northern BC. http://www.offshore-oilandgas.gov.bc.ca/OG/oilandgas/petroleumgeology/UnconventionalGas/Documents/C%20Adams.pdf. [Accessed on December 19, 2012]

British Columbia Ministry of Environment. (2009). Manual of British Columbia Hydrometric standards. http://www.geog.ubc.ca/~beaton/images/Establishing_a_station_leveling.pdf. [Accessed on January 8, 2014]

British Columbia Ministry of Forests and Range. (2008). Climate change, impacts, and adaptation scenarios: climate change and forests and range management in British

Columbia. Technical report 045. http://www.for.gov.bc.ca/hfd/pubs/Docs/Tr/Tr045.htm. [Accessed on May 21, 2013]

Canada Department of Agriculture. (1974). The system of soil classification for Canada. Queen's printer, Ottawa, 255 pp.

Canadian System of Soil Classification. (1998). 3rd edition. Available at http://sis.agr.gc.ca/cansis/taxa/cssc3/index.html. [Accessed on May 10, 2012]

Cannon, A.J., and McKendry, I.G. (2002). A graphical sensitivity analysis for statistical climate models: Application to Indian monsoon rainfall prediction by artificial neural networks and multiple linear regression models. *International Journal of Climatology*, 22, 1687–1708. DOI:10.1002/joc.811

Celik, I. (2005). Land-use effects on organic matter and physical properties of soil in a southern Mediterranean highland of Turkey. *Soil & Tillage Research*, 83, 270-277.

Chang, H.J. (2007). Comparative streamflow characteristics in urbanizing basins in the Portland Metropolitan Area, Oregon, USA. *Hydrological Processes*, 21(2), 211–222.

Chenini, I., Mammou, A.B., and May, M.E. (2010). Groundwater recharge zone mapping using GIS-based multi-criteria analysis: A case study in central Tunisia (Maknassy Basin). *Water Resources Management*, 24, 921-939.

Choi, M., and Jacobs, J.M. (2007). Soil moisture variability of root zone profiles within SMEX02 remote sensing footprints. *Advances in Water Resources*, 30 (4), 883-896.

Chow, V.T. (1959). Open Channel Hydraulics. McGraw-Hill, USA.

Christensen, J.H., and Christensen, O.B. (2007). A summary of the PRUDENCE model projections of changes in European climate by the end of this century. *Climate Change*, 81, 7-30.

Christophersen, N., and Hooper, R.P. (1992). Multivariate-Analysis of StreamWater Chemical Data – the Use of Principal Components- Analysis for the End-Member Mixing Problem. *Water Resources Research*, 28(1), 99–107.

Clapp, R.B., and Hornberger, G.M. (1978). Empirical equations for some soil hydraulic properties. *Water Resources Research*, 14, 601-604

Clow, D.W., Schrott, L., Webb, R., Campbell, D.H., Torizzo, A., and Dornblaser, M. (2003). Groundwater occurrence and contributions to stream flow in an Alpine catchment, Colorado Front Range. *Groundwater – Watershed Issue*, 41(7), 937-950.

Conant, B. (2004). Delineating and quantifying ground water discharge zones using streambed temperatures. *Ground Water*, 42(2), 243– 257.

Connor, J.A., Bowers, R.L., and Ahmed, F. (2005). Technical evaluation of Natural Resource Damage Assessment (NRDA) claims for groundwater resources. 2005 NGWA *Groundwater and Environmental Law Conference*, ID 45919385, July 21-22, 2005.

Cook, P.G., and Herczeg, A.L. (2000). (Eds): Environmental tracers in subsurface hydrology. Kluwer, Boston.

Covert, J. (1999). Washington State Department of Ecology, Personal communication.

Dams, J., Woldeamlak, S.T., and Batelaan, O. (2008). Predicting land-use change and its impact on the groundwater system of the Kleine Nete catchmenrt, Belgium. *Hydrology and Earth System Sciences*, 12, 1369-1385.

Dams, J., Salvadore, E., Van Daele, T., Ntegeka, V., Willems, P., and Batelaan, O. (2012). Spatio-temporal impact of climate change on the groundwater system. *Hydrology and Earth System Sciences*, 16, 1517-1531.

Diaz-Nieto, J., and Wilby, R.L. (2005). A comparison of statistical downscaling and climate change factor methods: Impacts on low flows in the River Thames, United Kingdom. *Climatic Change,* 69, 245–268.

Dobson Engineering Ltd. (2007). Kiskatinaw River watershed source protection plan. File 222-001. URL.http://www.dawsoncreek.ca/wordpress/wpcontent/uploads/2011/08/Kiskatinaw_Final.pdf.[Accessed on June 18, 2013].

Dobson Engineering Ltd., and Urban Systems Ltd. (2003). Kiskatinaw River Watershed Management Plan; File 0714.0046.01. URL http://www.dawsoncreek.ca/cityhall/departments/water/watershed/background-watershed-management-plans/ [Accessed on June 18, 2013].

Dotto, C.B.S., Mannina, G., Kleidorfer, M., Vezzaro, L., Henrichs, M., McCarthy, D.T., Freni, G., Rauch, W., and Deletic, A. (2012). Comparison of different uncertainty techniques in urban stormwater quantity and quality modeling. *Water Research*, 46, 2545-2558.

Downer, C.W. (2002): Identification and modeling of important stream flow producing processes in watersheds. Ph.D. dissertation, University of Connecticut.

Downer, C.W., James, W.F., Byrd, A., and Eggers, G.W. (2002a). Gridded Surface Subsurface Hydrologic Analysis (GSSHA) model simulation of hydrologic conditions and restoration scenarios for the Judicial Ditch 31 Watershed, Minnesota. Water Quality Technical Notes Collection (ERDCWQTN-AM-12)-June 2002, U.S. Army Engineer Research and Development Center: Vicksburg, MS.

Downer, C.W., Nelson, E.J., and Byrd, A. (2002b). Primer: Using Watershed Modeling System (WMS) for Gridded Surface Subsurface Hydrologic Analysis (GSSHA) Data Development—WMS 6.1 and GSSHA 1.43C. ERDC/CHL TR-02-XX, U.S. Army Engineer Research and Development Center, Vicksburg, MS.

Downer, C.W., and Ogden, F.L. (2006). Gridded Surface Subsurface Hydrologic Analysis (GSSHA) User's Manual; Version 1.43 for Watershed Modeling System 6.1. ERDC/CHL SR-06-1, U.S. Army Engineer Research and Development Center, Vicksburg, MS.

Drohan, P.J., Brittingham, M., Bishop, J., and Yoder, K. (2012). Early trends in land cover change and forest fragmentation due to shale-gas development in Pennsylvania: A potential outcome for the Northcentral Appalachains. *Environmental Assessment*, 49, 1061-1075.

Duan, Q., Sorooshia, S., and Gupta, V. (1992). Effective and Efficient Global Optimization for Conceptual Rainfall-Runoff models. *Water Resources Research*, 28(4), 1031-1051.

Durand, V., Aller, M.R., Greswell, R.B., Whelan, J., Rivett, M.O., Mackay, R, Smith, J.N.W., and Tellam, J.H. (2007). Natural attenuation potential of the urban hyporheic zone: field experiment set-up, baseline monitoring and modeling for extraction test design. *2nd SWITCH Scientific Meeting*, Israel, 27-29 Nov.

Eckhardt, K. (2005). How to construct recursive digital filters for base flow separation. *Hydrological Processes*, 19, 507–515.

Eckhardt, K. (2008). A comparison of base flow indices, which were calculated with seven different base flow separation methods. *Journal of Hydrology*, 352, 168–173.

El Hassan, A.A., Sharif, H.O., Jackson, T., and Chintalapudi, S. (2013). Performance of a conceptual and physically based model in simulating the response of a semi-urbanized watershed in San Antonio, Texas. *Hydrological Processes*, 27, 3394-3408.

Essaid, H.I., Zamora, C.M., McCarthy, K.A., Vogel, J.R., and Wilson, J.T. (2008). Using heat to characterize streambed water flux variability in four stream reaches. *Journal of Environmental Quality*, 37, 1010-1023.

Forest Practices Board. (2011). Cumulative effects assessment; A case study for the Kiskatinaw River watershed. FPB/SR/39.

Fowler, H.J., Blenkinsop, S., and Tebaldi, C. (2007). Linking climate change modeling to impact studies: recent advances in downscaling techniques for hydrological modeling. *International Journal of Climatology*, 27(12), 1547–1578.

Freer, J., Beven, K., and Ambroise, B. (1996). Bayesian estimation of uncertainty in runoff prediction and the value of data: An application of the GLUE approach. *Water Resources Research*, 32(7), 2161– 2173.

Fujieda, M., Kudoh, T., de Cicco, V., and de Calvarcho, J.L. (1997). Hydrological processes at two subtropical forest catchments: the Serra do Mar, Sao Paulo, Brazil. *Journal of Hydrology*, 196, 26-46.

Furukawa, Y., Inubushi, K., Ali, M., Itang, A.M., and Tsuruta, H. (2005). Effect of changing groundwater levels caused by land-use changes on greenhouse gas fluxes from tropical peat lands. *Nutrient Cycling in Agroecosystems*, 71, 81-91.

Gaiser, R.N. (1952). Root channels and roots in forest soils. *Proceedings – Soil Science Society of America,* 16, 62-65.

Gan, T.Y., Dlamini, E.M., and Biftu, G.F. (1997). Effects of model complexity and structure, data quality, and objective functions on hydrologic modeling. *Journal of Hydrology*, 192(1), 81-103.

Gauthier, M.J., Camporese, M., Rivard, C., Paniconi, C., and Larocque, M. (2009). A modeling study of heterogeneity and surface water-groundwater interactions in the Thomas Brook catchment, Annapolis valley (Nova Scotia, Canada). *Hydrology and Earth System Sciences*, 13, 1583-1596.

Geist, D.R., Joy, M.C., Lee, D.R., and Gonser, T. (1998). A method for installing piezometers in large cobble bed rivers. *Groundwater Monitoring & Remediation*, 18, 78-82.

Genereux, D.P., and Hooper, R.P. (1998). Oxygen and Hydrogen Isotopes in Rainfall-Runoff Studies, in: Isotope Tracers in Catchment Hydrology. Edited by: Kendall, C., and McDonnell, J.J., Elsevier Science, Amsterdam.

Ghaffari, G., Keesstra, S., Ghodousi, J., and Ahmadi, H. (2010). SWAT-simulated hydrological impact of land-use change in the Zanjanrood Basin, Northwest Iran. *Hydrological Processes*, 24, 892-903.

Gonzales, A.L., Nonner, J., Heijkers, J., and Uhlenbrook, S. (2009). Comparison of different base flow separation methods in a lowland catchment. *Hydrology and Earth System Sciences*, 13, 2055-2068.

Goderniaux, P., Brouy`ere, S., Fowler, H.J., Blenkinsop, S., Therrien, R., Orban, P., and Dassargues, A. (2009). Large scale surface-subsurface hydrological model to assess climate change impacts on groundwater reserves. *Journal of Hydrology*, 373, 122–138 doi:10.1016/j.jhydrol.2009.04.017

Goderniaux, P. (2010). Impact of climate change on groundwater reserves. Ph.D. dissertation, University of Liege.

Graham, L.P. (2004). Climate change effects on river flow to the Baltic Sea. *A Journal of the Human Environment,* 33(4–5), 235–241.

Graham, L.P., Andréasson, J., and Carlsson, B. (2007). Assessing climate change impacts on hydrology from an ensemble of regional climate models, model scales and linking methods – a case study on the Lule River basin. *Climatic Change*, 81(1), 293–307.

Guardiola-Claramonte, M., Troch, P.A., Breshears, D.B., Huxman, T.E., Switanek, M.B., Durcik, M., and Cobb, N.S. (2011). Decreased streamflow in semi-arid basins following drought-induced tree die-off: A counter-intuitive and indirect climate impact in hydrology. *Journal of Hydrology*, 406, 225-233.

Gupta, H.V., Sorooshian, S., and Yapo, P.O. (1999). Status of automatic calibration for hydrologic models: Comparison with multilevel expert calibration. *Journal of Hydrologic Engineering,* 4(2), 135-143.

Haith, D.A., and Shoemaker, I.L. (1987). Generalized watershed loading functions for stream flow nutrients. *Water Resources,* Bull. 107, 121-137.

Halford, K.J., and Mayer, G.C. (2000). Problems associated with estimating ground water discharge and recharge from stream-discharge records. *Ground Water*, 38(3), 331–342.

Hamby, D.M. (1994). A review of techniques for parameter sensitivity analysis of environmental models. *Environmental Monitoring and Assessment*, 32, 135–154.

Hannah, D.M., Brown, L.E., Milner, A.M., Gurnell, A.M., Mcgregor, G.R., Petts, G.E., Smith, B.P.G., and Snook, D.L. (2007). Integrating climate-hydrology-ecology for alpine river systems. *Aquatic Conservation: Marine and Freshwater Ecosystems*, 17, 636-656.

Harvey, F.E., Lee, D.R., Rudolph, D.L., and Frape, S.K. (1997). Locating groundwater discharge in large lakes using bottom sediment electrical conductivity mapping. *Water Resources Research*, 33(11), 2609– 2615.

Hatch, C.E., Fisher, A.T., Ruehl, C.R., and Stemler, G. (2010). Spatial and temporal variations in streambed hydraulic conductivity quantified with time-series thermal methods. *Journal of Hydrology*, 389, 276-288.

Hay, L.E., Wilby, R.L., and Leavesley, G.H. (2000). A comparison of delta change and downscaled GCM scenarios for three mountainous basins in the United States. *Journal of American Water Resources Association*, 36, 387–398.

Hester, E.T., and Doyle, M.W. (2008). In-stream geomorphic structures as drivers of hyporheic exchange. *Water Resources Research*, 44, W03417. doi:10.1029/2006WR005810

Hewlett, J.D., and Hibbert, A.R. (1967). Factors affecting the response of small watersheds to precipitation in humid areas. In: *Proceedings of. International Symposium on Forest Hydrology* (ed. by W. E. Sopper & H. W. Lull), p. 275–290, Pergamon Press, New York, USA.

Holtan, H.N., Minshall, N.E., and Harrold, L.L. (1962). Field manual for research in agricultural hydrology. SWCD ARS, Washington, D.C., 214 pp.

Hood, J.L., Roy, J.W., and Hayashi, M. (2006). Importance of groundwater in the water balance of an alpine headwater lake. *Geophysical Research Letters*, 33, L13405. doi:10.1029/2006GL026611

Hughes, D.A. (2004). Incorporating groundwater recharge and discharge functions into an existing monthly rainfall-runoff model. *Hydrological Sciences*, 49(2), 297-311.

IPCC. (2000). IPCC Special Report. Emission Scenarios. Cambridge University Press, Cambridge, United Kingdom, 570 pp.

IPCC. (2007). Climate Change 2007: The Physical Science Basis, Contribution of working Group I to the 4th assessment report (AR4) of the Intergovernmental Panel on Climate Change, Cambridge University Press, Cambridge, United Kingdom, 996 pp.

Jackson, C.R., and Spink, A.E.F. (2004). User's manual for the groundwater flow model ZOOMQ3D. British Geological Survey Internal Report, IR/04/140.

Jackson, C.R., Meister, R., and Prudhomme, C. (2011). Modeling the effects of climate change and its uncertainty on UK Chalk groundwater resources from an ensemble of global climate model projections. *Journal of Hydrology*, 399, 12-28.

Jagucki, M.L., Finton, C.D., Springer, A.E., and Bair, E.S. (1995). Hydrogeology and water quality at the Management Systems Evaluation Area near Piketon, Ohio. US Geological Survey Water Resources Investigations Report 95-4139, 117 pp.

Jenkins, R.N. (2006). The uses of GSSHA to model groundwater-surface water interaction. Master's Thesis, Brigham Young University.

Jinno, K., Tsutsumi, A., Alkaeed, O., Saita, S., and Berndtsson, R. (2009). Effects of land use change on groundwater recharge model parameters. *Hydrological Sciences Journal*, 54(2), 300-315.

Kala Groundwater Consulting Ltd. (2001). Groundwater potential evaluation Dawson Creek. British Columbia. Reference: R01332-0622. URL

http://www.dawsoncreek.ca/wordpress/wpcontent/uploads/watershed/2001DCk_Kala_GWPotential.pdf. [Accessed on June 18, 2013].

Kalbus, E., Reinstorf, F., and Schirmer, M. (2006). Measuring methods for groundwater-surface water interactions: a review. *Hydrology and Earth System Science*, 10, 873-887.

Karamouz, M., Nazif, S., and Falahi, M. (2012). Hydrology and Hydroclimatology: principles and applications. CRC Press, Florida, 740 pp.

Kasahara, T., and Wondzell, S.M. (2003). Geomorphic controls on hyporheic exchange flow in mountain streams. *Water Resources Research*, 39(1), 1005. doi:10.1029/2002WR001386

Kelly, S.E., and Murdoch, L.C. (2003). Measuring the hydraulic conductivity of shallow submerged sediments. *Ground Water*, 41(4), 431–439.

Kendall, C., and Caldwell, E.A. (1998). Fundamentals of Isotope Geochemistry, in: Isotope Tracers in Catchment Hydrology. Edited by: Kendall, C., and McDonnell, J.J., Elsevier Science, Amsterdam.

Kliner, K., and Knezek, M. (1974). The underground runoff separation method making use of the observation of ground water table. *Hydrology and Hydromechanics*, XXII(5), 457–466.

Klocking, B., and Haberlandt, U. (2002). Impacts of land use changes on water dynamics – a case study in temperate meso and macroscale river basins. *Physics and Chemistry of the Earth*, 27, 619-629.

Koeniger, P., Leibundgut, C., and Stichler, W. (2009). Spatial and temporal characterization of stable isotopes in river water as indicators of groundwater contribution and confirmation of modelling results; a study of the Weser river, Germany. *Isotopes in Environmental and Health Studies*, 45(4), 289-302. DOI: 10.1080/10256010903356953

Kollet, S.J., and Maxwell, R.M. (2006). Integrated surface-groundwater flow modeling a freesurface overland flow boundary condition in a parallel groundwater flow model. *Advances in Water Resources*, 29(7), 945-958.

Krause, S., and Bronstert, A. (2004). Approximation of groundwater-surface water interactions in a mesoscale lowland river catchment. *Hydrology: Science & Practice for the 21st Century*, Vol. II, British Hydrological Society.

Krause, S., Bronstert, A., and Zehe, E. (2007). Groundwater-surface water interactions in a North German lowland floodplain- Implications for the river discharge dynamics and riparian water balance. *Journal of Hydrology*, 347, 404-417.

Kristensen, K.J., and Jensen, S.E. (1975). A model for estimating actual evapotranspiration from potential transpiration. *Nordic Hydrology*, 6, 70-88.

Krupa, S.L., Belanger, T.V., Heck, H.H., Brock, J.T., and Jones, B.J. (1998). Krupaseep-the next generation seepage meter. *Interna tional Coastal Symposium (ICS 98)*, 26, 210–213.

Kubach, H., Ward, J., and Willey, S. (2011). Assessing land use changes due to Marcellus gas operations in Bradford County, PA. Geo 533 group project. http://webspace.ship.edu/cajant/student_white_papers.html. [Accessed on January 29, 2014].

Kuczera, G., and Mroczkowski, M. (1998). Assessment of hydrological parameter uncertainty and the worth of multiresponse data. *Water Resources Research*, 34(6), 1481–1489.

Kundzewicz, Z.W., Mata, L.J., Arnell, N.W., Doell, P., Jimenez, B., Miller, K., Oki, T., Sen, Z., and Shiklomanov, I. (2008). The implications of projected climate change for freshwater resources and their management. *Hydrological Sciences Journal*, 53, 3–10.

Kundzewicz, Z.W., and Doell, P. (2009). Will groundwater ease freshwater stress under climate change?, *Hydrological Sciences Journal*, 54, 665–675.

Kurtzman, D., and Kadmon, R. (1999). Mapping of temperature variables in Israel: a comparison of different interpolation methods. *Climate Research*, 13, 33-43.

Lahkim, M.B., and Garcia, L.A. (1999). Stochastic modeling of exposure and risk in a contaminated heterogeneous aquifer, 1: Monte Carlo uncertainty analysis. *Environmental Engineering Science*, 16(5), 315-328.

Land Resource Research Institute. (1985). Soils of Fort St. John-Dawson Creek, British Columbia. Soil Survey report No. 42, Agriculture Canada, Vancouver, BC.

Lee, D.R. (1977). Device for Measuring Seepage Flux in Lakes and Estuaries. *Limnology & Oceanography*, 22(1), 140–147.

Legates, D.R., and McCabe, G.J. (1999). Evaluating the use of "goodness-of-fit" measures in hydrologic and hydroclimatic model validation. *Water Resources Research,* 35(1), 233-241.

Leigh, D.S. (2010). Hydraulic geometry and channel evolution of small streams in the Blue Ridge of western North Carolina. *Southeastern Geographer*, 50(4), 394–421.

Lenhart, T., Eckhardt, K., Fohrer, N., and Frede, H.G. (2002). Comparison of two different approaches of sensitivity analysis. *Physics and Chemistry of the Earth,* 27, 645–654.

Lin, Y., Hong, N., Wu, P., Wu, C., and Verburg, P.H. (2007). Impacts of land use change scenarios on hydrology and land use patterns in the Wu-Tu watershed in Northern Taiwan. *Landscape and Urban Planning*, 80, 111-126.

Linsley, R.K., Kohler, M.A., Paulhus, J.L.H., and Wallace, J.S. (1958). Hydrology for engineers. McGraw Hill, New York.

Liu, Y.B., Gebremeskel, S., De Smedt, F., Hoffmann, L., and Pfister, L. (2003). A diffusive transport approach for flow routing in GIS-based flood modeling. *Journal of Hydrology*, 283, 91–106. doi:10.1016/S0022-1694(03)00242-7

Ma, T., Hathaway, D.L., and Hobson, A.N. (2002). MODFLOW simulation of transient surface water/groundwater interactions in a shallow riparian zone using HEC-2-based water surface profiles. S. S. Papadopulos & Associates, Inc. *(Contract No. 99-CS-20-2084)*

Mansour, M.M., and Hughes, A.G. (2004). User's manual for the distributed recharge model ZOODRM. British Geological Survey Internal Report, IR/04/150.

McCarthy, J.J., Canziani, O.F., Leary, N.A., Dokken, D.J., and White, K.S. (2001). Climate Change 2001: Impacts, Adaptation and Vulnerability. Intergovernmental Panel on Climate Change, Geneva.

McCarty, J.A.J. (2013). Long-term simulation in Parley's Canyon using GSSHA. M.Sc. Thesis, Brigham Young University.

McCuen, R.H. (2004). Hydrologic Analysis and Design. Prentice Hall, Upper Saddle River, New Jersey, 07458, 3rd edition, 2004. ISBN 0-13-142424-6.

McDonald, M.G., and Harbaugh, A.W. (1988). A modular three-dimensional finite difference groundwater flow model. OR-83-875, U.S. Geological Survey, Reston, VA.

McLaren, R.G. (2009). Gridbuilder: a pre-processor for 2-D, triangular element, finite element programs. Unpublished User Manual, Groundwater Simulations Group, Waterloo, Ontario. 87 pp.

McNamara, J.P., Kane, D.L., and Hinzman, L.D. (1997). Hydrograph separations in an Arctic watershed using mixing model and graphical techniques. *Water Resources Research*, 33(7), 1707–1719.

McWhorter, D.B., and Sunada, D.K. (1977). Ground-water Hydrology and Hydraulics. Water Resources Publications, LLC.

Miller, L.L., Hinkel, K.M., Nelson, F.E., Paetzold, R.F., and Outcalt, S.I. (1998). Spatial and temporal patterns of soil moisture and thaw depth at barrow, Alaska USA. *PERMAFROST – Seventh International Conference (Proceedings)*, Yellowknife, 55.

Minhas, P.S., and Sharma, D.R. (1986). Hydraulic conductivity and clay dispersion as affected by application sequence of saline and simulated rain water. *Irrigation Science*, 7, 159-167.

Mishra, S. (2009). Uncertainty and sensitivity analysis techniques for hydrologic modeling. *Journal of Hydroinformatics*, 11(3/4), 282-296.

Monteith, J.L. (1981). Evaporation and surface temperature, *Quarterly Journal of the Royal Meteorological Society,* 107, 1-27.

Moratatti, J., Moraes, J.M., Rodrigues, J.C., Victoria, R.L., and Martinelli, L.A. (1997). Hydrograph separation of the Amazon River using ^{18}O as an isotropic tracer. *Scientia Agricola*, 54(3), 167-173.

Moriasi, D.N., Arnold, J.G., Van Liew, M.W., Bingner, R.L., Harmel, R.D., and Veith, T.L. (2007). Model evaluation guidelines for systematic quantification of accuracy in watershed simulations. *American Society of Agricultural and Biological Engineers*, 50(3), 885-900.

Muleta, M.K., and Nicklow, J.W. (2004). Sensitivity and uncertainty analysis coupled with automatic calibration for a distributed watershed model. *Journal of Hydrology*, 306, 127–145.

Nash, J.E., and Sutcliffe, J.V. (1970). River flow forecasting through conceptual models: Part 1. A discussion of principles. *Journal of Hydrology*, 10(3), 282-290.

Naumburg, E., Mata-Gonzalez, R., Hunter, R., Mclendon, T., and Martin, D. (2005). Phreatophytic vegetation and groundwater fluctuations: A review of current research and application of ecosystem response modeling with an emphasis on Great Basin vegetation. *Environmental Management*, 35, 726–740. doi:10.1007/s00267-004-0194-7

Neff, B.P., Day, S.M., Piggott, A.R., and Fuller, L.M. (2005). Base Flow in the Great Lakes Basin. US Geological Survey Scientific Investigations Report 2005-5217, 23pp.

Nejadhashemi, A.P., Wardynski, B.J., and Munoz, J.D. (2011). Evaluating the impacts of land use changes on hydrologic responses in the agricultural regions of Michigan and Wisconsin. *Hydrology and Earth System Sciences Discussions,* 8, 3421-3468.

Ogden, F.L., and Saghafian, B. (1997). Green and ampt infiltration with redistribution, *Journal of Irrigation and Drainage. Engineering,* 123, 386-393.

Paudel, M. (2010). An examination of distributed hydrologic modeling methods as compared with traditional lumped parameter approaches. Ph.D. dissertation, Brigham Young University.

Paul, S.S. (2013). Analysis of land use and land cover change in Kiskatinaw River watershed: A remote sensing, GIS & modeling approach. M.Sc. Thesis, University of Northern British Columbia.

Paulsen, R.J., Smith, C.F., O'Rourke, D., and Wong, T.F. (2001). Development and evaluation of an ultrasonic ground water seepage meter. *Ground Water*, 39(6), 904–911.

Pettyjohn, W.A., and Henning, R. (1979). Preliminary estimate of groundwater recharge rates, related streamflow and water quality in Ohio: Ohio State. University Water Resources Center, Project Completion Report Number 552, 323.

Pinder, G.F., and Jones, J.F. (1969). Determination of the groundwater component of peak discharge from the chemistry of total runoff, *Water Resources Research*, 5(2), 438–445.

Price, K. (2011). Effects of watershed topography, soils, land use and climate on baseflow hydrology in humid regions: A review. *Progress in Physical Geography*, 35(4), 465-492.

Price, K., and Leigh, D.S. (2006). Morphological and sedimentological responses of streams to human impact in the southern Blue Ridge Mountains, USA. *Geomorphology*, 78, 142–160.

Prudhomme, C., Reynard, N., and Crooks, S. (2002). Downscaling of global climate models for flood frequency analysis: Where are we now?. *Hydrological Processes*, 16, 1137–1150.

Rao, M.N., and Yang, Z. (2010). Groundwater impacts due to conservation reserve program in Texas County, Oklahoma. *Applied Geography*, 30(3), 317-328.

Rawls, W.J., Brakensiek, R.L., and Saxton, K.E. (1982). Estimation of soil water properties. *Transactions of the American Society of Agricultural Engineers*, 25, 1316-1320.

Rawls, W.J., Brakensiek, D.L., and Miller, N. (1983). Green–Ampt infiltration parameters from soil data. *Journal of Hydraulic Engineering*, 109, 62–70.

Refsgaard, J.C. (1997). Parameterisation, calibration and validation of distributed hydrological models. *Journal of Hydrology*, 198(1-4), 69-97.

Refsgaard, J.C., and Storm, B. (1995). MIKE SHE. p. 809–846. *In* V.P. Singh (ed.) Computer models of watershed hydrology. Water Resources, Highlands Ranch, CO.

Reimchen, T.H.F. (1980). Surficial geology, Dawson Creek, British Columbia. Geological Survey of Canada, Map 1467A, scale 1:250 000, URL :ftp://ftp2.cits.rncan.gc.ca/pub/geott/ess_pubs/120/120060/gscmap-a_1467a_e_1980_mn01.pdf. [Accessed on November 21, 2012]. doi:10.4095/120060

Reynolds, W.D., Drury, C.F., Yang, X.M., Fox, C.A., Tan, C.S., and Zhang, T.Q. (2007). Land management effects on the near-surface physical quality of a clay loam soil. *Soil & Tillage Research*, 96, 316-330.

Rihani, J.F., and Maxwell, R.M. (2007). Numerical modeling of coupled groundwater and surface water interactions in an urban setting. University of California, Lawrence Livermore National Laboratory, Contract W-7405-Eng-48.

Rosenberry, D.O., and Morin, R.H. (2004). Use of an electromagnetic seepage meter to investigate temporal variability in lake seepage. *Ground Water*, 42(1), 68–77.

Rosenberry, D.O. (2008). A seepage meter designed for use in flowing water. *Journal of Hydrology*, 359(1–2), 118–130.

Rutledge, A.T. (1998). Computer programs for describing the recession of ground-water discharge and for estimating mean ground-water recharge and discharge from streamflow data – update. U.S. Geological Survey Water-Resources Investigations Report 98-4148, 43 pp.

Saha, G.C., Paul, S.S.. Li, J., Hirshfield, F., and Sui, J. (2013). Investigation of land-use change and groundwater-surface water interaction in the Kiskatinaw River Watershed, British Columbia (parts of NTS 093P/01, /02, /07-/10). in Geoscience BC Summary of Activities 2012, *Geoscience BC*, Report 2013-1, 139-148.

Saltelli, A., Chan, K., and Scott, E.M. (2000). Sensitivity Analysis. Wiley, New York.

Santhi, C., Arnold, J.G., Williams, J.R., Dugas, W.A., Srinivasan, R., and Hauck, L.M. (2001). Validation of the SWAT model on a large river basin with point and nonpoint sources. *Journal of American Water Resources Associations*, 37(5), 1169-1188.

Saskatchewan Ministry of Agriculture. (2008). Irrigation scheduling manual. November. http://www.agriculture.gov.sk.ca/Default.aspx?DN=288f45ad-5bab-41b1-9878-80acf555e3bf [Accessed on May19, 2013].

Saul'yev, V.K. (1957). On a method of numerical integration of a diffusion equation. in Russian, *Dokl Akad Nauk SSSR*, 115, 1077–1080.

Schilling, K.E., Li, Z., and Zhang, Y. (2006). Groundwater-surface water interaction in the riparian zone of an incised channel, Walnut Creek, Iowa. *Journal of Hydrology*, 327, 140-150.

Schilling, K.E., Chan, K.S., and Zhang, Y.K. (2010). Quantifying the effect of land use land cover change on increasing discharge in the Upper Mississippi River. *Journal of Hydrology*, 387, 433-345.

Schmidt, C., Bayer-Raich, M., and Schirmer, M. (2006). Characterization of spatial heterogeneity of groundwater-stream water interactions using multiple depth streambed temperature measurements at the reach scale. *Hydrology and Earth System Sciences*, 10, 849–859.

Scibek, J., Allen, D.M., Cannon, A., and Whitfield, P. (2006a). Groundwater-surface water interaction under scenarios of climate change using a high-resolution transient groundwater model. *Journal of Hydrology*, 333, 165-181.

Scibek, J., and Allen, D.M. (2006b). Modeled impacts of predicted climate change on recharge and groundwater levels. *Water Resources Research*, 42, W11405. doi:10.1029/2005WR004742

Sellinger, C.E. (1996). Computer program for performing hydrograph separation using the rating curve method. US Department of Commerce, National Oceanic and Atmospheric Administration, Technical Memorandum ERL GLERL-100.

Sharif, H.O., El Hassan, A.A., Bin-Shafique, S., Xie, H., and Zeitler, J. (2010). Hydrologic Modeling of an Extreme Flood in the Guadalupe River in Texas. *Journal of the American Water Resources Association*, 46(5), 881-891. DOI: 10.1111/j.1752-1688.2010.00459.x

Sharif, H.O., Yates, D., Roberts, R., and Mueller, C. (2006). The use of an automated now-casting system to forecast flash floods in an urban watershed. *Journal of Hydrometeorology,* 7(1), 190–202. DOI: 10.1175/JHM482.1

Shen, Z.Y., Chen, L., and Chen, T. (2012). Analysis of parameter uncertainty in hydrological and sediment modeling using GLUE method: a case study of SWAT model applied to Three Gorges Reservoir Region, China. *Hydrology and Earth System Sciences,* 16, 121-132. doi:10.5194/hess-16-121-2012

Shen, Z.Y., Chen, L., and Chen, T. (2013). The influence of parameter distribution uncertainty on hydrological and sediment modeling: a case study of SWAT model applied to the Daning watershed of the Three Gorges Reservoir Region, China. *Stochastic Environmental Research and Risk Assessment,* 27, 235-251. doi 10.1007/s00477-012-0579-8

Sholkovitz, E., Herbold, C., and Charette, M. (2003). An automated dyedilution based seepage meter for the time-series measurement of submarine groundwater discharge. *Limnology and Oceanography Methods,* 1, 16–28.

Sieber, A., and Uhlenbrook, S. (2005). Sensitivity analyses of a distributed catchment model to verify the model structure. *Journal of Hydrology,* 310, 216–235.

Singh, J., Knapp, H.V., and Demissie, M. (2004). Hydrologic modeling of the Iroquois River watershed using HSPF and SWAT. ISWS CR 2004-08, Champaign, Ill.: Illinois State Water Survey. Available at: www.sws.uiuc.edu/pubdoc/CR/ISWSCR2004-08.pdf. [Accessed on May19, 2013].

Sloto, R.A., and Crouse, M.Y. (1996). HYSEP: A computer program for streamflow hydrograph separation and analysis. US Geological Survey, Water Resources Investigation Report, 96-4040.

Smedema, L.K., and Rycroft, D.W. (1983). Land drainage: planning and design of Agricultural Drainage Systems. Batsford, London, 376 pp.

Solomon, S., Qin, D., Manning, M., Chen, Z., Marquis, M., Averyt, K.B., Tignor, M., and Miller, H.L. (2007). (Eds.): Climate change, 2007: the physical science basis, Contribution of Working Group I to the Fourth Assessment Report of the IPCC. Cambridge University Press, Cambridge, UK and New York, USA.

Sophocleous, M. (2002). Interactions between groundwater and surface water: the state of the science. *Journal of Hydrogeology*, 10, 52–67.

Soulsby, C., Tetzlaff, D., Rodgers, P., Dunn, S., and Waldron, S. (2006). Runoff processes, stream water residence times and controlling landscape characteristics in a mesoscale catchment: An initial evaluation. *Journal of hydrology*, 325, 197-221.

Starzyk, C.A. (2012). Simulating surface water-groundwater interaction in the Bertrand Creek watershed, B.C. Ph.D. Dissertation, The University of British Columbia.

Stewart, M.K., Mehlhorn, J., and Elliott, S. (2007). Hydrometric and natural tracer (oxygen-18, silica, tritium and sulphur hexafluoride) evidence for a dominant groundwater contribution to Pukemanga stream, New Zealand. *Hydrological Processes*, 21, 3340-3356.

Stoll, S., Hendricks Franssen, H.J., Butts, M., and Kinzelbach, W. (2011). Analysis of the impact of climate change on groundwater related hydrological fluxes: a multi-model approach including different downscaling methods. *Hydrology and Earth System Sciences,* 15, 21–38. doi:10.5194/hess-15-21-2011

Su, N. (1995). The unit hydrograph model for hydrograph separation, *Environment International*, 21(5), 509–515.

Sujono, J., Shikasho, S., and Hiramatsu, K. (2004). A comparison of techniques for hydrograph recession analysis. *Hydrological Processes*, 18(3), 403–413.

Swain, N., Christensen, S., Latu, K., Jones, N., Nelson, E., and Williams, G. (2013). A Geospatial Relational Data Model for Ingesting GSSHA Computational Models: A Step

Toward Two-Dimensional Hydrologic Modeling in the Cloud. *World Environmental and Water Resources Congress*, 201, 2716-2725. doi: 10.1061/9780784412947.269

Texas water Development Board. (1995). Aquifer of Texas. Report No. 345.

Tracy, F.T. (1977). A plane and axisymmetric finite element program for steady-state and transient seepage problems. Miscellaneous Paper K73-4, May 1973a, U.S. Army Engineer Waterways Experiment Section, PO Box 631, Vicksburg, MS 39180-0631.

USACE., Bureau of Reclamation., and NOAA. (2013). Short-term water management decisions: Users needs for improved climate, weather, and hydrologic information. Report No. CWTS 2013-1. URL: http://www.ccawwg.us/index.php/activities/short-term-water-management-decisions-user-needs-for-improved-climate-weather-and-hydrologic-information. [Accessed on October 10, 2013]

USDA (United States Department of Agriculture). (1987). USDA textural classification. ftp://ftp.wcc.nrcs.usda.gov/wntsc/H&H/training/soilsOther/soil-USDA-textural-class.pdf. [Accessed on May 10, 2012].

US EPA. (2007). Lecture#5: Hydrological processes, parameters and calibration. BASINS 4 Lectures, Data Sets, and Exercises.

US EPA. (2011). Figure 2: Long Term Scenarios for Greenhouse Gas Concentrations, based on data provided by IPCC WG1, on website "Future Atmosphere Changes in Greenhouse Gas and Aerosol Concentrations", Washington, D.C., U.S.A.

Van Liew, M.W., Arnold, J.G., and Garbrecht, J.D. (2003). Hydrologic simulation on agricultural watersheds: Choosing between two models. *Transactions of the American Society of Agricultural Engineers*, 46(6), 1539-1551.

Van Roosmalen, L., Christensen, B.S.B., and Sonnenborg, T.O. (2007). Regional differences in climate change impacts on groundwater and stream discharge in Denmark. *Vadose Zone Journal*, 6, 554-571.

Van Roosmalen, L., Sonnenborg, T.O., and Jensen, K.H. (2009). Impact of climate and land use change on the hydrology of a large-scale agricultural catchment. *Water Resources Research*, 45, W00A15. doi:10.1029/2007WR006760

Van Roosmalen, L., Christensen, J.H., Butts, M., Jensen, K.H., and Refsgaard, J.C. (2010). An intercomparison of regional climate model data for hydrological impact studies in Denmark. *Journal of Hydrology*, 380, 406-419.

Vansteenkiste, T., Tavakoli, M., Ntegeka, V., Willems, P., De Smedt, F., and Batelaan, O. (2012). Climate change impact on river flows and catchment hydrology: a comparison of two spatially distributed models. *Hydrological processes*. DOI: 10.1002/hyp.9480

Vivoni, E.R., Entekhabi, D., Bras, R.L., and Ivanov, V.Y. (2007). Controls on runoff generation and scale-dependence in a distributed hydrologic model. *Hydrology and Earth System Sciences,* 11(5), 1683–1701.

Vrugt, J.A., Gupta, H.V., Bouten, W., and Sorooshian, S. (2003). A Shuffled Complex Evolution Metropolis algorithm for optimization and uncertainty assessment of hydrologic model parameters. *Water Resources Research*, 39(8), 1201. doi:10.1029/2002WR001642

Vrugt, J.A., ter Braak, C.J.F., Clark, M.P., Hyman, J.M., and Robinson, B.A. (2008). Treatment of input uncertainty in hydrologic modeling: Doing hydrology backward with Markov chain Monte Carlo simulation. *Water Resources Research*, 44, W00B09. doi:10.1029/2007WR006720

Walvoord, M.A., and Striegl, R.G. (2007). Increased groundwater to stream discharge from permafrost thawing in the Yukon River basin: potential impacts on lateral export of carbon and nitrogen. *Geophysical Research letters*, 34, L12402. doi:10.1029/2007GL030216

Wang, B., Liu, J., Kim, H.J., Webster, P.J., and Yim, S.Y. (2012). Recent change of the global monsoon precipitation (1979-2008). *Climate Dynamics*, 39, 1123-1135.

Washington State Department of Ecology. (1999). Estimated baseflow characteristics of selected Washington Rivers and streams. Water Supply Bulletin No. 60, Publication No. 99-327.

Welderufael, W.A., and Woyessa, Y.E. (2010). Stream flow analysis and comparison of base flow separation methods: case study of the Modder River Basin in central South Africa. *European Water*, 31, 3-12.

Western, A.W., Grayson, R.B., and Bloschl, G. (2002). Scaling of soil moisture: A hydrologic perspective. *Annual Review of Earth and Planetary Sciences*, 30, 149-180.

Whisenant, S.G. (2008). Terrestrial systems. In Perrow Michael R. & Davy, Anthony Journal of Handbook of Ecological Restoration: Principles of Restoration, Cambridge University Press, 89 pp. ISBN 978-0-521-04983-2

Wijesekara, G.N., Gupta, A., Valeo, C., Hasbani, J.G., Qiao, Y., Delaney, P., and Marceau, D.J. (2012). Assessing the impact of future land-use changes on hydrological processes in the Elbow River watershed in southern Alberta, Canada. *Journal of Hydrology*, 412-413, 220-232.

Wilcox, L.J. (2003). Telescopic model of groundwater and surface water interactions near San Antonio, NM. Master's Thesis, New Mexico Institute of Mining and Technology.

Winter, T.C., Harvey, J.W., Franke, O.I., and Alley, W.M. (1998). Groundwater and surface water: A single resource. USGS Circular 1139.

World meteorological Organization (WMO). (1981). Guide to Hydrological Practices Volume I: Data Acquisition and Processing. World Meteorological Organization - No. 168.

Woessner, W.W., and Sullivan, K.E. (1984). Results of Seepage Meter and Mini-Piezometer Study, Lake Mead, Nevada. *Ground Water*, 22(5), 561–568.

Woessner, W.W. (1998). Changing views of stream-groundwater interaction. In Proceedings of the joint meeting of the XXVIII Congress of the International Association of Hydrogeologists and the annual meeting of the American Institute of Hydrology. Ed. Van Brahana, J., Eckstein, Y., Ongley, L.W., Schneider, R., and Moore, J.E. 1-6 St. Paul, Minnesota: American Institute of Hydrology.

Woldeamlak, S.T., Batelaan, O., and De Smedt, F. (2007). Effects of climate change on the groundwater system in the Grote-Nete catchment, Belgium. *Hydrogeology Journal*, 15, 891–901. doi:10.1007/s10040-006-0145-x.

Workman, S.R., Nokes, S.E., Ward, A.D., and Fausey, N.R. (1991). Overview of the Ohio Management Systems Evaluation Area. In: Ritter, W.F. (Editor), Proceedings of ASCE Irrigation and Drainage Conference, Honolulu, HI, 22-26 July, ASCE, New York, 725-731.

www.geobase.ca. [Accessed on January 15, 2012]

www.gov.bc.ca. [Accessed on August 10, 2011]

www.odysseydatarecording.com. [Accessed on June 15, 2010]

www.SoilsofCanada.ca. [Accessed on May 18, 2012]

www.solinst.com. [Accessed on May 20, 2012]

Xu, C.Y., Widen, E., and Halldin, S. (2005). Modelling hydrological consequences of climate change -Progress and challenges. *Advances in Atmospheric Sciences,* 22(6), 789–797.

Xu, J.H., Chen, Y.N., Li, W.H., and Dong, S. (2008a). Long-term trend and fractal of annual runoff process in mainstream of Tarim River. *Chinese Geographical Science*, 18(1), 77–84. DOI: 10.1007/s11769-008-0077-6

Xu, J.H., Chen, Y.N., Ji, M.H., and Lu, F. (2008b). Climate change and its effects on runoff of Kaidu River, Xinjiang, China: A multiple timescale analysis. *Chinese Geographical Science*, 18(4), 331–339. DOI:10.1007/s11769-008-0331-y

Xu, J.H., Chen, Y.N., Li, W.H., Ji, M.H., and Dong, S. (2009). The complex nonlinear systems with fractal as well as chaotic dynamics of annual runoff processes in the three headwaters of the Tarim River. *Journal of Geographical* Sciences, 19(1), 25–35. DOI: 10.1007/s11442-009-0025-0

Xu, J.H., Chen, Y.N., Lu, F., Li, W.H., Zhang, L., and Hong, Y. (2011). The nonlinear trend of runoff and its response to climate change in the Aksu River, western China. *International Journal of Climatology*, 31, 687-695.

Yimam, Y.T. (2010). Groundwater – surface water interaction modeling of the Grote-Nete catchment using GSFLOW. Master's Thesis, University Ghent.

Zehtabian, G., Azareh, A., Samani, A.N., and Rafei, J. (2013). Determing the most suitable geo-statistical method to develop zoning map of parameters EC, TDS and TH groundwater (case study: Garmsar Plain, IRand). *International Journal of Agronomy and Plant Production,* 4(8), 1855-1862.

Zhang, Y.K., and Schilling, K. (2004). Temporal scaling of hydraulic head and river base flow and its implication for groundwater recharge. *Water Resources Research*, 40, W03504. doi:10.1029/2003WR002094,2004

Zhang, G.P., Savenije, H.H.G., Fenicia, F., and Pfister, L. (2006a). Modeling subsurface storm flow with the Representative Elementary Watershed (REW) approach: application to the Alzette River Basin. *Hydrology and Earth System Sciences*, 10, 937-955.

Zhang, Y.K., and Schilling, K.E. (2006b). Increasing streamflow and baseflow in Mississippi River since the 1940 s: Effect of land use change. *Journal of Hydrology*, 324, 412-422.

Zhou, F., Xu, Y., Chen, Y., Xu, C.Y., Gao, Y., and Du, J. (2013). Hydrological response to urbanization at different spatio-temporal scales simulated by coupling of CLUE-S and the SWAT model in the Yangtze River delta region. *Journal of Hydrology*, 485, 113-125.